October 2024

INTERNATIONAL STUDIES AND EVALATIONS IN THE FIELD OF

SCIENCE AND MATHEMATICS

EDITORS

PROF. DR. ALPASLAN DAYANGAÇ

PROF. DR. HASAN AKGÜL

PROF. DR. GÜNAY ÖZTÜRK

INTERNATIONAL STUDIES AND EVALUATIONS IN THE FIELD OF SCIENCE AND MATHEMATICS

Ekim 2024

Editors

PROF. DR. ALPASLAN DAYANGAÇ
PROF. DR. HASAN AKGÜL
PROF. DR. GÜNAY ÖZTÜRK

CONTENTS

Chapter 1

PULSARS

E.Nihal Ercan[1]

1 Prof. Dr., Boğaziçi University,Physics Department, https://orcid.org/0000-0003-0639-704

1. Introduction

Pulsars are a type of compact star, along with neutron stars and white dwarfs, that is characterized by their emission of electromagnetic beams. They can be described as spinning neutron stars with high magnetization. They are no bigger than a large city but contain much more mass than the sun. [1]

The aim of this paper is to review the history of pulsars, their properties, and theories and research surrounding them. In this journey, Neutron stars will be mentioned almost as much as pulsars, as a lot of their existence is shared between them.
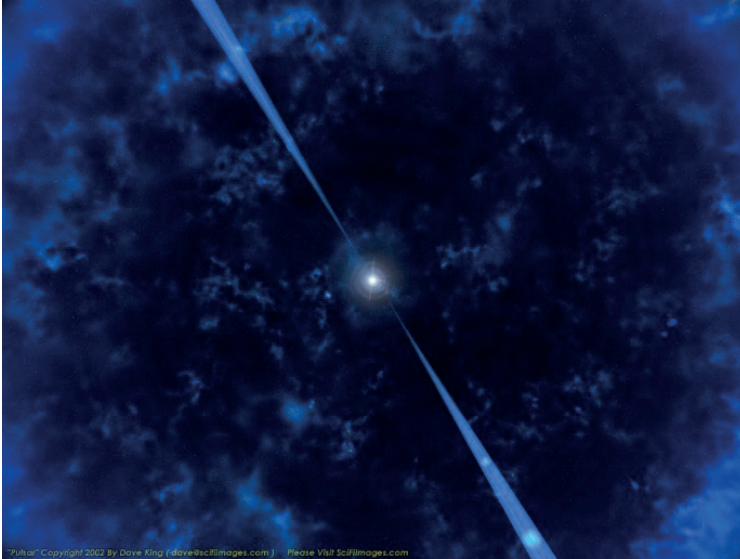
Figure 1 - An Artist's Rendering of a Pulsar [2]

Pulsars are a type of neutron star, super dense objects that are born from the death of a massive star. As the name implies, they are composed almost entirely of neutrons. They can be as massive as the sun but can have a diameter of about 20 km. They radiate strong electromagnetic radiations from their north and south poles, which can be quadrillion times stronger than the earth's. Of course, this much light emission indicates a huge energy reserve. How pulsars manage to shine this bright is still a subject of speculation to researchers. [3]

Another important property of pulsars is their ability to rotate at high speeds. Their speed can range from once a second to many hundred times a second. It is believed that their rotation speed originates from the conservation of angular momentum. In a nutshell, the massive "parent"

star is slowly rotating. Because of their giant size, even at the slow rotational speeds, their angular momentum is quite high. When the star implodes, and its core shrinks to about 20 km, forming a pulsar or a neutron star, that angular momentum is mostly preserved. However, the core is shrunk down to a fraction of its original size, meaning it must compensate for this by gaining rotational speed. [1] A good example of a conversation of angular momentum is when a ballerina pulls their arms to their chest, causing their rotational speed to increase.

2. Brief History of Pulsars

Discovery

The year is 1965. Jocelyn Bell, a graduate student in astronomy, was working at Mullard Radio Astronomy Observatory, close to Cambridge. Bell was born is Ireland in 1943, and she was inspired to pursue Ph.D. in astronomy. In particular, Bell was interested in the newly discovered Quasars. Bell and several other students were working together with Antony Hewish, who was involved in the development of a new technique to detect quasars, called interplanetary scintillation. A radio telescope was designed for this purpose, and the construction was carried out by the students help. [4]

Figure 2 - Jocelyn Bell Burnell [5]

Figure 3 - Mullard Radio Astronomy Observatory [6]

Bell and her fellow students spent around two years in the construction of the telescope. The telescope was finally operational in 1967, although the construction was still in progress. It was Bell's responsibility to operate the telescope and analyze the data. The data was enormous, more than 30 meters of paper each day, and no computer aid was possible at the time. [7]

After a while, Bell started to notice some oddities in the data, which she called "scruff". Something that didn't appear manmade but was remarkably regular in its pulse. Moreover, the signal was coming from the same part of the sky. Bell knew that no natural sources, at least all known at that time, could not produce a signal of such character. Intense sessions of elimination followed, where Bell and Hewish started ruling out various possible sources, including human interference. [4]
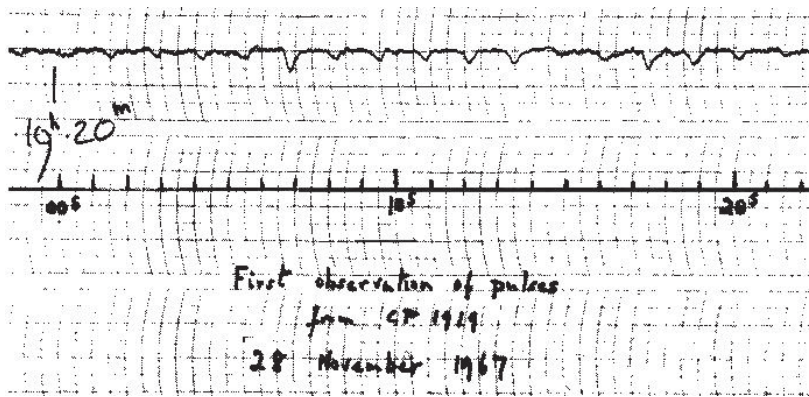
Figure 4 - First Recording of a Pulsar [8]

In the end, nothing would quite explain the signal. The signal had a period of 1.3 seconds, which was seen as unreasonably fast for something a star would produce. Because there was no explanation at the time, Bell and Hewish called the source of the signals LGM-1, which was a little joke, short for "Little Green Man", referring to extraterrestrial life. The source was later renamed CP 1919. [9]

However, Bell soon noticed another signal, this time with a frequency of 1.2 seconds, but from an entirely different part of the sky. Now, it was seen as unlikely that two separate alien civilizations would try to communicate with them at the exact same time, so the idea was ruled out. This decision was further supported when two more such signals were found by Bell. [4]

The idea of neutron stars was something already coined at the time. [9] Fritz Zwicky and Walter Baade hypothesized in 1934 that an exploding massive star, which they called a "supernova", could leave a dense core composed of neutrons behind as a remnant. At the time, this idea seemed very wild. And it has seemed impossible to detect such a small object, however bright they may be. For the longest time the idea was ignored. [9]

But now, with the discovery of LGM-1, Bell and Hewish computed the density of the source and found a density that was remarkably close to what a ball of neutrons would have. Suddenly, all the pieces fell into place. With the signal pulsating from a stellar object, Anthony Michaelis named the object a "pulsar". However, at that time, there was still a debate about whether the object was rotating or pulsating. Thus, the first neutron star that was discovered was a pulsar. And a huge leap was made in our understanding of the universe. [9] Antony Hewish was awarded with the Nobel Prize for Physics in 1974 for his discovery of pulsars. Jocelyn Bell Burnell, despite being the first one to discover the pulsars, was not awarded the Prize. [10]

Timeline of Pulsar Milestones

1974 - the Hulse-Taylor Binary System

In the year 1974, Russell A. Hulse and Joseph H. Taylor discovered the first binary pulsar system, PSR B1913+16, which is known as the Hulse-Taylor binary system. The binary system is composed of a neutron star and a pulsar. What made this discovery incredibly valuable, as well as earned the gentleman a Nobel Prize in 1993 [11], was that, according to Einstein's theory of relativity, systems such as these would emit strong gravitational radiation, which would cause the orbit to slowly lose its energy. Over time, their orbits would get closer and closer until the objects collapse. [12]
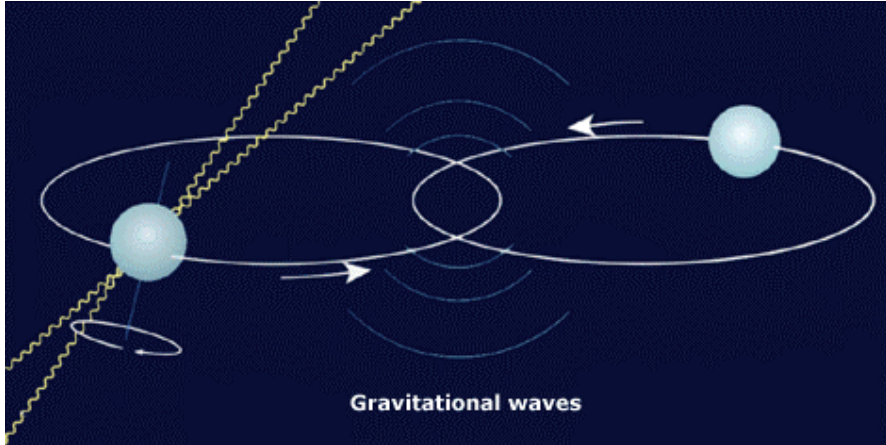
Figure 5 - Neutron Star and Pulsar Binary System [13]

The pulsar in PSR B1913+16 was very precise. And as a binary system its orbital period could be calculated, which turned out to be 7.75 hours. This system allowed astronomers to very accurately estimate the changes in orbital period. If what Einstein predicted was right, and the system was emitting gravitational waves, its orbital period would get shorter and shorter. Over the years, this was exactly what astronomers observed. Einstein was right, and General Relativity was once again proven correct. This discovery is still one of the most conclusive evidence for gravitational waves today. [12]

1982 – Millisecond Pulsars

Up until the year 1982, all discovered pulsars had a rotational period around 1 seconds or so. This all changed when Don Backer discovered the pulsar now known as PSR B1937+21. What made this pulsar special was that it had a rotational period of just 1.55 milliseconds, meaning it completed rotation around itself 38500 times per minute! [14]

This meant huge energy and momentum, which could not be from a parent star. This led some to hypothesize that the pulsar was gaining energy from another source, most reasonably another star. According to some, discovery of this pulsar led to a "theory frenzy" and rekindled the interest in pulsars. [15] One such theory was that these millisecond pulsars were the result of X-ray binary systems, which will be covered later in this paper.
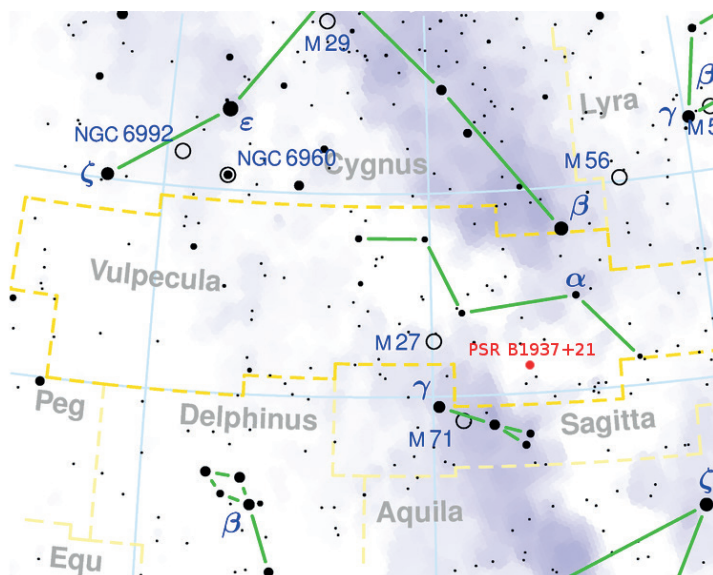
Figure 6 - PSR B1937+21 in the Sky [16]

1992 – Planets around Pulsars

In 1990, Polish astronomer Aleksander Wolszczan discovered the pulsar PSR B1257+12, a millisecond pulsar with a rotational period of 6.2 milliseconds. This pulsar was special because it had an abnormal pulse period, which was further investigated. In 1992, Polish astronomers published the now well-known paper in which the first confirmed discovery of a planet outside of our solar system was made. Not only was an exoplanet found for the first time, but the long suspicion of whether planets could orbit a neutron star was also concluded. After some refinements, another planet was found in the same system. [17] It is not believed that these planets can sustain life as we know it, due to extreme conditions of the pulsar.

Figure 7 – An Artist Impression of PSR B1257+12 System [18]

2006 – White Dwarf Pulsar

This discovery is important in many aspects. First, its unusual nature was first noticed by amateur astronomers, showing that anyone could make a change. [19] The second one requires a bit more explanation. While it was said previously in this paper that pulsars were neutron stars with special characteristics, this does not need to be so. On paper, a white dwarf could be a pulsar as well. But for the longest time, no such white dwarf was observed. This all changed when, in 2006, AR Scorpii, a binary pulsar system consisting of a white dwarf and a red dwarf, was noticed by some amateur astronomers to show odd characteristics. When the amateur astronomers could not quite grasp what was the reason for the oddity, they contacted professional astronomers, who immediately started taking a spectrum of AR Scorpii. This eventually led to the discovery that the white dwarf in the binary system was a white dwarf. [19] At long last the theory had proof.

Figure 8 – An Artists Impression of AR Scorpii System [20]

As a white dwarf-pulsar, AR Scorpii shows a very slow rotational period of 3.56 hours due to low inertia. As a white dwarf, it is about the size of the Earth, making it one of the biggest pulsars.

To summarize the milestones regarding Pulsars:

- **1934:** Fritz Zwicky and Walter Baade hypothesized that an exploding massive star could leave behind a remnant composed solely of neutrons, named "neutron star".

- **1967:** Pulsars were discovered by Jocelyn Bell and Antony Hewish. They were the first neutron stars to be discovered. Antony Hewish was awarded the Nobel Prize in 1974.

- **1974:** Joseph Hooton Taylor and Russell Hulse discovered the first pulsar in a binary system. This discovery also proved the first existence of gravitational waves. They were both awarded the Nobel Prize in Physics in 1993.

- **1982:** Don Backer and his group discovered the first millisecond pulsar, PSR B1937+21. This rekindled the interest in pulsars.

- **1992:** Aleksander Wolszczan discovered the first exoplanet around pulsar PSR B1257+12 by noticing the irregularities in the pulsing period of the pulsar.

- **2016:** AR Scorpii was identified to be a white dwarf-pulsar, a concept that existed up until that point in the paper.

3. Science of Pulsars

This section of the paper aims to review properties and phenomenon associated with neutron stars and pulsars.

Birth of Pulsars

Pulsars and Neutron stars begin their life in a similar, violent manner. A star lives in a balancing act. Its gravity constantly tries to compress it, whereas the pressure from the gas and heat fueled by fusion reactions tries to expand it. For a massive star, which burns its fuel much faster until the core cannot sustain hydrogen fusion anymore. Then gravity wins momentarily, and the core of the star contracts, heating up as a result. This heat allows other fusion reactions to take place. The cycle continues until the star burns the last of its fuel to iron, essentially nuclear ash that does not fuse into anything. [21]

When all of the star's fuel is burnt, a star cannot fight against its gravity anymore. The core collapses rapidly. What happens now depends on the star mass. If a star's mass is around the mass of the sun, the Star creates a planetary nebula, where the outer layers of the star are expanded outwards into space. The core of the stars will compress until it cannot overcome the electron degeneracy pressure and forms a white dwarf. [22] [23]
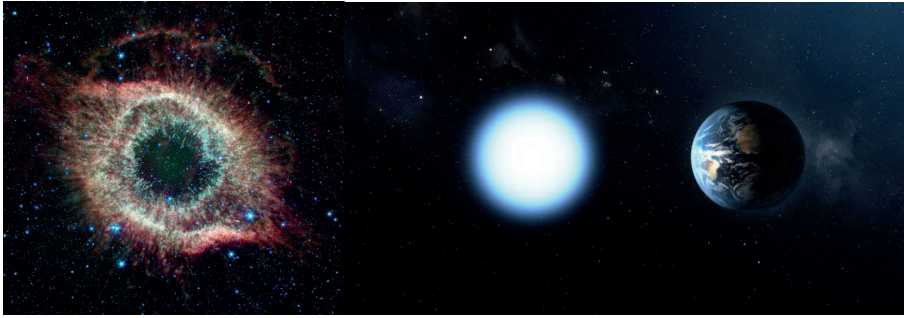
Figure 9 - A Planetary Nebula [24]   Figure 10 - White Dwarf Size Compared to Earth [25]

For a star much more massive than our sun, for example, around 8-10 solar masses, the star goes out with a much more violent process. The electron degeneracy pressure cannot stop the collapse of the core. The star forces electrons to collapse into protons, creating neutrons. These neutrons, in turn, exhibit neutron degeneracy, and this degenerate pressure violently stops the core's collapse. [26] The star's outer layers are blown off into space in a spectacular explosion, creating a supernova. What is left of the star is an incredibly dense neutron star spinning extremely fast due to the conservation of angular momentum, a pulsar. [22] If a star is any bigger, the neutron degeneracy can't hold the core together either, and the star creates a black hole.
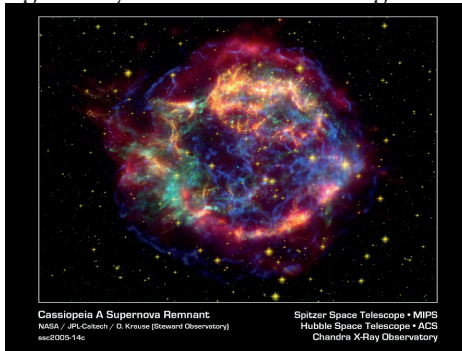
Figure 11 - A Supernova Remnant [27]   Figure 12 - Neutron Star Size [28]
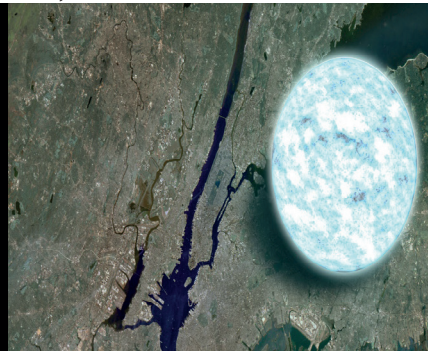
Categories of Pulsars

Currently, pulsars can be divided into three distinct classes. These classes are chosen depending on what powers the electromagnetic radiations emitted by pulsars. [29]

- Rotation-powered pulsars
- Accretion-powered pulsars
- Magnetars

Rotation-Powered Pulsars

This type of pulsar is what is mostly comes to mind when we say "pulsars". They are the first type of pulsars to be discovered. They were also known as radio pulsars, but the term was dropped when it was realized they emitted X-rays instead of radio waves. This type of pulsar uses its rotational energy from its parent star to emit radiation. As a result, these pulsars slow down over time as they lose rotational energy. [30]

Accretion-Powered Pulsars

Otherwise known as X-ray pulsars, they are characterized by their periodic variations in X-ray intensity. X-ray emission period can vary from a fraction of a second to several minutes. [29]

X-ray pulsars are from binary systems composed of one another companion star. Because of the powerful magnetic field of the pulsar, the gases of the companion star will gravitate into the pulsar, creating an accretion disk around the neutron star and powering it in the process. Because of this, they can spin incredibly fast, making them millisecond pulsars simultaneously. [31]
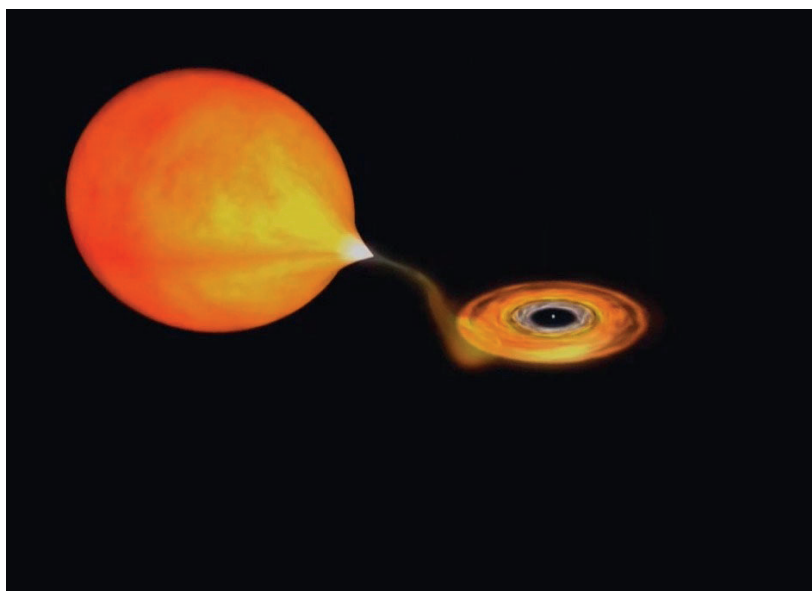
Figure 13 - Artist's Impression of an X-ray Pulsar and Its Companion [32]

Because accretion disks power X-ray pulsars, they can be observed speeding up instead of slowing down like rotation-powered pulsars. However, this is not the norm; most others have relatively stable spins. [31]

Magnetars

Magnetars are neutron stars with extremely strong magnetic fields. They have the strongest magnetic fields in the entire universe. [33] Due to their extremely strong magnetic fields, they rotate much more slowly, in order of a couple of seconds. Their magnetic fields power their radiation, and as such, their magnetic fields gradually decay. This decay is quite fast on a cosmic scale, around 10000 years. After their magnetic fields are weakened, the active life of a magnetar ends. They are one of the most extreme objects in the universe, close second to black holes. [34]

Figure 14 - An Artist's Impression of a Magnetar [35]

Magnetars are home to one of the most powerful surface activities in the universe, called Starquakes. Slight movements in the surface of magnetars can lead to extremely powerful gamma-ray flares, which can be recorded from Earth. [36]

Interior of Pulsars

The insides of neutron stars, and therefore of pulsars, are not completely understood. They are believed to have layers similar to a planet, with an atmosphere, crust, and a liquid core. The crust is extremely hard, made from iron from the supernova, with a crystal lattice structure, where a sea of electrons flows through. [37]
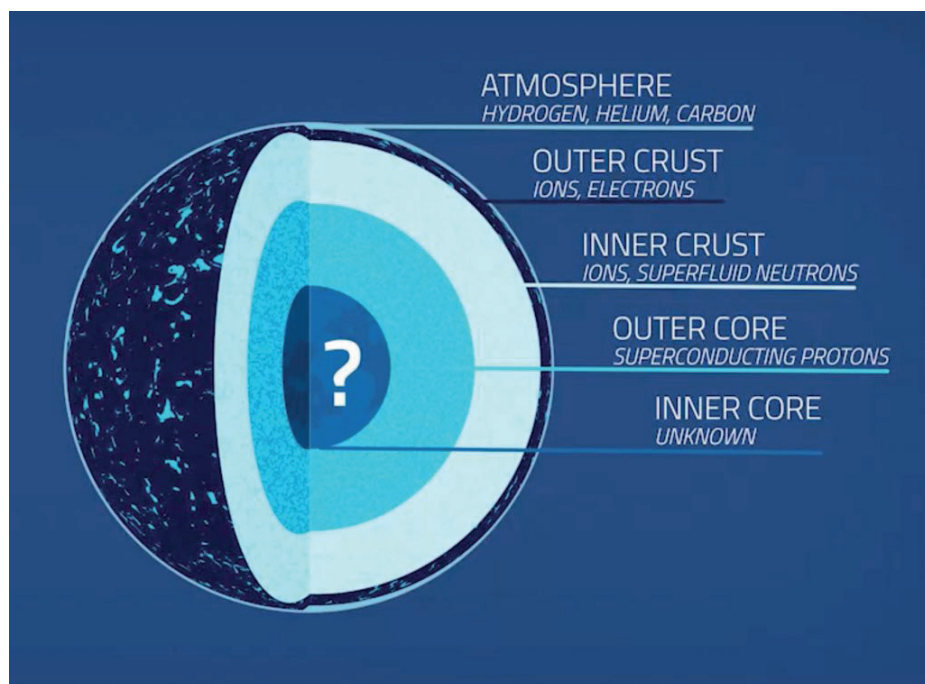
Figure 15 - Diagram of Neutron Star Interior [38]

Going down deeper means that gravity is pulling things stronger and stronger. Fewer protons and more neutrons can be seen as the electrons and protons merge. The crust and the outer core can be divided into multiple sections. Together, they form Nuclear Pasta, theorized to be the strongest material in the universe. [39]

The types of Nuclear Pasta are named after different types of actual pasta, and these are:

• Gnocchi Phase: In the inner crust, between the conventional matter at the outer crust and the ultra-dense material at the core, lies the gnocchi phase, condensed semi-spherical collections of matter not quite as extreme as the core.

• Spaghetti Phase: Deeper into the crust, the pressure is so great that the gnocchi phase matter is compressed, forming long rods instead of individual spheres of nucleons. This matter is immersed in a superfluid of neutrons.

• Lasagna Phase: Further into the neutron star, the rods of matter are compressed into a sheet of nuclear matter that resembles lasagna, which is its name.

This highly theoretical matter is collectively called Nuclear Pasta, and neutron stars can have "mountains" of nuclear pasta, at most a few centimetres high but many times heavier than the mountain ranges on Earth! [39]
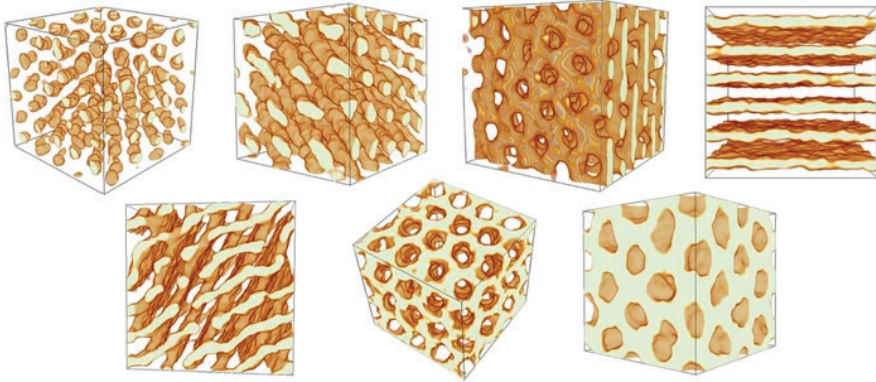
Figure 16 - Simulations of Nuclear Pasta Inside Neutron Stars [40]

We do not know what lies in the centre of the neutron stars. It is unknown what happens to matter when compressed that much. However, some theorize that nucleons can break apart, resulting in a sea of quarks and gluons, appropriately called Quark-Gluon Plasma. [41]

Synchrotron Radiation

Synchrotron radiation is the phenomenon in which ultra-relativistic particles emit radiation, i.e., particles moving close to the speed of light in a magnetic field. [42] It is a type of non-thermal radiation that occurs in nature around black holes and neutron stars, but most known cosmic radio sources are known to emit them. They are useful in estimating the strength of magnetic fields and relativistic particles. [42] Synchrotron radiation is extremely polarized and continuous. Its intensity and frequency are tied to the strength of the magnetic field and the energy of the charged particles affected by the said magnetic field. This means a stronger magnetic field and higher energy particles create greater intensity and frequency of emitted radiation. [43]

Figure 17 - Jet of Synchrotron Radiation from M87 Black Hole [44]

Pulsar Wind Nebulae

Pulsar Wind Nebulae are a nebula found inside a supernova remnant around a pulsar. They are composed of charged particles at very high speeds; therefore, these nebulae evolve over time. They are known to be gamma ray, x-ray, optical and infrared radiation sources. Therefore, most of their properties will be covered later in the Observational Properties of Pulsars section.

Kilonova

We know by observation that two neutron stars can form a binary system. It was also shown that these systems slowly lose their orbital energy through gravitational waves. The neutron star binary system gets closer and closer to each other as they lose orbital energy, and at some point, they collide and merge. This gives a short gamma-ray burst and may create a black hole from the two neutron stars. This phenomenon is known as a Kilonova. It has been hypothesized that most known heavy elements in the universe, also called r-process nuclei, are created during this process. [45] These elements are important for biological functions and electronics; as such, these collisions can be seen as important to life in the universe.

Figure 18 - An Artist's Impression of a Kilonova [46]

Neutron Degeneracy

Degenerate matter is an exotic form packed so closely that pressure is of thermal origin and quantum. Degenerate matter is closely related to the Pauli exclusion principle, which states that no two fermions, such as electrons, can have identical quantum mechanical states in the same quantum system at the same time. [47] Various particles can exert significant pressures via the Pauli exclusion principle in dense matter until they can expand enough. In white dwarfs, the electron degeneracy pressure is enough to stop the collapse of the core, resulting in a star about the size of the Earth. In neutron stars, electron degeneracy is insufficient pressure to hold off the gravitational collapse, and electrons are fused with protons to form neutrons. [48] These neutrons also exhibit degeneracy pressure as the core collapses. Neutron stars' collapse is finally halted by this pressure, resulting in the incredibly dense object, more massive than the sun but slightly bigger than a city.
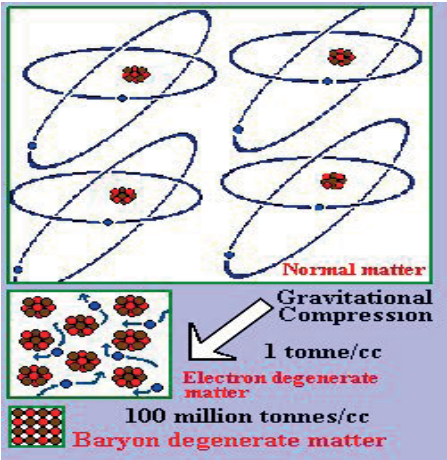
Figure 19 - Comparison between Normal and Degenerate Matter [49]

4. Observational Properties of Pulsars

Pulsars are immensely helpful for astronomers because they emit a wide range of radiation and can be observed differently. Their periodic emission makes them one of the best candidates for regular study. In this section, different ways to observe pulsars will be discussed. Throughout this section, images of the Crab Nebula, which has a pulsar in its centre, will be used whenever possible to show how pulsar emits different radiation.

Radio

In radio wavelengths, pulsars act like lighthouses, shining periodically if their magnetic poles are facing towards Earth. They are particularly strong radio wave emitters. Pulsars were also discovered thanks to a radio telescope, as mentioned before. Because of their emissions, Pulsars are easily detected with radio telescopes despite their extremely small size.
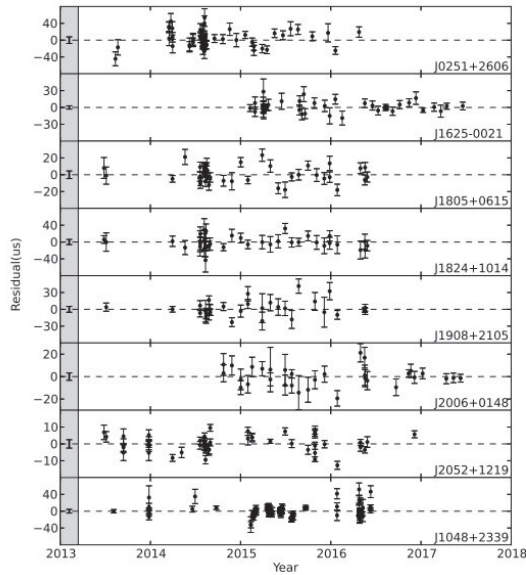
Figure 20 - Data from Binary Pulsars captured via Radio Telescope [50]
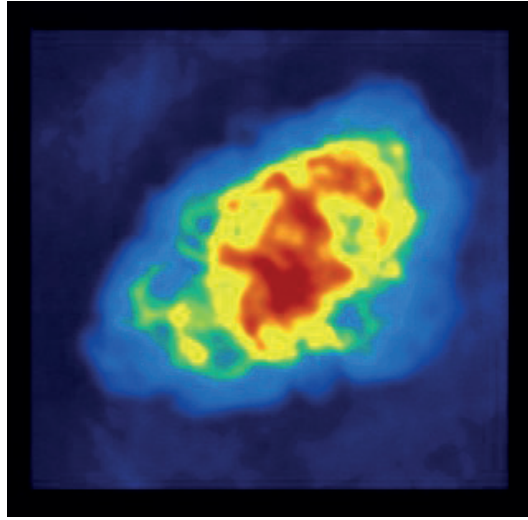
Figure 21 - Crab Nebula Image Constructed by Radio Emissions [51]

Microwave

Pulsars are very strong sources of microwave radiation. Since they produce a broad spectrum of radiation, microwave emissions, which are close to radio wavelengths, are also particularly strong. We already mentioned that most pulsars are usually categorized as "radio pulsars", but some can also be "microwave-bright". [52]

Infrared (IR)

While infrared and near-infrared astronomy are useful for identifying galaxies and supernova remnants, pulsars are not usually known as infrared emitters. Although this is not a rule, astronomers found at least one such pulsar. The reason behind this is not clearly understood, but the experts say it is impossible for a neutron star to emit by itself. The actual infrared emitter is thought to be the pulsar wind nebula or fallback disk. [53]

Figure 22 - Crab Nebula in Infrared Radiation [54]

Visible Light (Optical Pulsars)

Pulsars are extremely small objects. Because of this, even though their surface can be millions of degrees Celsius, they do not shine as bright as other stars. This makes detecting them via optical telescopes quite difficult. Pulsars are one of the dimmest objects ever discovered via optical telescope, with absolute magnitudes as low as 25.7! These pulsars, that is, pulsars observed with visible light, are called optical pulsars. [55] However, this has not stopped us from discovering them anyway, and there are now six known optical pulsars today.

Table 1 - List of Known Optical Pulsars [56]

Name of Pulsar	Magnitude (B)
Crab Pulsar (CM Tauri, PSR B0531+21)	16.5
Vela Pulsar	24
PSR B0540-69	23
PSR B0656+14	26
PSR B0633+17	25.5
PSR B1509-58	25.7

Of these six, Crab Pulsar, located inside Crab Nebula, and Vela Pulsar are the most well-known and studied. Some images of crab pulsar are given below.
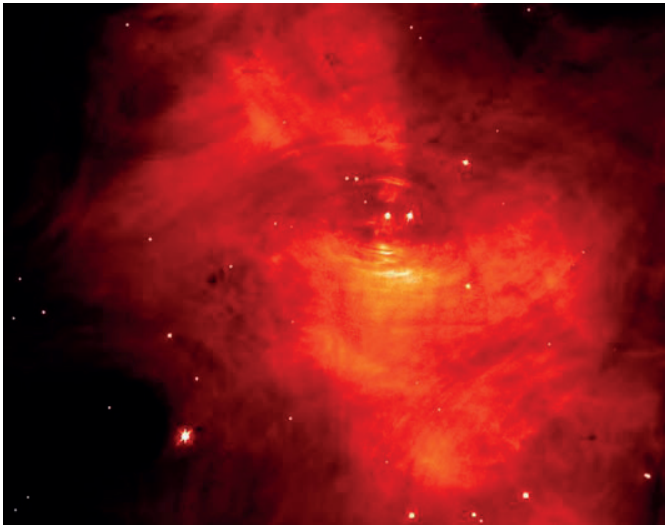
Figure 23 - Crab Pulsar in Visible Light [57]

Figure 24 - Crab Pulsar, Combination of Visible and X-ray Images [58]

Above is a composite image where the image taken via visible light (red) is combined with X-ray emission data (blue) to show the pulsar more clearly.
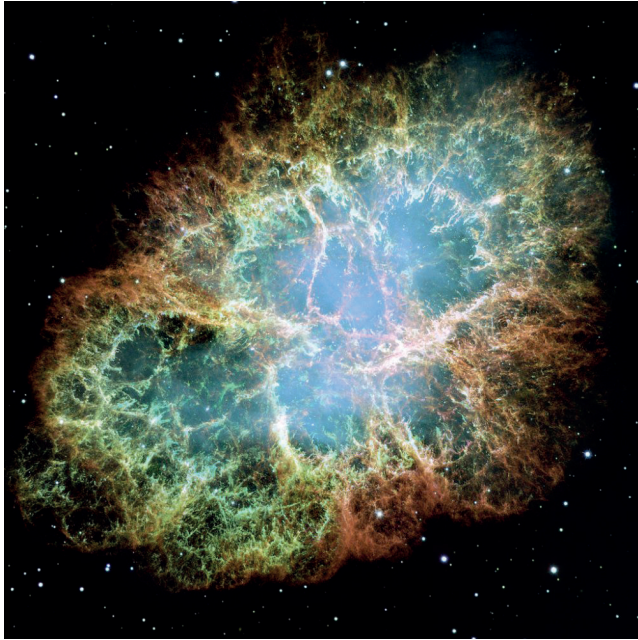
Figure 25 - Crab Nebula in Visible Light [59]

Ultraviolet (UV)

Ultraviolet radiation comes from hotter objects, such as interstellar gas at 1 million kelvins. [60] This might help create temperature maps of nebulas, although they are more helpful in analysing white dwarfs than neutron stars.
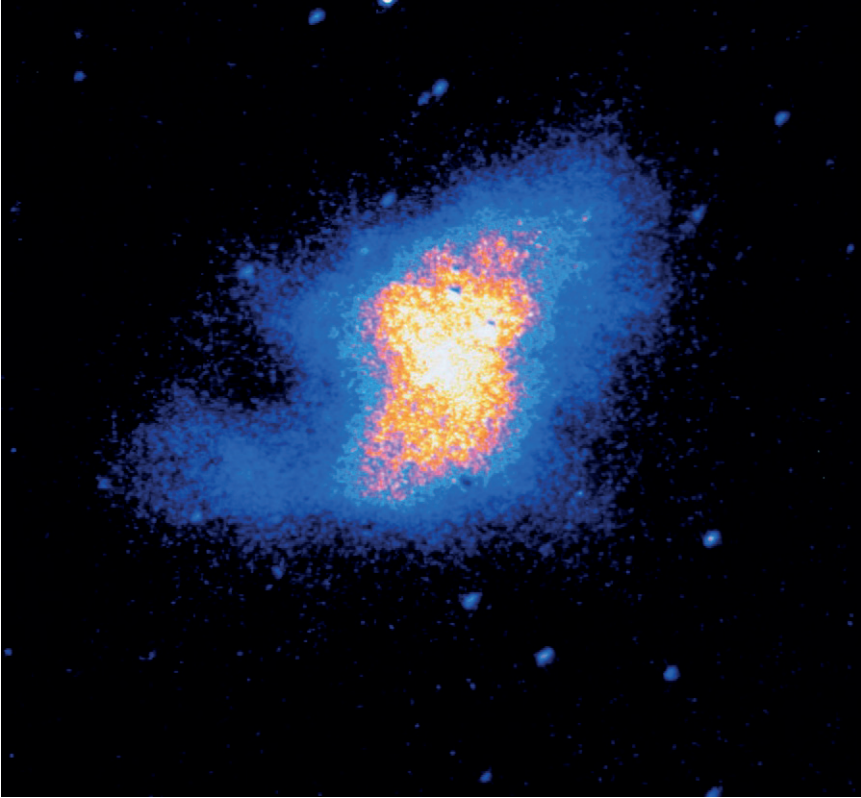
Figure 26 - Crab Nebula in UV Spectrum [61]

X-ray

Pulsars are very powerful X-ray emitters, as the synchrotron radiation mostly comprises X-ray and gamma rays. Because of this, both Crab pulsar and Vela pulsar are imaged via X-rays, creating spectacular images. [1] In these images, not only the pulsar itself can be seen, but also the jets of matter they are ejecting can. At this point, I would like to remind you that the pulsar itself is no bigger than 20 km.
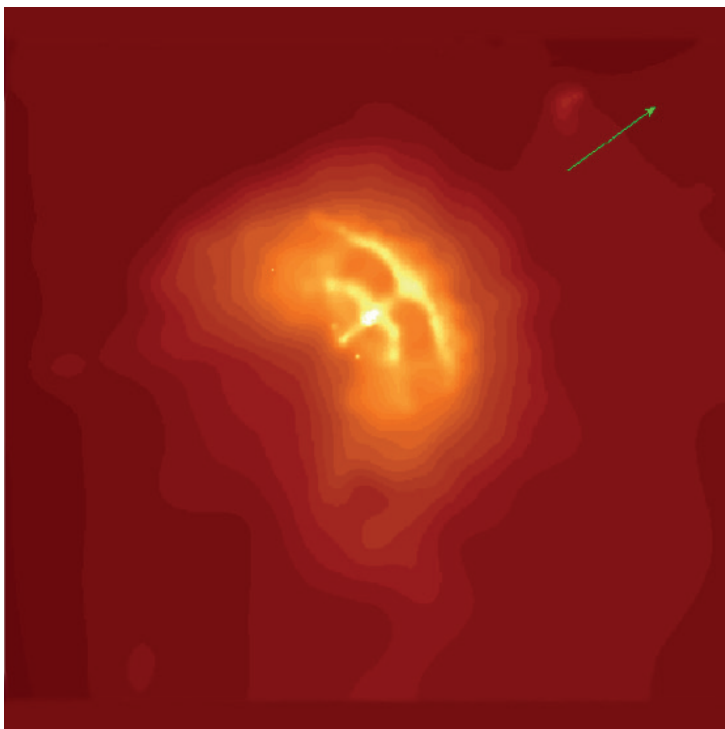
Figure 27 - Vela Pulsar in X-ray [62]
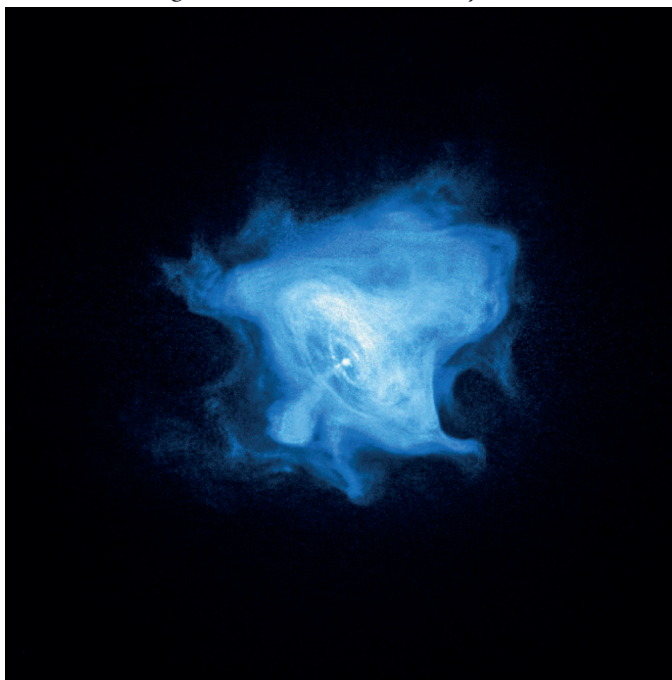
Figure 28 - Crab Pulsar in X-ray [63]

Gamma Rays

Supernova remnants were already connected to gamma-ray sources. Studies show that pulsars can drive gamma-ray radiations. These radiations are observed from Earth. The fastest spinning pulsars emit strong gamma rays, which beam towards or away from Earth as the pulsar rotates. [64]

These very-high-energy gamma rays are observed with ground-based Cherenkov telescopes. The gamma rays are observed, and they create "a short-lived shower" of subatomic particles as they pass through the telescope. The Cherenkov telescope is built to detect the faint and short flashes of light emitted from these particles. The images can be used to calculate gamma rays' direction and intensity. [65]
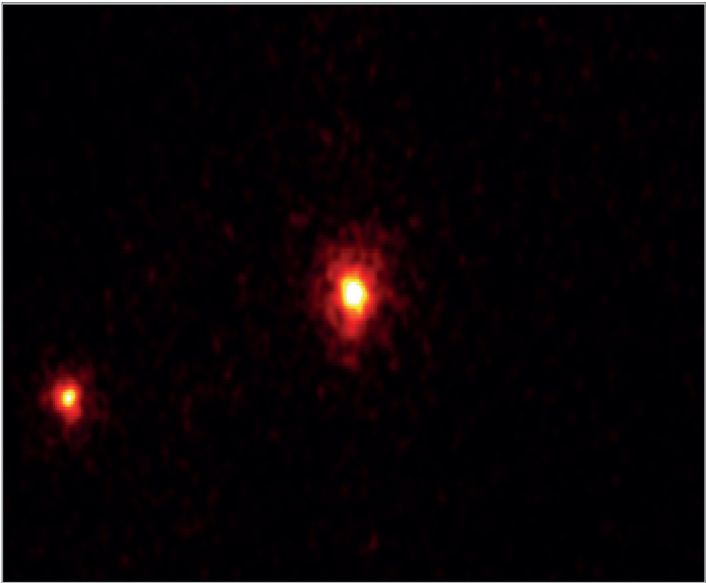
Figure 29 - Crab Pulsar in Gamma Rays [66]
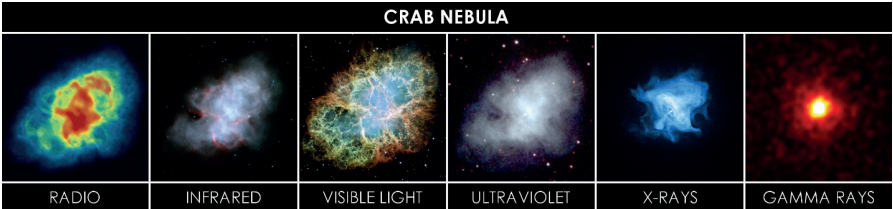
Figure 30 - Crab Nebula in Various Wavelengths [67]

5. Applications of Pulsars

Pulsars are very peculiar objects in the universe, and because of this, we can take advantage of them in various ways.

Pulsar Clocks

We have mentioned before that radio pulses emitted from pulsars are very accurate. But to what extent is truly extraordinary? For example, J0437-4715 has an orbital period 0f 0.005757451936712637 seconds with an error of 1.7×10^{-17} seconds. This is more precise than any clock, except for atomic clocks built for special circumstances. They also provide an external source of reference for time, something not easily found anywhere else in the universe. [68]

There is a pulsar clock located in Gdansk, Poland. The clock was built in 2011 and is one of the most accurate clocks in the world. Outside of sun dials, it is the first clock to count the time using an extraterrestrial signal. [69]

Figure 31 - A Pulsar Clock [70]

Maps

Because they act like lighthouses, pulsars are immensely useful in astronomy and mapping the sky.

Astronomer Frank Drake designed the pulsar map while working with his fellow astronomer Carl Sagan. The map shows the location of the nearest pulsars relative to the solar system. Frank Drake used 14 pulsars to create the map. Now, we have discovered many more pulsars close to the solar system, meaning the map is more difficult to read, both for humans and any possible extraterrestrial life. These maps were used in Pioneer and Voyager missions,

where various facts about humanity and the solar system were embedded in a golden plaque. These plaques were sent with Voyager and Pioneer to the edges of the solar system. [71]
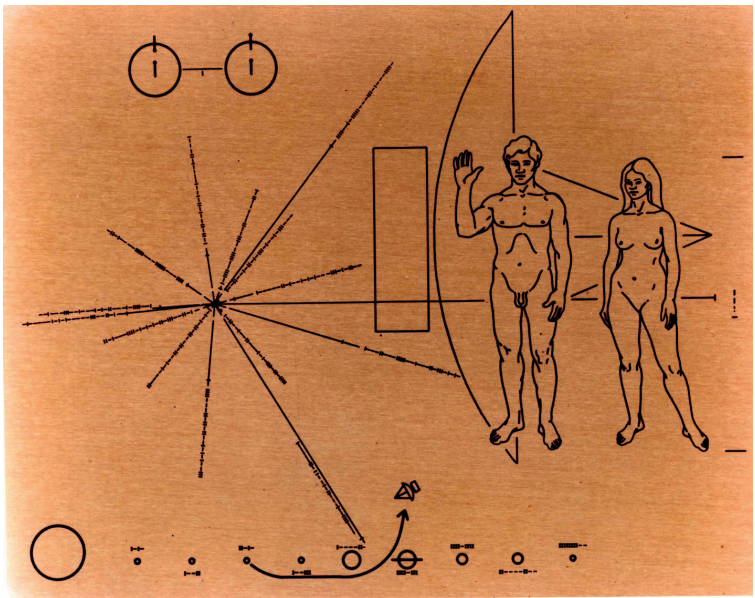
Figure 32 - Pioneer Plaque [72]
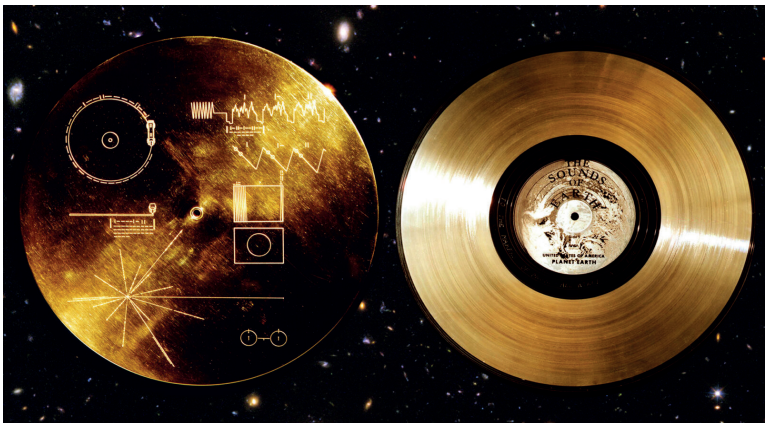
Figure 33 - Voyager Plaque [73]

Gravitational Wave Detection

As mentioned, binary star systems emit gravitational waves and slowly lose their orbital energy until they collapse and create a Kilonova. These binary pulsar systems are among the first and most prominent proofs of the existence of gravitational waves.

Three operational research centres around the world use pulsars to detect gravitational waves. These are: [74]

- The European Pulsar Timing Array (EPTA) is located in Europe, and the project is known as the Large European Array for Pulsars (LEAP).

- Parkes Pulsar Timing Array (PPTA) in Australia.

- North American Nanohertz Observatory for Gravitational Waves (NANOGrav) in Canada and US.

They work together to form the International Pulsar Timing Array (IPTA).
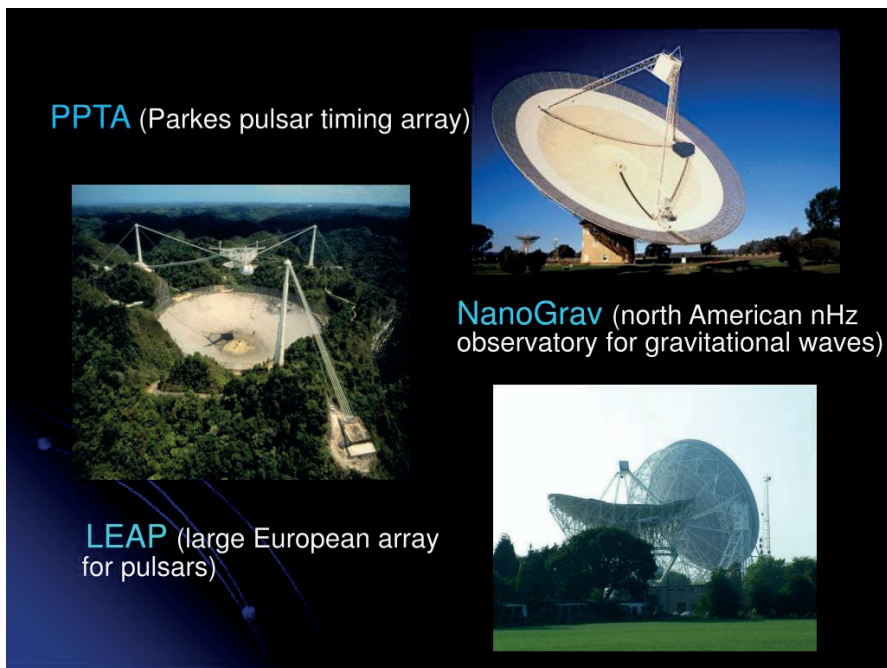
Figure 34 - Pulsar Timing Arrays [75]

Conclusion

Pulsars are extreme objects. Some of their properties are so insane that it is difficult to truly imagine. From their birth to their deaths, pulsars live a violent but spectacular life. We learned that they are born from the death of a massive star. They are small objects around 20 km in diameter but more massive than the sun. Their density is difficult to grasp, and one teaspoon of pulsar matter is as massive as an entire mountain range. What gives them the name "pulsar" is that they emit radiation beams from their magnetic poles. If these beams hit aim towards Earth, we can see them almost like a lighthouse in the sea. They also spin extremely fast, with some spinning hundreds of times each second. Their magnetic fields are also the strongest in the universe. All these properties make them one of the most interesting objects in the universe.

We had not known about these objects for a long time. They were virtually unknown to us until 1967. But now, we have come a long way, and by studying these magnificent objects, we have learned a lot about the universe and how it works. They provided us with one of the best evidence of gravitational waves, which Einstein predicted in his theory of general relativity.

Pulsars are objects of fascination in the hearts of many people, astronomers or otherwise. As a species, we always pursue extremes and the unknown. And maybe because of this, pulsars, more than 50 years after their discovery, are still one of the most fascinating topics in astronomy.

References

[1] C. Cofield, "What Are Pulsars?," 22 05 2016. [Online]. Available: https://www.space.com/32661-pulsars.html. [Accessed 12 01 2021].

[2] D. King, "Pulsar," [Online]. Available: http://2.bp.blogspot.com/_tjmBBHq3HRI/TEx3mkdFSQI/AAAAAAAAAAU/D3pxVYi9yA8/s1600/pulsar.jpg. [Accessed 12 01 2020].

[3] "What Is a Pulsar?," [Online]. Available: https://www.sciencealert.com/pulsar. [Accessed 17 01 2021].

[4] E. Tretkoff, "aps.org," 02 2006. [Online]. Available: https://www.aps.org/publications/apsnews/200602/history.cfm. [Accessed 18 01 2021].

[5] "4.bp.blogspot.com," [Online]. Available: https://assets.teenvogue.com/photos/581c962ec1cacbb91ceb18c6/master/pass/GettyImages-102730646.jpg. [Accessed 18 01 2021].

[6] "4.bp.blogspot.com," [Online]. Available: https://4.bp.blogspot.com/-qXl6h_oHVcI/T0v9OOxnHZI/AAAAAAAACAM/UVCh-5A7Yxs/s1600/AA+(5).jpg. [Accessed 18 01 2021].

[7] "history.aip.org," [Online]. Available: https://history.aip.org/history/exhibits/mod/pulsar/pulsar1/01.html.

[8] "cv.nrao.edu," [Online]. Available: https://www.cv.nrao.edu/course/astr534/images/PSRs_discovery.jpg. [Accessed 18 01 2021].

[9] C. R. James, "astronomy.com," [Online]. Available: https://astronomy.com/bonus/pulsars. [Accessed 18 01 2021].

[10] I. Hargittai, The road to Stockholm: Nobel Prizes, science, and scientists, Oxford University Press, 2006.

[11] "The Nobel Prize in Physics 1993," Nobel Media AB 2021, [Online]. Available: https://www.nobelprize.org/prizes/physics/1993/summary/. [Accessed 19 01 2020].

[12] K. Mukai, "We Knew That Already," NASA, 17 03 2016. [Online]. Available: https://asd.gsfc.nasa.gov/blueshift/index.php/2016/03/17/we-knew-that-already/. [Accessed 19 01 2021].

[13] "johnhartnettdotorg.files," [Online]. Available: https://johnhartnettdotorg.files.wordpress.com/2015/07/ht-binary.gif. [Accessed 19 01 2021].

[14] D. Backer, S. Kulkarni, C. Heiles, M. Davis and M. Goss, "Millisecond Pulsar in 4C 21.53," 1982.

[15] D. E. Thomsen, "Pulsar Encounters of a Third Kind," *Science News,* no. 123, 1984.

[16] T. Bronger, "wikimedia," 13 02 2010. [Online]. Available: https://commons. wikimedia.org/wiki/File:Vulpecula_constellation_map.png. [Accessed 19 01 2021].

[17] A. Wolszczan and D. A. Frail, "A planetary system around the millisecond pulsar PSR1257 + 12," *Nature,* vol. 355, no. 6356, pp. 145-147, 1992.

[18] "earthlyuniverse.com," [Online]. Available: https://i1.wp.com/earthlyuniverse. com/wp-content/uploads/2017/03/Draugr-Ron-Miller-NASA-Blueshift.jpg?resize=750%2C439. [Accessed 19 01 2021].

[19] "skyandtelescope.org," [Online]. Available: https://skyandtelescope.org/ observing/stargazers-corner/amateurs-aid-discovery-pulsing-white-dwarf-ar-scorpii/. [Accessed 19 01 2021].

[20] "research.nd.edu," [Online]. Available: https://research.nd.edu/assets/249938/ ar_scorpii_feature.jpg. [Accessed 19 01 2021].

[21] "What Happens When Stars Produce Iron?," Futurism, 14 07 2014. [Online]. Available: https://futurism.com/what-happens-when-stars-produce-iron. [Accessed 20 01 2020].

[22] N. Ercan, Astrofizik, Ankara: Nobel Akademik Yayincilik, 2019.

[23] "hyperphysics," [Online]. Available: http://hyperphysics.phy-astr.gsu.edu/ hbase/Astro/whdwar.html. [Accessed 20 01 2021].

[24] "meteoritegallery," [Online]. Available: https://meteoritegallery.com/wp-content/uploads/2014/04/hires1.jpg. [Accessed 20 01 2021].

[25] "cdn-images," [Online]. Available: https://cdn-images-1.medium.com/ max/1600/1*Big8C5PNb_wNFxo31qDLOA.jpeg. [Accessed 20 01 2021].

[26] "stanford.edu," [Online]. Available: https://kipac.stanford.edu/research/ topics/neutron-stars-and-pulsars. [Accessed 20 01 2021].

[27] "4.bp.blogspot," NASA, [Online]. Available: https://4.bp.blogspot.com/-C2aIi1yP3HY/UFrlH2PinyI/AAAAAAAAANE/3qwr57hmpsM/ s1600/Kepler-s-Supernova-remnant-By-NASA.jpeg. [Accessed 20 01 2021].

[28] J. Diaz, "gizmodo," 09 03 2012. [Online]. Available: https://gizmodo.com/how-big-is-a-neutron-star-compared-to-new-york-5892029. [Accessed 20 01 2021].

[29] "medium.com," 21 08 2019. [Online]. Available: https://medium.com/@sin_ gularity/9-types-of-neutron-stars-3566cb18c7b8. [Accessed 20 01 2021].

[30] "enacademic.com," [Online]. Available: https://enacademic.com/dic.nsf/ enwiki/14412/Rotation-powered_pulsar. [Accessed 20 01 2020].

[31] "astronomy.swin.edu," [Online]. Available: https://astronomy.swin.edu.au/cosmos/X/X-ray+Pulsar. [Accessed 20 01 2020].

[32] "images.spaceref.com," [Online]. Available: http://images.spaceref.com/news/2013/xray_radio_pulsar_945.jpg. [Accessed 20 01 2021].

[33] P. Sutter, "space.com," 14 08 2015. [Online]. Available: https://www.space.com/30263-paul-sutter-on-why-magnetars-are-scary.html. [Accessed 20 01 2021].

[34] "Magnetars, the Most Magnetic Stars In the Universe," NASA, 02 02 2004. [Online]. Available: https://www.nasa.gov/missions/deepspace/f_magnetars.html. [Accessed 20 01 2021].

[35] "nasa.go," NASA, [Online]. Available: https://www.nasa.gov/images/content/55304main_magnetar.jpg. [Accessed 20 01 2021].

[36] R. C. Duncan. [Online]. Available: https://web.archive.org/web/20070611144829/http://solomon.as.utexas.edu/~duncan/sciam.pdf. [Accessed 20 01 2021].

[37] J. Emspak, "space.com," 06 10 2015. [Online]. Available: https://www.space.com/30748-pulsar-glitches-due-to-superfluid-interior.html. [Accessed 20 01 2021].

[38] NASA, [Online]. Available: https://asd.gsfc.nasa.gov/blueshift/wp-content/uploads/2017/08/neutronstardiagram-1024x753.jpg. [Accessed 20 01 2021].

[39] Kurzgesagt, "youtube.com," Kurzgesagt, 10 10 2019. [Online]. Available: https://www.youtube.com/watch?v=udFxKZRyQt4. [Accessed 20 01 2021].

[40] "theatlantic," [Online]. Available: https://cdn.theatlantic.com/thumbor/jvc4xur6wzORj7etkLvqm0dt7js=/720x405/media/img/mt/2018/10/pasta_1/original.jpg. [Accessed 20 01 2021].

[41] "MIT News," 09 06 2010. [Online]. Available: https://news.mit.edu/2010/exp-quark-gluon-0609. [Accessed 20 01 2021].

[42] NASA, [Online]. Available: https://asd.gsfc.nasa.gov/Volker.Beckmann/school/download/Longair_Radiation2.pdf. [Accessed 20 01 2021].

[43] "Britannica," [Online]. Available: https://www.britannica.com/science/synchrotron-radiation. [Accessed 20 01 2021].

[44] "upload.wikimedia.org," [Online]. Available: https://upload.wikimedia.org/wikipedia/commons/3/39/M87_jet.jpg. [Accessed 20 01 2021].

[45] E. Howell, "universetoday.com," 5 08 2013. [Online]. Available: https://www.universetoday.com/103940/whats-a-kilonova-youre-looking-at-it/. [Accessed 20 01 2021].

[46] "dailycaller.com/," [Online]. Available: https://cdn01.dailycaller.com/wp-content/uploads/2017/10/Colliding-neutron-stars-e1508172068189.png. [Accessed 20 01 2021].

[47] A. M. Helmenstine, "thoughtco.com," 02 02 2019. [Online]. Available: https://www.thoughtco.com/definition-of-pauli-exclusion-principle-605486. [Accessed 20 01 2021].

[48] M. Anissimov, "wisegeek.com," 24 12 2020. [Online]. Available: https://www.wisegeek.com/what-is-degenerate-matter.htm. [Accessed 20 01 2021].

[49] "bis.babylon.com," [Online]. Available: http://bis.babylon.com/?rt=GetFile&uri=!!5AMGUJXGFE&type=0&index=75. [Accessed 20 01 2021].

[50] [Online]. Available: https://scx2.b-cdn.net/gfx/news/2021/eightbinarym.jpg. [Accessed 21 01 2021].

[51] "staticflickr," [Online]. Available: https://c1.staticflickr.com/5/4087/5039185926_c1c0e5577e_n.jpg. [Accessed 21 01 2021].

[52] J. P. Millis, "thoughtco.com," 03 10 2019. [Online]. Available: https://www.thoughtco.com/microwave-radiation-3072280. [Accessed 21 01 2021].

[53] J. Daley, 19 09 2018. [Online]. Available: https://www.smithsonianmag.com/smart-news/pulsar-giving-weird-infrared-light-and-were-not-sure-why-180970331/. [Accessed 21 01 2021].

[54] [Online]. Available: https://www.constellation-guide.com/wp-content/uploads/2013/06/Crab-Nebula-supernova-remnant.jpg. [Accessed 21 01 2021].

[55] [Online]. Available: https://history.aip.org/history/exhibits/mod/. [Accessed 21 01 2021].

[56] A. Shearer and A. Golden, "Why study pulsars optically?," in *Neutron Stars, Pulsars, and Supernova Remnants*, 2002, p. 44.

[57] "history.aip.org," [Online]. Available: https://history.aip.org/history/exhibits/mod/images/pulsar/crab_hst.jpg. [Accessed 21 01 2021].

[58] [Online]. Available: https://upload.wikimedia.org/wikipedia/commons/c/c9/Chandra-crab.jpg. [Accessed 21 01 2021].

[59] [Online]. Available: https://www.constellation-guide.com/wp-content/uploads/2013/06/Crab-Nebula-Messier-1.jpg. [Accessed 21 01 2021].

[60] "britannica," [Online]. Available: https://www.britannica.com/science/ultraviolet-astronomy. [Accessed 21 01 2021].

[61] "fineartamerica," [Online]. Available: https://images.fineartamerica.com/images-medium-large-5/uv-image-of-crab-nebula-by-astro-1-nasascience-photo-library.jpg. [Accessed 21 01 2021].

[62] "wikimedia," [Online]. Available: https://upload.wikimedia.org/wikipedia/commons/6/6f/Vela_Pulsar_xray.jpg. [Accessed 21 01 2021].

[63] "blogspot," [Online]. Available: https://1.bp.blogspot.com/-YbTyXgGCJas/WKy0fUIqUVI/AAAAAAAAik8/JlJ035in_2I_Ht7x862uvkavIy1wKoT0ACLcB/s1600/Crab_Nebula_pulsar_x-ray.jpg. [Accessed 21 01 2021].

[64] "space.com," [Online]. Available: https://www.space.com/27911-fast-spinning-pulsar-gamma-rays.html. [Accessed 21 01 2021].

[65] "harvard.edu," [Online]. Available: https://www.cfa.harvard.edu/news/2011-28. [Accessed 21 01 2021].

[66] NASA, [Online]. Available: https://svs.gsfc.nasa.gov/vis/a010000/a010700/a010767/crabmovie_frame4.png. [Accessed 21 01 2021].

[67] "wikimedia," [Online]. Available: https://upload.wikimedia.org/wikipedia/commons/6/6b/Crab_Nebula_in_Multiple_Wavelengths.png. [Accessed 21 01 2021].

[68] "procaffenation," [Online]. Available: https://procaffenation.com/pulsars-the-most-accurate-clocks-in-space/. [Accessed 21 01 2021].

[69] "web.archive.org," [Online]. Available: https://web.archive.org/web/20111213061916/http://www.mhmg.gda.pl/index.php?view=event,339&oddzial=5. [Accessed 21 01 2021].

[70] "wikimedia," [Online]. Available: https://upload.wikimedia.org/wikipedia/commons/b/b4/Gda%C5%84sk_%E2%80%93_zegar_pulsarowy_ekran.JPG. [Accessed 21 01 2021].

[71] [Online]. Available: https://www.pbs.org/the-farthest/science/pulsar-map/. [Accessed 21 01 2021].

[72] NASA, [Online]. Available: https://solarsystem.nasa.gov/system/internal_resources/details/original/709_Pioneer_Plaque.png. [Accessed 21 01 2021].

[73] NASA, [Online]. Available: https://www.wfmt.com/wp-content/uploads/2019/03/golden-1.jpg. [Accessed 21 01 2021].

[74] "smithsonianmag," [Online]. Available: https://www.smithsonianmag.com/smart-news/gravitational-wave-detection-earns-nobel-prize-physics-180965094/. [Accessed 21 01 2021].

[75] [Online]. Available: https://image3.slideserve.com/5426456/slide12-l.jpg. [Accessed 21 01 2021].
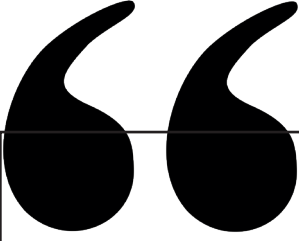
Chapter 2

PERFORMANCE EVALUATION OF OPTIMIZATION METHODS: A STUDY ON GENETIC ALGORITHM, PARTICLE SWARM OPTIMIZATION, AND ANT COLONY OPTIMIZATION

Pelin AKIN[1]

1 Dr.Öğr.Üyesi Pelin AKIN, Çankırı Karatekin Üniversitesi, Fen Fakültesi, İstatistik Bölümü, pelinakin@karatekin.edu.tr, ORCID: 0000-0003-3798-4827.

INTRODUCTION

Optimization can be defined as the process of employing mathematical and algorithmic methods to identify the optimal solution to a given problem. In the present era, many optimization techniques have assumed a pivotal role across diverse fields, particularly in machine learning and artificial intelligence. The earliest known optimization methods date back to the late 19th and early 20th centuries and are related to mathematical programming. The linear programming by George Dantzig in the mid-1940s constituted a revolutionary innovation in optimization. This method represents one of the earliest instances of mathematical modeling to yield optimal results in complex systems (Gill, Murray, Saunders, Tomlin, & Wright, 2008). The advent of advanced optimization techniques can be traced back to the 1960s and subsequent years. The concept of the genetic algorithm was first introduced by John Holland in 1975, drawing inspiration from the evolutionary processes observed in nature (Holland, 1992). GA is an optimization method that uses concepts from natural selection, genetic variation, and evolution to improve solutions. This approach has rapidly gained acceptance as an effective tool for solving complex problems. In the 1980s, Drs. Dr. Russell Eberhardt, James, and Kennedy developed particle swarm optimization (PSO). Methodologically, colonies exhibited collective behaviors that could be imitated to increase detection efficiency (Kennedy & Eberhart, 1995). PSO has attracted attention in many application areas as an optimization technique for continuous variable control. The ability of PSO to perform efficiently, especially in multidimensional space, has been popular in fields such as engineering and computer science. The concept of ant colony adaptation (ACO) was first proposed by Marco Dorigo in the 1990s, inspired by observations of foraging behavior in ants (Dorigo & Di Caro, 1999). ACO is considered an effective strategy if it is used to solve problems that require discovering many solutions. This is a common approach in combinatorial optimization, as evidenced by its application to the transportation sales assistant problem. The fundamental premise of ACO is derived from the pheromone trails left by ants while foraging, which other ants subsequently follow to ascertain the most direct route.

Several studies have recently been conducted to compare GA, PSO, and ACO algorithms. Agrawal and Kaur (2018)Agarwal, and Kaur (2018) compare the effectiveness of Ant Colony Optimization (ACO) and Hybrid Particle Swarm Optimization (PSO) algorithms for selecting and prioritizing test cases in the software testing process. Studies show that hybrid PSO provides better computational efficiency and fault coverage than traditional ACO. Papazoglou and Biskas (2023) present a comparison of genetic algorithm (GA) and particle swarm optimization (PSO) methods for solving the optimal power flow (OPF) problem, an essential issue in the management of power

grids. Research shows that GA often gives good results when severe problems are present.

Adrian, Utamima, and Wang (2015) examined three metaheuristic methods for structuring construction sites: genetic algorithm (GA), particle swarm optimization (PSO), and ant colony optimization (ACO). According to the study, GA provided the best results in general, while PSO and ACO produced effective solutions.

(Le, 2013) investigated the optimal methods of gate placement using genetic algorithm (GA), ant colony optimization (ACO), and particle swarm optimization (PSO) methods. As a result, GA and PSO stand out as efficient methods for solving the gating problem. Three metaheuristic approaches, namely Genetic Algorithm (GA), Particle Swarm Optimisation (PSO), and Ant Colony Optimisation (ACO), were investigated for the arrangement of construction sites. The study's objective is to optimize the location of the facilities to minimize the construction and interaction costs due to facility layout constraints. According to the study, GA generally gave the best results, while PSO and ACO produced effective solutions.

Chen and Shang (2021) The study by Chen and Shang (2021) compares Genetic Algorithms (GA), Ant Colony Optimisation (ACO), and Particle Swarm Optimisation (PSO) algorithms for measurement path optimization on free-form surfaces. The research examines the efficiency and effectiveness of these algorithms in improving measurement path planning. The results show that PSO offers a faster convergence and better solution quality than GA and ACO in path optimization tasks.

Yarat, Senan, and Orman (2021) compare the Particle Swarm Optimisation (PSO) algorithm with other metaheuristic methods. The research examines the advantages and disadvantages of PSO in optimization problems and evaluates its performance with other methods, such as GA and ACO. The results show that PSO provides fast and efficient solutions in many applications but may have limitations compared to other methods in certain situations. The study highlights the role of PSO in the field of optimization.

This paper will demonstrate GA, PSO, and ACO applications of these three optimization methods through two different problems: Determining the minimum value using a simple mathematical function $f(x)=(x-2)2$ and the Iris dataset. Iris data set is used to develop a linear regression model to predict the dependent variable ("sepal.length"). The model will be constructed using the independent variable "sepal.width", "petal.length" and "petal.width". We aim to find a way to minimize the overall squared error.

1. OPTIMIZATION

Optimization involves finding the most efficient or optimal solution to a given problem Optimization involves finding the most efficient or optimal solution to a given problem. For example, an automobile manufacturer may aim to reduce costs and increase productivity by improving production processes, while in agriculture, the focus could be on maximizing yield with minimal water use. The optimization process can be implemented once the decision variables, objective functions, and constraints are defined (Yuan et al., 2022).

The mathematical definition of an optimization problem is as follows.

Objective: minimum or maximum f(x)

Variables $X = (x_1, x_2, x_2, ..., x_n)^T$

Inequality constraints: $gk(x) \leq 0$, j = 1,...,m

Equality constraints: $h_k(x) = 0$, k = 1,...,l

Here, $g_k(x)$ represents inequality constraints, and $h_k(x)$ refers to equality constraints in the optimization model.

Optimization problems are usually classified as single-objective and multi-objective. Single-objective optimization seeks to achieve a single objective, while multi-objective optimization aims to balance conflicting objectives. For example, a food company wants to cut costs while improving productivity. Optimization problems can also be classified according to the nature of the variables (continuous or discrete), the presence of constraints (mandatory or unconstrained), the nature of the solution (global or local), and the solution design (deterministic or stochastic).

Two main optimization procedures are used: exact and approximate methods. The specific methods aim at finding a globally optimal solution to the problem and include techniques such as linear programming. The goal of approximate methods is to find a fast and acceptable solution. These methods often include algorithms inspired by nature (e.g., genetic algorithms and particle swarm optimization).

1.1.ANT COLONY OPTIMIZATION (ACO)

Ant Colony Optimization (ACO) is an algorithm inspired by the foraging behavior of ants. Ants find the shortest path through pheromone trails they leave in their environment. Although the ants initially disperse in random directions, these paths are preferred over time as more pheromones accumulate on shorter paths. ACO was first proposed by Dorigo et al. (1991) to solve the traveling salesperson problem(Dorigo & Di Caro, 1999).

Figure 1 illustrates the path previously discovered by the ants to reach the food, while the second image depicts an obstacle that influences the movement dynamics of the colony. In this position, the ant's new directional options are equally likely to be chosen. In this situation, the new directional options for the ants are equally likely to be chosen, leading to a balanced division between right and left turns. This randomness allows the colony to explore various routes. Ants use a chemical called pheromone to communicate among themselves. The shorter the path, the faster the passage per unit of time, the greater the amount of pheromone released. Accordingly, the number of ants that prefer the shorter path increases over time. After a certain period, all ants prefer the shorter path.
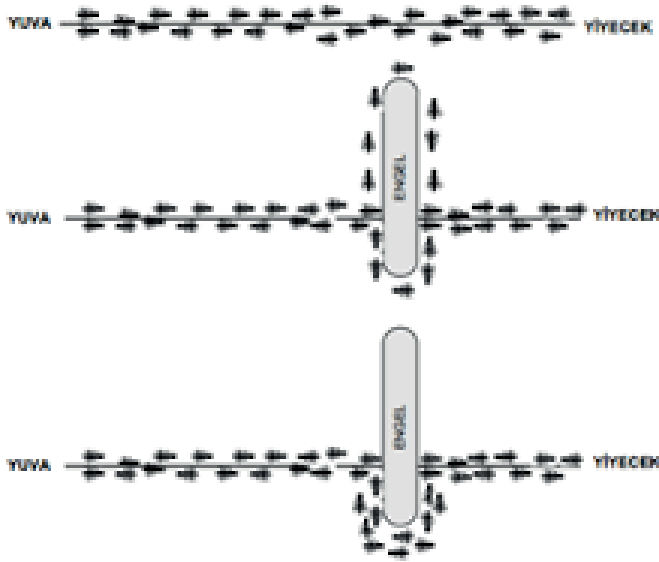
Figure 1. Ant Movement Dynamics

Artificial ants communicate through pheromone trails, like ants in nature, but artificial ants are additionally endowed with some capabilities. For example, artificial ants can access some information about the problem and have a specific memory. The ACO algorithm is an iterative process, and in each iteration, the pheromone trails left by the artificial ants are updated, thus approaching the optimal solution. (Fidanova & Fidanova, 2021). Steps of the ACO algorithm,

Steps of the ACO algorithm:

1. Determine initial pheromone values.

2. Randomly place ants in all cities.

3. Each ant completes its tour by selecting the next city based on local search probability.

4. Calculate the lengths of the paths traveled by each ant and update the local pheromone levels.

5. Determine the best solution and use it for global pheromone renewal.

The advantages of ACO include its ability to reach global optimums in complex, multimodal problems and its adaptability to environmental changes. However, the algorithm's computational time can increase significantly for larger problem sizes, and inaccurate pheromone updates may lead to sub-optimal solutions.

1.2. Particle Swarm Optimization-(PSO)

Particle Swarm Optimization is inspired by the behavior of animals living in herds (Koç, Dünder, Gümüştekin, Koç, & Cengiz, 2018). Each particle is updated according to its own best (pBest) and the group's best (gBest) solutions (Marini & Walczak, 2015).

The basic flow diagram of the PSO algorithm is as follows(Koç, Koç, & Dünder, 2019)

1. Set initial parameters (maximum number of iterations, number of particles, velocity and position ranges)

2. Initialize each particle at random position and speed

3. Determine the best global location

4. Update the velocity and position of the particles for each iteration

5. Rotate the best solution

The advantages of PSO are fast convergence and easy applicability. However, it has disadvantages, such as early convergence problems and parameter sensitivity (Yarat et al., 2021).

1.3. Genetic Algorithm (GA)

Genetic algorithms (GA) are optimization methods that mimic biological evolutionary processes. Random mutations between chromosomes and natural selection processes are used to solve optimization problems. GA can effectively solve continuous, discrete optimization problems (Sivanandam & Deepa, 2008).

The main steps of the GA algorithm are as follows.

1. Set initial parameters (population, genetic operator, maximum number of generations).

2. Create a random starting population

3. For each generation:

- Requires individual eligibility

- Selection of new populations by selection, crossover, and mutation

4. Bring back the best man

The advantages of GA are that it is effective for complex problems and parallel applications and can adapt to dynamic environments. However, it has disadvantages, such as moving computing costs and slow assembly. Moreover, incorrect choices in personnel selection may lead to poor results (Shabir & Singla, 2016).

APPLICATION

Three different optimization algorithms (genetic algorithm, particle swarm optimization, and ant colony optimization) were tested on two different problems. The first problem used a simple mathematical function $f(x)=(x-2)^2$, which is the minimum value of this function. The learned algorithms are compared in terms of speed and accuracy. The second problem used the Iris dataset.

In the first example, three optimization methods, genetic algorithm (GA), particle swarm optimization (PSO), and ant colony optimization (ACO), were applied to an objective function $f(x)=(x-2)^2$. The minimum value of this function is at x =2, where the function This results in zero. The performance of each algorithm was compared by measuring the optimal value and the time taken to find a solution. Figure 2 shows the genetic algorithm codes.


```
# Fonksiyon (örnek optimizasyon fonksiyonu)
objective_function <- function(x) {
  return ((x - 2)^2)  # x = 2'de minimum olan bir fonksiyon
}

# Genetic Algorithm
library(GA)
ga_model <- ga(type = "real-valued", fitness = function(x) -objective_function(x),
          lower = -10, upper = 10, popSize = 50, maxiter = 100)
ga_best <- ga_model@fitnessValue
ga_time <- system.time(ga_model)
```

Figure 2. Genetic algorithm optimization

First, the function $(x-2)^2$ is defined as objective_function. The difference between the calculated fitness function ga_function(x) from the genetic algorithm and objective_function is evaluated. The best value, denoted as ga_best, is found when this difference is minimal. The ga_time records the duration of the program's execution. Figure 3 presents the PSO optimization codes.

```
# Particle Swarm Optimization
library(pso)
pso_model <- psoptim(par = 5, fn = objective_function, lower = -10, upper = 10)
pso_best <- pso_model$value
pso_time <- system.time(psoptim(par = 5, fn = objective_function, lower = -10, upper = 10))
```

Figure 3. PSO algorithm optimization Code

Unlike the GA algorithm, the PSO algorithm does not have a fitness function. Instead, lower and upper bounds are defined. In this study, the minimum value x that can be taken is -10, and the maximum is 10. Figure 4 presents the Ant Optimization codes.

```
# Fonksiyon (örnek optimizasyon fonksiyonu)
objective_function <- function(x) {
  return ((x - 2)^2)  # x = 2'de minimum olan bir fonksiyon
}

# ACO kullanarak optimizasyon
lower_bound <- -10  # Arama aralığı alt sınırı
upper_bound <- 10   # Arama aralığı üst sınırı

start_time <- Sys.time()  # Zaman ölçümünü başlat
aco_result <- aco_continuous(objective_function, lower_bound, upper_bound,
                      num_ants = 10, iterations = 100, evaporation_rate = 0.5)
end_time <- Sys.time()  # Zaman ölçümünü bitir
```

Figure 4. Ant Colony Optimization Code

The Ant Optimization algorithm requires the number of ants and the pheromone rate in addition to the parameters of the PSO algorithm. Figure 5 provides the code for comparing the results of these three optimization methods.

```
# Sonuçların Karşılaştırılması
results <- data.frame(
  Algorithm = c("GA", "PSO", "ACO"),
  Best_Value = c(ga_best, pso_best, aco_best),
  Time = c(ga_time["elapsed"], pso_time["elapsed"], aco_time["elapsed"])
)

print(results)
```

Figure 5. *Compare result code*

Table 1 presents the best results and the time these three algorithms take.

Table 1. Comparison of Best Values and Execution Time for GA, PSO, and ACO Algorithms

Algorithm	Best_Value	Time
GA	-1.28e-10	0.00
PSO	0.00	0.22
ACO	0.0001	0.00

The Genetic Algorithm (GA) predicted the minimum of the function quite accurately with the Best Value result of -1.28e-10. This value is close to zero and indicates that the optimization process was successful. Moreover, GA obtained this result in as little as 0.00 seconds, which shows that the algorithm is effective in terms of solution quality and speed. Particle Swarm Optimization (PSO) found the minimum of the function with exactly zero (0.00). This shows that PSO also correctly detects the minimum of the function. However, this result took 0.25 seconds, i.e., more time than the GA. While PSO has good accuracy, it is slower than GA in speed. Ant Colony Optimization (ACO) performed the worst. ACO found a Best Value of 0.0001, far from the minimum value. ACO was not as successful as the other algorithms. However, the solution time is relatively fast at 0.00 seconds. Despite the speed advantage, the low quality of the solution shows that ACO is unsuitable for this problem. As a result, GA shows the best performance regarding both solution quality and speed, while PSO produces accurate solutions but works slower. Despite its speed advantage, ACO performs poorly in terms of solution quality.

In the second analysis, a simple linear regression model was built using the famous Iris dataset, and optimization algorithms were applied to find the best parameters for this model. The Iris dataset contains 150 observations on three different iris flower species (Setosa, Versicolor, and Virginica). Four features were recorded for each observation: Sepal Length (sepal length), Sepal Width (sepal width), Petal Length (petal length), and Petal Width (petal width). This study aimed to find the parameters of a linear regression model that best estimates the dependent variable Sepal Length. In this model, which is formed by combining the independent variables Sepal Width, Petal Length, and Petal Width, we aim to model the relationship between the independent variables and the dependent variable in the best way and to find the set of parameters that minimizes the sum of squared error. Figure 1 shows the codes of the algorithms, for iris data.

```
# Iris veri setini yükleme
data(iris)

# Bağımlı ve bağımsız değişkenler
y <- iris$Sepal.Length
X <- as.matrix(iris[, c("Sepal.Width", "Petal.Length", "Petal.Width")])

# Hedef fonksiyon: Hata kareler toplamı
objective_function <- function(params) {
  # Basit bir lineer regresyon modelinin tahminleri
  predictions <- X %*% params
  # Gerçek değerlerle tahminler arasındaki hata kareler toplamı
  return (sum((y - predictions)^2))
}

# Genetic Algorithm ile optimizasyon
library(GA)
ga_model <- ga(type = "real-valued", fitness = function(params) -objective_function(params),
        lower = rep(-10, 3), upper = rep(10, 3), popSize = 50, maxiter = 100)
ga_best <- ga_model@fitnessValue
ga_time <- system.time(ga_model)

# Particle Swarm Optimization ile optimizasyon
library(pso)
pso_model <- psoptim(par = rep(0, 3), fn = objective_function, lower = rep(-10, 3), upper = rep(10, 3))
pso_best <- pso_model$value
pso_time <- system.time(psoptim(par = rep(0, 3), fn = objective_function, lower = rep(-10, 3), upper = rep(10, 3)))

# Ant Colony Optimization: Sürekli ACO için basit bir fonksiyon
aco_function <- function(objective_function, n_ants, n_iterations, lower, upper) {▆}

# ACO ile optimizasyon
aco_result <- aco_function(objective_function, n_ants = 20, n_iterations = 100, lower = rep(-10, 3), upper = rep(10, 3))
aco_best <- aco_result$best_distance
aco_time <- system.time(aco_function(objective_function, n_ants = 20, n_iterations = 100, lower = rep(-10, 3), upper = rep(10,

# Sonuçların Karşılaştırılması
results <- data.frame(
  Algorithm = c("GA", "PSO", "ACO"),
  Best_Value = c(ga_best, pso_best, aco_best),
  Time = c(ga_time["elapsed"], pso_time["elapsed"], aco_time["elapsed"])
)

print(results)
```

Figure 6. Optimization algorithms for iris data

In Figure 6, considering the error rates of the iris dataset, the error has been considered as the fitness function for the genetic algorithm. The lower bound is set to -10, and the upper bound is set to +10 for the three variables. Table 2 presents the comparison table.

Table 2. Comparison of Best Values and Execution Time for GA, PSO, and ACO Algorithms

Algorithm	Best_Value	Time
GA	-24.3770	0.00
PSO	19.8649	0.36
ACO	249.4587	0.00

The results detail the performance of the genetic algorithm (GA), particle swarm optimization (PSO), and ant colony optimization (ACO) algorithms that optimize the parameters of a linear regression model on the iris data set. Genetic internal strategy obtained the least squared error of -24.37705 and, in this case, was the most successful strategy in the optimization problem. This result indicates that the model predictions of the GA are very close to the actual target, and the algorithm reaches the optimal solution instantaneously

within 0.00 seconds. On the other hand, particle swarm optimization (PSO) yielded a higher squared error of 19.86486, with a computation time of 0.36 seconds, indicating that it requires more computation time compared to GA. This finding suggests that PSO is not an effective tool for this dataset. On the other hand, Ant Colony Optimization (ACO) obtained the highest squared error of 249.45870. ACO was recorded as the least effective method for this problem at an execution time of 0.00 seconds; that is, although the algorithm performs fast, its quality of results is very low.

CONCLUSION AND DISCUSSION

Optimization methods are critical for solving scientific and technical problems. In this study, the performance of the genetic algorithm (GA), particle swarm optimization (PSO), and ant colony optimization (ACO) methods is evaluated using the Iris dataset and a simple function.

The first experiment used GA, PSO, and ACO methods to optimize the simple function. The results show that GA obtained the best value of -1.278853e-10, PSO 0, and ACO 0.0001e+00. The running time of each algorithm was also recorded. These findings highlight the ability of GA optimization to produce results quicker than PSO and the ability of ACO to make appropriate choices for particular problems.
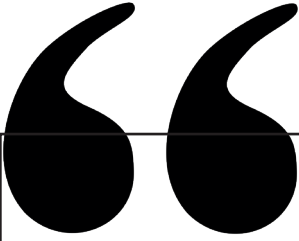
The second example is that the total error squared was an objective function in further optimization analysis with the Iris data set. In this study, the GA, PSO, and ACO algorithms obtained errors of -24.37705, 19.86486, and 249.45870, respectively. The results show that GA performs the best on this dataset. However, ACOs produce the worst results.

In conclusion, optimization techniques such as GA, PSO, and ACO can exhibit different performance for different problems. Each approach offers advantages and disadvantages and different solutions in a particular situation. This study highlights potential application areas for optimization algorithms and emphasizes the importance of blending these techniques and developing new optimization techniques in the future.

REFERENCES

Adrian, A. M., Utamima, A., & Wang, K.-J. (2015). A comparative study of GA, PSO and ACO for solving construction site layout optimization. *KSCE Journal of Civil Engineering, 19*, 520-527.

Agrawal, A. P., & Kaur, A. (2018). *A comprehensive comparison of ant colony and hybrid particle swarm optimization algorithms through test case selection.* Paper presented at the Data Engineering and Intelligent Computing: Proceedings of IC3T 2016.

Chen, Y., & Shang, N. (2021). Comparison of GA, ACO algorithm, and PSO algorithm for path optimization on free-form surfaces using coordinate measuring machines. *Engineering Research Express, 3*(4), 045039.

Dorigo, M., & Di Caro, G. (1999). *Ant colony optimization: a new meta-heuristic.* Paper presented at the Proceedings of the 1999 congress on evolutionary computation-CEC99 (Cat. No. 99TH8406).

Fidanova, S., & Fidanova, S. (2021). Ant colony optimization. *Ant Colony Optimization and Applications*, 3-8.

Gill, P. E., Murray, W., Saunders, M. A., Tomlin, J. A., & Wright, M. H. (2008). George B. Dantzig and systems optimization. *Discrete Optimization, 5*(2), 151-158.

Holland, J. H. (1992). *Adaptation in natural and artificial systems: an introductory analysis with applications to biology, control, and artificial intelligence*: MIT press.

Kennedy, J., & Eberhart, R. (1995). *Particle swarm optimization.* Paper presented at the Proceedings of ICNN'95-international conference on neural networks.

Koç, H., Dünder, E., Gümüştekin, S., Koç, T., & Cengiz, M. A. (2018). Particle swarm optimization-based variable selection in Poisson regression analysis via information complexity-type criteria. *Communications in Statistics-Theory and Methods, 47*(21), 5298-5306.

Koç, H., Koç, T., & Dünder, E. (2019). Parçacık Sürü Optimizasyonu Yöntemi ile Sayım Modelleri için En Uygun Değişken Kümesinin Belirlenmesi. *Süleyman Demirel Üniversitesi Fen Bilimleri Enstitüsü Dergisi, 23*, 76-83.

Le, D.-N. (2013). A comparatives study of gateway placement optimization in wireless mesh network using ga, pso and aco. *International Journal of Information and Network Security, 2*(4), 292.

Marini, F., & Walczak, B. (2015). Particle swarm optimization (PSO). A tutorial. *Chemometrics and Intelligent Laboratory Systems, 149*, 153-165.

Papazoglou, G., & Biskas, P. (2023). Review and comparison of genetic algorithm and particle swarm optimization in the optimal power flow problem. *Energies, 16*(3), 1152.

Shabir, S., & Singla, R. (2016). A comparative study of genetic algorithm and the particle swarm optimization. *International Journal of electrical engineering, 9*(2), 215-223.

Sivanandam, S., & Deepa, S. (2008). Genetic algorithms. In *Introduction to genetic algorithms* (pp. 15-37): Springer.

Yarat, S., Senan, S., & Orman, Z. (2021). A comparative study on PSO with other metaheuristic methods. *Applying particle swarm optimization: New solutions and cases for optimized portfolios*, 49-72.

Yuan, Y., Ren, J., Wang, S., Wang, Z., Mu, X., & Zhao, W. (2022). Alpine skiing optimization: A new bio-inspired optimization algorithm. *Advances in Engineering Software, 170*, 103158.

Chapter 3

VITAMIN C (ASCORBIC ACID) AND ITS FUNCTIONS IN THE METABOLISM

Ebru COTELI[1]

1 Assist Prof, Ahi Evran University Vocational School of Health Services, Kirsehir, e.coteli@ahievran.edu.tr, ORCID: 0009-0005-7193-8711

1. INTRODUCTION

1.1. Vitamin definition

Vitamins are nutrients that ensure healthy growth and development of metabolism and are essential for the continuation of life [1]. It is derived from the words vita (life) + amine. It means amen of life. Vitamins are nutrients that enable human beings to grow and develop in a healthy way and are necessary for the continuation of life. Our body generates the energy it needs from nutrients, the stable functioning of the nervous and digestive systems, and growth and protection of body health. They help with matters. Vitamins are divided into two classes: fat-soluble and water-soluble vitamins. Fat-soluble vitamins are A, D, E, and K. When fat soluble vitamins (A-D-E-K) are consumed excessively for a long time, they can accumulate in the body and cause poisoning. While there is an extra load on the liver and kidneys during excretion, it harms the kidneys and therefore our health. Water-soluble vitamins are the B complex group and vitamin C (ascorbic acid). Human body vitamins cannot synthesize them, so it is vital to obtain vitamins through diet [2].

1.2. Vitamin C (ascorbic acid)

Vitamin C, also known as ascorbic acid, is an organic compound with antioxidant properties. is a compound. Chemical formula: $C_6H_8O_6$, density: 1.65 g/cm3, and the molecular weight is 176.12 g/mol. Its melting point is 189 ºC, its decomposition point is 190-192 ºC, and in water its solubility is approximately 33 g/mL [3, 4]. It is one of the water-soluble vitamins. It is especially abundant in green vegetables, fruits, and citrus fruits. Vitamin C is unstable to heating and resistant to freezing. Vitamin C acts as a coenzyme in the hydroxylation reactions of proline and lysine units of collagen [5-7]. Vitamin C (ascorbic acid) is similar to glucose in structure. Like it, it consists of six carbons. Additionally, this vitamin is a hydrophilic molecule [8]. In metabolism, this vitamin exists in its reduced form ascorbic acid, ascorbate, and dehydroascorbic acid forms [9]. This vitamin is widely used in the fields of cosmetics, pharmaceuticals, and food [10]. White and solid appearance, but impure samples may appear in shades of yellow. Acid reaction ascorbic acid has a slightly specific odor and sour taste. Very little in acetone while it is soluble, it is insoluble in ether, benzene, chloroform, and oil [3, 4]. The exact formula of vitamin C is shown in Figure 1.
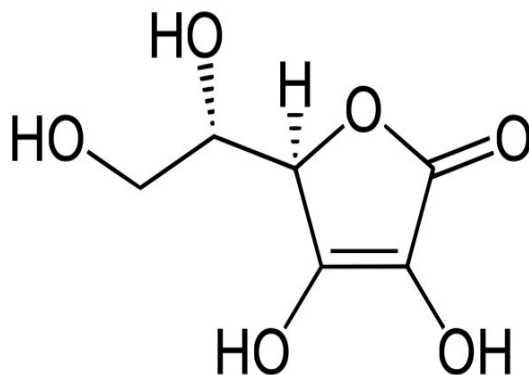
Figure 1. *Vitamin C (ascorbic acid) structure*

Vitamin C is easily absorbed from the small intestines. In particular, this vitamin acts as an antioxidant by easily reacting with superoxide and hydroxyl radicals. In addition, this vitamin is important for the synthesis of bile acids, the absorption of iron, and wound healing. It is effective in healing. Especially foods containing fat such as fish, margarine, and milk are oxidative. protects against deterioration. Vitamin C regenerates radical tocopherols by forming ascorbate radicals [11].

Vitamin C, which has a lactone structure, has both reduced and oxidized forms. These two forms of vitamin C are biologically active [12, 13]. These forms are called L-ascorbic acid and L-dehydroascorbic acid. These substances occur naturally, especially in fruits and vegetables.
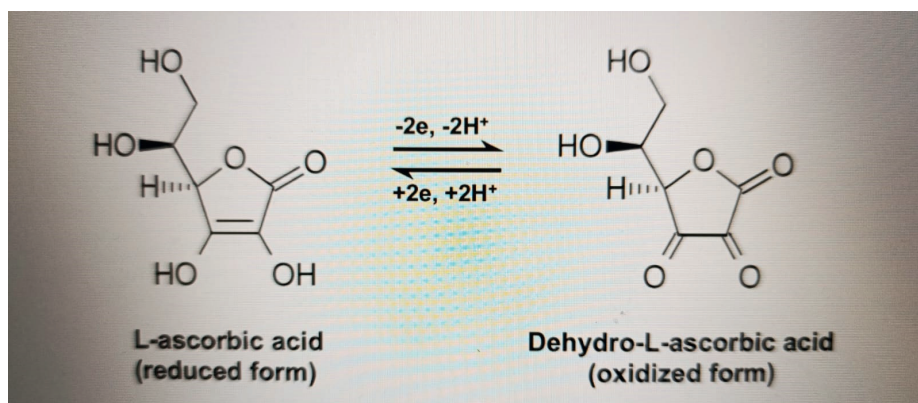
Figure 2. *Reduced and oxidized forms of ascorbic acid*

1.3. Synthesis of ascorbic acid

Most plants and animals synthesize ascorbic acid from D-glucose or D-galactose. Most animals produce relatively high levels of glucose in the liver. produces ascorbic acid. The biosynthetic pathways of ascorbate and its analogues are shown in Figure 3 [14].
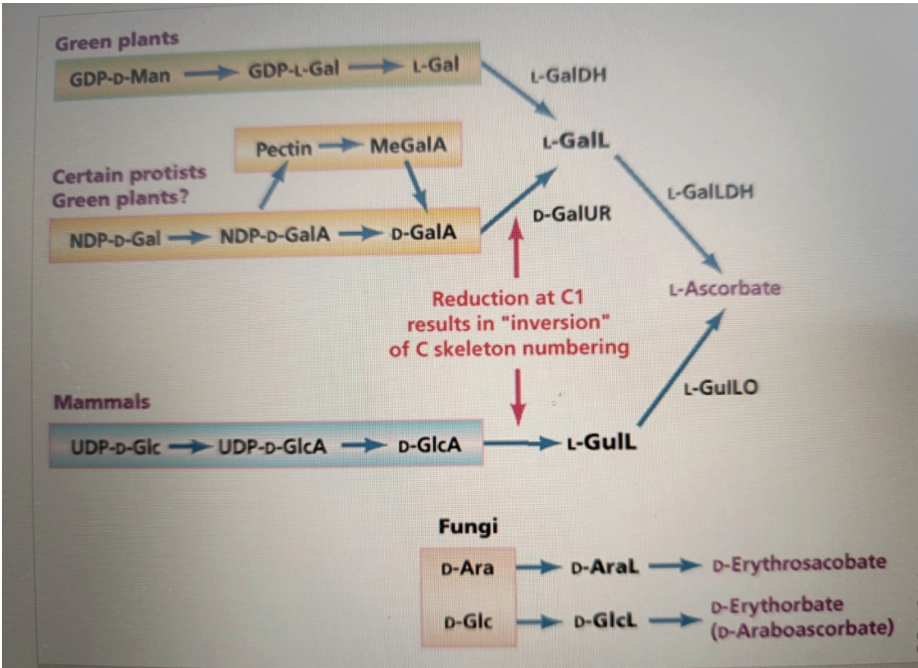
Figure 3. *Biosynthetic pathways of ascorbate and its analogues [14].*

Abbreviations: Ara/AraL, arabinose/arabinonolactone; Gal/GalA/GalL, galactose/galacturonic acid/galactonolactone; L-GalDH, galactose dehydrogenase; L-GalLDH, galactonolactone dehydrogenase; D-GalUR, galacturonic acid reductase; Glc/GlcA/GlcL, glucose/glucuronic acid/gluconolactone; GulL, gulonolactone; L-GulO, gulonolactone oxidase; GDP, guanosine diphosphate; Man, mannose; MeGalA, methyl D-galacturonic acid; NDP, nucleoside diphosphate; UDP, uridine diphosphate.

1.4. Sources of vitamin C

Many vegetables and fruits contain vitamin C (Ascorbate). Fruits such as mango, strawberry, melon, cherry, kiwi, papaya, and watermelon are rich in this vitamin. Additionally, vegetables such as Brussels sprouts, broccoli, tomatoes, peas, cabbage, beans, cauliflower, red and green peppers, and potatoes are rich in vitamin C [15].

1.5. Vitamin C requirement

The daily requirement of vitamin C is kept slightly high due to its low stability. Vitamin C requirement depends on diet, metabolic status, age, and varies depending on renal clearance. In addition to smoking, physical and mental stress, and chronic stress, its requirement increases in many conditions such as alcoholism, metabolic status, and infectious diseases [16].

1.6. Vitamin C absorption and excretion

Absorption of vitamin C occurs in the mouth, stomach, and small intestine cells [16]. However, absorption of vitamin C occurs mostly in the stomach. Because ascorbic acid turns into its dehydro form in the stomach, and since dehydroascorbic acid is uncharged, it passes through membranes more quickly than L-ascorbic acid [17].

1.7. Functions of Vitamin C in Metabolism

1.7.1. Collagen synthesis

Collagen, which constitutes approximately 1/3 of all proteins in our body [18], increases the body's resistance to external and internal factors and helps cells to come together. It is an important protein that ensures retention. On the other hand, flexibility in skin tissue, while providing shine and softness, also serves as support for bone and cartilage tissue [19]. Literature studies have shown that ascorbic acid is effective in collagen synthesis. Proline and lysine amino acids in vitamin C deficiency hydroxylation decreases, and as a result, the synthesis of collagen decreases [20].

1.7.2. Antioxidant function

Free radicals have one or more unpaired electrons in their outer orbital. It is defined as an atom or molecule containing high energy [21]. Oxidative stress occurs when free radicals become overloaded and accumulate in the body. This process can cause cancer, autoimmune disorders, aging, cataracts, rheumatoid arthritis, and chronic and degenerative diseases such as cardiovascular and neurodegenerative diseases to lead to its development [22]. Structures that function to prevent the formation of reactive oxygen species in the body and prevent the damage caused by these substances are called antioxidants. Antioxidants are substances that prevent the progression of peroxidation by reacting with radicals [23]. Especially vitamin C acts as a powerful reducing agent and free radical scavenger in biological systems. This vitamin is in the first step of antioxidant defense. It especially functions to protect lipid membranes and proteins against oxidative damage [24]. In addition to these functions, ferric iron (Fe^{+3}) is a ferrous enzyme that increases lipid peroxidation. It shows oxidant properties by converting it into iron (Fe^{+2}) [25]. Also vitamin C; it acts to clean superoxide, singlet oxygen,

peroxynitrite and hydroperoxyl, reactive oxygen, and reactive nitrogen species such as hypochlorous acid and ozone. Because of this function, it protects the metabolism against oxidative damage [26].

1.7.3. Vitamin C and the cardiovascular system

Studies have shown that dietary antioxidants contribute to metabolism and hypertension. showed that it is inversely proportional [27, 28]. Additionally, studies have shown that treatment with ascorbic acid increases systolic and diastolic blood pressure in hypertensive patients significantly [29]. Studies in hypertension patients show that vitamin C or a mixture of vitamin C and vitamin E increases nitric oxide synthesis and reduces blood pressure [29, 30]. Vitamin C deficiency in metabolism causes a pathological disease called scurvy. In this disorder, it causes slow healing wounds, bleeding, joint pain, and loss of teeth and hair [31].

1.7.4. Vitamin C and Scurvy

Scurvy is caused by vitamin C deficiency resulting from long journeys and fruits. It is a disease that occurs due to a diet without vegetables. Studies have shown that consumption of foods rich in vitamin C prevents scurvy [32]. In addition, the main cause of scurvy is that it causes bleeding that can occur in almost every organ. Especially also in bones, it is a disease that causes frailty. Therefore, the use of vitamin C is essential [33].

1.7.5. Vitamin C and neurodegenerative diseases

Ascorbic acid exerts its direct antioxidant effect by clearing reactive oxygen and nitrogen species produced during normal cell metabolism [34]. Especially in vivo studies have shown that ascorbate is the main by-product of the rapid metabolism of mitochondrial neurons. reported that it has the ability to inactivate superoxide radicals [35]. A non-antioxidant function of vitamin C is central nervous function via neurotransmitters. system participates in signal transmission [36]. Especially ascorbic acid and neurotransmitter substances It serves as a cofactor in the synthesis reaction of catecholamines. Regarding the effect of vitamin C on cognitive processes such as learning, memory, and movement reports, the exact mechanism of this effect is still under investigation. Additionally, animal experiments have shown that ascorbate has a cholinergic effect and demonstrated a clear relationship between dopaminergic systems [37].

1.7.6. Vitamin C and the immune system

Vitamin C has important functions in protecting the immune system. In vitamin C deficiency, the immune system weakens and causes infections. Decreases in vitamin C levels have been observed in the organism in many diseases, especially bacterial infections, influenza, hepatitis, and HIV [38]. It has

been found that vitamin C intake can reduce the incidence of colds, pneumonia, and respiratory infections and shorten the duration of symptoms [39]. The common cold is one of the most common diseases in the general population. It refers to a group of symptoms such as nasal congestion, sore throat, cough, lethargy, and asthenia, with or without fever. There is a common belief that vitamin C helps relieve cold symptoms. However, the scientific data to support this belief is still controversial [40]. It has been found that the use of vitamin C can reduce the incidence of colds, pneumonia, and respiratory infections and shorten the duration of symptoms [39]. Vitamin C levels have been found to decrease in plasma, leukocytes, and urine during various infections, including colds and pneumonia. This decrease is thought to be due to the reaction of vitamin C with phagocytes, which are responsible for preventing the potential damage of many oxidizing agents during infections [41].

1.7.7. Vitamin C and eye health

Vitamin C ensures the integrity of blood vessels and connective tissues, especially in the eye. It also inhibits the formation of free radicals resulting from high metabolic activity in the eye and prevents oxidative damage [42]. Cataract, age-related macular degeneration, and glaucoma are the main ocular diseases and are associated with oxidative damage and lead to severe vision loss. Since vitamin C is an antioxidant, it reduces or eliminates the effects of oxidative damage [43]. There are many studies on eye health and vitamin C. For example, in a study consisting of a macular degeneration patient group and a control group, dietary vitamin C intake was found to be associated with a reduced risk of macular degeneration [44].

1.7.8. Vitamin C and cancer

The effect of vitamin C on cancer is not fully known. However, it is thought to protect against molecular damage associated with carcinogenesis, modulate gene expression, induce cancer cell apoptosis by regulating cellular signaling, inhibit cell proliferation, and is anti-cancer due to its antioxidant properties [45, 46]. In addition, this vitamin protects cells and tissues against oxidative damage and suppresses reactions that increase cancer formation, such as nitrosamines. Many studies on vitamin C and cancer have shown that many of the mechanisms used by cancer cells to survive and grow are targeted by vitamin C. Vitamin C, with its anticancer properties, caused redox imbalance, weakness in epigenetic reprogramming, and disorder in oxygen perception regulation, which are common points for many cancer cells. Therefore, vitamin C is of great importance in cancer treatments [47, 48].

1.7.9. Vitamin C and diabetes

Nowadays, an increase in diabetes is observed. This disease manifests itself with hyperglycemia, an increase in glycated hemoglobin (HbA1c) level, and

disorders in antioxidant enzyme activities. There are two types of this disease: Type 1 and Type 2 [49, 50]. Studies show that oxidative stress, which occurs as a result of the imbalance between reactive oxygen species and antioxidant levels, causes disruption of glucose metabolism and hyperglycemia. It has also been reported that oxidative stress levels are high in patients with diabetes [51]. A study reported that vitamin C supplementation in metabolism reduces increased oxidative stress, reduces glucose toxicity, and prevents the decrease in the number of beta cells of the pancreas [52].

REFERENCES

[1] Lykkesfeldt, J. (2012). Ascorbate and dehydroascorbic acid as biomarkers of oxidative stress: validity of clinical data depends on vacutainer system used. *Nutrition research*, *32*(1), 66-69.

[2] Milisav, I., Ribarič, S., & Poljsak, B. (2018). Antioxidant vitamins and ageing. *Biochemistry and Cell Biology of Ageing: Part I Biomedical Science*, 1-23.

[3] Tan, B. (2018). Spectrophotometric determination of vitamin C in fruit juices. *Master's thesis*. Ondokuz Mayıs University Institute of Science and Technology, Samsun.

[4] Chiu, A., & Kimball, A.B. (2003). Topical vitamins, minerals and botanical ingredients as modulators of environmental and chronological skin damage. *British Journal of Dermatology*, *149*(4), 681-691.

[5] Akkuş, İ. (1995). Free oxygen radicals and their physiopathological effects. *Mimoza Publishing and Distribution*, 1-15, Konya.

[6] Tüzün, C. (1997). Biochemistry, 3rd Edition, Palme Publishing, 151-187, Ankara.

[7] Emerk, K., & Onat, T. (1997). Basic Biochemistry. 2nd Edition, Saray Medikal Publishing, İzmir-Türkiye.

[8] Telang, P.S. (2013). Vitamin C in dermatology. *Indian Dermatol Online J, 4* (2), 142.

[9] Kocot, J., Luchowska-Kocot, D., Kiełczykowska, M., Musik, I., & Kurzepa, J. (2017). Does vitamin C influence neurodegenerative diseases and psychiatric disorders? *Nutrients*, *9*(7):659.

[10] Sunil, K., Singh, S., & Verma, R. (2017). Anticancer potential of dietary vitamin D and ascorbic acid: a review. *Crit Rev Food Sci Nutr.*, *57*(12), 2623-2635.

[11] Wolf, R., Wolf, D., & Ruocco, V. (1998). Vitamin E: The radical protector. *Journal of the European Academy of Dermatology and Venereology, 10*, 103-117.

[12] Nishikawa, Y., & Kurata, T. (2000). Interconversion between dehydro-L-ascorbic acid and L-ascorbic acid. *Biosci Biotechnol Biochem.*, *64*(3), 476–483.

[13] Dewhirst, R.A., & Fry, S.C. (2018). The oxidation of dehydroascorbic acid and 2,3-diketogulonate by distinct reactive oxygen species. *Biochem. J.*, *475*(21), 3451–3470.

[14] De Tullio, M.C. (2010). The Mystery of Vitamin C. *Nature Education*, *3*(9), 48.

[15] Haytowitz, D. (1995). Information from USDA's Nutrient Data Book. *J. Nutr.*, *125*, 1952-1955.

[16] Aksoy, M. (2011). Nutritional biochemistry (3rd ed.), Hatiboğlu Publishing, Ankara.

[17] Bilişli, A. (2012). Food biochemistry, Sidas publications, Izmir.

[18] Sinanoğlu, G. (2013). Collagenase enzyme inhibitors. Master's thesis. Istanbul

University Institute of Science and Technology. Istanbul.

[19] Bilek, S.E., & Bayram, S.K. (2015). Use of collagen hydrolyzate as a functional ingredient in the food industry. *Academic Food*, *13*(4), 327-334.

[20] Türközü, D. (2014). The evaluation of the effect of implementation some disinfectants on the vitamin C content of lettuce and rocket salad. Master's thesis, Gazi University Institute of Health Sciences, Ankara.

[21] Sen, S., Chakraborty, R., Sridhar, C., Reddy, Y.S.R., & De, B. (2010). Free radicals, antioxidants, diseases and phytomedicines: current status and future prospect. *International journal of pharmaceutical sciences review and research*, *3*(1), 91-100.

[22] Aguirre, R., & May, J.M. (2008). Inflammation in the vascular bed: importance of vitamin C. *Pharmacology & therapeutics*, *119*(1), 96-103.

[23] Karabulut, H., & Gülay, M.Ş. (2016). Free radicals. *Mehmet Akif Ersoy University Health Sciences Institute Journal*, *4*(1).

[24] Pehlivan, F.E. (2017). Vitamin C: An antioxidant agent. In book: Vitamin C, 23-35.

[25] Huan, H., Huan, H., Qiao, Y., Zhang, Z., Wu, Z., Liu, D., Liao, Z., Yin, D., & He, M.F. (2018). Dual action of vitamin C in iron supplement therapeutics for iron deficiency anemia: prevention of liver damage induced by iron overload. *Food & function*, *9*(10), 5390-5401.

[26] Carr, A.C., & Frei, B. (1999). Toward a new recommended dietary allowance for vitamin C based on antioxidant and health effects in humans. *The American journal of clinical nutrition*, *69*(6), 1086-1107.

[27] Salonen, R.M., Nyyssönen, K., Kaikkonen, J., Porkkala-Sarataho, E., Voutilainen, S., Rissanen, T.H., Tuomainen, T.P., Valkonen, V.P., Ristonmaa, U., Lakka, H.M., Vanharanta, M., Salonen, J.T., & Poulsen, H.E. (2003). Six-year effect of combined vitamin C and E supplementation on atherosclerotic progression: the Antioxidant Supplementation in Atherosclerosis Prevention (ASAP) Study. *Circulation*, *107*(7), 947-953.

[28] Myint, P.K., Luben, R.N., Welch, A.A., Bingham, S.A., Wareham, N.J., & Khaw, K.T. (2008). Plasma vitamin C concentrations predict risk of incident stroke over 10 y in 20 649 participants of the European prospective investigation into cancer–norfolk prospective population study. *The American journal of clinical nutrition*, *87*(1), 64-69.

[29] Ellulu, M.S. (2017). Obesity, cardiovascular disease, and role of vitamin C on inflammation: a review of facts and underlying mechanisms. *Inflammopharmacology*, *25*(3), 313-328.

[30] Sherman, D.L., Keaney Jr, J.F., Biegelsen, E.S., Duffy, S.J., Coffman, J.D., & Vita, J.A. (2000). Pharmacological concentrations of ascorbic acid are required for the beneficial effect on endothelial vasomotor function in hypertension. *Hypertension*, *35*(4), 936-941.

[31] Carpenter, K.J. (2012). The discovery of vitamin C. *Ann. Nutr Metab.*, *61*(3), 259–264.

[32] Khalife, R., Grieco, A., Khamisa, K., Tinmouh, A., McCudden, C., & Saidenberg, E. (2019). Scurvy, an old story in a new time: The hematologist's experience. *Blood Cells, Molecules, and Diseases*, *76*, 40-44.

[33] Desai, V.D., Hegde, S., Bailoor, D.N., & Patil, N. (2009). Scurvy extinct? Think again! Int J Clin Pediatr Dent., *2*(3), 39-42.

[34] Kocot, J., Luchowska-Kocot, D., Kiełczykowska, M., Musik, I., & Kurzepa, J. (2017). Does vitamin C influence neurodegenerative diseases and psychiatric disorders? *Nutrients*, *9*(7), 659.

[35] Jackson, T.S., Xu, A., Vita, J.A., & Keaney Jr, J.F. (1998). Ascorbate prevents the interaction of superoxide and nitric oxide only at very high physiological concentrations. *Circulation research*, *83*(9), 916-922.

[36] Hansen, S.N., Tveden-Nyborg, P., & Lykkesfeldt, J. (2014). Does vitamin C deficiency affect cognitive development and function? *Nutrients*, *6*(9), 3818- 3846.

[37] Harrison, F.E., & May, J.M. (2009). Vitamin C function in the brain: vital role of the ascorbate transporter SVCT2. *Free Radical Biology and Medicine*, *46*(6), 719-730.

[38] Kalokerinos A, Dettman I, & Meakin M. (2005). Endotoxin and vitamin C part1— Sepsis, endotoxin and vitamin C. *Journal of Australasian College Nutritional and Environmental Medicine*, *24*(1), 17-21.

[39] Kim, T.K., Lim, H.R., & Byun, J.S. (2022). Vitamin C supplementation reduces the odds of developing a common cold in Republic of Korea Army recruits: randomised controlled trial. *BMJ Mil Health*. 168(2), 117-123.

[40] Quidel, S., Gómez, E., Bravo-Soto, G., & Ortigoza, Á. (2018). What are the effects of vitamin C on the duration and severity of the common cold? *Medwave*, *18*(06), e7261.

[41] Hemilä, H. (2003). Vitamin C, respiratory infections and the immune system. *Trends in Immunology*, *24*(11), 579-580.

[42] McCusker, M.M., Durrani, K., Payette, M.J., & Suchecki, J. (2016). An eye on nutrition: The role of vitamins, essential fatty acids, and antioxidants in age-related macular degeneration, dry eye syndrome, and cataract. *Clinics in dermatology, 34*(2), 276-285.

[43] Raman, R., Vaghefi, E., & Braakhuis, A.J. (2017). Food components and ocular pathophysiology: a critical appraisal of the role of oxidative mechanisms. *Asia Pacific journal of clinical nutrition, 26*(4), 572-585.

[44] Aoki, A., Inoue, M., Nguyen, E., Obata, R., Kadonosono, K., Shinkai, S., Hashimoto, H., Sasaki, S., & Yanagi, Y. (2016). Dietary n-3 fatty acid, α-tocopherol, zinc, vitamin D, vitamin C, and β-carotene are associated with age-related macular degeneration in Japan. *Scientific reports, 6,* 20723.

[45] Schlueter, A.K., & Johnston, C.S. (2011). Vitamin C: overview and update. *Journal*

of Evidence-Based Complementary & Alternative Medicine, *16*(1), 49-57.

[46] Barrita, J.L.S., & Sánchez, M.D.S.S. (2013). Antioxidant role of ascorbic acid and his protective effects on chronic diseases. *Oxidative Stress and Chronic Degenerative Diseases-A Role for Antioxidants*, 449.

[47] Pawlowska, E., Szczepanska, J., & Blasiak, J. (2019). Pro-and antioxidant effects of vitamin C in cancer in correspondence to its dietary and pharmacological concentrations. *Oxidative Medicine and Cellular Longevity, 2019,* 7286737.

[48] Ngo, B., Van Riper, J.M., Cantley, L.C., & Yun, J. (2019). Targeting cancer vulnerabilities with high-dose vitamin C. *Nature Reviews Cancer*, *19*(5), 271-282.

[49] Rafighi, Z., Shiva, A., Arab, S., & Yusuf, R.M. (2013). Association of dietary vitamin C and E intake and antioxidant enzymes in type 2 diabetes mellitus patients. *Global journal of health science*, *5*(3), 183-187.

[50] Çatak, J. 2019. Determination of glycemic indexes of some food products and biscuits consumed in our country using in vitro methods. *European Journal of Science and Technology*, 16, 940-947.

[51] Harding, A.H., Wareham, N.J., Bingham, S.A., Khaw, K., Luben, R., Welch, A., & Forouhi, N.G. (2008). Plasma vitamin C level, fruit and vegetable consumption, and the risk of new-onset type 2 diabetes mellitus: the European prospective investigation of cancer–Norfolk prospective study. *Archives of internal medicine*, *168*(14), 1493-1499.

[52] Dakhale, G.N., Chaudhari, H.V., & Shrivastava, M. (2011). Supplementation of vitamin C reduces blood glucose and improves glycosylated hemoglobin in type 2 diabetes mellitus: a randomized, double-blind study. *Advances in pharmacological sciences*, *2011*, 195271.

Chapter 4

COSMIC RAYS

E.Nihal Ercan[1]

1 Prof. Dr., Boğaziçi University,Physics Department, https://orcid.org/0000-0003-0639-704

What are Cosmic Rays?

Cosmic ray particles rain over Earth's atmosphere from interstellar space with intense flux (1000 per square meter per second). They arrive evenly from all directions, but cosmic ray sources do not spread around us similarly. They deflected and scattered in the Galaxy, which hides their actual trace from their origin. The origin of cosmic rays is not fully known, but we know most come from the solar system and somewhere in the Galaxy. They consist of electrons, neutrons, and atomic nuclei. The atmosphere of the Earth doesn't let cosmic radiation arrive at the Earth's surface. Earth's magnetic field is also a protector of us. When they arrive in the atmosphere, they collide with nuclei, creating more particles. The particle which occurs after those collisions are pions. After that, charged pions emit muons. Muons do not interact efficiently with matter as pions do. Muon's average flux to the Earth's surface is 1 muon per square cm per minute.

Figure 1. A view for cosmic rays (credit: NASA)

History of Cosmic Ray Researches

Cosmic rays were discovered in 1912 by Victor Hess. In 1908, Theodor Wulf perfected the electroscope to 1V. He thought that measuring radioactivity at different heights may give different results. Till then, the dominant opinion was radioactivity came from the soil. Victor Hess ascended an electroscope with a balloon and found that the electroscope discharges more and more as

the balloon goes up. It is generally believed that cosmic radiation was gamma rays because of its penetrating power. The geomagnetic effect of cosmic radiation was found later in 1927, accidentally by J. Clay. With that result, astronomers concluded cosmic rays must be charged particles. In 1931, Fritz Zwicky introduced the term super-nova idea. He said such explosions produce cosmic rays. In 1932, Anderson made a cloud chamber under a magnetic field. In his experiments, he realised there is a positively charged electron, which is the positron. In 1937, Neddemayer discovered the muon. In 1947, Pion was discovered by Lattes, Occhialini &Powell, and Rochester and Butler discovered Kaon. Before particle accelerators reached high energies, cosmic rays were used in high-energy physics research. Those researchers discovered subatomic particles, mainly positrons and muons. Cosmic Ray research led scientists to particle physics research. Today, astrophysics researchers mainly focus on the origin of cosmic rays, how they are accelerated to those high velocities, and what role they play in Galaxy dynamics, and they give us information about matter from outside the solar system. One of the most important findings of cosmic ray research is that the neutrino has zero mass.

Some Observational Aspects

In 1896, Antoine Henri Becquerel discovered spontaneous radioactivity. By accident, he observed uranium salts emitting radiation on a photographic plate. Afterwards, in 1898, Marie and Pierre Curie discovered that polonium and radium could generate radioactivity.

Theodor Wulf, a Jesuit and professor, measured the radioactivity difference between the Eiffel and the ground, and he was expecting an exponential decrease $e-h/\lambda$ was expected because, till that time, scientists were considering radioactivity came from the ground. With the results of that experiment, scientists convicted that radioactivity.

In 1911, Pacini found an important reduction of radioactivity under 3m deep in the sea. That experiment showed that due to water absorption, the amount of radioactive substances in the sea was 20% less than that in the ground. Scientists discovered that radiation comes from somewhere outside of the sea.

After those experiments, Victor Hess 1911 made 2 balloons to ascend the electroscope and measure the radiation difference between the ground and above. But he found no effect. In 1912, he had a chance to repeat the same experiment with 7 balloons, and the results were significant. He realised that as height increases, ionisation also increases, and that happens because of radiation coming from above. But he considered gamma rays were causing this effect.

Milikan and Cameron also measured water depths and higher places. They reproduced Pacini's effect and realised particles come from space homogenously in every direction. They named them cosmic rays. However, it was still believed that gamma rays caused cosmic radiation.

Then, the geomagnetic effect was discovered accidentally by J. Clay in 1927. Then Hans Geinger developed Geiger counters, which are easier to measure and give a more rapid response. Arthur Compton organised a survey of cosmic radiation depending on the geomagnetic latitude. In 1933, scientists found that cosmic radiation is greater in the West than in the East, which led to the opinion most cosmic rays are positively charged. In 1932, Anderson designed an experiment with a cloud chamber with a magnetic field. By the direction the particle moved, the particle he observed was positively charged. If that particle was a proton or something has mass like a proton, that particle would fall down in a shorter time. He concluded, that particle is positive charged electron. Later it will be named positron. After the development of high-energy accelerators, cosmic ray experiments were mainly made with accelerators. And those experiments mainly focused to find the origin of cosmic rays, their composition, and the properties of those particles.
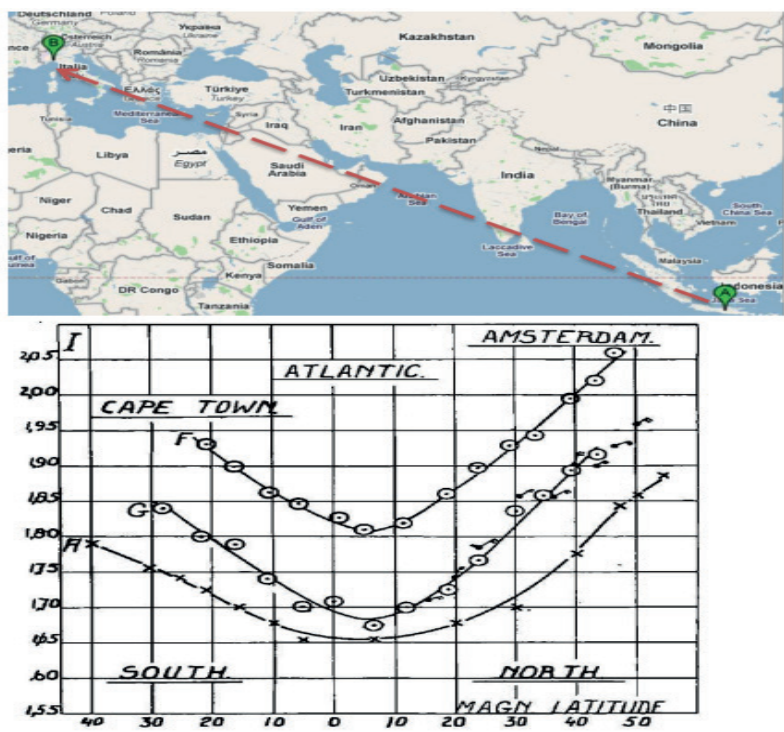
Figure 2. Distribution of Cosmic rays on Earth (Credit: NASA)

Theoretical Aspects and The Properties of Cosmic Rays

Cosmic rays are extremely high-speed particles, and their composition gives information about the chemical properties of their origin. Cosmic ray isotopes give even more information about the region of the source, as well as the initial acceleration from the source. Those pieces of information are key to understanding galactic and extragalactic parts of the universe. With better measurements of ultrahigh energies becoming possible, we will better understand the galactic and extragalactic origins of those interstellar particles. The most useful property of cosmic rays is their energy spectrum. From 10^9 to 10^{20} eV, that energy spectrum is relatively powerless. Energies around 40 GeV, solar modulation effects become significant. Under some MeV, anomalous cosmic rays can be observed. Around 10 MeV, particles of solar origin that are accelerated by solar flare events can be observed. We can't observe the intensity of solar rays greater than 3×10^{20} eV. The composition of particles that have over 1012 eV energy is not well known either. Supernova events accelerate those particles. Cosmic ray particles are mainly hydrogen, some helium, and very small amounts of carbon, oxygen, and heavier elements. Except for some exceptions, cosmic ray compositions are the elements that are plenty in our solar system. Exceptions give us great information about matter composition outside of our solar system. $^{22}Ne/^{20}Ne$ ratio is an important exception for that purpose. Those compositions give important information about the origins of the cosmic rays.
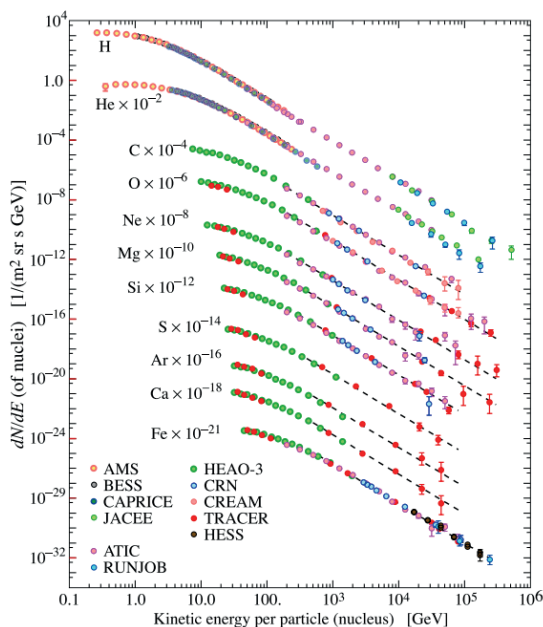
Figure 3. Energy density versus Kinetic energy per nucleus (Credit: NASA)
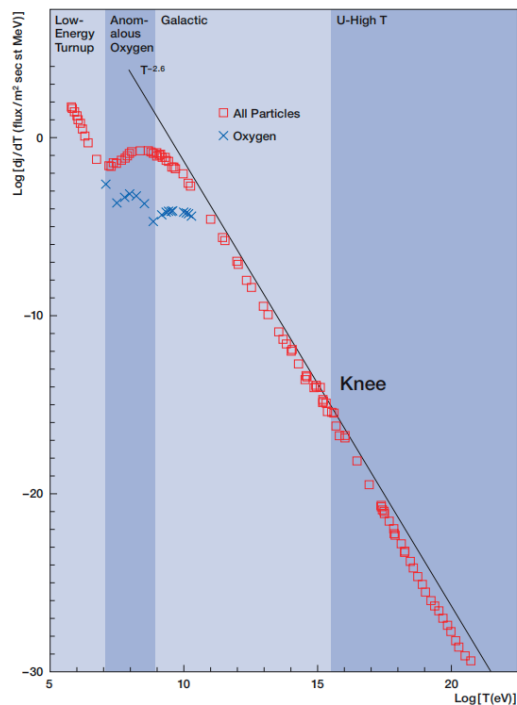
Figure 4. Logarithmic energy distribution of cosmic particles (Credit: NASA)

Primary and Secondary Cosmic Rays

Cosmic rays that are accelerated by interstellar objects are called primary cosmic rays. The particles produced by the interaction of those cosmic rays with gas are called secondaries. Electrons, carbon, protons, and all particles produced in stars are primaries. Elements that are not products of stars are secondaries. Positrons and antiprotons are the most common particles of secondary cosmic rays. Cosmic radiation originates from outside the solar system except for solar flares. We can describe the spectral components of cosmic particles in four different ways. First, by particles per unit rigidity, and the second, by particles per unit energy per one nucleon. Third is nucleons/ energy. And the last one is particles/energy*nucleon.
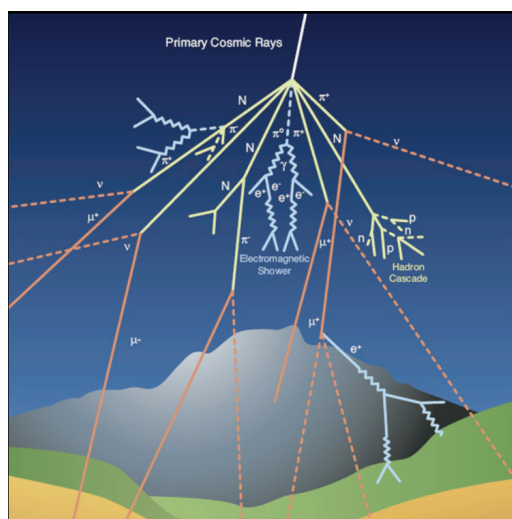
Figure 5. Primary Cosmic rays and the rest of the produced parts (Credit: NASA)

Cosmic Rays on Earth

Cosmic particle rain primarily reaches Earth's atmosphere and is affected by the Earth's magnetic field. All particles except protons and electrons are made of interactions of primary cosmic rays in the air. Mesons are decays to neutrino and muons. Natural mesons also decay into protons and electrons. The most common particles at sea level are muons. Muons are produced in the atmosphere with the decay of mesons . They are the most numbered charged particles on the ground . They lose 2 GeV in ionisation while going down to Earth . Muon decay is the main reason for low-energised electrons on the ground level. Neutral meson decay is also the reason for protons . Neutrinos are also other particles that are produced by cosmic rays . Their interaction is hard to measure, and because of that, experiments require sharp detectors. We can't directly measure neutrino flux, but we can measure the convolution of the neutrino flux with the detector.
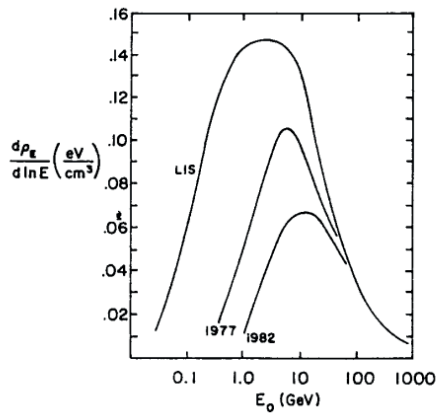
Figure 1.6: Distribution of the energy density in cosmic rays (integrand of equation (1.2)).

Figure 6. Energy density distribution at high energies (Credit: NASA)
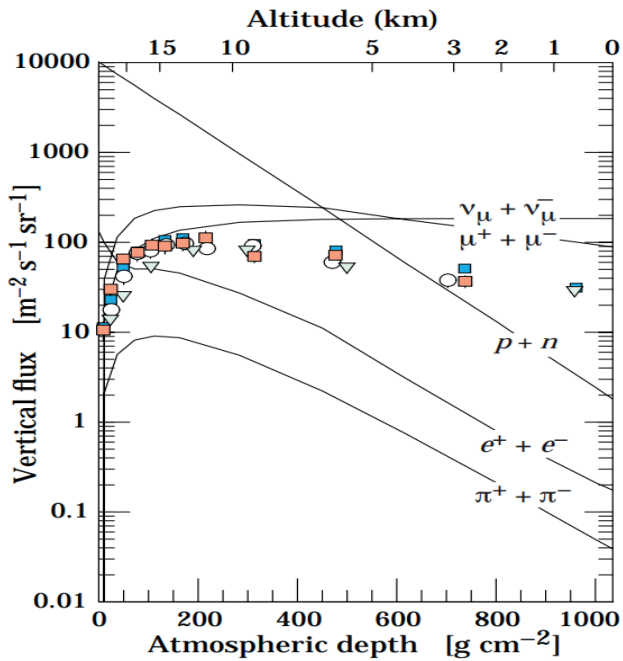
Figure 7. Vertical Flux versus atmospherics depth (Credit: NASA)
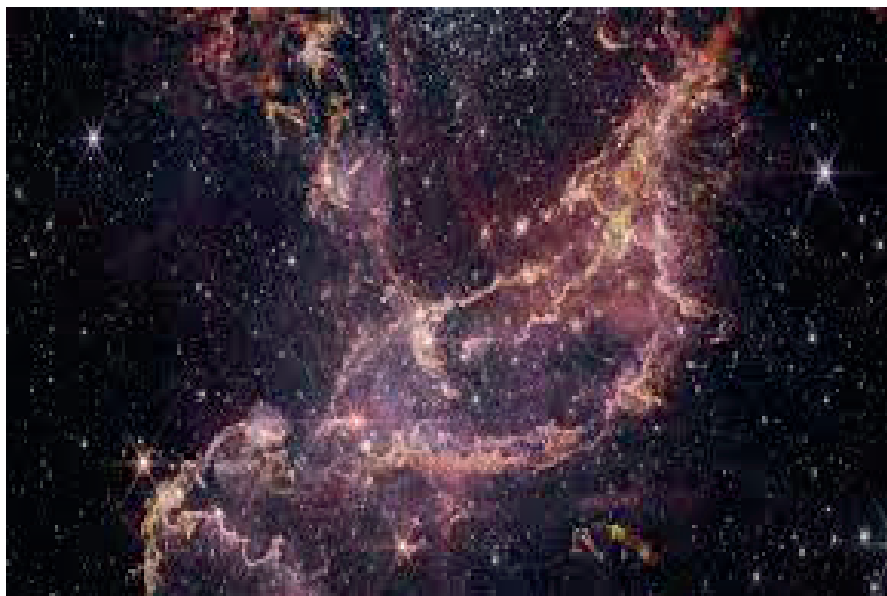
Figure 8. A nice view of Cosmic rays in the cosmos (Credit: NASA)

Cosmic Ray Effects on Life

The climate is mainly affected by natural causes, but recently, it was suggested that the intensity of cosmic particles is related to Earth's cloud cover. Ionisation can change the transparency of the atmosphere, and that can directly affect the climate of Earth. Scientists are still researching this hypothesis.

Since cosmic radiation is correlated with altitude, people living at higher altitudes are affected by cosmic rays. After examining medical records, researchers concluded that there is no correlation to the hazardous outcome of cosmic rays. Since cosmic rays existed from the beginning, they were a boundary condition for life to occur. Their energy is not critical to excite electrons in cells. Above the atmosphere and magnetosphere, cosmic rays affect organisms and become hazardous since those layers are why hazardous rays can't reach the surface of Earth. Because of this, the cosmic ray effect should be considered when planning a mission above those layers and, obviously, in missions to other planets.

Cosmic rays affect organisms and materials. For example, aircraft solar panels are damaged by cosmic rays, which causes a loss in power production. If the effect of cosmic rays on those panels is not calculated, the space mission will fail.

Conclusion

Cosmic rays are keys to understanding distant regions of our galaxy and the composition of matter on our planet. They give us information about their source and what their source consists of. For example, solar cosmic rays give detailed information about the Sun's composition. Cosmic ray studies open new windows for understanding the universe and how it works. Cosmic rays study not only astronomers' topics but also, it is topic of particle physics since they give a lot of information about the composition of matter and its components. They also give information about dynamic processes in the universe, not only matter. Cosmic rays are like messages from our galaxy and other galaxies.

The Figures are mainly searched through the NASA websites and the references at the end of the manuscript.

References

SPATIUM 11 Published by the Association Pro ISSI (Hansjörg Schlaepfer , 2003)

Cosmic Rays , Bruno Rossi, 1964

Cosmic Rays , .K. Gaisser and T. Stanev , 2007
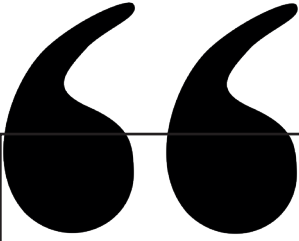
Cosmic Rays and Particle Physics, Thomas G. Gaisser, 1990

https://home.cern/science/physics/cosmic-rays-particles-outer-space

https://imagine.gsfc.nasa.gov/science/toolbox/cosmic_rays2_orig.html

https://indico.cern.ch/event/197799/contributions/371924/attachments/291924/408037/12SpacepartDeangelis.pdf

A century of cosmic rays, Michael Friedlander, Nature , March 2012

Chapter 5

EXOPLANETS

E.Nihal Ercan[1]

1 Prof. Dr., Boğaziçi University,Physics Department, https://orcid.org/0000-0003-0639-704

Exoplanets are planets detected outside of our solar system. They usually orbit stars in a small portion of our galaxy (NASA, 2022). The discovery of exoplanets brought new horizons and, of course, questions to the field of astronomy. How do planets form? Could there actually be any life other than ours in the universe? It is important to learn about exoplanets and the process involved in discovering one to answer these questions and better understand the universe we live in.

The first confirmed discovery of exoplanets came 1992 around a pulsar called PSR B1257+12. Not one but two exoplanets, namely Poltergeist and Phobetor, were found orbiting the pulsar (National Schools Observatory, 2023). A third one, called Draugr, orbiting the same pulsar, was discovered in 1994. The first-ever finding of an exoplanet, a polluted white dwarf, was actually by Van Maanen in 1917, but it wasn't confirmed until later (NASA, 2022). The nearest exoplanet was detected approximately four light years away, around the star Proxima Centauri, a red dwarf (May 2022). This was an important discovery because the planet is comparable in size to Earth and positioned in the star's habitable zone, which means that it might contain life. NASA says that the launch of the Kepler Space Telescope greatly advanced the discovery of exoplanets (2022). Kepler was specially designed to find exoplanets in our neighbourhood in the Milky Way, and it helped detect more than 2,700 exoplanets until it retired in 2018 after completing its prime and extended missions. After Kepler, Transiting Exoplanet Survey Satellite (TESS) was launched and it searched around the most luminous stars in our galaxy. In addition, NASA's Spitzer Space Telescope was not intended for exoplanet discovery but was still quite beneficial thanks to its infrared instruments. According to the National Schools Observatory (NSO), Spitzer made the first *direct* detection of an exoplanet in 2005 (2023). James Webb Space Telescope also brings hope in exploring exoplanets, NASA states (2022).

The criteria for an object to be classified as an exoplanet according to NASA Exoplanet Archive is as follows: The mass of the object should be equal to or less than 30 Jupiter masses, the planet should not free float, there have been enough observations made to confirm its existence, the information about these must be in publications reviewed by peers, and accepted in the literature of astrophysics (2022). An exoplanet stays as a candidate until these criteria are met, and then it can be confirmed as an exoplanet. It is also worth to mention the process of naming exoplanets. Names of exoplanets can be somewhat confusing, but there is a simple logic behind them. NASA explains that the first name of an exoplanet is the name of the telescope or survey that found it. The number indicates the star's position, and the order in which the planet was found corresponds to the lowercase letter, starting with b and continuing as c, d, e and so on. The first name of an exoplanet could also be the name of the parent star. For instance, if Earth were an exoplanet, its

name would be "Sun d", as in the Sun being the parent star Earth orbits and d corresponds to the Earth being the third planet found in the Solar system (NASA, 2022).

There are several useful ways to detect exoplanets. Siegel (2022) states that the transit method is the most successful, with 4,060 discoveries, but it wasn't until 2004 that the first transiting exoplanet was discovered. The transit method is finding an exoplanet from the shadow it casts when it moves in between the star and the observer (NASA, 2022). In the radial velocity method, a star wobbles and the observed colour of the star changes, and astronomers assume this to be due to the planets orbiting that star. According to Siegel, the most complex method is the direct imaging method, where you can directly collect photons from the exoplanet. Still, it only works if the exoplanet is big, luminous enough, and positioned not too far from the star or close to the Earth (2022). Gravitational microlensing happens similarly to the transit method but in microlensing, the star that the planet moves in between and the observer is a *distant* star. In this case, instead of the planet blocking the light, the mass of the earth curves the space and behaves like a lens.

The different types of exoplanets are divided into four categories: Gas giant, super-Earth, Neptunian and terrestrial (NASA, 2022). Gas giants are massive planets that primarily consist of helium and hydrogen. They are similar to Jupiter and Saturn since they have a solid core and gases that gyrate above their core instead of hard surfaces. Gas giants can be so much bigger than Jupiter; unlike Jupiter, they are near their parent stars. Their closeness to their star makes their temperature go up to thousands of degrees Celsius, and that's why they are often called "hot Jupiters". Hot Jupiters cause a spectral shift of the light from the stars and make them wobble in space due to their compact orbits. Scientists try to figure out if hot Jupiters form near their stars or if they migrate afterwards to their stars. It would be more likely that they would form farther away from their star, and the gravity of the star would cause them to migrate inwards since the planet wouldn't last in such an intense environment that happens during the formation (NASA, 2022).

Neptune-like planets are planets that are about the size of Neptune or Uranus. These exoplanets have atmospheres that consist primarily of hydrogen and helium and have cores of rock and heavy metals (NASA, 2023). They are referred to as "ice giants" since their atmospheres contain water, ammonia, and methane, usually found in the cold outer portions of the solar system as frozen ice. In 2014, the first ice giant was discovered 25,000 light years away. NASA asserts that there are hot Neptunes, although they are hard to come across. Recently, astronomers found that one of the hottest Neptunes, GJ 436b, is evaporating. GJ 436b is not expected to vanish any time soon because of evaporation, but this might not be the case for warmer Neptunes where the rate of losing atmosphere is much faster.

The name can be misleading, but a super-Earth is related to Earth only by its size. A super-Earth can be twice the size of Earth and ten times its size (NASA, 2022). Astronomers agree that various types of super-Earths might be composed of water, snow or mostly dense gas. Observations from NASA's Spitzer Space Telescope made possible the construction of a super-Earth's temperature map, which revealed significant temperature swings on the planet's surface from one point to another. The most considerable temperature difference on this exoplanet, 55 Cancri, was 1,300 Kelvin. This is because one side of the planet always experienced heat from its star while the other stayed in the dark.

For a planet to be considered terrestrial (or rocky), it must be half the size of Earth, up to twice its radius (NASA, 2022). Not all rocky planets are terrestrial; if they are twice the size of the Earth, they are still considered super-Earths. The composition of terrestrial planets is mainly of rock and iron with either a solid or a liquid surface. Some of these terrestrial planets are within just the proper distance to contain water in liquid, which is known as the habitable zone. According to NASA (2021), the habitable zone or "the Goldilocks zone" is defined as "the distance from a star at which liquid water could exist on orbiting planets' surfaces." It doesn't precisely mean those planets are habitable, but they can lead us correctly, bringing us to an important finding.

The discovery of the most significant number of Earth-sized planets was in 2017, orbiting the star called TRAPPIST-1, NASA claims (2022). This impressive finding sparked hopes of finding a possibly habitable planet among the seven exoplanets that orbit TRAPPIST-1. In 2018, scientists noticed that some had more water than the Earth's oceans after looking closer at these seven planets. Since these planets are so far away and the light from them is so weak, it is impossible to know their appearance. Scientists can only guess how they look based on the data they have. Only the planet TRAPPIST-1e is considered the most similar to Earth due to its size and density and how much radiation it takes from the host star. One of the seven planets' potential to harbour life is still up for future study.

There is one more thing to be of particular interest about exoplanet types. We know that types of exoplanets are generally determined by their size and mass. When classifying exoplanets, astronomers noticed a gap between planet sizes. Benjamin Fulton explained this phenomenon in his paper as the lead author in 2017 (NASA, 2022). The Fulton gap corresponds to an interval of 1.5 to 2.0 times the radius of Earth, where the number of exoplanets is much less than in other intervals (Vaporia, n.d.). *Evaporation valley* is another term for the Fulton gap because a planet's atmosphere so close to its parent star will be either intact or gone due to photoevaporation.

In short, many studies have been conducted about exoplanets. Studying different types of exoplanets using various kinds of telescopes and methods of searching helps us uncover the truth about the diverse worlds in our universe, and maybe, one day, we can find the answers to our questions.

References

May, A. (2022). 10 Amazing Exoplanet Discoveries. https://www.space.com/amazing-exoplanet-discoveries

NASA Exoplanet Archive. (2022). Exoplanet Criteria for Inclusion in the Archive. https://exoplanetarchive.ipac.caltech.edu/docs/exoplanet_criteria.html

NASA. (2022). What is an Exoplanet? – Exoplanet Exploration: Planets Beyond our Solar System. https://exoplanets.nasa.gov/what-is-an-exoplanet/in-depth/

NASA. (2022). Gas Giant. https://exoplanets.nasa.gov/what-is-an-exoplanet/planet-types/gas-giant/

NASA. (2023). Neptune-like. https://exoplanets.nasa.gov/what-is-an-exoplanet/planet-types/neptune-like/

NASA. (2022). Super-Earth. https://exoplanets.nasa.gov/what-is-an-exoplanet/planet-types/super-earth/

NASA. (2022). Terrestrial. https://exoplanets.nasa.gov/what-is-an-exoplanet/planet-types/terrestrial/

National Schools Observatory. (2023). The History of Exoplanets. https://www.schoolsobservatory.org/learn/astro/exoplanets/history

Siegel, E. (2022). Here's what the first 5000 exoplanets have taught us. *Big Think.* https://bigthink.com/starts-with-a-bang/first-5000-exoplanets/

The Planetary Society. (2023). Exoplanets, Worlds Orbiting Other Stars. https://www.planetary.org/worlds/exoplanets

Vaporia. (n. d.). Fulton Gap. http://astro.vaporia.com/start/fultongap.html

Chapter 6

ON THE CONTINUITY PROPERTY OF S-NUMERICAL RADIUS AND S-CRAWFORD NUMBER FUNCTIONS

Rukiye Öztürk Mert[1]

1 Asst. Prof. Dr. Hitit University, Faculty of Sciences and Arts, Department of Mathematics, Çorum, Türkiye, rukiyeozturkmert@hitit.edu.tr,
ORCID: 0000-0001-8083-5304

1. Introduction

Remember that the numerical range, numerical radius and Crawford number of a linear bounded operator T in complex Hilbert space $(H, (\cdot, \cdot))$, stated as

$$W(T) = \{(Tx, x): x \in H, \ \|x\| = 1 \},$$

$$w(T) = \sup\{|\mu|: \mu \in W(T)\}$$

and

$$c(T) = \inf\{|\mu|: \mu \in W(T)\}$$

respectively.

The general information of these subjects can be found in [1-3]. On the other numerical ranges and numerical radius functions deeply explanation has been made in [1].

Give one definition.

Definition [4]: For the operators $\mathcal{A}, S \in B(H), S = S^*$,

$$W_S(\mathcal{A}) = \{\frac{(\mathcal{A}x, x)_S}{(x, x)_S}: x \in H, \ (x, x)_S \neq 0\}, \quad \text{where} \quad (x, x)_S = (x, Sx),$$

$$w_S(\mathcal{A}) = \sup \{|\mu|: \mu \in W_S(\mathcal{A})\},$$

$$c_S(\mathcal{A}) = \inf \{|\mu|: \mu \in W_S(\mathcal{A})\}$$

are called S-numerical range, S-numerical radius and S-Cranford number of the $\mathcal{A}$.

In the work [4], S-numerical range of some differential operators and block differential operators has been computed numerically.

It is noted for nxn complex matrix A and nxn Hermitian matrix S this definition has been given in [5]. Some detail description of the $W_S(A)$ (in particular convexity properties) has been investigated in it.

In the present study, the continuity properties of S-numerical radius and S-Crawford number function are investigated.

2. Convergence of S-Numerical Radius and S-Crawford Number Sequences

To start with, explain the concept of uniform convergence for sequences of operators.

Definition 2.1. [6] Let H be any complex Hilbert space and $(\mathcal{A}_n)$ be an operator sequences in $B(H)$. The sequence $(\mathcal{A}_n)$ is said uniformly converges to the $\mathcal{A} \in B(H)$, if for any $\varepsilon > 0$, there is some $n_0 = n_0(\varepsilon) \in \mathbb{N}$, such that for all $n > n_0$ is true $\|\mathcal{A}_n - \mathcal{A}\| < \varepsilon$.

Theorem 2.2. For any operators $\mathcal{A}, \mathcal{B} \in B(H)$ and selfadjoint operator $S \in B(H)$ with property $c(S) = \inf\limits_{\|x\|=1} |(Sx, x)| > 0$ it is true

$$|w_S(\mathcal{A}) - w_S(\mathcal{B})| \leq \frac{\|\mathcal{A} - \mathcal{B}\| \, \|S\|}{c(S)}$$

and

$$|c_S(\mathcal{A}) - c_S(\mathcal{B})| \leq \frac{\|\mathcal{A} - \mathcal{B}\| \, \|S\|}{c(S)}.$$

Proof. Here, for any $\mathcal{A}, \ \mathcal{B} \in B(H)$ we have

$$\left| \frac{(\mathcal{A}x, x)_S}{(x, x)_S} \right| \leq \left| \frac{((\mathcal{A} - \mathcal{B})x, x)_S}{(x, x)_S} \right| + \left| \frac{(\mathcal{B}x, x)_S}{(x, x)_S} \right|$$

and from this

$$w_S(\mathcal{A}) \leq \sup_{(Sx,x)_S \neq 0} \left| \frac{((\mathcal{A} - \mathcal{B})x, x)_S}{(x, x)_S} \right| + w_S(\mathcal{B}),$$

$$c_S(\mathcal{A}) \leq \sup_{(Sx,x)_S \neq 0} \left| \frac{((\mathcal{A} - \mathcal{B})x, x)_S}{(x, x)_S} \right| + c_S(\mathcal{B}).$$

Similarly

$$w_S(\mathcal{B}) \leq \sup_{(x,x)_S \neq 0} \left| \frac{((\mathcal{A} - \mathcal{B})x, x)_S}{(x, x)_S} \right| + w_S(\mathcal{A}),$$

$$c_S(\mathcal{B}) \leq \sup_{(x,x)_S \neq 0} \left| \frac{((\mathcal{A} - \mathcal{B})x, x)_S}{(x, x)_S} \right| + c_S(\mathcal{A}).$$

Consequently,

$$|w_S(\mathcal{A}) - w_S(\mathcal{B})| \leq \sup_{(x,x)_S \neq 0} \left| \frac{((\mathcal{A} - \mathcal{B})x, x)_S}{(x, x)_S} \right|$$

and

$$|c_S(\mathcal{A}) - c_S(\mathcal{B})| \leq \sup_{(x,x)_S \neq 0} \left| \frac{((\mathcal{A} - \mathcal{B})x, x)_S}{(x, x)_S} \right|.$$

Moreover

$$\left| \frac{((\mathcal{A} - \mathcal{B})x, x)_S}{(x, x)_S} \right| \leq \frac{\|\mathcal{A} - \mathcal{B}\| \|S\| \|x\|^2}{|(Sx, x)|}$$

$$= \|\mathcal{A} - \mathcal{B}\| \|S\| \frac{1}{\left| (S\left(\frac{x}{\|x\|}\right), \frac{x}{\|x\|}) \right|}$$

$$= \|\mathcal{A} - \mathcal{B}\| \|S\| \frac{1}{|(Sy, y)|}$$

$$= \|\mathcal{A} - \mathcal{B}\| \|S\| \frac{1}{|(y, y)_S|}, \qquad y = \frac{x}{\|x\|}$$

From last inequality, the validity of theorem is clear.

Theorem 2.3. Assume that $\mathcal{A}_n \in B(H)$, $n \geq 1$ and $S = S^* \in B(H)$ with property $c(S) > 0$. If the operator sequences $(\mathcal{A}_n)$ uniformly converges to the o$\mathcal{A} \in B(H)$, then

$$\lim_{n \to \infty} w_S(\mathcal{A}_n) = w_S(\mathcal{A})$$

and

$$\lim_{n \to \infty} c_S(\mathcal{A}_n) = c_S(\mathcal{A}).$$

Proof. By Theorem 2.2 it is clear

$$|w_S(\mathcal{A}_n) - w_S(\mathcal{A})| \leq \frac{\|S\|}{c(S)} \|\mathcal{A}_n - \mathcal{A}\|$$

and

$$|c_S(\mathcal{A}_n) - c_S(\mathcal{A})| \leq \frac{\|S\|}{c(S)} \|\mathcal{A}_n - \mathcal{A}\|, \quad n \geq 1.$$

From above inequalities the validity of theorem is clear.

Now will be investigate the continuous property of $w_S(\cdot)$ and $c_S(\cdot)$ functions on the operator S.

Firstly, demonstrate the results below.

Lemma 2.4. Let $\mathcal{A},\ S,\ T \in B(H), S = S^*, T = T^*$ with properties $c(S) > 0$ and $c(T) > 0$. Then

$$|w_S(\mathcal{A}) - w_T(\mathcal{A})| \leq \alpha \|S - T\|$$

and

$$|c_S(\mathcal{A}) - c_T(\mathcal{A})| \leq \alpha \|S - T\|,$$

where $= \frac{2\|T\|\|\mathcal{A}\|}{c(S)c(T)}$.

Proof. For any $x \in H$ with $(Sx, x) \neq 0, (Tx, x) \neq 0$ we have

$$\left|\frac{(\mathcal{A}x, Sx)}{(Sx, x)}\right| \leq \left|\frac{(\mathcal{A}x, Sx)}{(Sx, x)} - \frac{(\mathcal{A}x, Tx)}{(Tx, x)}\right| + \left|\frac{(\mathcal{A}x, Tx)}{(Tx, x)}\right| \qquad (1)$$

Then

$$\left|\frac{(\mathcal{A}x, Sx)}{(Sx, x)} - \frac{(\mathcal{A}x, Tx)}{(Tx, x)}\right| = \frac{|(\mathcal{A}x, Sx)(Tx, x) - (\mathcal{A}x, Tx)(Sx, x)|}{|(Sx, x)|\,|(Tx, x)|}$$

$$\leq \frac{|(\mathcal{A}x, (Tx, x)Sx - (Sx, x)Tx)|}{c(s)c(T)}$$

$$\leq \frac{\|\mathcal{A}\|}{c(s)c(T)} \|(Tx, x)(Sx - Tx) + (Tx, x)Tx - (Sx, x)Tx\|$$

$$\leq \frac{\|\mathcal{A}\|}{c(s)c(T)} (\|T\|\,\|S - T\| + \|T\|\,\|T - S\|)$$

$$= \frac{2\|\mathcal{A}\|\,\|T\|}{c(s)c(T)} \|S - T\|,\ x \in H, \qquad (Sx, x) \neq 0,$$
$$(Tx, x) \neq 0.$$

Then from relation (1) we have

$$w_S(\mathcal{A}) \leq \alpha \|S - T\| + w_T(\mathcal{A})$$

$$c_S(\mathcal{A}) \leq \alpha \|S - T\| + c_T(\mathcal{A}), \quad \alpha = \frac{2\|\mathcal{A}\|\|T\|}{c(S)c(T)}.$$

From last inequalities it is obtained that

$$|w_S(\mathcal{A}) - w_T(\mathcal{A})| \leq \alpha \|S - T\|$$

and

$$|c_S(\mathcal{A}) - c_T(\mathcal{A})| \leq \alpha \|S - T\| \, .$$

From last lemma it is implies the results below.

Theorem 2.5. Let us $\mathcal{A}, S_n \in B(H)$, $S_n^* = S_n$, $n \geq 1$. If operator sequences (S_n) uniformly converges to the $S \in B(H)$, $c(S) > 0$, then

$$w_S(\mathcal{A}) = \lim_{n \to \infty} w_{S_n}(\mathcal{A})$$

and

$$c_S(\mathcal{A}) = \lim_{n \to \infty} c_{S_n}(\mathcal{A}).$$

Proof. In this case for the sequences (S_n) from Lemma 2.4 we have

$$\left|w_{S_n}(\mathcal{A}) - w_S(\mathcal{A})\right| \leq \alpha_n \|S_n - S\| \, ,$$

$$\left|c_{S_n}(\mathcal{A}) - c_S(\mathcal{A})\right| \leq \alpha_n \|S_n - S\| \, , \qquad n \geq 1,$$

Where $\alpha_n = \frac{2\|\mathcal{A}\|\|S_n\|}{c(S)c(S_n)}, n \geq 1$.

Since (S_n) uniformly converges to the operator S, then $(\|S_n\|)$ is bounded sequences. On the other hand it is known that

$c(S) = \lim_{n \to \infty} c(S_n) \qquad$ (see [1]).

Then, since $c(S) > 0$, then

$$\lim_{n \to \infty} \alpha_n = \frac{2\|\mathcal{A}\|\|S\|}{c^2(S)}.$$

Consequently, from above mentioned inequalities we have

$$w_S(\mathcal{A}) = \lim_{n \to \infty} w_{S_n}(\mathcal{A})$$

and

$$c_S(\mathcal{A}) = \lim_{n \to \infty} c_{S_n}(\mathcal{A}).$$

Actually, it is true the following theorem.

Theorem 2.6. Assume that $\mathcal{A}_n,\ S_n \in B(H)$, $S_n^* = S_n$, $n \geq 1$. If operator sequences $(\mathcal{A}_n)$ and (S_n) uniformly converges to the operators $\mathcal{A}, S \in B(H)$, $c(S) > 0$, respectively, then

$$w_S(\mathcal{A}) = \lim_{n \to \infty} w_{S_n}(\mathcal{A}_n)$$

and

$$c_S(\mathcal{A}) = \lim_{n \to \infty} c_{S_n}(\mathcal{A}_n).$$

Proof. By Theorem 2.2 and Lemma 2.4, it is clear that

$$\left| w_{S_n}(\mathcal{A}_n) - w_S(\mathcal{A}) \right|$$
$$\leq \left| w_{S_n}(\mathcal{A}_n) - w_{S_n}(\mathcal{A}) \right| + \left| w_{S_n}(\mathcal{A}) - w_S(\mathcal{A}) \right|$$
$$\leq \frac{\|\mathcal{A}_n - \mathcal{A}\| \|S_n\|}{c(S_n)} + \frac{2\|\mathcal{A}\| \|S_n\|}{c(S)c(S_n)} \|S_n - S\|$$

and

$$\left| c_{S_n}(\mathcal{A}_n) - c_S(\mathcal{A}) \right| \leq \left| c_{S_n}(\mathcal{A}_n) - c_{S_n}(\mathcal{A}) \right| + \left| c_{S_n}(\mathcal{A}) - c_S(\mathcal{A}) \right|$$
$$\leq \frac{\|\mathcal{A}_n - \mathcal{A}\| \|S_n\|}{c(S_n)} + \frac{2\|\mathcal{A}\| \|S_n\|}{c(S)c(S_n)} \|S_n - \mathcal{A}\|,$$

$n \geq 1$.

From this, since

$$\lim_{n \to \infty} \frac{\|S_n\|}{c(S_n)} = \frac{\|S\|}{c(S)}$$

and

$$\lim_{n \to \infty} \frac{\|S_n\|}{c(S)c(S_n)} = \frac{\|S\|}{c^2(S)},$$

then from last inequalities it is obtained

$$w_S(\mathcal{A}) = \lim_{n \to \infty} w_{S_n}(\mathcal{A}_n)$$

and

$$c_S(\mathcal{A}) = \lim_{n \to \infty} c_{S_n}(\mathcal{A}_n).$$

Remark. For recently development research in this area, it can be found in [7-19].

Example. Let us $H = L^2(0,1)$, $\psi_n : [0,1] \longrightarrow \mathbb{C}$, $\varphi_n : [0,1] \longrightarrow \mathbb{R}$, $\psi_n, \varphi_n \in C[0,1], n \geq 1$,

$$\psi_n \xrightarrow{[0,1]} \psi = 1, n \to \infty,$$

$$\varphi_n \xrightarrow{[0,1]} \varphi \geq 1, n \to \infty,$$

and for $n \geq 1$ assume that

$$A_n g(\mathrm{x}) = \psi_n(x) g(x), \ g \in L^2(0,1), A_n : L^2(0,1) \to L^2(0,1),$$

$$S_n g(\mathrm{x}) = \varphi_n(x) g(x), \ g \in L^2(0,1), S_n : L^2(0,1) \to L^2(0,1).$$

It is clear that $A_n, S_n \in B(L^2(0,1))$, $n \geq 1$, and operator sequences (A_n) and (S_n) uniformly convergence to the operator $A = I$ and $Sg(x) = \varphi(x)g(x), g \in L^2(0,1)$ respectively. In addition

$$c(S) = \inf_{\|g\|=1} |(Sg, g)| = \inf_{\|g\|=1} \left| \int_0^1 \varphi \, |g|^2(t) dt \right| \geq 1.$$

Then by last theorem, it is established that

$$\lim_{n \to \infty} w_{S_n}(A_n) = w_S(A) = \sup_{\|g\| \neq 0} \left| \frac{(Ag, Sg)}{(Sg, g)} \right|$$

$$= \sup_{(Sg,g) \neq 0} \left| \frac{\int_0^1 Ag(t) \, \overline{Sg(t)} dt}{\int_0^1 Sg(t) \, \overline{g(t)} dt} \right|$$

$$= \sup_{(Sg,g) \neq 0} \frac{\int_0^1 \varphi(t) \, |g|^2(t) dt}{\int_0^1 \varphi(t) \, |g|^2(t) dt} = 1$$

and

$$\lim_{n \to \infty} c_{S_n}(A_n) = c_S(A) = \inf_{(Sg,g) \neq 0} \left| \frac{(Ag, Sg)}{(Sg, g)} \right|$$

$$= \sup_{(Sg,g) \neq 0} \left| \frac{\int_0^1 Ag(t) \, \overline{Sg(t)} dt}{\int_0^1 Sg(t) \, \overline{g(t)} dt} \right|$$

$$= \sup_{(Sg,g) \neq 0} \left| \frac{\int_0^1 \varphi(t) \, |g|^2(t) dt}{\int_0^1 \varphi(t) \, |g|^2(t) dt} \right| = 1.$$

References

1. Bhunia, P., Dragomir, S. S., Moslehian, M. S., & Paul, K. (2022). Lectures on numerical radius inequalities. Infosys Science Foundation Series. New York: Springer.

2. Gustafson K. E., and Rao, D. K. M. (1997). Numerical Range: The Field of Values of Linear Operators and Matrices. New York: Springer.

3. Halmos, P. R. (1982). A Hilbert space problem book. New York: Springer –Verlag.

4. Muhammad, A., Azeez B., and Taheri F. E. (2023). Computing the s-numerical ranges of differential operators. Operators and Matrices, 17(3), 583-598.

5. Li, Chi-Kwong, Tsing, Nam-Kiu, and Uhlig, F. (1996). Numerical ranges of an operator on an indefinite inner product space. The Electronic Journal of Linear Algebra, 1, 1-17.

6. Bachman, G., and Narici, L. (1966). Functional Analysis. New York: Academic Press.

7. İsmailov, Z., and Öztürk Mert, R. (2022). Gaps between some spectral characteristics of direct sum of Hilbert space operators. Operators and Matrices, 16(2), 337-347.

8. Otkun Çevik, E., and Ismailov, Z. I. (2022). Some Gap Relations Between Operator Norm with Spectral and Numerical Radii of Direct Sum Hilbert Space Operators. Lobachevskii Journal of Mathematics, 43(2), 366-375.

9. Ismailov, Z. I., and Ipek Al, P. (2022). Some Spectral Characteristic Numbers of Direct Sum of Operators. Turkish Journal of Analysis and Number Theory, 10(1), 21-26.

10. İpek Al, P., and Ismailov, Z. I. (2021). On the spectral radius of antidiagonal block operator matrices. Journal of Mathematical Chemistry, 59(10), 2206-2217.

11. Otkun Çevik, E., and Ismailov, Z. I. (2021). Radius and Operator Norm of Infinite Upper Triangular Double Band Block Operator Matrices. Journal of Analysis & Number Theory, 9(2), 19-22.

12. Ipek Al, P., and Ismailov, Z. I. (2021). Gaps Between Operator Norm and Spectral and Numerical Radii of the Tensor Product of Operators. Turkish Journal of Analysis and Number Theory, 9(2), 22-24.

13. Otkun Çevik, E., and Ismailov, Z. I. (2021). Spectral Radius and Operator Norm of Infinite Upper Triangular Double Band Block Operator Matrices. Journal of Analysis & Number Theory, 9(2), 19-22.

14. Ismailov Z. I. and Otkun Çevik E. (2022). On the one spectral relation for analytic function of operator. Journal of Nonlinear Science and Applications, 15, 301-307.

15. Cağlayan Ü., and Ismailov Z.I. (2024). On The Convergence Properties Of p-Numerical Radii And p-Crawford Numbers Sequences. O. Talaz, A. Demirçalı. içinde, Current Studies in Science and Mathematics (s. 5-18), Ankara: Platanus Publishing.

16. Cağlayan Ü., and Ismailov Z.I. (2024). On The Continuity Properties of Davis-Wielandt Radius and Crawford Number Functions. E. Otkun Çevik içinde, Matematik Alanında Analizler (s. 16-24), Afyonkarahisar: Yaz Yayınları.

17. Otkun Çevik E., and Ismailov Z.I. (2024). On The Continuity of Ratio Numerical Radius and Ratio Crawford Number Functions. E. Otkun Çevik içinde, Matematik Alanında Analizler (s. 25-34), Afyonkarahisar: Yaz Yayınları.

18. Bhunia, P., Ipek Al, P., and Ismailov, Z. I. (2024). On the convergence of some spectral characteristics of the converging operator sequences. Proceedings-Mathematical Sciences, 134(1), 1-15.

19. Cağlayan Ü., and Ipek Al, P. (2024). On the Continuity with Respect to Denominator of Ratio Numerical Radius and Ratio Crawford Number Functions. International Academic Studies in Sciences and Mathematics, June 2024 (s. 121-132), Ankara: Serüven Yayınevi.

Chapter 7

THE INVOLUTE CURVES OF ANY NON-UNIT SPEED TIMELIKE CURVE IN MINKOWSKI 3-SPACE

Sümeyye GÜR MAZLUM¹

1 Gümüşhane University, Kelkit Aydın Doğan Vocational School, Department of Computer Technology, Gümüşhane, Türkiye, E-mail: sumeyyegur@gumushane.edu.tr, ORCID: https://orcid.org/0000-0003-2471-1627

1. Introduction

Involute curves are curves derived from a curve and reflect the geometric properties of that curve. When considered in the context of classical differential geometry, involute curves are used to understand the physical or geometric meaning of the curve more deeply. Involute curves have various applications in mathematical and physical systems. Since these curves are usually defined in relation to a main curve, they play important roles in solving geometric and mechanical problems. Involute curves are widely used in the design of gears. When the profile of gears is designed in the form of an involute curve, a smooth motion transfer between gears is achieved. This design allows the contact points of the gears to change continuously, reducing friction and wear. Thus, increasing efficiency and long-lasting gears are obtained. Involute curves are used in the analysis of motion in systems related to acceleration and forces. In particular, in systems where the motion is nonlinear, curvilinear or rotational, involutes simplify the analysis of speed and acceleration. In the motion of robot arms or in the kinematic analysis of mechanical systems, involute curves provide precise definition of motion paths. These curves are used especially in the motion planning of robotic manipulators to provide continuous motion and minimize mechanical stress. In the field of optics, involute curves can be helpful in geometric optics calculations, especially in the problems of focusing and reflecting light in mirror and lens systems. When the curved paths formed during the reflection and refraction of light rays are modelled with involutes, more precise results can be obtained. Beyond these application areas, involute curves are widely used to solve theoretical and practical problems in disciplines such as differential geometry, mechanics, engineering and computer graphics. There are some of the studies on involute curves made by geometricians in various spaces, (Bilici and Çalışkan, 2011; Bilici and Çalışkan, 2009; Bükcü and Karacan, 2007a; Bükcü and Karacan, 2007b; Gür and Şenyurt, 2013; Şenyurt and Gür, 2012; Gür Mazlum and Bektaş, 2023). On the other hand, basic concepts and advanced studies on Minkowski 3-space are available in various sources (Akutagava and Nishikawa, 1990; Beem, Paul and Kevin, 2017; Birman and Nomizu, 1984; Lopez, 2014; O'Neill, 1983; Ratcliffe, 1994; Uğurlu, 1997; Uğurlu and Çalışkan, 2012; Woestijne, 1990). In this study, the involute curves of a timelike curve in Minkowski 3-space are examined and some characteristic properties of these curves are detailed.

In addition, the relationships between these properties of two curves are given.

2. Preliminaries

Let $\vec{\mathfrak{A}} = \left(\mathfrak{u}_1, \ \mathfrak{u}_2, \ \mathfrak{u}_3 \right)$ and $\vec{\mathfrak{R}} = \left(\mathfrak{r}_1, \ \mathfrak{r}_2, \ \mathfrak{r}_3 \right) \in \mathbb{E}_1^3$ be two vectors. For these vectors, the Lorentzian inner product function and Lorentzian vector product function are defined as follows:

$$\langle , \rangle_L \ : \mathbb{E}_1^3 \times \mathbb{E}_1^3 \to \mathbb{E}_1^3, \qquad \left\langle \vec{\mathfrak{A}}, \ \vec{\mathfrak{R}} \right\rangle = \mathfrak{u}_1 \mathfrak{r}_1 + \mathfrak{u}_2 \mathfrak{r}_2 - \mathfrak{u}_3 \mathfrak{r}_3$$

and

$$\wedge_L \ : \mathbb{E}_1^3 \times \mathbb{E}_1^3 \to \mathbb{E}_1^3 \ , \qquad \vec{\mathfrak{A}} \wedge_L \vec{\mathfrak{R}} = (\mathfrak{u}_3 \mathfrak{r}_2 - \mathfrak{u}_2 \mathfrak{r}_3, \ \mathfrak{u}_1 \mathfrak{r}_3 - \mathfrak{u}_3 \mathfrak{r}_{11}, \ \mathfrak{u}_1 \mathfrak{r}_2 - \mathfrak{u}_2 \mathfrak{r}_1).$$

Here, the space $\mathbb{E}_1^3$ is called the Minkowski 3-space. In Minkowski 3-space, the causal character of any vector $\vec{\mathfrak{A}} = \left(\mathfrak{u}_1, \ \mathfrak{u}_2, \ \mathfrak{u}_3 \right)$, if $\left\langle \vec{\mathfrak{A}}, \ \vec{\mathfrak{A}} \right\rangle_L > 0$ or $\vec{\mathfrak{A}} = \vec{0}$, then $\vec{\mathfrak{A}}$ is spacelike, if $\left\langle \vec{\mathfrak{A}}, \ \vec{\mathfrak{A}} \right\rangle_L < 0$, then $\vec{\mathfrak{A}}$ is timelike, or if $\left\langle \vec{\mathfrak{A}}, \ \vec{\mathfrak{A}} \right\rangle_L = 0$ and $\vec{\mathfrak{A}} \neq \vec{0}$, then $\vec{\mathfrak{A}}$ is lightlike (or null). The Lorentzian norm of $\vec{\mathfrak{A}}$ is $\left\| \vec{\mathfrak{A}} \right\|_L = \sqrt{\left| \left\langle \vec{\mathfrak{A}}, \vec{\mathfrak{A}} \right\rangle_L \right|}$ and if $\left\| \vec{\mathfrak{A}} \right\|_L = 1$, $\vec{\mathfrak{A}}$ is a unit vector. For $\vec{\mathfrak{A}}$ and $\vec{\mathfrak{R}} \in \mathbb{E}_1^3$, if $\left\langle \vec{\mathfrak{A}}, \ \vec{\mathfrak{R}} \right\rangle_L = 0$, $\vec{\mathfrak{A}}$ and $\vec{\mathfrak{R}}$ are Lorentzian orthogonal vectors. Let $\vec{\mathfrak{A}}$ and $\vec{\mathfrak{R}}$ be nonzero Lorentzian orthogonal vectors in $\mathbb{E}_1^3$, in this case if $\vec{\mathfrak{A}}$ is timelike, then $\vec{\mathfrak{R}}$ is spacelike, (Ratcliffe, 1994). An differentiable curve $\left(\vec{\mathfrak{I}} \right)$ in $\mathbb{E}_1^3$ is called the timelike, spacelike or lightlike curve, if the tangent vector at every point $\vec{\mathfrak{I}}[t]$ of the curve is timelike, spacelike or lightlike, respectively. Let $\left\{ \vec{\mathbb{V}_1}, \ \vec{\mathbb{V}_2}, \ \vec{\mathbb{V}_3} \right\}$ be Frenet frame, ρ_1 and ρ_2 be the curvature and torsion $\left(\vec{\mathfrak{I}} \right)$. According to the causal character of the curve $\left(\vec{\mathfrak{I}} \right)$, there are the following equations between these elements (Uğurlu and Çalışkan, 2012):

- if $\left(\vec{\mathfrak{I}} \right)$ is spacelike, $\vec{\mathbb{V}_1}$ and $\vec{\mathbb{V}_2}$ are spacelike, $\vec{\mathbb{V}_3}$ is timelike, then

$$\overrightarrow{\mathbb{V}_1} = \frac{\overrightarrow{\mathfrak{I}'}}{\left\|\overrightarrow{\mathfrak{I}'}\right\|_L}, \quad \overrightarrow{\mathbb{V}_2}[t] = -\overrightarrow{\mathbb{V}_3} \wedge_L \overrightarrow{\mathbb{V}_1}, \quad \overrightarrow{\mathbb{V}_3}[t] = \frac{\overrightarrow{\mathfrak{I}'} \wedge_L \overrightarrow{\mathfrak{I}''}}{\left\|\overrightarrow{\mathfrak{I}'} \wedge_L \overrightarrow{\mathfrak{I}''}\right\|_L}, \qquad (1)$$

$$\overrightarrow{\mathbb{V}_1} \wedge_L \overrightarrow{\mathbb{V}_2} = \overrightarrow{\mathbb{V}_3}, \quad \overrightarrow{\mathbb{V}_2} \wedge_L \overrightarrow{\mathbb{V}_3} = -\overrightarrow{\mathbb{V}_1}, \quad \overrightarrow{\mathbb{V}_3} \wedge_L \overrightarrow{\mathbb{V}_1} = -\overrightarrow{\mathbb{V}_2} \qquad (2)$$

and

$$\overrightarrow{\mathbb{V}_1'} = \left\|\overrightarrow{\mathfrak{I}'}\right\|_L \rho_1 \overrightarrow{\mathbb{V}_2}, \quad \overrightarrow{\mathbb{V}_2'} = \left\|\overrightarrow{\mathfrak{I}'}\right\|_L \left(-\rho_1 \overrightarrow{\mathbb{V}_1} + \rho_2 \overrightarrow{\mathbb{V}_3}\right), \quad \overrightarrow{\mathbb{V}_3'} = \left\|\overrightarrow{\mathfrak{I}'}\right\|_L \rho_2 \overrightarrow{\mathbb{V}_2}, (3)$$

- if $\left(\vec{\mathfrak{I}}\right)$ is spacelike, $\overrightarrow{\mathbb{V}_1}$ and $\overrightarrow{\mathbb{V}_3}$ are spacelike, $\overrightarrow{\mathbb{V}_2}$ is timelike, then

$$\overrightarrow{\mathbb{V}_1} = \frac{\overrightarrow{\mathfrak{I}'}}{\left\|\overrightarrow{\mathfrak{I}'}\right\|_L}, \quad \overrightarrow{\mathbb{V}_2} = \overrightarrow{\mathbb{V}_3} \wedge_L \overrightarrow{\mathbb{V}_1}, \quad \overrightarrow{\mathbb{V}_3} = \frac{\overrightarrow{\mathfrak{I}'} \wedge_L \overrightarrow{\mathfrak{I}''}}{\left\|\overrightarrow{\mathfrak{I}'} \wedge_L \overrightarrow{\mathfrak{I}''}\right\|_L}, \qquad (4)$$

$$\overrightarrow{\mathbb{V}_1} \wedge_L \overrightarrow{\mathbb{V}_2} = -\overrightarrow{\mathbb{V}_3}, \quad \overrightarrow{\mathbb{V}_2} \wedge_L \overrightarrow{\mathbb{V}_3} = -\overrightarrow{\mathbb{V}_1}, \quad \overrightarrow{\mathbb{V}_3} \wedge_L \overrightarrow{\mathbb{V}_1} = \overrightarrow{\mathbb{V}_2} \qquad (5)$$

and

$$\overrightarrow{\mathbb{V}_1'} = \left\|\overrightarrow{\mathfrak{I}'}\right\|_L \rho_1 \overrightarrow{\mathbb{V}_2}, \quad \overrightarrow{\mathbb{V}_2'} = \left\|\overrightarrow{\mathfrak{I}'}\right\|_L \left(\rho_1 \overrightarrow{\mathbb{V}_1} + \rho_2 \overrightarrow{\mathbb{V}_3}\right), \quad \overrightarrow{\mathbb{V}_3'} = \left\|\overrightarrow{\mathfrak{I}'}\right\|_L \rho_2 \overrightarrow{\mathbb{V}_2} \qquad (6)$$

- if $\left(\vec{\mathfrak{I}}\right)$ is timelike, $\overrightarrow{\mathbb{V}_1}$ is timelike, $\overrightarrow{\mathbb{V}_2}$ and $\overrightarrow{\mathbb{V}_3}$ are spacelike, then

$$\overrightarrow{\mathbb{V}_1} = \frac{\overrightarrow{\mathfrak{I}'}}{\left\|\overrightarrow{\mathfrak{I}'}\right\|_L}, \quad \overrightarrow{\mathbb{V}_2} = -\overrightarrow{\mathbb{V}_3} \wedge_L \overrightarrow{\mathbb{V}_1}, \quad \overrightarrow{\mathbb{V}_3} = -\frac{\overrightarrow{\mathfrak{I}'} \wedge_L \overrightarrow{\mathfrak{I}''}}{\left\|\overrightarrow{\mathfrak{I}'} \wedge_L \overrightarrow{\mathfrak{I}''}\right\|_L}, \qquad (7)$$

$$\overrightarrow{\mathbb{V}_1} \wedge_L \overrightarrow{\mathbb{V}_2} = -\overrightarrow{\mathbb{V}_3}, \quad \overrightarrow{\mathbb{V}_2} \wedge_L \overrightarrow{\mathbb{V}_3} = \overrightarrow{\mathbb{V}_1}, \quad \overrightarrow{\mathbb{V}_3} \wedge_L \overrightarrow{\mathbb{V}_1} = -\overrightarrow{\mathbb{V}_2} \qquad (8)$$

and

$$\overrightarrow{\mathbb{V}_1'} = \left\|\overrightarrow{\mathfrak{I}'}\right\|_L \rho_1 \overrightarrow{\mathbb{V}_2}, \quad \overrightarrow{\mathbb{V}_2'} = \left\|\overrightarrow{\mathfrak{I}'}\right\|_L \left(\rho_1 \overrightarrow{\mathbb{V}_1} - \rho_2 \overrightarrow{\mathbb{V}_3}\right), \quad \overrightarrow{\mathbb{V}_3'} = \left\|\overrightarrow{\mathfrak{I}'}\right\|_L \rho_2 \overrightarrow{\mathbb{V}_2}. \qquad (9)$$

3. The Involute Curves of Any Non-Unit Speed Timelike Curve in Minkowski 3-Space

Let $\left(\vec{\mathfrak{I}}\right) = \vec{\mathfrak{I}}[t]$ be any regular timelike curve in $\mathbb{E}_1^3$. By definition of involute curves (see Definition 3.1) and because the Lorentzian inner product of two timelike vectors cannot be zero (Ratcliffe, 1994), the involute curve $\left(\vec{\hat{\mathfrak{I}}}\right) = \vec{\hat{\mathfrak{I}}}[\hat{t}]$ of $\left(\vec{\mathfrak{I}}\right)$ must be a spacelike curve. In the

following sections, it will be seen that the binormal or principal normal vectors $\left(\vec{\hat{\mathfrak{I}}} \right)$ can be both spacelike and timelike. Let's give the following equations for these curves, respectively:

$$\sigma[t] = \left\| \frac{\overrightarrow{d\mathfrak{I}[t]}}{dt} \right\|_L = \left\| \vec{\mathfrak{I}}'[t] \right\|_L,$$

$$\hat{\sigma}[\hat{t}] = \left\| \frac{\overrightarrow{d\hat{\mathfrak{I}}[\hat{t}]}}{d\hat{t}} \right\|_L = \left\| \vec{\hat{\mathfrak{I}}}'[\hat{t}] \right\|_L.$$

Definition 3.1. Let timelike $\overrightarrow{V}_1[t]$ and spacelike $\overrightarrow{\hat{V}}_1[\hat{t}]$ be the tangent vectors of the timelike curve $\left(\vec{\mathfrak{I}} \right)$ and the spacelike curve $\left(\vec{\hat{\mathfrak{I}}} \right)$, respectively. If $\left\langle \overrightarrow{\hat{V}}_1[\hat{t}], \ \overrightarrow{V}_1[t] \right\rangle_L = 0$, then $\left(\vec{\hat{\mathfrak{I}}} \right)$ is a involute of $\left(\vec{\mathfrak{I}} \right)$ at any point $\vec{\mathfrak{I}}[t]$ in $\mathbb{E}_1^3$, Figure 1.
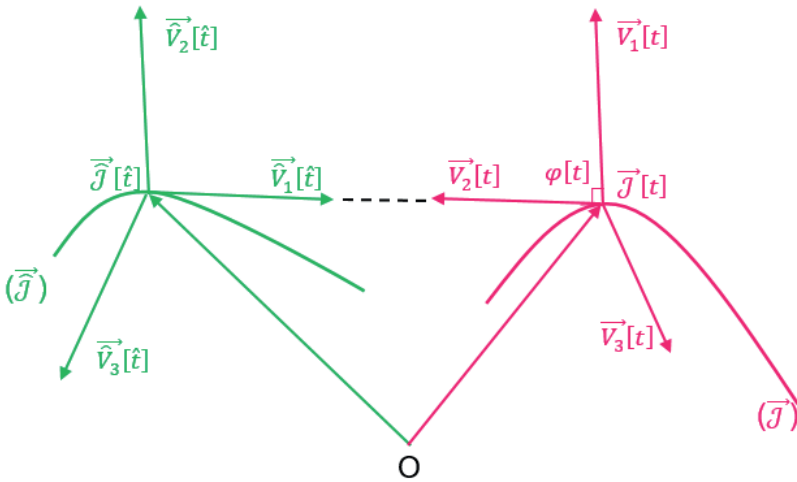
Figure 1. The spacelike involute curve $\left(\vec{\hat{\mathfrak{I}}} \right)$ of the timelike curve $\left(\vec{\mathfrak{I}} \right)$

In Figure 1, the angle $\varphi[t]$ between the $\overrightarrow{V}_1[t]$ and $\overrightarrow{\hat{V}}_1[\hat{t}]$ is shown as a perpendicular in the familiar way. In fact, $\varphi[t]$ is a Lorentzian timelike

angle, corresponding to zero degrees. Because $\left\langle \overrightarrow{\hat{\mathbb{V}}_1}[\hat{t}],\ \overrightarrow{\mathbb{V}_1}[t] \right\rangle_L = \sinh(\varphi[t]) = 0$ (Ratcliffe, 1994).

Theorem 3.2. The relationship between the timelike curve $(\vec{\mathfrak{I}})$ and its spacelike involute curve $(\vec{\hat{\mathfrak{I}}})$ is

$$\vec{\hat{\mathfrak{I}}}[\hat{t}] = \left(\vec{\mathfrak{I}} - \left(\int \sigma dt\right)\overrightarrow{\mathbb{V}_1}\right)[t]. \tag{10}$$

Proof. From Figure 1, we write

$$\vec{\hat{\mathfrak{I}}}[\hat{t}] = \left(\vec{\mathfrak{I}} + a\overrightarrow{\mathbb{V}_1}\right)[t], \tag{11}$$

where a is an function of t. The first derivative of (11) with respect to t is

$$\frac{d\hat{t}}{dt}\vec{\hat{\mathfrak{I}}}'[\hat{t}] = \left(\vec{\mathfrak{I}}' + a\overrightarrow{\mathbb{V}_1'} + a'\overrightarrow{\mathbb{V}_1}\right)[t]. \tag{12}$$

If we substitute (6) and (9) into (12), then we have

$$\frac{d\hat{t}}{dt}\left(\hat{\sigma}\overrightarrow{\hat{\mathbb{V}}_1}\right)[\hat{t}] = \left((a' + \sigma)\overrightarrow{\mathbb{V}_1} + \sigma a \rho_1 \overrightarrow{\mathbb{V}_2}\right)[t]. \tag{13}$$

If we apply Lorentzian inner product with the spacelike vector $\overrightarrow{\mathbb{V}_1}[t]$ to (13), then we obtain

$$a'[t] = -\sigma[t], \tag{14}$$

so

$$a[t] = -\int \sigma[t]dt. \tag{15}$$

If we substitute (15) into (11), then we have (10).

Corollary 3.3. Let the spacelike curve $(\vec{\hat{\mathfrak{I}}})$ be a involute of the timelike curve $(\vec{\mathfrak{I}})$. The Lorentzian distance between the points $\vec{\hat{\mathfrak{I}}}[\hat{t}]$ and $\vec{\mathfrak{I}}[t]$ is

$$|a[t]| = \left|\int \sigma[t]dt\right|. \tag{16}$$

Proof. From (11), we get

$$\vec{\hat{\gamma}}\big[\hat{t}\big] - \vec{\gamma}[t] = \big(a\overrightarrow{V_1}\big)[t].$$ (17)

If we take the Lorentzian norm of both sides of (17), then we attain

$$\Big\|\vec{\hat{\Im}}\big[\hat{t}\big] - \vec{\Im}[t]\Big\|_L = \big|a[t]\big|.$$ (18)

From (15) and (18), we obtain (16).

Theorem 3.4. Let the spacelike curve $\big(\vec{\hat{\Im}}\big)$ be a involute of the timelike curve $\big(\vec{\Im}\big)$. For curvature $\rho_1[t] \neq 0$ of $\big(\vec{\Im}\big)$, the curvature $\hat{\rho}_1\big[\hat{t}\big]$ of $\big(\vec{\hat{\Im}}\big)$ is

$$\hat{\rho}_1\big[\hat{t}\big] = \left(\frac{\sqrt{\big|\rho_1^2 - \rho_2^2\big|}}{\rho_1\big|\int \sigma dt\big|}\right)[t].$$ (19)

Proof. If we substitute (14) and (15) into (13), then we get

$$\frac{d\hat{t}}{dt}\big(\hat{\sigma}\overrightarrow{\hat{V}_1}\big)\big[\hat{t}\big] = \Big(-\rho_1\big(\int \sigma dt\big)\sigma\overrightarrow{V_2}\Big)[t].$$ (20)

If we take the Lorentzian norm of (20), then we have

$$\frac{d\hat{t}}{dt} = \frac{\big(\rho_1\big|\int \sigma dt\big|\sigma\big)[t]}{\hat{\sigma}\big[\hat{t}\big]}.$$ (21)

Thus, from (20) and (21), we obtain

$$\overrightarrow{\hat{V}_1}\big[\hat{t}\big] = \pm\overrightarrow{V_2}[t].$$

Here, we choose

$$\overrightarrow{\hat{V}_1}\big[\hat{t}\big] = -\overrightarrow{V_2}[t].$$ (22)

The first derivative of (22) with respect to t is

$$\frac{d\hat{t}}{dt}\overrightarrow{\hat{V}_1'}\big[\hat{t}\big] = -\overrightarrow{V_2'}[t]$$

and so by considering (6) and (9),

$$\frac{d\hat{t}}{dt}\left(\hat{\sigma}\hat{\rho}_1\overrightarrow{\hat{V}_2}\right)[\hat{t}] = \left(\sigma\left(\rho_1\overline{V_1} - \rho_2\overline{V_3}\right)\right)[t],$$

also from (21),

$$\left(\hat{\rho}_1\overrightarrow{\hat{V}_2}\right)[\hat{t}] = \left(\frac{\rho_1\overline{V_1} - \rho_2\overline{V_3}}{\rho_1\left|\int\sigma dt\right|}\right)[t]. \qquad (23)$$

The Lorentzian norm of (23) is (19).

Theorem 3.5. Let the spacelike curve $\left(\vec{\hat{\Im}}\right)$ be a involute of the timelike curve $\left(\vec{\Im}\right)$. The torsion $\hat{\rho}_2\left[\hat{t}\right]$ of $\left(\vec{\hat{\Im}}\right)$ is

$$\hat{\rho}_2\left[\hat{t}\right] = \left(\frac{\rho_1\rho_2{}' - \rho_1{}'\rho_2}{\sigma\rho_1\left(\int\sigma dt\right)\left(\rho_2^2 - \rho_1^2\right)}\right)[t]. \qquad (24)$$

Proof. The first, second and third derivatives of (10) with respect to t are

$$\frac{d\hat{t}}{dt}\overrightarrow{\hat{\Im}'}[\hat{t}] = \left(-\sigma\rho_1\left(\int\sigma dt\right)\overline{V_2}\right)[t], \qquad (25)$$

$$\left(\frac{d\hat{t}}{dt}\right)^2\overrightarrow{\hat{\Im}''}[\hat{t}] = -\left(\sigma^2\rho_1^2\left(\int\sigma dt\right)\overline{V_1}\right)[t] - \left(\left(\left[\sigma\rho_1' + \sigma'\rho_1\right]\left(\int\sigma dt\right) + \sigma^2\rho_1\right)\overline{V_2}\right)[t] \qquad (26)$$
$$+ \left(\sigma^2\rho_1\rho_2\left(\int\sigma dt\right)\overline{V_3}\right)[t]$$

and

$$\left(\frac{d\hat{t}}{dt}\right)^3\overrightarrow{\hat{\Im}'''}[\hat{t}] = \left(\left(\left[-3\sigma\hat{\sigma}\rho_1^2 - 3\sigma^2\rho_1\rho_1'\right]\left(\int\sigma dt\right) - 2\sigma^3\rho_1^2\right)\overline{V_1}\right)[t] \qquad (27)$$
$$- \left[\left(\left[\sigma^3\rho_1^3 - \sigma^3\rho_1^2\rho_2 - 2\rho_1'\sigma' + \rho_1''\sigma + \rho_1\sigma''\right]\left(\int\sigma dt\right) + \left(2\rho_1'\sigma'^2 + 3\rho_1\sigma\sigma'\right)\right)\overline{V_2}\right][t]$$
$$+ \left(\left(\left[\sigma^2\rho_1'\rho_2 + 3\sigma\sigma'\rho_1\rho_2 + \sigma^2\left(\rho_1'\sigma + \rho_1\sigma'\right)\right]\left(\int\sigma dt\right) + \sigma^2\rho_1 + \sigma^3\rho_1\rho_2\right)\overline{V_3}\right)[t],$$

respectively. If we apply the Lorentzian vector product (25) and (26), then we have

$$\left(\overrightarrow{\hat{\Im}'}\wedge_L\overrightarrow{\hat{\Im}''}\right)[\hat{t}] = \left(\frac{dt}{d\hat{t}}\right)^3\left(\rho_1^2\sigma^3\left(\int\sigma dt\right)^2\left(-\rho_2\overrightarrow{V_1} + \rho_1\overrightarrow{V_3}\right)\right)[t]. \qquad (28)$$

If we apply the Lorentzian inner product (27) and (28), then we attain

$$\left\langle \overrightarrow{\hat{\mathfrak{I}}'} \wedge_L \overrightarrow{\hat{\mathfrak{I}}''}, \overrightarrow{\hat{\mathfrak{I}}'''} \right\rangle_L \left[\hat{t} \right] = \left(\frac{dt}{d\hat{t}} \right)^6 \left(\rho_1^3 \sigma^5 \left(\int \sigma dt \right)^3 \left(\rho_1 \rho_2' - \rho_1' \rho_2 \right) \right) [t]. \quad (29)$$

Also, the Lorentzian norm of (28) is

$$\left\| \overrightarrow{\hat{\mathfrak{I}}'} \wedge_L \overrightarrow{\hat{\mathfrak{I}}''} \right\|_L \left[\hat{t} \right] = \left(\frac{dt}{d\hat{t}} \right)^3 \left(\rho_1^2 \sigma^3 \left(\int \sigma dt \right)^2 \sqrt{\left| \rho_1^2 - \rho_2^2 \right|} \right) [t]. \quad (30)$$

If we substitute (29) and (30) into the equality

$$\hat{\rho}_2 \left[\hat{t} \right] = \left(\frac{\left\langle \overrightarrow{\hat{\mathfrak{I}}'} \wedge_L \overrightarrow{\hat{\mathfrak{I}}''}, \ \overrightarrow{\hat{\mathfrak{I}}'''} \right\rangle_L}{\left\| \overrightarrow{\hat{\mathfrak{I}}'} \wedge_L \overrightarrow{\hat{\mathfrak{I}}''} \right\|_L^2} \right) \left[\hat{t} \right],$$

then we obtain (24).

Theorem 3.6. The relationship between of the Frenet frames of the timelike curve $\left(\vec{\mathfrak{I}} \right)$ and its spacelike involute curve $\left(\vec{\hat{\mathfrak{I}}} \right)$ is

$$\begin{bmatrix} \overrightarrow{\hat{\mathbb{V}}_1} \\ \overrightarrow{\hat{\mathbb{V}}_2} \\ \overrightarrow{\hat{\mathbb{V}}_3} \end{bmatrix} \left[\hat{t} \right] = \left(\frac{1}{\sqrt{\left| \rho_1^2 - \rho_2^2 \right|}} \begin{bmatrix} 0 & -1 & 0 \\ \varepsilon \rho_1 & 0 & -\varepsilon \rho_2 \\ -\rho_2 & 0 & \rho_1 \end{bmatrix} \right) \begin{bmatrix} \overrightarrow{\mathbb{V}_1} \\ \overrightarrow{\mathbb{V}_2} \\ \overrightarrow{\mathbb{V}_3} \end{bmatrix} [t], \quad (31)$$

where, if $\overrightarrow{\hat{\mathbb{V}}_3} \left[\hat{t} \right]$ is timelike, then $\varepsilon = -1$ or if $\overrightarrow{\hat{\mathbb{V}}_3} \left[\hat{t} \right]$ is spacelike, then $\varepsilon = 1$.

Proof. If we substitute (28) and (30) into (1) or (4), then we get

$$\overrightarrow{\hat{\mathbb{V}}_3} \left[\hat{t} \right] = \left(\frac{-\rho_2 \overrightarrow{\mathbb{V}_1} + \rho_1 \overrightarrow{\mathbb{V}_3}}{\sqrt{\left| \rho_1^2 - \rho_2^2 \right|}} \right) [t]. \quad (32)$$

From (32), $\left\langle \overrightarrow{\hat{\mathbb{V}}_3}\left[\hat{t}\right], \overrightarrow{\hat{\mathbb{V}}_3}\left[\hat{t}\right] \right\rangle_L = \varepsilon$. Thus, if $\overrightarrow{\hat{\mathbb{V}}_3}\left[\hat{t}\right]$ is spacelike, then $\overrightarrow{\hat{\mathbb{V}}_2}\left[\hat{t}\right]$ is timelike, or $\overrightarrow{\hat{\mathbb{V}}_3}\left[\hat{t}\right]$ is timelike, then $\overrightarrow{\hat{\mathbb{V}}_2}\left[\hat{t}\right]$ is spacelike. Moreover, if we consider (22) and (32) in (1) or (4), then we have

$$\overrightarrow{\hat{\mathbb{V}}_2}\left[\hat{t}\right] = \varepsilon \left(\frac{-\rho_1 \overrightarrow{\mathbb{V}_1} + \rho_2 \overrightarrow{\mathbb{V}_3}}{\sqrt{\left|\rho_1^2 - \rho_2^2\right|}} \right)[t]. \tag{33}$$

From (22), (32) and (33), we obtain (31).

Theorem 3.7. Let the Darboux vector be $\vec{D}[t]$ of the timelike curve $\left(\vec{\Im}\right)$. The Darboux vector $\vec{\hat{D}}\left[\hat{t}\right]$ of its spacelike involute curve $\left(\vec{\hat{\Im}}\right)$ is

$$\vec{\hat{D}}\left[\hat{t}\right] = -\hat{\sigma}\left[\hat{t}\right] \left(\frac{\varepsilon \vec{D} + \theta' \overrightarrow{\mathbb{V}_2}}{\rho_1 \sigma \left(\int \sigma dt\right)} \right)[t] \tag{34}$$

or

$$\vec{\hat{D}}\left[\hat{t}\right] = -\frac{dt}{d\hat{t}} \left(\varepsilon \vec{D} + \theta' \overrightarrow{\mathbb{V}_2} \right)[t], \tag{35}$$

where $\theta[t]$ is the Lorentzian timelike angle between $\vec{D}(t)$ and $\overrightarrow{\mathbb{V}_3}(t)$.

Proof. If we substitute (19), (22), (24) and (32) into

$$\vec{\hat{D}}\left[\hat{t}\right] = \left(\hat{\sigma} \varepsilon \left[-\hat{\rho}_2 \overrightarrow{\hat{\mathbb{V}}_1} + \hat{\rho}_1 \overrightarrow{\hat{\mathbb{V}}_3} \right] \right)\left[\hat{t}\right],$$

(Uğurlu and Çalışkan, 2012), then we get

$$\vec{\hat{D}}\left[\hat{t}\right] = \frac{\hat{\sigma}\left[\hat{t}\right]}{\rho_1 \int \sigma[t] dt} \varepsilon \left(-\rho_2 \overrightarrow{\mathbb{V}_1} - \frac{\rho_1' \rho_2 - \rho_1 \rho_2'}{\sigma \rho_1 \left(\rho_1^2 - \rho_2^2\right)} \overrightarrow{\mathbb{V}_2} + \rho_1 \overrightarrow{\mathbb{V}_3} \right)[t]. \tag{36}$$

For the timelike curve $\left(\vec{\Im}\right)$, since

$$\vec{D}[t] = \left(\sigma \left[\rho_2 \overrightarrow{\mathbb{V}_1} - \rho_1 \overrightarrow{\mathbb{V}_3} \right] \right)[t], \tag{37}$$

(Uğurlu and Çalışkan, 2012), instead (36) we write

$$\vec{D}\big[\hat{t}\,\big] = \frac{\hat{\sigma}\big[\hat{t}\,\big]}{\big(\rho_1\sigma\big(\int\sigma dt\big)\big)[t]} \varepsilon\left(-\vec{D} - \frac{\rho_1'\rho_2 - \rho_1\rho_2'}{\rho_1^2 - \rho_2^2}\,\overrightarrow{\mathbb{V}_2}\right)[t]. \qquad (38)$$

In this case, if $\big|\rho_1[t]\big| > \big|\rho_2[t]\big|$, then $\vec{D}[t]$ is a spacelike vector and so

$$\begin{cases} \cosh\big(\theta[t]\big) = \left(\dfrac{\rho_1}{\sqrt{\rho_1^2 - \rho_2^2}}\right)[t], \\[4mm] \sinh\big(\theta[t]\big) = \left(\dfrac{\rho_2}{\sqrt{\rho_1^2 - \rho_2^2}}\right)[t] \end{cases} \qquad (39)$$

or if $\big|\rho_1[t]\big| < \big|\rho_2[t]\big|$, then $\vec{D}[t]$ is a timelike vector and so

$$\begin{cases} \sinh\big(\theta[t]\big) = \left(\dfrac{\rho_1}{\sqrt{\rho_2^2 - \rho_1^2}}\right)[t], \\[4mm] \cosh\big(\theta[t]\big) = \left(\dfrac{\rho_2}{\sqrt{\rho_2^2 - \rho_1^2}}\right)[t], \end{cases} \qquad (40)$$

(Uğurlu and Çalışkan, 2012). from (39) and (40), we get

$$\theta'[t] = \varepsilon\left(\frac{\rho_1'\rho_2 - \rho_1\rho_2'}{\rho_2^2 - \rho_1^2}\right)[t]. \qquad (41)$$

If we substitute (41) into (38), then we have (34). Or from (21) and (34), we obtain (35).

Corollary 3.8. The relationship between the Frenet frames of the timelike curve $\big(\vec{\mathfrak{J}}\big)$ and its spacelike involute curve $\big(\vec{\tilde{\mathfrak{J}}}\big)$ is as follows:

• if $\big|\rho_1[t]\big| > \big|\rho_2[t]\big|$, then

$$
\begin{bmatrix} \overrightarrow{\hat{V}_1} \\ \overrightarrow{\hat{V}_2} \\ \overrightarrow{\hat{V}_3} \end{bmatrix} [\hat{t}] = \begin{bmatrix} 0 & -1 & 0 \\ \varepsilon \cosh(\theta) & 0 & -\varepsilon \sinh(\theta) \\ -\sinh(\theta) & 0 & \cosh(\theta) \end{bmatrix} \begin{bmatrix} \overrightarrow{V_1} \\ \overrightarrow{V_2} \\ \overrightarrow{V_3} \end{bmatrix} [t] \tag{42}
$$

or

- if $\left| \rho_1[t] \right| < \left| \rho_2[t] \right|$, then

$$
\begin{bmatrix} \overrightarrow{\hat{V}_1} \\ \overrightarrow{\hat{V}_2} \\ \overrightarrow{\hat{V}_3} \end{bmatrix} [\hat{t}] = \sigma \begin{bmatrix} 0 & -1 & 0 \\ \varepsilon \sinh(\theta) & 0 & -\varepsilon \cosh(\theta) \\ -\cosh(\theta) & 0 & \sinh(\theta) \end{bmatrix} \begin{bmatrix} \overrightarrow{V_1} \\ \overrightarrow{V_2} \\ \overrightarrow{V_3} \end{bmatrix} [t]. \tag{43}
$$

Proof. It is clear that (31), (39) and (40).

Corollary 3.9. Let the spacelike curve $\left(\vec{\tilde{\Im}} \right)$ be a involute of the timelike curve $\left(\vec{\Im} \right)$. $\overrightarrow{\hat{V}_3}[\hat{t}]$ is the opposite of pole vector $\vec{P}[t]$.

Proof. The pole vector $\vec{P}[t]$ of $\left(\vec{\Im} \right)$ is

$$
\vec{P}[t] = \left(\sinh(\theta) \overrightarrow{V_1} - \cosh(\theta) \overrightarrow{V_3} \right)[t],
$$

if $\left| \rho_1[t] \right| > \left| \rho_2[t] \right|$,

or

$$
\vec{P}[t] = \left(\cosh(\theta) \overrightarrow{V_1} - \sinh(\theta) \overrightarrow{V_3} \right)[t],
$$

if $\left| \rho_1[t] \right| < \left| \rho_2[t] \right|$,

(Uğurlu and Çalışkan, 2012). From (42) and (43), we obtain

$$
\vec{P}[t] = -\overrightarrow{\hat{V}_3}[\hat{t}]. \tag{44}
$$

Corollary 3.10. Let the spacelike curve $\left(\vec{\tilde{\Im}}\right)$ be a involute of the timelike curve $\left(\vec{\Im}\right)$. If $\left(\vec{\Im}\right)$ with non-zero curvature is a helix,

- the Darboux vectors $\vec{\hat{D}}\left[\hat{t}\right]$ and $\vec{D}\left[t\right]$ are linearly dependent,
- the binormal vector $\vec{\hat{V}}_3\left[\hat{t}\right]$ and Darboux vector $\vec{\hat{D}}\left[\hat{t}\right]$ are linearly dependent.

Proof. If $\left(\vec{\Im}\right)$ with non-zero curvature is a helix, we know

$$\frac{\rho_2\left[t\right]}{\rho_1\left[t\right]} = \text{constant}. \tag{45}$$

The first derivative of (45) with respect to t is

$$\left(\rho_1'\rho_2 - \rho_1\rho_2'\right)\left[t\right] = 0. \tag{46}$$

So, from (41) and (46), we obtain

$$\theta'\left[t\right] = 0. \tag{47}$$

On the other hand, from (39) and (45) or (40) and (45), we get

$$\tan\left(\theta\left[t\right]\right) = \text{constant}. \tag{48}$$

The first derivative of (48) with respect to t is

$$\left(\left(\theta'\right)\operatorname{sech}^2\left(\theta\right)\right)\left[t\right] = 0. \tag{49}$$

Thus, from (49), we obtain (47) again. If we substitute (47) into (35), then we get

$$\vec{\hat{D}}\left[\hat{t}\right] = -\frac{dt}{d\hat{t}}\vec{D}\left[t\right]. \tag{50}$$

From (7), (44) and (50), we obtain

$$\vec{\hat{D}}\left[\hat{t}\right] = \frac{dt}{d\hat{t}}\left\|\vec{D}\left[t\right]\right\|_L \vec{\hat{V}}_3\left[\hat{t}\right]. \tag{51}$$

The corollary is clear, from (50) and (51).

Theorem 3.11. Let the spacelike curve $\left(\vec{\hat{\Im}}\right)$ be a involute of the timelike curve $\left(\vec{\Im}\right)$. The pole vector $\vec{\hat{P}}\left[\hat{t}\right]$ of $\left(\vec{\hat{\Im}}\right)$ is

$$\vec{\hat{P}}\left[\hat{t}\right] = \left(-\frac{\varepsilon\sigma\sqrt{\left|\rho_1^2 - \rho_2^2\right|}\,\vec{P}\theta'\,\vec{\mathbb{V}_2}}{\sqrt{\theta'^2 + \sigma^2\left|\rho_1^2 - \rho_2^2\right|}}\right)[t].$$

(52)

Proof. The Lorentzian norm of (35) is

$$\vec{\hat{D}}\left[\hat{t}\right] = -\frac{dt}{d\hat{t}}\left(\varepsilon\vec{D} + \theta'\vec{\mathbb{V}_2}\right)[t]$$

$$\left\|\vec{\hat{D}}\left[\hat{t}\right]\right\|_L = \frac{dt}{d\hat{t}}\left(\sqrt{\left\|\vec{D}\right\|_L} + \theta'^2\right)[t] \qquad .$$

(53)

From (35), (37), (53) and the equality

$$\vec{\hat{P}}\left[\hat{t}\right] = \left(\frac{\vec{\hat{D}}}{\left\|\vec{\hat{D}}\right\|_L}\right)\left[\hat{t}\right],$$

we have

$$\vec{\hat{P}}\left[\hat{t}\right] = \left(-\frac{\varepsilon\vec{D} + \theta'\vec{\mathbb{V}_2}}{\sqrt{\theta'^2 + \sigma^2\left|\rho_1^2 - \rho_2^2\right|}}\right)[t].$$

(54)

From (37) and (54), we obtain (52).

Corollary 3.12. Let the spacelike curve $\left(\vec{\hat{\Im}}\right)$ be a involute of the timelike curve $\left(\vec{\Im}\right)$. If $\left(\vec{\Im}\right)$ is a helix with non-zero curvature, the pole vector $\vec{\hat{P}}\left[\hat{t}\right]$ is the opposite of the pole vector $\vec{P}\left[t\right]$.

Proof. If we substitute (47) into (52), then we get

$$\vec{\hat{P}}\left[\hat{t}\right] = -\vec{P}\left[t\right].$$

(55)

The corollary is clear from (55).

Theorem 3.13. Let $\theta[t]$ be the Lorentzian timelike angle between $\overrightarrow{V}_3[t]$ and $\overrightarrow{D}[t]$ of the timelike curve $(\vec{\Im})$. The Lorentzian spacelike angle $\hat{\theta}[\hat{t}]$ between $\overrightarrow{\hat{V}}_3[\hat{t}]$ and $\overrightarrow{\hat{D}}[\hat{t}]$ of its spacelike involute curve $(\vec{\hat{\Im}})$ is

$$\hat{\theta}[\hat{t}] = \arctan\left(\pm\frac{\theta'}{\sigma\sqrt{\left|\rho_1^2 - \rho_2^2\right|}}\right)[t]. \tag{56}$$

Proof. We know

$$\tan\left(\hat{\theta}[\hat{t}]\right) = \left(\frac{\hat{\rho}_2}{\hat{\rho}_1}\right)[\hat{t}], \tag{57}$$

(Uğurlu and Çalışkan, 2012). If we substitute (19) and (24) into (57), then we get

$$\tan\left(\hat{\theta}[\hat{t}]\right) = \pm\left(\frac{\rho_1'\rho_2 - \rho_1\rho_2'}{\sigma\left(\rho_1^2 - \rho_2^2\right)^{3/2}}\right)[t]. \tag{58}$$

If we substitute (41) into (58), then we obtain (56).

Corollary 3.14. Let the spacelike curve $(\vec{\hat{\Im}})$ be a involute of the timelike curve $(\vec{\Im})$. The pole vector $\overrightarrow{\hat{P}}[\hat{t}]$ of $(\vec{\hat{\Im}})$ is as follows:

- if $\left|\rho_1[t]\right| > \left|\rho_2[t]\right|$, then

$$
\vec{P}\left[\hat{t}\right] = -\left(\sinh\left(\theta\right)\cos\left(\arctan\left(\pm\frac{\theta'}{\sigma\sqrt{\left|\rho_1^2 - \rho_2^2\right|}} \right) \right) \overrightarrow{\mathbb{V}_1} \right)\left[t\right]
$$

$$
-\left(\sin\left(\arctan\left(\pm\frac{\theta'}{\sigma\sqrt{\left|\rho_1^2 - \rho_2^2\right|}} \right) \right) \overrightarrow{\mathbb{V}_2} \right)\left[t\right] \qquad (59)
$$

$$
+\left(\cosh\left(\theta\right)\cos\left(\arctan\left(\pm\frac{\theta'}{\sigma\sqrt{\left|\rho_1^2 - \rho_2^2\right|}} \right) \right) \overrightarrow{\mathbb{V}_3} \right)\left[t\right],
$$

- if $\left|\rho_1\left[t\right]\right| < \left|\rho_2\left[t\right]\right|$, then

$$
\vec{P}\left[\hat{t}\right] = -\left(\cosh\left(\theta\right)\cos\left(\arctan\left(\pm\frac{\theta'}{\sigma\sqrt{\left|\rho_1^2 - \rho_2^2\right|}} \right) \right) \overrightarrow{\mathbb{V}_1} \right)\left[t\right]
$$

$$
\mp\left(\sin\left(\arctan\left(\pm\frac{\theta'}{\sigma\sqrt{\left|\rho_1^2 - \rho_2^2\right|}} \right) \right) \overrightarrow{\mathbb{V}_2} \right)\left[t\right] \qquad (60)
$$

$$
+\left(\sinh\left(\theta\right)\cos\left(\arctan\left(\pm\frac{\theta'}{\sigma\sqrt{\left|\rho_1^2 - \rho_2^2\right|}} \right) \right) \overrightarrow{\mathbb{V}_3} \right)\left[t\right].
$$

Proof. For the spacelike curve $\left(\vec{\tilde{\Im}}\right)$, we know

$$
\vec{P}\left[\hat{t}\right] = \left(-\sin\left(\hat{\theta}\right)\overrightarrow{\hat{\mathbb{V}}_1} + \cos\left(\hat{\theta}\right)\overrightarrow{\hat{\mathbb{V}}_3} \right)\left[\hat{t}\right], \qquad (61)
$$

(Uğurlu and Çalışkan, 2012). If we substitute (42), (43) and (56) into (61), then we obtain (59) and (60).

Corollary 3.15. Let the spacelike curve $\left(\vec{\tilde{\Im}}\right)$ be a involute of the timelike curve $\left(\vec{\Im}\right)$. $\left(\vec{\Im}\right)$ is a helix with non-zero curvature if only if $\left(\vec{\tilde{\Im}}\right)$ is planar curve.

Proof. From (24) and (46), since $\left(\vec{\mathfrak{I}}\right)$ is a helix,

$$\hat{\rho}_2\left[\hat{t}\right]=0. \tag{62}$$

So, the corollary is clear from (62).

Example. Let's take into account the timelike curve

$$\vec{\mathfrak{I}}[t]=\left(t,\sqrt{3}\cosh[t],\sqrt{3}\sinh[t]\right). \tag{63}$$

From (63),

$$\sigma[t]=\left\|\vec{\mathfrak{I}}'[t]\right\|_L=\sqrt{2}, \tag{64}$$

$$a[t]=-\int\sigma[t]dt=-\sqrt{2}t-c, \quad c\in\mathbb{R}. \tag{65}$$

The Frenet frame of $\left(\vec{\mathfrak{I}}\right)$ from (7) is

$$\begin{cases} \vec{\mathbb{V}_1}[t]=\dfrac{1}{\sqrt{2}}\left(1,\sqrt{3}\sinh[t],\sqrt{3}\cosh[t]\right) & \text{(timelike)}, \\[2mm] \vec{\mathbb{V}_2}[t]=\left(0,\cosh[t],\sinh[t]\right) & \text{(spacelike)}, \\[2mm] \vec{\mathbb{V}_3}[t]=-\dfrac{1}{\sqrt{2}}\left(\sqrt{3},\sinh[t],\cosh[t]\right) & \text{(spacelike)}. \end{cases} \tag{66}$$

The curvatures of $\left(\vec{\mathfrak{I}}\right)$ are

$$\rho_1[t]=\frac{\sqrt{3}}{2} \quad\text{and}\quad \rho_2[t]=-\frac{1}{2}. \tag{67}$$

Here, since $\dfrac{\rho_2[t]}{\rho_1[t]}=\text{constant}$, $\left(\vec{\mathfrak{I}}\right)$ is a helix.

The Darboux and pole vectors $\left(\vec{\mathfrak{I}}\right)$ from (37) are

$$\vec{D}[t]=\vec{P}[t]=(1,0,0) \quad \text{(spacelike)}. \tag{68}$$

Since $\left|\rho_1[t]\right|>\left|\rho_2[t]\right|$, from (39), (64), (67) and (68),

$$\cosh\big(\theta[t]\big) = \frac{\sqrt{6}}{2} \quad \text{and} \quad \sinh\big(\theta[t]\big) = -\frac{\sqrt{2}}{2}. \tag{69}$$

So, the Lorentzian spacelike angle between spacelike vectors $\overrightarrow{V_3}[t]$ and $\overrightarrow{D}[t]$ is found as

$$\theta[t] \cong -0,6584.$$

Moreover, the spacelike involute curve $\left(\vec{\tilde{\Im}}\right)$ with spacelike binormal of the timelike curve $\left(\vec{\Im}\right)$ from (10), (63), (65) and (66) is obtained as

$$\vec{\tilde{\Im}}[t] = \left(-\frac{c}{\sqrt{2}}, \ \sqrt{3}\left(\cosh[t] - \left(t + \frac{c\sqrt{2}}{2}\right)\sinh[t]\right), \ \sqrt{3}\left(\sinh[t] - \left(t + \frac{c\sqrt{2}}{2}\right)\cosh[t]\right) \right) \tag{70}$$

Figure 2. Here, for each value of c, there is an involute curve of $\left(\vec{\Im}\right)$ belonging to a different point $\vec{\Im}[t]$. From (70),

$$\hat{\sigma}[t] = \left\|\vec{\tilde{\Im}}'[t]\right\|_L = \sqrt{3}\left|t + \frac{c\sqrt{2}}{2}\right|. \tag{71}$$

Thus, from (21), (64), (65), (67) and (71), it is seen that

$$\frac{d\hat{t}}{dt} = 1.$$

Frenet frame of $\left(\vec{\tilde{\Im}}\right)$ from (4) is

$$\begin{cases} \overrightarrow{\tilde{V}_1}[t] = \big(0, -\cosh[t], -\sinh[t]\big) & \text{(spacelike)}, \\ \overrightarrow{\tilde{V}_2}[t] = \big(0, \sinh[t], \cosh[t]\big) & \text{(timelike)}, \\ \overrightarrow{\tilde{V}_3}[t] = \big(-1, 0, 0\big) & \text{(spacelike)}. \end{cases} \tag{72}$$
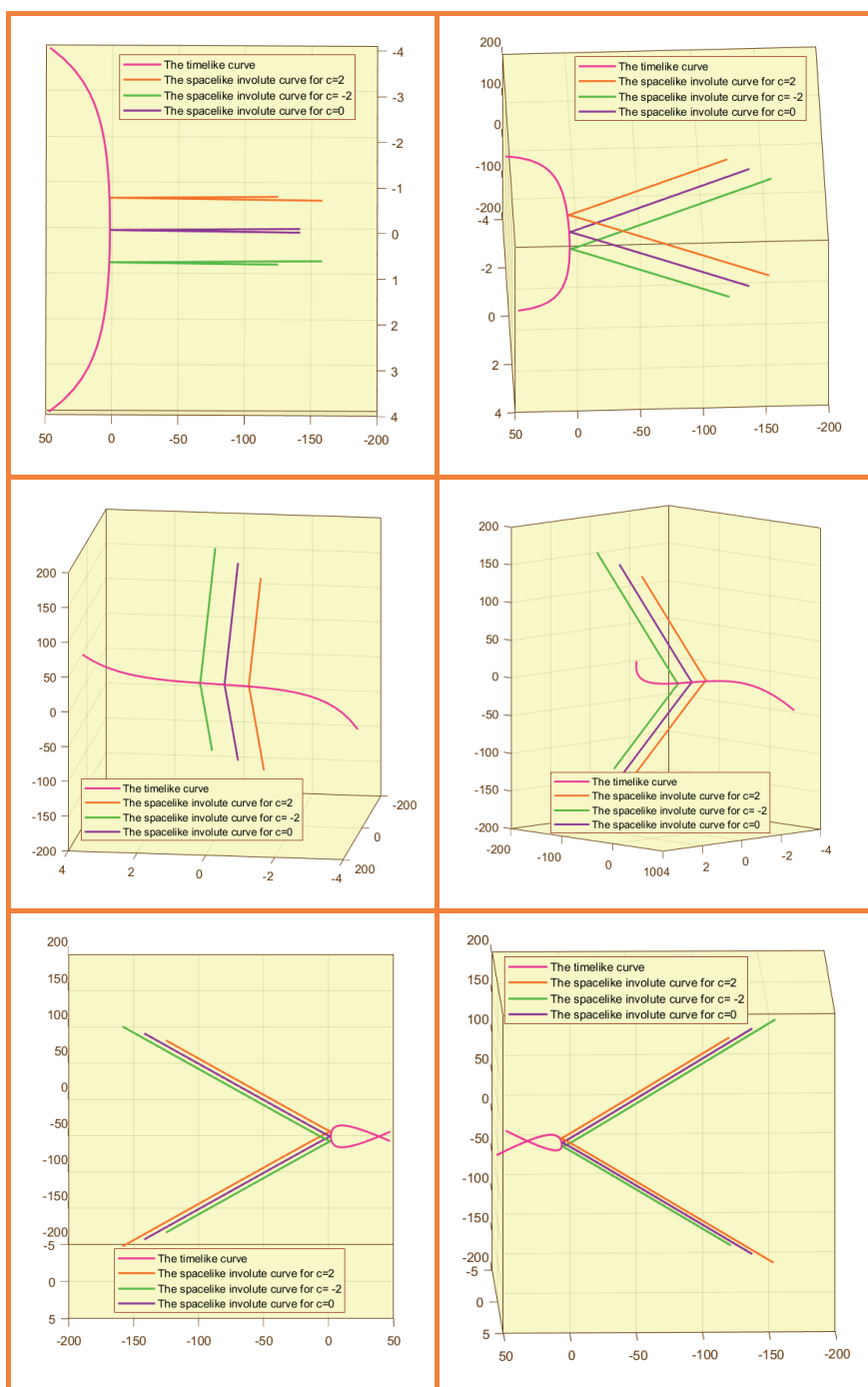
Figure 2. The timelike curve $\left(\vec{\mathfrak{I}}\right)$ and its spacelike involute curves

So, from (66) and (72), it is seen that $\left\langle \overrightarrow{\hat{V}_1}[t], \, \overrightarrow{V_1}[t] \right\rangle_L = 0$. Besides, from (66), (67), (69) and (72), it is clear that (31) and (42) is provided:

$$
\begin{bmatrix} \overrightarrow{\hat{V}_1} \\ \overrightarrow{\hat{V}_2} \\ \overrightarrow{\hat{V}_3} \end{bmatrix}[t] = \frac{\sqrt{2}}{2} \begin{bmatrix} 0 & -1 & 0 \\ \sqrt{3} & 0 & 1 \\ 1 & 0 & \sqrt{3} \end{bmatrix} \begin{bmatrix} \overrightarrow{V_1} \\ \overrightarrow{V_2} \\ \overrightarrow{V_3} \end{bmatrix}[t].
$$

The curvatures of $\left(\overrightarrow{\hat{\Im}} \right)$ are

$$
\hat{\rho}_1[t] = \frac{\sqrt{3}}{3\left| t + \dfrac{c\sqrt{2}}{2} \right|} \qquad \text{and} \qquad \hat{\rho}_2[t] = 0.
$$

From (65) and (67), it is clear that (19) and (24) are provided. Besides, $\left(\overrightarrow{\Im} \right)$ is a helix and so its involute $\left(\overrightarrow{\hat{\Im}} \right)$ is planar (Corollary 3.15). In addition, the Darboux and pole vectors of $\left(\overrightarrow{\hat{\Im}} \right)$ are

$$
\overrightarrow{\hat{D}}[t] = \overrightarrow{\hat{P}}[t] = (-1, 0, 0) \qquad \text{(spacelike)}.
$$

So, it is clear that (34), (35) and (52) are provided. Since $\left(\overrightarrow{\Im} \right)$ is a helix, (50) and (55) are seen clearly (Corollary 3.9 and Corollary 3.12). Moreover, for the spacelike involute curve $\left(\overrightarrow{\hat{\Im}} \right)$,

$$
\begin{cases} \cos\left(\hat{\theta}[t] \right) = \left(\dfrac{\hat{\sigma}\hat{\rho}_1}{\left\| \overrightarrow{\hat{D}} \right\|_L} \right)[t] = 1, \\[4mm] \sin\left(\hat{\theta}[t] \right) = \left(\dfrac{\hat{\sigma}\hat{\rho}_2}{\left\| \overrightarrow{\hat{D}} \right\|_L} \right)[t] = 0. \end{cases}
$$

So, the real angle between the spacelike vectors $\overrightarrow{\hat{\mathbb{V}}_3}[t]$ and $\overrightarrow{\hat{D}}[t]$ is

$$\hat{\theta}[t] = 0.$$

Thus, it is clear that, (56) is indeed provided.

4. Conclusions

In present study, we examine the involute curves of a non-unit speed timelike curve in Minkowski 3-space and evaluate the relations between some elements. Involute curves of a timelike curve are definitely spacelike, but they can have spacelike or timelike binormal vector. We saw that the involutes of the timelike helix in the example we examined are spacelike curves with spacelike binormal. Similarly, the involutes of a non-unit speed spacelike curve are discussed. In addition, the evolute curves of the same curve can be investigated.

REFERENCES

Akutagava, K., Nishikawa, S. (1990). The Gauss map and space-like surfaces with prescribed mean curvature in Minkowski 3-space. Tohoku Math. J., 42, 67–82.

Beem, J. K., Paul, E. E., Kevin, L. E. (2017). Global lorentzian geometry. Routledge.

Bilici, M., Çalışkan, M. (2011). Some new notes on the involutes of the timelike curves in Minkowski 3-space. Int. J. Math. Sciences, 6(41), 2019–2030.

Bilici, M., Çalışkan, M. (2019). Some new results on the curvatures of the spherical indicatrices of the involutes of a spacelike curve with a spacelike binormal in Minkowski 3-space, MathLAB Journal, 2(1), 110–119.

Birman, G. S., Nomizu, K. (1984). Trigonometry in Lorentzian geometry. Ann. Math. Mont. 91, 534–549.

Bükcü, B., Karacan, M. K. (2007a). On the involute and evolute curves of the spacelike curve with a spacelike binormal in Minkowski 3-space. Int. J. Contemp. Math. Sciences, 2(5), 221–232.

Bükcü, B., Karacan, M. K. (2007b). On the involute and evolute curves of the timelike curve in Minkowski 3-space. Demonstratio Mathematica, 40(3), 721–732.

Gür, S., Şenyurt, S. (2013). Spacelike–timelike involute–evolute curve couple on dual Lorentzian space. J. Math. Comput. Sci., 3(4), 1054–1075.

Gür Mazlum, S., Bektaş, M. (2023). Involute curves of any non-unit speed curve in Euclidean 3-space. International Studies in Science and Mathematics. (Eds. Akgül, H., Baba H., İyit, N.) 177–195, Serüven Publishing, Ankara.

Lopez, R. (2014). Differential geometry of curves and surfaces in Lorentz-Minkowski space. International Electronic Journal of Geometry, 7, 44–107.

O'Neill, B. (1983). Semi-Riemannian geometry with applications to relativity. Academic Press: London, England.

Ratcliffe, J. G. (1994). Foundations of hyperbolic manifolds. Springer-Verlag: Tokyo, Japanese.

Şenyurt, S., Gür, S. (2012). Timelike–spacelike involute–evolute curve couple on dual Lorentzian space, J. Math. Comput. Sci., 2(6), 1808–1823.

Uğurlu, H. H. (1997). On the geometry of time-like surfaces, Communications Faculty of Sciences, University of Ankara, A1 Series, 46, 211–223.

Uğurlu, H. H., Çalışkan, A. (2012). Darboux ani dönme vektörleri ile spacelike ve timelike yüzeyler geometrisi. Celal Bayar University Press: Manisa, Turkiye.

Woestijne, I. V. (1990). Minimal surfaces of the 3-dimensional Minkowski space, Geometry and Topology of Submanifolds: II, Word Scientific, Singapore, 344–369.
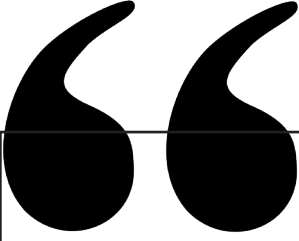
Chapter 8

EIGENFUNCTION EXPANSION OF THE STURM-LIOUVILLE PROBLEM WITH DISCONTINUITY CONDITION AND EIGENPARAMETER DEPENDENCE ON THE BOUNDARY CONDITION

Nida PALAMUT KOŞAR[1]

Özge AKÇAY[2]

1 Dr. Öğr. Üyesi Nida PALAMUT KOŞAR,, Gaziantep Üniversitesi Nizip Eğitim Fakültesi, Matematik ve Fen Bilimleri Eğitimi Bölümü, Matematik Eğitim Anabilim Dalı, ,ORCİD ID: 0000-0003-2421-7872

2 Doç. Dr. Özge AKÇAY,Munzur Üniversitersi, Mühendislik Fakültesi, Bilgisayar Mühendisliği Bölümü , ORCİD ID:0000-0001-9691-666X

1.Introduction

In recent years, discontinuous Sturm-Liouville problems have been encountered in mathematics, physics and engineering fields; therefore, many studies have been done on these problems and the studies done are remarkable (see Anderssen, 1997; Freiling and Yurko, 2001; Gomilko and Pivovarchik, 2002; Tikhonov and Samarskii, 1990 and the references therein).

In this paper, we consider the Sturm-Liouville equation

$$-\xi'' + q(s)\xi = \lambda^2\xi, \quad s \in (0, \infty) \tag{1.1}$$

under the discontinuity conditions at the point $x = a \in (0, \infty)$,

$$\xi(a - 0) = \alpha\xi(a + 0), \quad \xi'(a - 0) = \alpha^{-1}\xi'(a + 0) \tag{1.2}$$

and the boundary conditions

$$\xi'(0) + \lambda^2\xi(0) = 0 \tag{1.3}$$

where λ is a spectral parameter, $1 \neq \alpha > 0$ and $q(s)$ is a real-valued function satisfying the condition

$$\int_0^{+\infty} s|q(s)|ds < \infty. \tag{1.4}$$

In mathematical physics, when we investigate the solution of partial differential equations under given initial and boundary conditions using the Fourier method, we encounter the following types of problems: to determine the eigenvalues and eigenfunctions of differential operators and to expand an arbitrary function as a series of eigenfunctions. An important and interesting problem is that of the examination of the spectrum and expanding a given function in term of eigenfunctions of a differential operator.

In this study, our aim is to obtain the expansion formula with respect to the eigenfunctions of boundary value problem (1.1)-(1.3). For this purpose, first of all, we construct the resolvent operator of problem (1.1)-(1.3). Then, by applying the method of Titchmarsh (see Titchmarsh, 1962), we obtain the eigenfunction expansion formula of boundary value problem (1.1) -(1.3).

The direct and inverse problem for Sturm-Liouville problems containing discontinuity conditions at the point on the positive half line under different boundary conditions are studied in (Akcay, 2021; El-Reheem and Nasser, 2014; Huseynov and Osmanova, 2007; Huseynov and Osmanli, 2009; Huseynov and Mammadova, 2013). Moreover, the direct and inverse problem for Sturm Liouville problems involving discontinuous coefficients are examined in (Guseinov and Pashaev, 2002; Mamedov and Palamut, 2009; Mamedov and Cetinkaya, 2015; Mamedov, Kosar and Cetinkaya, 2015).

2.The Jost Solution

To obtain the eigenfunction expansion formula, we use the Jost solution of equation (1.1) with discontinuity conditions (1.2) and in this section, we give this Jost solution. The existence of the discontinuity condition seriously affects the Jost solution. Therefore, the Jost solution of equation (1.1) under the discontinuity conditions (1.2) is different from the transmission operator and this Jost solution obtained by (Huseynov and Osmanova, 2007) has an integral representation as follows:

For all λ from the closed upper half plane (1.1) has a Jost solution $e(s, \lambda)$ which satisfied the conditions (1.3) and (1.4) can be represented in the form

$$e(s, \lambda) = e_0(s, \lambda) + \int\limits_{s}^{+\infty} K(s,t)e^{i\lambda t}dt$$

where

$$e_0(s, \lambda) = \begin{cases} e^{i\lambda s}, & s > a, \\ \alpha^+ e^{i\lambda s} + \alpha^- e^{i\lambda(2a-s)}, & 0 < s < a, \end{cases}$$

and $\alpha^{\mp} = 1/2(\alpha \mp \frac{1}{\alpha})$. For all fixed $s \in (0,a) \cup (a, \infty)$ the kernel $K(s, \cdot) \in L_1(s, \infty)$ and

satisfies the inequality

$$\int\limits_{s}^{\infty} |K(s,t)|dt \leq e^{c\sigma_1(s)} - 1, \quad c = \alpha^+ + |\alpha^-|, \quad \sigma_1(s)\int\limits_{s}^{\infty} t|q(t)|dt.$$

Moreover, the following properties holds:

$$K(s,s) = \begin{cases} \dfrac{\alpha^+}{2} \displaystyle\int_s^{+\infty} q(t)dt, & 0 < s < a, \\ \dfrac{1}{2} \displaystyle\int_s^{+\infty} q(t)dt, & s > a \end{cases}$$

$$K(s, 2a - s + 0) - K(s, 2a - s - 0) = \frac{\alpha^-}{2}\left(\int_a^{+\infty} q(t)dt - \int_s^a q(t)dt\right),\ 0 < s < a.$$

The solution $e(s,\lambda)$ is analitic for λ in $Im\lambda > 0$ and it is continuous for $Im\lambda \geq 0$. For reel $\lambda \neq 0$ the functions $e(s,\lambda)$ and $\overline{e(s,\lambda)}$ form the fundamental system for solutions of equation (1.1) with condition (1.3) and the Wronskian of this system is equal to

$$W\{e(s,\lambda), \overline{e(s,\lambda)} = e'(s,\lambda)\overline{e(s,\lambda)} - e(s,\lambda)\overline{e'(s,\lambda)} = 2i\lambda\}.$$

The scattering data of the problem (1.1) -(1.3) as defined as $\{S(\lambda), (-\infty < \lambda < \infty), \lambda_k, \mu_k\}$ and determines the behavior of normalized eigenfunctions at infinity. The normalized eigenfunctions of the problem (1)-(3) is given with the form as

$$u(s,\lambda) = \overline{e(s,\lambda)} - S(\lambda)e(s,\lambda), \quad (-\infty < \lambda < \infty)$$

(2.1)

$$u(s, i\lambda_k) = \mu_k e(s, i\lambda_k), \quad (k = 1,2,\dots,n)$$

(2.2)

Here we denote $S(\lambda), \lambda_k$ and μ_k are the the scattering function, eigenfunction and normalized number of the problem (1.1) -(1.3) respectively.

3. Resolvent Operator

To obtain the eigenfunction expansion of problem (1.1) -(1.3), we first need to construct the resolvent operator of this problem.

Let us defined the inner product in Hilbert space, $H = L_2(0, \infty) \times \mathbb{C}$ as follows:

$$\langle F, G \rangle = \int_0^\infty f_1(s)\overline{g_1(s)}ds + f_2\overline{g_2},$$

where

$$F = \begin{pmatrix} f_1(s) \\ f_2 \end{pmatrix} \;,\; G = \begin{pmatrix} g_1(s) \\ g_2 \end{pmatrix} \in H.$$

We define the operator with domain

$D(L) = \{F \in H: f_1(s), f_1'(s) \in AC[0, a] \cap AC[a, \infty),\; \ell(f_1) \in L_2(0, \infty),\; f_2 = -f_1(0)\}$

as

$$L(F) = \begin{pmatrix} \ell(f_1) \\ f_1'(0) \end{pmatrix}, \quad \ell(f_1) = \{-f_1'' + q(s)f_1\}.$$

Assume that λ^2 is a spectrum point of operator L. Then there exist a resolvent operator

$$R_{\lambda^2}(L) = (L - \lambda^2 I)^{-1}.$$

Let find the expression of operator $R_{\lambda^2}(L)$.

Lemma 3.1: The resolvent operator of L is

$$\xi(s, \lambda) = f_2 \frac{e(s, \lambda)}{w(\lambda)} + \int_0^{+\infty} G(s, t, \lambda)f_1(t)dt$$

where

$$G(s, t, \lambda) = \begin{cases} e(s, \lambda)\varphi(t, \lambda), & t \leq s \\ \varphi(s, \lambda)e(t, \lambda), & t \geq s. \end{cases}$$

Proof: Let $F \in D(L)$ and $f_1(s)$ is a finite function. To construct the resolvent operator we need to solve the boundary problem

$$-\xi'' + q(s)\xi = \lambda^2\xi + f_1(s) \tag{3.1}$$

$$\xi'(0) + \lambda^2\xi(0) = f_2 \tag{3.2}$$

Let us find the solutions of the problem (3.1) -(3.2) which has a form

$$\xi(s,\lambda) = c_1(s,\lambda)\varphi(s,\lambda) + c_2(s,\lambda)e(s,\lambda) \tag{3.3}$$

where $\varphi(s,\lambda)$ is a solution of equation (3.1) which satisfies the conditions;

$$\varphi(0,\lambda) = -1, \; \varphi'(0,\lambda) = \lambda^2.$$

By applying the method of variation of constants we get

$$\begin{cases} c'(s,\lambda)\varphi(s,\lambda) + c'_2(s,\lambda)e(s,\lambda) = 0 \\ c'(s,\lambda)\varphi'(s,\lambda) + c'_2(s,\lambda)e'(s,\lambda) = -f_1(s). \end{cases} \tag{3.4}$$

Since $\xi(s,\lambda) \in L_2(0,\infty)$, then $\lim \top(s \to \infty)$ $⟦c\_1\,(s,\lambda = 0)⟧$. Using this relation and equation system (3.4) we get,

$$\begin{cases} c_1(s,\lambda) = \frac{1}{w(\lambda)}\int_s^\infty f_1(t)e(t,\lambda)dt \\ c_2(s,\lambda) = c_2(0,\lambda) + \frac{1}{w(\lambda)}\int_0^s f_1(t)\varphi(t,\lambda)dt. \end{cases} \tag{3.5}$$

Substituting (3.5) into (3.3) we get

$$\xi(s,\lambda) = \frac{f_2 e(s,\lambda)}{w(\lambda)} + \int_0^\infty G(s,t,\lambda)f_1(t)dt$$

where

$$G(s,t,\lambda) = \begin{cases} e(s,\lambda)\varphi(t,\lambda), & 0 \le t \le s, \\ \varphi(s,\lambda)e(t,\lambda), & s \le t < \infty. \end{cases}$$

Lemma 3.2: Let the function $f_1(s) \in D(L)$ continously differentiable two times and finite at ∞. Then as $|\lambda| \longrightarrow \infty$, $Im\lambda \ge 0$, the following is valid:

$$\xi(s,\lambda) = f_2 \frac{e(s,\lambda)}{w(\lambda)} + \int_0^\infty G(s,t,\lambda)f_1(t)dt = -\frac{f_1(s)}{\lambda^2} + O\left(\frac{1}{\lambda^2}\right)$$

Proof: Using Lemma 3.1 and integrating by parts we get

$$\int\limits_0^\infty G(s,t,\lambda)f_1(t)dt$$

$$= \frac{1}{w(\lambda)}\int\limits_0^s e(s,\lambda)\varphi(t,\lambda)f_1(t)dt$$

$$+ \int\limits_s^\infty \varphi(s,\lambda)e(t,\lambda)f_1(t)dt$$

$$= \frac{e(s,\lambda)}{w(\lambda)\int_0^s\{-\varphi''(t,\lambda)+q(t)\varphi(t,\lambda)\}f_1(t)dt}$$

$$+ \frac{\varphi(s,\lambda)}{w(\lambda)}\int\limits_0^s\{-e''(t,\lambda)+q(t)e(t,\lambda)\}f_1(t)dt$$

$$= \frac{1}{\lambda^2 w(\lambda)}\left\{\int\limits_0^s \varphi(t,\lambda)[-f_1''(t)+q(t)f_1(t)]dt\right.$$

$$\left. + \int\limits_s^\infty e(t,\lambda)[-f_1''(t)+q(t)f_1(t)]dt\right\}$$

$$= \frac{W\{e(s,\lambda),\varphi(s,\lambda)\}}{\lambda^2 w(\lambda)}f_1(s) + \frac{1}{\lambda^2}\int\limits_0^\infty G(s,t,\lambda)\widehat{f_1(t)}\,dt$$

where

$$\widehat{f_1(t)} = -f_1''(t)+q(t)f_1(t).$$

Therefore, we can find

$$\int_0^\infty G(s,t,\lambda)f_1(t)\,dt = -\frac{f_1(s)}{\lambda^2} + \frac{1}{\lambda^2}\int_0^\infty G(s,t,\lambda)\widehat{f_1(t)}dt. \tag{3.6}$$

So

$$\xi(s,\lambda) = f_2\frac{e(s,\lambda)}{w(\lambda)} + \int_0^\infty G(s,t,\lambda)f_1(t)\,dt$$

$$= -\frac{f'_1(0)e(s,\lambda)}{\lambda^2 w(\lambda)} - \frac{f_1(s)}{\lambda^2} + \frac{1}{\lambda^2\int_0^\infty G(s,t,\lambda)\widehat{f_1(t)}\,dt}$$

$$= -\frac{f_1(s)}{\lambda^2}\left\{-\frac{f_1'(0)e(s,\lambda)}{w(\lambda)} + \int\limits_0^\infty G(s,t,\lambda)\widehat{f_1(t)}\,dt\right\}$$

Lemma is proved.

4. The Expansion Formula

In this section, we will obtain the expansion formula with respect to the eigenfunctions of discontinuous boundary value problem (1.1)-(1.3).

Let us denote the circle of radius R as Γ_R which center is zero and boundary contour is positive oriented. We let $\Gamma'_{R,\varepsilon}$ denote boundary contour positive oriented in plane

$D_1 = \{z: [z] \leq R, |Im\ Z| \geq \varepsilon\}$ and $\Gamma''_{R,\varepsilon}$ denote boundary contour negative oriented in plane $D_2 = \{z: [z] \leq R, |Im\ Z| \leq \varepsilon\}$.

Then with the properties of integration we can write

$$\int_{\Gamma'_{R,\varepsilon}} d\lambda = \int_{\Gamma_R} d\lambda + \int_{\Gamma''_{R,\varepsilon}} d\lambda$$

$$(4.1)$$

Now multiplying both sides of equality (3.6) with $\frac{\lambda}{2i\pi}$ and integrating counter Γ_R over λ we obtain

$$\frac{1}{2\pi i}\int_{\Gamma_R} \lambda\xi(s,\lambda)d\lambda = \frac{1}{2\pi i}\int_{\Gamma_R} \frac{f_1(s)}{\lambda}d\lambda + \frac{1}{2\pi i}\int_{\Gamma_R} \frac{z_1(s,\lambda)}{\lambda}d\lambda +$$
$$\frac{1}{2\pi i}\int_{\Gamma_R} \frac{z_2(s,\lambda)}{\lambda}d\lambda \qquad (4.2)$$

where $z_1(s,\lambda) = -\frac{f_1'(0)e(s,\lambda)}{w(\lambda)}$, $z_2(s,\lambda) = \int_0^\infty G(s,t,\lambda)\widehat{f_1(t)}dt$.

According to the equation (4.1) we obtain

$$\frac{1}{2\pi i}\int_{\Gamma'_{R,\varepsilon}} \lambda\xi(s,\lambda)d\lambda = \frac{1}{2\pi i}\int_{\Gamma_R} \lambda\xi(s,\lambda)d\lambda + \frac{1}{2\pi i}\int_{\Gamma''_{R,\varepsilon}} \lambda\xi(s,\lambda)d\lambda$$

$$(4.3)$$

By considering equation (4.2) into (4.3) we get

$$\frac{1}{2\pi i}\int_{\Gamma'_{R,\varepsilon}}\lambda\xi(s,\lambda)d\lambda = -\frac{1}{2\pi i}\int_{\Gamma_R}\frac{f_1(s)}{\lambda}d\lambda + \frac{1}{2\pi i}\int_{\Gamma_R}\frac{z_1(s,\lambda)}{\lambda}d\lambda +$$
$$\frac{1}{2\pi i}\int_{\Gamma_R}\frac{z_1(s,\lambda)}{\lambda}d\lambda$$

$$+\frac{1}{2\pi i}\int_{-R+i\varepsilon}^{R+i\varepsilon}\lambda\xi(s,\lambda)d\lambda + \frac{1}{2\pi i}\int_{R+i\varepsilon}^{R-i\varepsilon}\lambda\xi(s,\lambda)d\lambda$$
$$+\frac{1}{2\pi i}\int_{R-i\varepsilon}^{-R-i\varepsilon}\lambda\xi(s,\lambda)d\lambda$$
$$+\frac{1}{2\pi i}\int_{-R-i\varepsilon}^{-R+i\varepsilon}\lambda\xi(s,\lambda)d\lambda.$$

By taking limit as $R \to \infty$, $\varepsilon \to 0$ we get

$$\lim_{\substack{R\to\infty\\\varepsilon\to 0}}\frac{1}{2\pi i}\int_{\Gamma'_{R,\varepsilon}}\lambda\xi(s,\lambda)d\lambda$$

$$= -f_1 + \frac{1}{2\pi i}\int_{-\infty}^{\infty}\lambda[\xi(s,\lambda+i0)-\xi(\xi,\lambda-i0)]d\lambda.$$

On the other hand, using the residue theorem we can write

$$\frac{1}{2\pi i}\int_{\Gamma'_{R,\varepsilon}}\lambda\xi(s,\lambda)d\lambda = \sum_{k=1}^{n}\operatorname*{Res}_{\lambda=i\lambda_k}\lambda\xi(s,\lambda) + \sum_{k=1}^{n}\operatorname*{Res}_{\lambda=-i\lambda_k}\overline{\lambda\xi(s,\lambda}$$

From the last two equations we get

$$f_1(s) = -\sum_{k=1}^{n}\operatorname*{Res}_{\lambda=i\lambda_k}\lambda\xi(s,\lambda) - \sum_{k=1}^{n}\operatorname*{Res}_{\lambda=-i\lambda_k}\overline{\lambda\xi(s,\lambda)}$$

$$+\frac{1}{2\pi i}\int_{-\infty}^{\infty}\lambda[\xi(s,\lambda+i0)-\xi(s,\lambda-i0)]d\lambda \qquad (4.4)$$

Let $\psi(s,\lambda)$ be the solution of (1.1) satisfying the initial conditions

$\psi(0,\lambda) = 0$, $\psi'(0,\lambda) = 1$.

It is clear that $W\{\varphi(s,\lambda),\psi(s,\lambda)\} = \varphi'(0,\lambda)\psi(s,\lambda) - \varphi(0,\lambda)\psi'(0,\lambda) = 1$. Then for $Im\lambda > 0$

$e(s, \lambda)$ is written is the linear combination with the solutions of $\varphi(x, \lambda)$ and $\psi(x, \lambda)$ i.e.

$$e(s, \lambda) = c_1 \varphi(s, \lambda) + c_2 \psi(s, \lambda)$$

where $\quad c_1 = -e(0, \lambda)$, $c_2 = w(\lambda)$. Then get $\quad e(s, \lambda) = -e(0, \lambda)\varphi(s, \lambda) + w(\lambda)\psi(s, \lambda)$.

It is easy that

$$G(s, t, \lambda) = -\frac{1}{w(\lambda)} e(0, \lambda)\varphi(s, \lambda)\varphi(t, \lambda) + \begin{cases} \psi(s, \lambda)\varphi(t, \lambda), & t \leq s \\ \varphi(s, \lambda)\psi(t, \lambda), & t \geq s. \end{cases}$$

Then for $Im\lambda > 0$

$$\xi(s, \lambda) = \int_0^\infty G(s, t, \lambda)f_1(t) \, dt + f_2 \frac{e(s, \lambda)}{w(\lambda)}$$

$$= -\frac{e(0, \lambda)}{w(\lambda)} \int_0^\infty \varphi(s, \lambda)\varphi(t, \lambda)f_1(t)dt$$

$$+ \int_0^s \psi(s, \lambda)\varphi(t, \lambda)f_1(t)dt + \int_s^\infty \varphi(s, \lambda)\psi(t, \lambda)f_1(t)dt$$

$$- f_2 \frac{e(0, \lambda)\varphi(s, \lambda)}{w(\lambda)} + f_2 \psi(s, \lambda).$$

It follows that

$$\underset{\lambda = i\lambda_k}{Res} \lambda \xi(s, \lambda) = -\frac{i\lambda_k e(0, i\lambda_k)}{\dot{w}(i\lambda_k)} \int_0^\infty \varphi(s, i\lambda_k)\varphi(t, i\lambda_k)f_1(t)dt$$

$$- f_2 \frac{i\lambda_k e(0, i\lambda_k)\varphi(s, i\lambda_k)}{\dot{w}(i\lambda_k)}$$

$$\underset{\lambda = -i\lambda_k}{Res} \overline{\lambda \xi(s, \lambda)} = \frac{\overline{(\iota\lambda_k)}e(0, -i\lambda_k)}{\overline{\dot{w}}(-\iota\lambda_k)} \int_0^\infty \overline{\varphi(s, -\iota\lambda_k)} \; \overline{\varphi(t, -\iota\lambda_k)} \, f_1(t)dt$$

$$-f_2 \frac{\overline{(-\iota\lambda_k)} \ \overline{e(0,-\iota\lambda_k)} \ \overline{\varphi(s,-\iota\lambda_k)}}{\overline{\dot{w}(-\iota\lambda_k)}}$$

It can be seen that

$$\sum_{k=1}^{n} \operatorname*{Res}_{\lambda \,=\, i\lambda_k} \lambda\xi(s,\lambda) + \sum_{k=1}^{n} \operatorname*{Res}_{\lambda \,=\, -i\lambda_k} \overline{\lambda\xi(s,\lambda)}$$

$$= \sum_{k=1}^{n} \frac{-2i\lambda_k e(0,i\lambda_k)}{\dot{w}(i\lambda_k)} \int_0^{\infty} \varphi(s,i\lambda_k)\varphi(t,i\lambda_k)f_1(t)dt -$$
$$\sum_{k=1}^{n} \frac{2i\lambda_k \ f_2 \ e(0,i\lambda_k) \ \varphi(s,i\lambda_k)}{\dot{w}(i\lambda_k)} \tag{4.5}$$

Now let us calculate the integral

$$\frac{1}{2\pi i} \int_{-\infty}^{\infty} \lambda[\xi(s,\lambda+i0) - \xi(s,\lambda-i0)]d\lambda$$

$$= \frac{1}{2\pi i} \int_{-\infty}^{\infty} \lambda \frac{2i\lambda}{|w(\lambda)|^2} \int_0^{\infty} \varphi(s,\lambda) \overline{\varphi(t,\lambda)} f_1(t) \ dt \ d\lambda$$

$$+ \frac{1}{2\pi i} \int_{-\infty}^{\infty} \lambda \ f_2 \frac{2i\lambda \ \varphi(s,\lambda)}{|w(\lambda)|^2} d\lambda$$

$$=$$
$$\frac{2}{\pi} \int_0^{\infty} \frac{\lambda^2}{|w(\lambda)|^2} \varphi(s,\lambda) \int_0^{\infty} \overline{\varphi(t,\lambda)} f_1(t) \ dt \ d\lambda +$$
$$\frac{2f_2}{\pi} \int_0^{\infty} \frac{\lambda^2}{|w(\lambda)|^2} \varphi(s,\lambda)d\lambda$$
$$\tag{4.6}$$

By taking the equations (4.5) and (4.6) into (4.4), for the expansion of eigenfunctions of operator L we obtain the formula

$$f_1(s) = \sum_{k=1}^{n} \frac{2i\lambda_k e(0, i\lambda_k)}{\dot{w}(i\lambda_k)} \int_0^\infty \varphi(s, i\lambda_k)\varphi(t, i\lambda_k)f_1(t)dt$$

$$+ \sum_{k=1}^{n} \frac{2i\lambda_k \, f_2 e(0, i\lambda_k)\varphi(s, i\lambda_k)}{\dot{w}(i\lambda_k)}$$

$$+ \frac{2f_2}{\pi} \int_0^\infty \frac{\lambda^2}{|w(\lambda)|^2} \varphi(s, \lambda)d\lambda + \frac{2}{\pi} \int_0^\infty \frac{\lambda^2}{|w(\lambda)|^2} \varphi(s, \lambda) \int_0^\infty \overline{\varphi(t, \lambda)}f_1(t)dtd\lambda$$

$$(4.7)$$

Now let us write this formula with normalized eigenfunctions $u(x, \lambda)$ and $u(x, i\lambda_k)$

$$u(s, \lambda) = \overline{e(s, \lambda} - S(\lambda)e(s, \lambda), \quad -\infty < \lambda < \infty$$

$$u(s, i\lambda_k) = m_k e(s, i\lambda_k), \qquad\qquad k = \overline{1, n}$$

$$\frac{-2i\lambda\varphi(s,\lambda)}{w(\lambda)} = \overline{e(s, \lambda)} - S(\lambda)e(s, \lambda) = u(s, \lambda) \qquad (4.8)$$

$$\mu_k^{-2} = \frac{\dot{w}(i\lambda_k)e(0, i\lambda_k)}{2i\lambda_k}$$

From (4.8) we can write

$$\varphi(s, \lambda) = -\frac{u(s, \lambda)w(\lambda)}{2i\lambda}$$

Put this equation into (4.6) we get

$$\frac{1}{2\pi i} \int_{-\infty}^{\infty} \lambda[\xi(s, \lambda + i0) - \xi(s, \lambda - i0)]d\lambda$$

$$= \frac{2}{\pi} \int_0^{\infty} \frac{\lambda^2}{|w(\lambda)|^2}$$

$$- \frac{u(s, \lambda)w(\lambda)}{2i\lambda} \int_0^{\infty} - \frac{\overline{u(t, \lambda)}}{-2i\lambda} \overline{w(\lambda)} \, f_1(t)dtd\lambda$$

$$+ \frac{2}{\pi} f_2 \int_0^{\infty} \frac{\lambda^2}{|w(\lambda)|^2} - \frac{u(s, \lambda)w(\lambda)}{2i\lambda} d\lambda$$

$$= \frac{1}{2\pi} \int\limits_0^\infty \int\limits_0^\infty u(s,\lambda)\,\overline{u(t,\lambda)} f_1(t)\,dt\,d\lambda$$

$$+ \frac{f_2}{2\pi} \int\limits_0^\infty 2i\lambda \frac{u(s,\lambda)}{w(\lambda)}\,d\lambda.$$

Now examine the expression of residue;

$$u(s,i\lambda_k) = \mu_k e(s,i\lambda_k) = \left(\frac{2i\lambda_k}{\dot{w}(i\lambda_k)e(0,i\lambda_k)}\right)^{\frac{1}{2}} e(s,i\lambda_k)$$

$$e(s,\lambda) = -e(0,\lambda)\varphi(s,\lambda) \Longrightarrow \varphi(s,\lambda) = -\frac{e(s,\lambda)}{e(0,\lambda)}$$

can be written. So we obtain

$$\sum_{k=1}^n \frac{2i\lambda_k e(0,i\lambda_k)}{\dot{w}(i\lambda_k)} \int\limits_0^\infty \varphi(s,i\lambda_k)\varphi(t,i\lambda_k)f_1(t)\,dt$$

$$+ \sum_{k=1}^n \frac{2i\lambda_k\, f_2 e(0,i\lambda_k)\varphi(s,i\lambda_k)}{\dot{w}(i\lambda_k)}$$

$$= \sum_{k=1}^n \frac{2i\lambda_k e(0,i\lambda_k)}{\dot{w}(i\lambda_k)} \int\limits_0^\infty \frac{e(s,i\lambda_k)}{e(0,i\lambda_k)} \frac{e(t,i\lambda_k)}{e(0,i\lambda_k)} f_1(t)\,dt$$

$$+ \sum_{k=1}^n \frac{2i\lambda_k\, f_2 e(0,i\lambda_k)}{\dot{w}(i\lambda_k)} \frac{-e(s,i\lambda_k)}{e(0,i\lambda_k}$$

$$= \sum_{k=1}^n \int\limits_0^\infty u(s,i\lambda_k)u(t,i\lambda_k)f_1(t)\,dt + \sum_{k=1}^n f_1(0)\,\mu_k e(0,i\lambda_k)u(x,i\lambda_k)$$

If we write what we found in (4.7) we get the expansion of eigenfunctions

$$f_1(s) = \sum_{k=1}^{n} \int_0^{\infty} u(s, i\lambda_k) u(t, i\lambda_k) f_1(t) dt$$

$$+ f_1(0) \sum_{k=1}^{n} \mu_k e(0, i\lambda_k) u(s, i\lambda_k)$$

$$+ \frac{1}{2\pi} \int_0^{\infty} \int_0^{\infty} u(s, \lambda) \overline{u(t, \lambda)} f_1(t) dt + \frac{f_2}{2\pi} \int_0^{\infty} \frac{2i\lambda}{w(\lambda)} u(s, \lambda) d\lambda.$$

As a result we prove the following theorem:

Theorem: The expansion formula according to the eigenfunctions of the boundary value problem (1.1)-(1.3) is as follows:

$$F(s) = \binom{f_1(s)}{f_2} = \sum_{k=1}^{n} \langle F, U_k(s) \rangle U_k(s) + \frac{1}{2\pi} \int_0^{\infty} S(F, \lambda) U(s, \lambda) d\lambda,$$

where

$$U_k(s) = \binom{u(s, i\lambda_k)}{-u(0, i\lambda_k)}, \quad U(s, \lambda) = \binom{u(s, \lambda)}{-u(0, \lambda)}$$

and

$$S(F, \lambda) = \int_0^{\infty} f_1(t) \overline{u(t, \lambda)} dt + \frac{2i\lambda}{\omega(\lambda)} f_2.$$

References

Akcay, O. (2021). Inverse scattering problem for Sturm-Liouville operator with discontinuity conditions on the positive half line. *Int. J. Pure Appl. Sci.*, 7, 401-409.

Anderssen, R.S. (1997). The effect of discontinuous in density and shear velocity on the asymptotic overtone structure of torsional eigenfrequencies of the earth. *Geophys J. R. Astr. Soc.* 50, 303-309.

El-Reheem, Z. FA and Nasser, A. H. (2014). On the spectral investigation of the scattering problem for some version of one-dimensional Schrödinger equation with turning point, *Bound. Value Probl.*, 97, doi: 10.1186/1687-2770-2014-97.

Freiling, G. and Yurko, V.A. (2001). *Inverse Sturm-Liouville problems and their applications.* Huntington, NY: Nova Science Publishers Inc.

Gomilko, A. and Pivovarchik, V. (2002). On basis properties of a part of eigenfunctions of the problem of vibrations of a smooth inhomogeneous string damped at the midpoint. *Math. Nachr.* 245, 72-93.

Guseinov, I.M. and Pashaev, R.T. (2002). On an inverse problem for a second-order differential equation. *Usp. Mat. Nauk,* 57, 147-148.

Huseynov, H. M. and Osmanova, J. A. (2007). On jost solution of Sturm-Liouville equation with discontinuity conditions. *Trans. Natl. Acad. Sci. Azerb. Ser. Phys.-Tech. Math. Sci.*, 27(1), 63-70.

Huseynov, H. M. and Osmanli, J.A. (2009). Uniqueness of the solution of the inverse scattering problem for discontinuous Sturm-Liouville operator, *Trans. Acad. Sci. Azerb. Ser. Phys.-Tech. Math. Sci.*, 29, 43-50.

Huseynov, H.M. and Mammadova, L.I. (2013). The inverse scattering problem for Sturm-Liouville operator with discontinuity conditions on the semi-axis, *Proc. Inst. Math. Mech. Natl. Acad. Sci. Azerb.*, 39, 63-68.

Mamedov, K.R. and Palamut, N. (2009). On a direct problem of scattering theory for a class of Sturm-Liouville operator with discontinuous coefficient. *Proc. Jangjeon Math. Soc.,* 12, 243-251.

Mamedov, K.R. and Cetinkaya, F.A. (2015). Boundary value problem for a Sturm-Liouville operator with piecewise continuous coefficient. *Hacettepe Journal of Mathematics and Statistics*, 44(4), 867-874.

Mamedov, K.R., Kosar, N.P. and Cetinkaya, F.A. (2015). Inverse scattering problem for a piecewise continuous Sturm-Liouville equation with eigenparameter dependence in the boundary condition. *Proceedings of the Institute of Mathematics and Mechanics, National Academy of Sciences of Azerbaijan,* 41(1), 16-24.

Tikhonov, A.N. and Samarskii, A.A. (1990). *Equations of mathematical physics.* Dover, NewYork: Dover Books on Physics and Chemistry.

Titchmarsh, E.C. (1962). *Eigenfunctions Expansions*, Oxford.

Chapter 9

ON PYTHAGOREAN FUZZY SEMİ δ-SETS

Adem YOLCU[1]
Taha Yasin ÖZTÜRK[2]

1 Department of Mathematics, Faculty of Science and Letter, Kafkas University, Kars, Türkiye, yolcu.adem@gmail.com, ORCID: 0000-0002-4317-652X
2 Department of Mathematics, Faculty of Science and Letter, Kafkas University, Kars, Türkiye, taha36100@hotmail.com, ORCID: 0000-0003-2402-6507

1. INTRODUCTION

In 1965, Zadeh (Zadeh,1965) created fuzzy set theory to deal with unclear or imprecise information in decision making. Fuzzy set theory is distinguished by a membership function that assigns each target a membership value between 0 and 1. Chang (Chang,1968) explored fuzzy topological spaces and fundamental topological concepts including open set, closed set, and continuity. Later, Lowen (Lowen,1976;Lowen, 1977) conducted several investigations on fuzzy topological spaces. Atanassov (Atanassov,1986) introduced the intuitionistic fuzzy set (IFS), which includes the degree of non-membership ψ and the degree of membership φ in such a way that $\varphi + \psi \leq 1$. Coker (Coker,1997) proposed intuitionistic fuzzy topological spaces and investigated continuity and compactness. Several investigations were conducted on intuitionistic fuzzy topological spaces (Gou et.al.,2016;Hur et.al,2004;Saadati and Park,2006). Although intuitionistic fuzzy set theory is popular, in some pragmatic decision-making procedures, the total of degree of membership and degree of non-membership, in which an option that fits the requirements of competence is provided, can be more than one; nonetheless, their square sum is one or less.

Yager devised the Pythagorean fuzzy set (PFS) (Yager,2013). defined by a membership degree and a non-membership degree such that the square sum of its membership and non-membership degrees is less than or equal to 1. Clearly, PFS is more successful than IFS. Yager (Yager and Abbasov,2014) demonstrated this scenario with an example. An expert's support for participation in an alternative is $\frac{\sqrt{3}}{2}$ while his opposition to membership is $\frac{1}{2}$. Since the total of the two numbers is more than one. They are not available for IFS. However, they are eligible for PFS since $\left(\frac{\sqrt{3}}{2}\right)^2 + \left(\frac{1}{2}\right)^2 \leq 1$. PFS has been studied from various perspectives, including decision-making technologies (Ren et.al,2016;Zeng et.al,2016;Zhang and Xu,2014), aggregation operators (Garg, 2016a;Garg, 2019;Liang et.al,2015;Ma and Xu,2016), information measures (Garg, 2016b;Zhang, 2016), PFS extensions (Du et.al,2017;Liu et.al,2017;Peng,2019;Peng and Selvachandran,2019), and basic properties (Gou et.al,2016;Peng and Yang,2015;Yager,2013). In 2019, Olgun et al.

(Olgun et.al,2019) introduced pythagorean fuzzy topological spaces and examined their characteristics.

In this chapter, we initiate and define the topological structures of pythagorean fuzzy semi δ −open sets and pythagorean fuzzy semi-closed sets. We also investigate the properties of pythagorean fuzzy semi δ −interior, pythagorean fuzzy semi-closure, and discuss the relationship between them.

2. PRELIMINARIES

In this section, we will give some preliminary information for the present study.

Definition 2.1 *(Zadeh,1965) Let $\mathfrak{I}$ be an universe. A fuzzy set (FS for short) A in $\mathfrak{I}$, $A = \{(\varsigma, \varphi_A(\varsigma)): \varsigma \in \mathfrak{I}\}$, where $\mu_A: \mathfrak{I} \to 0,1]$ is the membership function of the fuzzy set A; $\varphi_A(\varsigma) \in 0,1]$ is the membership of $\varsigma \in \mathfrak{I}$ in A.*

Definition 2.2 *(Atanassov,1986) Let $\mathfrak{I}$ be a nonempty fixed set. An intuitionistic fuzzy set (IFS for short) A in $\mathfrak{I}$ is an object having the form $A = \{\langle \varsigma, \varphi_A(\varsigma), \psi_A(\varsigma) \rangle: \varsigma \in \mathfrak{I}\}$ where the functions $\varphi_A: \mathfrak{I} \to 0,1]$ and $\psi_A: \mathfrak{I} \to 0,1]$ denote the degree of membership ana the degree of nonmembership of each element $\varsigma \in \mathfrak{I}$ to the set A, respectively, and $0 \leq \mu_A(\varsigma) + \gamma_A(\varsigma) \leq 1$ for each $\varsigma \in \mathfrak{I}$.*

The degree of indeterminacy $I_A = 1 - \mu_A(\varsigma) - \gamma_A(\varsigma)$.

Definition 2.3 *(Yager,2013) Let $\mathfrak{I}$ be a universe of discourse. A pythagorean fuzzy set $\aleph$ in $\mathfrak{I}$ is given by $\aleph = \{\langle \varsigma, \varphi_\aleph(\varsigma), \psi_\aleph(\varsigma) \rangle: \varsigma \in \mathfrak{I}\}$ where the functions $\varphi_\aleph(\varsigma): \mathfrak{I} \to 0,1]$ denotes the degree of membership and $\psi_\aleph(\varsigma): \mathfrak{I} \to 0,1]$ denotes the degree of nonmembership of the element $\varsigma \in \mathfrak{I}$ to the set $\aleph$, respectively, with the condition that $0 \leq (\varphi_\aleph(\varsigma))^2 + (\psi_\aleph(\varsigma))^2 \leq 1$.*

The degree of indeterminacy $I_\aleph = \sqrt{1 - (\varphi_\aleph(\varsigma))^2 - (\psi_\aleph(\varsigma))^2}$.

Definition 2.4 *(Yager,2013) Let* $\aleph_1 = \{\langle \varsigma, \varphi_{\aleph_1}(\varsigma), \psi_{\aleph_1}(\varsigma) \rangle \colon \varsigma \in \mathfrak{I}\}$ *and* $\aleph_2 = \{\langle \varsigma, \varphi_{\aleph_2}(\varsigma), \psi_{\aleph_2}(\varsigma) \rangle \colon \varsigma \in \mathfrak{I}\}$ *be two pythagorean fuzzy sets over* $\mathfrak{I}$. *Then,*

1. the pythagorean fuzzy complement of $\aleph_1$ is defined by

$$\aleph_1^c = \{\langle \varsigma, \psi_{\aleph_1}(\varsigma), \varphi_{\aleph_1}(\varsigma) \rangle \colon \varsigma \in \mathfrak{I}\},$$

2. the pythagorean fuzzy intersection of $\aleph_1$ and $\aleph_2$ is defined by

$$\aleph_1 \cap \aleph_2 = \{\langle \varsigma, \min\{\varphi_{\aleph_1}(\varsigma), \varphi_{\aleph_2}(\varsigma)\}, \max\{\psi_{\aleph_1}(\varsigma), \psi_{\aleph_2}(\varsigma)\} \rangle \colon \varsigma \in \mathfrak{I}\},$$

3. the pythagorean fuzzy union of $\aleph_1$ and $\aleph_2$ is defined by

$$\aleph_1 \cup \aleph_2 = \{\langle \varsigma, \max\{\varphi_{\aleph_1}(\varsigma), \varphi_{\aleph_2}(\varsigma)\}, \min\{\psi_{\aleph_1}(\varsigma), \psi_{\aleph_2}(\varsigma)\} \rangle \colon \varsigma \in \mathfrak{I}\},$$

we say $\aleph_1$ is a pythagorean fuzzy subset of $\aleph_2$ and we write $\aleph_1 \subseteq \aleph_2$ if $\varphi_{\aleph_1}(\varsigma) \leq \varphi_{\aleph_2}(\varsigma)$ and $\psi_{\aleph_1}(\varsigma) \geq \psi_{\aleph_2}(\varsigma)$ for each $\varsigma \in \mathfrak{I}$, $0_{\mathfrak{I}} = \{\langle \varsigma, 0, 1 \rangle \colon \varsigma \in \mathfrak{I}\}$ and $1_{\mathfrak{I}} = \{\langle \varsigma, 1, 0 \rangle \colon \varsigma \in \mathfrak{I}\}$.

Definition 2.5 *(Olgun et.al.,2019) Let* $\mathfrak{I} \neq \emptyset$ *be a set and* $\tilde{\tau}$ *be a family of pythagorean fuzzy subsets of* $\mathfrak{I}$. *If*

1. $0_{\mathfrak{I}}$, $1_{\mathfrak{I}} \in \tilde{\tau}$,
2. for any $\aleph_1$, $\aleph_2 \in \tilde{\tau}$, we have $\aleph_1 \cap \aleph_2 \in \tilde{\tau}$,
3. for any $\{\aleph_i\}_{i \in I} \subseteq \tilde{\tau}$, we have $\underset{i \in I}{\cup} \aleph_i \in \tilde{\tau}$

then $\tilde{\tau}$ is called a pythagorean fuzzy topology on $\mathfrak{I}$ and the pair $(\mathfrak{I}, \tilde{\tau})_p$ is said to be a pythagorean fuzzy topological space ($PFTS$ for short).Each member of $\tilde{\tau}$ is called a pythagorean fuzzy open set ($PFOS$ for short). The complement of a pythagorean fuzzy open set is called a pythagorean fuzzy closed set ($PFCS$ for short).

Remark 2.1 *As any fuzzy set or intuitionistic fuzzy set can be considered as a pythagorean fuzzy set, we observe that any fuzzy topological space or intuitionistic fuzzy topological space is a pythagorean fuzzy topological space as well. Conversely, it is obvious that pythagorean fuzzy topological space needs not to be a fuzzy topological space or intuitionistic fuzzy topological space. Even a pythagorean fuzzy open set may be neither a fuzzy set nor an intuitionistic fuzzy set (see following example).*

Example 2.1 *(Olgun et.al.,2019) Let $\Im = \{\varsigma_1, \varsigma_2\}$. Consider the following family of pythagorean fuzzy subsets $\tilde{\tau} = \{0_\Im, 1_\Im, \aleph_1, \ldots, \aleph_5\}$ where*

$$\aleph_1 = \{\langle \varsigma_1, 0.5, 0.7 \rangle, \langle \varsigma_2, 0.2, 0.4 \rangle\},$$

$$\aleph_2 = \{\langle \varsigma_1, 0.6, 0.5 \rangle, \langle \varsigma_2, 0.3, 0.9 \rangle\},$$

$$\aleph_3 = \{\langle \varsigma_1, 0.4, 0.8 \rangle, \langle \varsigma_2, 0.1, 0.95 \rangle\},$$

$$\aleph_4 = \{\langle \varsigma_1, 0.6, 0.5 \rangle, \langle \varsigma_2, 0.3, 0.4 \rangle\},$$

$$\aleph_5 = \{\langle \varsigma_1, 0.5, 0.7 \rangle, \langle \varsigma_2, 0.2, 0.9 \rangle\}.$$

Observe that $(\Im, \tilde{\tau})_p$ is a pythagorean fuzzy topological space.

Definition 2.6 *(Olgun et.al.,2019) Let $\Im$ and Y be two non-empty sets, let $f : \Im \to Y$ be a function and let A and B be Pythagorean fuzzy subsets of $\Im$ and Y, respectively. Then, the membership and non-membership functions of image of A with respect to f that is denoted by $f[A]$ are defined by*

$$\mu_{f[A]}(y) = \begin{cases} \sup_{z \in f^{-1}(y)} \mu_A(z), & \text{if } f^{-1}(y) \neq \emptyset \\ 0, & \text{otherwise} \end{cases}$$

and

$$v_{f[A]}(y) = \begin{cases} \inf_{z \in f^{-1}(y)} v_A(z), & \text{if } f^{-1}(y) \neq \emptyset \\ 0, & \text{otherwise} \end{cases}$$

respectively. The membership and non-membership functions of pre-image of B with respect to f that is denoted by $f^{-1}[B]$ are defined by

$$\mu_{f^{-1}[B]}(\varsigma) = \mu_B(f(\varsigma)) \qquad \text{and} \qquad \nu_{f^{-1}[B]}(\varsigma) = \nu_B(f(\varsigma))$$

respectively.

In the study [16], they showed that $\mu_{f[A]}^2 + \nu_{f[A]}^2 \leq 1$ pythagorean fuzzy membership condition is provide for pythagorean fuzzy image and pre-image.

Proposition 2.1 *(Olgun et.al.,2019) Let $\Im$ and Y be two non-empty sets and $f: \Im \rightarrow Y$ be a pythagorean fuzzy function. Then, we have*

1. $f^{-1}[B^c] = (f^{-1}[B])^c$ for any pythagorean fuzzy subset B of Y.

2. $(f[A])^c \subseteq f[A^c]$ for any pythagorean fuzzy subset A of $\Im$.

3. If $B_1 \subseteq B_2$ then $f^{-1}[B_1] \subseteq f^{-1}[B_2]$ where B_1 and B_2 are pythagorean fuzzy subset of Y.

4. If $A_1 \subseteq A_2$ then $f[A_1] \subseteq f[A_2]$ where A_1 and A_2 are pythagorean fuzzy subset of $\Im$.

5. $f[f^{-1}[B]] \subseteq B$ for any pythagorean fuzzy subset B of Y.

6. $A \subseteq f^{-1}[f[A]]$ for any pythagorean fuzzy subset A of $\Im$.

Definition 2.7 *(Olgun et.al.,2019) Let $(\Im, \tilde{\tau}_1)_p$ and $(Y, \tilde{\tau}_2)_p$ be two pythagorean fuzzy topological spaces and $f: \Im \rightarrow Y$ be a pythagorean fuzzy function. Then, f is said to be pythagorean fuzzy continuous if for any pythagorean fuzzy subset A of $\Im$ and for any neighbourhood V of $f[A]$ there exists a neighbourhood U of A such that $f[U] \subseteq V$.*

Theorem 2.1 *(Olgun et.al.,2019) Let $(\Im, \tilde{\tau}_1)_p$ and $(Y, \tilde{\tau}_2)_p$ be two pythagorean fuzzy topological spaces. A function $f: \Im \rightarrow Y$ is pythagorean fuzzy continuous iff for each open (closed) pythagorean fuzzy subset B of*

Y we have $f^{-1}[B]$ is an open (closed) pythagorean fuzzy subset of $\mathfrak{I}$.

Definition 2.8 *(Ozturk and Yolcu,2020) Let* $(\mathfrak{I}, \tilde{\tau})_p$ *be a PFTS and* $\aleph = \{\langle \varsigma, \varphi_\aleph(\varsigma), \psi_\aleph(\varsigma) \rangle : \varsigma \in \mathfrak{I}\}$ *be a PFS over* $\mathfrak{I}$. *Then the pythagorean fuzzy interior, pythagorean fuzzy closure and pythagorean fuzzy boundary of* $\aleph$ *are defined by;*

1. $int(\aleph) = \cup \{G : G \text{ is a } PFOS \text{ in } \mathfrak{I} \text{ and } G \subseteq \aleph\}$,
2. $cl(\aleph) = \cap \{K : K \text{ is a } PFCS \text{ in } \mathfrak{I} \text{ and } \aleph \subseteq K\}$,
3. $Fr(\aleph) = cl(\aleph) \cap cl(\aleph^c)$.

It is clear that,

1. $int(\aleph)$ is the biggest pythagorean fuzzy open set contained $\aleph$,
2. $cl(\aleph)$ is the smallest pythagorean fuzzy closed set containing $\aleph$.

Proposition 2.2 *(Ozturk and Yolcu,2020)Let* $(\mathfrak{I}, \tilde{\tau})_p$ *be a PFTS and* $\aleph$, $\aleph_1$, $\aleph_2$ *be PFSs over* $\mathfrak{I}$. *Then the following properties hold;*

1. $int(\aleph) \subseteq \aleph$,
2. $int(int(\aleph)) = int(\aleph)$,
3. $\aleph_1 \subseteq \aleph_2 \Rightarrow int(\aleph_1) \subseteq int(\aleph_2)$,
4. $int(\aleph_1 \cap \aleph_2) = int(\aleph_1) \cap int(\aleph_2)$,
5. $int(1_\mathfrak{I}) = 1_\mathfrak{I}$, $int(0_\mathfrak{I}) = 0_\mathfrak{I}$.

Proposition 2.3 *(Ozturk and Yolcu,2020)Let* $(\mathfrak{I}, \tilde{\tau})_p$ *be a PFTS and* $\aleph$, $\aleph_1$, $\aleph_2$ *be PFSs over* $\mathfrak{I}$. *Then the following properties hold;*

1. $\aleph \subseteq cl(\aleph)$,
2. $cl(cl(\aleph)) = cl(\aleph)$,
3. $\aleph_1 \subseteq \aleph_2 \Rightarrow cl(\aleph_1) \subseteq cl(\aleph_2)$,
4. $cl(\aleph_1 \cup \aleph_2) = cl(\aleph_1) \cup cl(\aleph_2)$,
5. $cl(1_\mathfrak{I}) = 1_\mathfrak{I}$, $cl(0_\mathfrak{I}) = 0_\mathfrak{I}$.

Theorem 2.2 *(Ozturk and Yolcu,2020) Let* $(\mathfrak{I}, \tilde{\tau})_p$ *be a PFTS and* $\aleph$ *be*

a PFS over $\mathfrak{I}$. Then,

1. $cl(\aleph^c) = \big(int(\aleph)\big)^c,$
2. $int(\aleph^c) = \big(cl(\aleph)\big)^c.$

3. Main Results

Definition 3.1 *Let $(\mathfrak{I}, \tilde{\tau})_p$ be a pythagorean fuzzy topological space over $\mathfrak{I}$ and $\Sigma \tilde{\subseteq} PFS(\mathfrak{I})$. If there exists a pythagorean fuzzy open set $\aleph$ such that $\aleph \tilde{\subseteq} \Sigma \tilde{\subseteq} pcl(\aleph)$, then Σ is called pythagorean fuzzy semi $\delta -open$ set over $\mathfrak{I}$.*

Definition 3.2 *Let $(\mathfrak{I}, \tilde{\tau})_p$ be a pythagorean fuzzy topological space over $\mathfrak{I}$ and $\Sigma \tilde{\subseteq} PFS(\mathfrak{I})$. Σ is pythagorean fuzzy semi $\delta -closed$ set if and only if its complement Σ^c is pythagorean fuzzy semi $\delta -open$ set.*

Remark 3.1 *It is obvious that a pythagorean fuzzy open set is pythagorean fuzzy semi $\delta -open$ set. But the converse is not true in general. This is shown in following example.*

Example 3.1 *Let $\mathfrak{I} = \{\varsigma_1, \varsigma_2\}$ and*

$$\tilde{\tau} = \big\{\tilde{0}_{\mathfrak{I}}, \tilde{1}_{\mathfrak{I}}, \aleph_1, \aleph_2, \aleph_3\big\}$$

where $(\aleph_1, E), (\aleph_2, E), (\aleph_3, E)$ pythagorean fuzzy sets over $\mathfrak{I}$, defined as;

$$\aleph_1 = \{((\varsigma_1, 0.3, 0.7), (\varsigma_2, 0.4, 0.8))\}$$

$$\aleph_2 = \{((\varsigma_1, 0.5, 0.3), (\varsigma_2, 0.5, 0.6))\}$$

$$\aleph_3 = \{((\varsigma_1, 0.6, 0.2), (\varsigma_2, 0.6, 0.3))\}$$

It is clear that $\tilde{\tau}$ is a pythagorean fuzzy topological spaces and $(\mathfrak{I}, \tilde{\tau})_p$ is pythagorean fuzzy topological spaces. The pythagorean fuzzy closed sets as follow;

$$\left(\tilde{0}_{\Im}\right)^{c} = \tilde{1}_{\Im}$$

$$\left(\tilde{1}_{\Im}\right)^{c} = \tilde{0}_{\Im}$$

$$\aleph_{1}^{c} = \{(\varsigma_{1}, 0.7, 0.3), \varsigma_{2}, (0.8, 0.4)\}$$

$$\aleph_{2}^{c} = \{(\varsigma_{1}, 0.3, 0.5), (\varsigma_{2}, 0.6, 0.5)\}$$

$$\aleph_{3}^{c} = \{(\varsigma_{1}, 0.2, 0.6), (\varsigma_{2}, 0.3, 0.6)\}$$

Now we consider a pythagorean fuzzy set Σ over $\Im$ defined by,

$$\Sigma = \{(\varsigma_{1}, 0.4, 0.5), (\varsigma_{2}, 0.7, 0.6)\}$$

Then there exist a pythagorean fuzzy open set $\aleph_{2}$ such that $\aleph_{2} \subseteq \Sigma \subseteq pcl\aleph_{2} = \aleph_{1}^{c}$.

Hence Σ is a pythagorean fuzzy semi δ − open set, but Σ is not pythagorean fuzzy open set.

Proposition 3.1 *Let* $(\Im, \tilde{\tau})_{p}$ *be a pythagorean fuzzy topological space over* $\Im$ *and* $\aleph \subseteq PFS(\Im)$. *Then* $\aleph$ *is pythagorean fuzzy semi* δ −*open set if and only if* $\aleph \subseteq pcl(pint\aleph)$.

Proof. ($\Rightarrow$)Suppose that $\aleph$ is pythagorean fuzzy semi δ −open set, then there exists a pythagorean fuzzy open set Σ such that $\Sigma \subseteq \aleph \subseteq pcl(\Sigma)$. Now $\Sigma \subseteq pint\aleph$ implies that $pcl(\Sigma) \subseteq pcl(pint\aleph)$. Therefore (

$$(\aleph, E) \subseteq pcl(\Sigma) \subseteq pcl(pint\aleph)$$

.

($\Leftarrow$) Suppose that $\aleph \subseteq pcl(pint\aleph)$. Take $\Sigma = pint\aleph$, we have

$$\Sigma \subseteq \aleph \subseteq pcl(\Sigma)$$

This complete this proof.

Theorem 3.1 *Let* $(\mathfrak{I}, \tilde{\tau})_p$ *be a pythagorean fuzzy topological space over* $\mathfrak{I}$. *Then an arbitrary union of pythagorean fuzzy semi* $\delta -open$ *sets is pythagorean fuzzy semi* $\delta -open$ *set.*

Proof. Let $\{\aleph_i : i \in I\}$ be a collection of pythagorean fuzzy semi $\delta -open$ sets and $\Sigma = \underset{i \in I}{\cup} \aleph_i$. Since each $\aleph_i$ is PFS semi $\delta -open$, then there exist a pythagorean fuzzy open set Σ_i such that $\Sigma_i \tilde{\subseteq} \aleph_i \tilde{\subseteq} pclS_i$ and so $\underset{i \in I}{\cup} \Sigma_i \tilde{\subseteq} \underset{i \in I}{\cup} \aleph_i \tilde{\subseteq} \underset{i \in I}{\cup} pclS_i \tilde{\subseteq} pcl\left(\underset{i \in I}{\cup} \Sigma_i \right)$. Let $\Sigma = \underset{i \in I}{\cup} \Sigma_i$. Then Σ is pythagorean fuzzy open and $\Sigma \tilde{\subseteq} \underset{i \in I}{\cup} \aleph_i \tilde{\subseteq} pclS$. Therefore, $\underset{i \in I}{\cup} \aleph_i$ is a pythagorean fuzzy semi $\delta -open$ set.

Corollary 3.1 *Let* $(\mathfrak{I}, \tilde{\tau})_p$ *be a pythagorean fuzzy topological space over* $\mathfrak{I}$. *Then the family of all pythagorean fuzzy semi* $\delta -open$ *sets are a pythagorean fuzzy supra topology on* $\mathfrak{I}$.

Proposition 3.2 *Let* $\aleph$ *be a pythagorean fuzzy semi* $\delta -open$ *set and* Σ *be a pythagorean fuzzy set in* $(\mathfrak{I}, \tilde{\tau})_p$. *Suppose* $\aleph \tilde{\subseteq} \Sigma \tilde{\subseteq} pcl\aleph$. *Then* Σ *is a pythagorean fuzzy semi* $\delta -open$ *set over* $\mathfrak{I}$.

Proof. $\aleph$ be a pythagorean fuzzy semi $\delta -open$ set implies that there exist a pythagorean fuzzy open set Σ such that $\Sigma \tilde{\subseteq} \aleph \tilde{\subseteq} pclS$. Now $\Sigma \tilde{\subseteq} \Sigma$ and $pcl\aleph \tilde{\subseteq} pclS$ implies that $\Sigma \tilde{\subseteq} pclS$. Therefore $\Sigma \tilde{\subseteq} \Sigma \tilde{\subseteq} pclS$. Hence Σ is a pythagorean fuzzy semi $\delta -open$ set in $\mathfrak{I}$.

Proposition 3.3 *Let* $(\mathfrak{I}, \tilde{\tau})_p$ *be a pythagorean fuzzy topological space over* $\mathfrak{I}$ *and* $\aleph \tilde{\subseteq} PFS(\mathfrak{I})$. *Then* $\aleph$ *is pythagorean fuzzy semi* $\delta -closed$ *if and only if there exist a pythagorean fuzzy closed set* Σ *such that* $pint(\Sigma) \tilde{\subseteq} \aleph \tilde{\subseteq} \Sigma$.

Proof. This proof is clear that from the definition of pythagorean fuzzy semi $\delta -closed$ set.

Proposition 3.4 *Every pythagorean fuzzy closed set is pythagorean fuzzy semi* $\delta -closed$ *set in a pythagorean fuzzy topological spaces* $(\mathfrak{I}, \tilde{\tau})_p$.

Proof. Straightforward.

Remark 3.2 *The converse of Proposition 3.4 may not be provide in general. It is shown in following example.*

Example 3.2 *Consider the Example 3.1.*

$$\Sigma^c = \{(\varsigma_1, 0.5, 0.4), (\varsigma_2, 0.6, 0.7)\}$$

is pythagorean fuzzy semi $\delta-$closed set. But Σ^c is not pythagorean fuzzy closed set.

Theorem 3.2 *Let $(\mathfrak{I}, \tilde{\tau})_p$ be a pythagorean fuzzy topological space over $\mathfrak{I}$ and $\aleph \in PFS(\mathfrak{I})$. Then $\aleph$ is pythagorean fuzzy semi $\delta-$closed set if and only if $pint(pcl\aleph) \widetilde{\subseteq} \aleph$.*

Proof. ($\Rightarrow$) Suppose that $\aleph$ is a pythagorean fuzzy closed set, then by Proposition 6, there exists a pythagorean fuzzy closed set Σ such that $pint(\Sigma) \widetilde{\subseteq} \aleph \widetilde{\subseteq} \Sigma$. This follows that $pcl\aleph \widetilde{\subseteq} pcl(\Sigma) = \Sigma$. Thus $pint(pcl\aleph) \widetilde{\subseteq} pint(\Sigma)$. Therefore, $pint(pcl\aleph) \widetilde{\subseteq} pint(\Sigma) \widetilde{\subseteq} \aleph$.

($\Leftarrow$) Suppose that $\aleph$ be a pythagorean fuzzy set in $(\mathfrak{I}, \tilde{\tau})_p$ such that $pint(pcl\aleph) \widetilde{\subseteq} \aleph$. We take $pcl\aleph = \Sigma$. Then $pint(\Sigma) \widetilde{\subseteq} \aleph \widetilde{\subseteq} \Sigma$. This implies that $\aleph$ is a pythagorean fuzzy semi $\delta-$closed set.

Theorem 3.3 *Let $(\mathfrak{I}, \tilde{\tau})_p$ be a pythagorean fuzzy topological space over $\mathfrak{I}$. Then an arbitrary intersection of pythagorean fuzzy semi $\delta-$closed sets is pythagorean fuzzy semi $\delta-$closed set.*

Proof. Suppose that $\{\aleph_i : i \in I\}$ be a collection of pythagorean fuzzy semi $\delta-$closed sets. Since each $i \in I$, $\aleph_i$ is a pythagorean fuzzy semi $\delta-$closed set, then by Proposition 6, there exist a pythagorean fuzzy closed set (G_i, E) such that $pint(G_i, E) \widetilde{\subseteq} \aleph_i \widetilde{\subseteq} (G_i, E)$. This follows that $\underset{i \in I}{\cap}(pint(G_i, E)) \widetilde{\subseteq} \underset{i \in I}{\cap} \aleph_i \widetilde{\subseteq} \underset{i \in I}{\cap} (G_i, E)$. We take $\underset{i \in I}{\cap} (G_i, E) = \Sigma$. Then by Theorem 3.2, Σ is a pythagorean fuzzy closed set and hence $\underset{i \in I}{\cap} \aleph_i$ is a pytahgorean fuzzy semi $\delta-$closed set.

Theorem 3.4 *Let $(\mathfrak{I}, \tilde{\tau})_p$ be a pythagorean fuzzy topological space over $\mathfrak{I}$, $\aleph$ be a pythagoren fuzzy semi $\delta-$closed set and Σ be a pythagorean fuzzy set over $\mathfrak{I}$. If $pint\aleph \widetilde{\subseteq} \Sigma \widetilde{\subseteq} \aleph$, then Σ is a pythagorean fuzzy semi $\delta-$closed set.*

Proof. Since $\aleph$ is a pythagorean fuzzy semi $\delta-$closed set, then by Prosoposition 6, tehere exists an pythagorean fuzzy closed set Σ such that $pintS \widetilde{\subseteq} \aleph \widetilde{\subseteq} \Sigma$. Then $\Sigma \widetilde{\subseteq} \Sigma$. Also $pint(pintS) = pintS \widetilde{\subseteq} pint\aleph$. This implies that $pintS \widetilde{\subseteq} \Sigma$.

Therefore, $pintS \widetilde{\subseteq} \Sigma \widetilde{\subseteq} \Sigma$. Hence Σ is a pythagorean fuzzy semi $\delta-$closed set.

Definition 3.3 *Let* $(\mathfrak{I}, \tilde{\tau})_p$ *be a pythagorean fuzzy topological space over* $\mathfrak{I}$ *and* $\aleph \in PFS(\mathfrak{I})$.

1. The pythagorean fuzzy semi $\delta-$interior of $\aleph$, denoted by $s\delta pint\aleph$, is the union of all the pythagorean fuzzy semi $\delta-$open sets contained in $\aleph$.

Clearly, $s\delta pint\aleph$ is the largest pythagorean fuzzy semi $\delta-$open set over $\mathfrak{I}$ contained in $\aleph$.

2. The pythagorean fuzzy semi $\delta-$closure of $\aleph$, denoted by $s\delta pcl\aleph$, is the intersection of all the pythagorean fuzzy semi $\delta-$closed sets contains $\aleph$.

Clearly, $s\delta pcl\aleph$ is the smallest pythagorean fuzzy semi $\delta-$closed set over $\mathfrak{I}$ which contains $\aleph$.

Remark 3.3 *It is clear that, If* $\aleph$ *be a pythagorean fuzzy set, then*

$$pint\aleph \widetilde{\subseteq} s\delta pint\aleph \widetilde{\subseteq} \aleph \widetilde{\subseteq} s\delta pcl\aleph \widetilde{\subseteq} pcl\aleph$$

Theorem 3.5 *Let* $(\mathfrak{I}, \tilde{\tau})_p$ *be a pythagorean fuzzy topological space over* $\mathfrak{I}$ *and* $\aleph, \Sigma \in PFS(\mathfrak{I})$. *Then,*

1. $s\delta pint(\tilde{0}_{\mathfrak{I}}) = s\delta pcl(\tilde{0}_{\mathfrak{I}}) = \tilde{0}_{\mathfrak{I}}$ and $s\delta pint(\tilde{1}_{\mathfrak{I}}) = s\delta pcl(\tilde{1}_{\mathfrak{I}}) = \tilde{1}_{\mathfrak{I}}$,

2. $\aleph$ is a pythagorean fuzzy semi $\delta-$open(semi $\delta-$closed) set if and only if $s\delta pint\aleph = \aleph$ $(s\delta pcl\aleph = \aleph)$.

3. $s\delta pint(s\delta pint\aleph) = \aleph$.

4. $\aleph \widetilde{\subseteq} \Sigma$ implies $s\delta pint\aleph \widetilde{\subseteq} spintS$ and $s\delta pcl\aleph \widetilde{\subseteq} spclS$,

5. (i) $s\delta pint\aleph \widetilde{\cap}_E spintS = s\delta pint(\aleph \widetilde{\cap}_E \Sigma)$

  (ii) $s\delta pcl\aleph \widetilde{\cap}_E spclS \widetilde{\supseteq} s\delta pcl(\aleph \widetilde{\cap}_E \Sigma)$

6. $s\delta pint\aleph \widetilde{\cup}_E spintS \widetilde{\subseteq} s\delta pint(\aleph \widetilde{\cup}_E \Sigma)$

    $s\delta pcl\aleph \widetilde{\cup}_E spclS = s\delta pcl(\aleph \widetilde{\cup}_E \Sigma)$

Proof. (1)-(4) follow directly from the definition of pythagorean fuzzy semi δ −interior and pythagorean fuzzy semi δ −closure .

(5) (i) By (4), we have $(\aleph \widetilde{\cap}_E \Sigma) \widetilde{\subseteq} \aleph$, $(\aleph \widetilde{\cap}_E \Sigma) \widetilde{\subseteq} \Sigma$ implies

$$s\delta pint(\aleph \widetilde{\cap}_E \Sigma) \widetilde{\subseteq} s\delta pint\aleph, s\delta pint(\aleph \widetilde{\cap}_E \Sigma) \widetilde{\subseteq} spintS,$$

so that $s\delta pint(\aleph \widetilde{\cap}_E \Sigma) \widetilde{\subseteq} s\delta pint\aleph \widetilde{\cap}_E spintS$. Also, since $s\delta pint\aleph \widetilde{\subseteq} \aleph$ and $spintS \widetilde{\subseteq} \Sigma$ implies $s\delta pint\aleph \widetilde{\cap}_E spintS \widetilde{\subseteq} (\aleph \widetilde{\cap}_E \Sigma)$.

Thus $s\delta pint\aleph \widetilde{\cap}_E spintS$ is a pythagorean fuzzy semi δ −open subsets of $(\aleph \widetilde{\cap}_E \Sigma)$. Hence $s\delta pint\aleph \widetilde{\cap}_E spintS \widetilde{\subseteq} s\delta pint(\aleph \widetilde{\cap}_E \Sigma)$. Thus $s\delta pint\aleph \widetilde{\cap}_E spintS = (\aleph \widetilde{\cap}_E \Sigma)$.

(ii) By (4), we have $(\aleph \widetilde{\cap}_E \Sigma) \widetilde{\subseteq} \aleph$, $(\aleph \widetilde{\cap}_E \Sigma) \widetilde{\subseteq} \Sigma$ implies

$$s\delta pcl(\aleph \widetilde{\cap}_E \Sigma) \widetilde{\subseteq} s\delta pcl\aleph, s\delta pcl(\aleph \widetilde{\cap}_E \Sigma) \widetilde{\subseteq} spclS,$$

so that $s\delta pcl(\aleph \widetilde{\cap}_E \Sigma) \widetilde{\subseteq} s\delta pcl\aleph \widetilde{\cap}_E spclS$.

(6) The proof is similar to (5) by using property that $\aleph \widetilde{\subseteq} (\aleph \widetilde{\cup}_E \Sigma)$, $\Sigma \widetilde{\subseteq} (\aleph \widetilde{\cup}_E \Sigma)$.

Theorem 3.6 *Let* $(\mathfrak{I}, \widetilde{\tau})_p$ *be a pythagorean fuzzy topological space over* $\mathfrak{I}$ *and* $\aleph \in PFS(\mathfrak{I})$. *Then,*

1. $(s\delta pint\aleph)^c = s\delta pcl(\aleph^c)$.

2. $(pcl\aleph)^c = s\delta pint(\aleph^c)$.

3. $s\delta pint(pint\aleph) = pint(s\delta pint\aleph) = pint\aleph$.

4. $s\delta pcl(pcl\aleph) = pcl(s\delta pcl\aleph) = pcl\aleph$.

Proof. (1) $s\delta pint\aleph \cong \aleph$ implies that $\aleph^c \cong (s\delta pint\aleph)^c$. Now by Theorem 7 (2), and since $(s\delta pint\aleph)^c$ is a pythagorean fuzzy semi δ −closed set, we have $s\delta pcl(\aleph^c) \cong s\delta pcl((s\delta pint\aleph)^c) = (s\delta pint\aleph)^c$. For the reverse inclusion, $\aleph^c \cong s\delta pcl(\aleph^c)$ implies that $(s\delta pcl(\aleph^c))^c \cong (\aleph^c)^c = \aleph$. $s\delta pcl(\aleph^c)$ being pythagorean fuzzy semi $\delta -$ closed implies that $(s\delta pcl(\aleph^c))^c$ is pythagorean fuzzy semi $\delta -$ open. Thus $(s\delta pcl(\aleph^c))^c \cong s\delta pint\aleph$ and hence $(s\delta pint\aleph)^c \cong ((s\delta pcl(\aleph^c))^c)^c = s\delta pcl(\aleph^c)$.

(2) It is similar to (1).

(3) By Remark 2, $pint\aleph$ is a pythagorean fuzzy open set implies that it is pythagorean fuzzy semi δ −open set. Therefore, by Theorem 7(2), $s\delta pint(pint\aleph) = pint\aleph$. $pint\aleph \cong s\delta pint\aleph = \aleph$. This implies that $s\delta pint(pint\aleph) = pint\aleph$.

(4) $pcl\aleph$ is pythagorean fuzzy closed set implies that it is pythagorean fuzzy semi $\delta -$ closed. Therefore $s\delta pcl(pcl\aleph) = pcl\aleph$. Then $\aleph \cong s\delta pcl\aleph \cong pcl\aleph$. Hence $s\delta pcl\aleph \cong pcl(s\delta pcl\aleph) \cong s\delta pcl\aleph$. This implies that $pcl(s\delta pcl\aleph) = pcl\aleph$.

4. Conclusion

In this chapter,we presented topological structures of pythagorean fuzzy semi δ −open and pythagorean fuzzy semi δ −closed sets. We also investigated and explored some properties of pythagorean fuzzy semi δ − interior and pythagorean fuzzy semi δ − closure and discussed relationship between them. We hope that the findings in this chapter will enhance and promote the further study in the pythagorean fuzzy set theory.

References

Atanassov, K. (1986). Intuitionistic fuzzy sets. *Fuzzy Sets and Systems, 20*, 87-96.

Chang, C. (1968). Fuzzy topological spaces. *Journal of Mathematical Analysis and Applications, 24*, 182–190.

Coker, D. (1997). An introduction to intuitionistic fuzzy topological spaces. *Fuzzy Sets and Systems, 88*, 81-89.

Du, Y., Hou, F., Zafar, W., Yu, Q., & Zhai, Y. (2017). A novel method for multi-attribute decision making with interval-valued Pythagorean fuzzy linguistic information. *International Journal of Intelligent Systems, 32*(10), 1085-1112.

Garg, H. (2019). New logarithmic operational laws and their aggregation operators for Pythagorean fuzzy sets and their applications. *International Journal of Intelligent Systems, 34*(1), 82-106.

Garg, H. (2016a). A new generalized Pythagorean fuzzy information aggregation using Einstein operations and its application to decision making. *International Journal of Intelligent Systems, 31*(9), 886-920.

Garg, H. (2016b). A novel correlation coefficient between Pythagorean fuzzy sets and its applications to decision-making processes. *International Journal of Intelligent Systems, 31*(12), 1234-1252.

Gou, X., Xu, Z., & Ren, P. (2016). The properties of continuous Pythagorean fuzzy information. *International Journal of Intelligent Systems, 31*(5), 401-424.

Hanafy, I. M. (2003). Completely continuous functions in intuitionistic fuzzy topological spaces. *Czechoslovak Mathematical Journal, 53*(4), 793-803.

Hur, K., Kim, J. H., & Ryou, J. H. (2004). Intuitionistic fuzzy topological spaces. *The Pure and Applied Mathematics, 11*(3), 243-265.

Liang, W., Zhang, X., & Liu, M. (2015). The maximizing deviation method based on interval-valued Pythagorean fuzzy weighted aggregating operator for

multiple criteria group decision analysis. *Discrete Dynamics in Nature and Society, 2015.*

Liu, Z., Liu, P., Liu, W., & Pang, J. (2017). Pythagorean uncertain linguistic partitioned Bonferroni mean operators and their application in multi-attribute decision making. *Journal of Intelligent & Fuzzy Systems, 32*(3), 2779-2790.

Lowen, R. (1976). Fuzzy topological spaces and fuzzy compactness. *Journal of Mathematical Analysis and Applications, 56*(3), 621–633.

Lowen, R. (1977). Initial and final fuzzy topologies and the fuzzy Tychonoff theorem. *Journal of Mathematical Analysis and Applications, 58*(1), 11–21.

Ma, Z., & Xu, Z. (2016). Symmetric Pythagorean fuzzy weighted geometric/averaging operators and their application in multicriteria decision-making problems. *International Journal of Intelligent Systems, 31*(12), 1198-1219.

Olgun, M., Ünver, M., & Yardımcı, Ş. (2019). Pythagorean fuzzy topological spaces. *Complex and Intelligent Systems, 5*(2), 177-183.

Öztürk, T. Y., & Yolcu, A. (2020). Some structures on Pythagorean fuzzy topological spaces. *Journal of New Theory, 33*, 15-25.

Peng, X., & Yang, Y. (2015). Some results for Pythagorean fuzzy sets. *International Journal of Intelligent Systems, 30*(11), 1133–1160.

Peng, X. (2019). New operations for interval-valued Pythagorean fuzzy sets. *Scientia Iranica E, 26*(2), 1049–1076.

Peng, X., & Selvachandran, G. (2019). Pythagorean fuzzy sets: State of the art and future directions. *Artificial Intelligence Review, 52*, 1873–1927. https://doi.org/10.1007/s10462-017-9596-9

Ren, P., Xu, Z., & Gou, X. (2016). Pythagorean fuzzy TODIM approach to multi-criteria decision making. *Applied Soft Computing, 42*, 246-259.

Saadati, R., & Park, J. H. (2006). On the intuitionistic fuzzy topological spaces. *Chaos, Solitons & Fractals, 27*(2), 331-344.

Yager, R. R. (2013). Pythagorean fuzzy subsets. In *Proceedings of the Joint IFSA World Congress NAFIPS Annual Meeting* (Vol. 1, pp. 57-61). Edmonton, Canada.

Yager, R. R., & Abbasov, A. M. (2014). Pythagorean membership grades, complex numbers, and decision making. *International Journal of Intelligent Systems, 28*(5), 436-452.

Zadeh, L. A. (1965). Fuzzy sets. *Information and Control, 8*, 338-353.

Zeng, S., Chen, J., & Li, X. (2016). A hybrid method for Pythagorean fuzzy multiple-criteria decision making. *International Journal of Information Technology and Decision Making, 15*(2), 403–422. https://doi.org/10.1142/S0219622016500012

Zhang, X. (2016). A novel approach based on similarity measure for Pythagorean fuzzy multiple criteria group decision making. *International Journal of Intelligent Systems, 31*(6), 593-611.

Zhang, X., & Xu, Z. (2014). Extension of TOPSIS to multiple criteria decision making with Pythagorean fuzzy sets. *International Journal of Intelligent Systems, 29*(12), 1061-1078.

Chapter 10

POINT ESTIMATION FOR THE BETA DISTRIBUTION PARAMETERS USING GENETIC ALGORITHM

Adil KILIÇ[1]

Birdal ŞENOĞLU[2]

1 Res. Asst., Kırıkkale University, ORCID: 0000-0003-3114-9118, adilkilic@kku.edu.tr
2 Prof. Dr., Ankara University, ORCID: 0000-0003-3707-2393, senoglu@science.ankara.edu.tr

1 INTRODUCTION

The standard beta distribution is characterized by two shape parameters α and β, see Jambunathan (1954). It is used for modelling random variables such as percentages and proportions defined in the $[0, 1]$ interval. The beta distribution is generally preferred to be the conjugate prior distribution for binomial probabilities in Bayesian statistics, see Gelman et al. (1995). There are also many applications of the beta distribution across a range of scientific fields in the literature, see for example Olea (2011), Jun and Yoo (2012), and Santana-e-Silva et al. (2022).

There exist a vast literature focusing on the beta distribution within the framework of parameter estimation. For example, Gnanadesikan et al. (1967) investigated the maximum likelihood (ML) estimates of two parameters of the beta distribution using the smallest observations in a random sample. Fielitz and Myers (1975) obtained the method of moment estimators of the parameters of the beta distribution and examined the properties of these estimators. Romesburg (1976) demonstrated that the ML estimation method can be used by formulating the beta distribution parameters in terms of smallest order statistics, although it is slightly more difficult to calculate than the method of moments. Kottas and Lau (1978) showed that the ML estimators of the beta distribution parameters are generally superior to moment estimators. Beckman and Tietjen (1978) proposed a method for calculating ML estimates of the beta distribution that does not require initial values and is mostly free of convergence problems. Lau and Lau (1991) compared various methods for calculating ML estimators of the beta distribution parameters and also presented a practical way to create confidence intervals for them. Bowman and Shenton (1992) demonstrated that method of moment estimators for beta distribution parameters are preferable compared to the corresponding ML estimators when the computer oriented extended Taylor series method is used. Corderio et al. (1997) introduced closed-form expressions for bias-corrected ML estimates of the parameters of the beta distribution. Cribari-Neto and Vasconcellos (2002) analyzed the finite-sample behavior of three second-order bias-corrected alternatives to the ML estimators of the parameters of the beta distribution. Owen (2008) compared the performances of many different estimation methods for the parameters of the beta distribution. Ma and Leijon (2010) compared the performances of

different approaches for Bayesian estimation of the parameters of the beta distribution. Othman (2022) proposed a methodology to obtain prior distributions for the shape parameters of the beta distribution. Yugandhar and Haragopal (2023) estimated the parameters of the beta distribution with the local frequency ratio method and compared them with method of moments estimators. Ali et al. (2023) examined the efficiencies of method of moments and ML estimators of the beta distribution with respect to the change in sample size.

In this study, we focus on the beta distribution, which has location, scale, and shape parameters, rather than the standard beta distribution, and obtain the ML and modified ML (MML) estimators of the distribution parameters in cases where it is assumed that the shape parameters are known. For obtaining the ML estimates of the unknown parameters, it is preferred to use genetic algorithm (GA) among the various numerical methods, because of its advantages over derivative-based numerical methods. Note that the search space, which is one of the initial parameters of GA, is determined with two different methods: the commonly used fixed search space (FSS) and the reduced search space (RSS) proposed by Yalcinkaya et al. (2018). The effectiveness of these search spaces are also compared in evaluating the efficiencies of ML estimates. The reason for including MML estimators of beta distribution parameters into the study is to compare the efficiencies of estimators obtained in closed form and estimators obtained numerically.

2 STANDARD BETA DISTRIBUTION

The probability density function (pdf) of the standard beta distribution with the shape parameters $\alpha > 0$ and $\beta > 0$ is given by

$$f(x) = \frac{1}{B(\alpha, \beta)} x^{\alpha-1} (1-x)^{\beta-1}, \qquad 0 < x < 1 \qquad (1)$$

where $B(\alpha, \beta) = \frac{\Gamma(\alpha)\Gamma(\beta)}{\Gamma(\alpha+\beta)}$. If the random variable X has the standard beta distribution, then it is denoted by $X \sim beta(\alpha, \beta)$, see Jambunathan (1954) for the details on the mathematical properties of it.

For the various values of shape parameters α and β, the curves of $beta(\alpha, \beta)$ distribution pdf are illustrated in Figure 1.
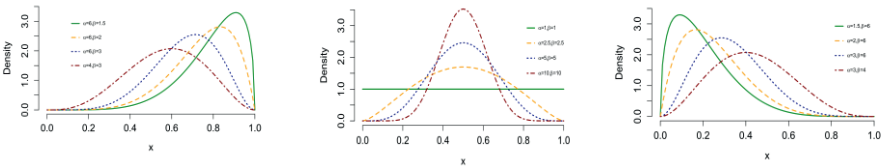
Figure 1. The curves of the $beta(\alpha, \beta)$ distribution pdf for the various values of shape parameters α and β.

Additionally, the skewness (γ_1) and kurtosis (γ_2) values for the beta distribution are given in Table 1.

Table 1. The values of kurtosis and skewness for the beta distribution.

β	3	5	10	20
		$\alpha = 3$		
γ_1	0	0.310	0.638	0.860
γ_2	2.333	2.585	3.197	3.837
		$\alpha = 5$		
γ_1	-0.310	0	0.333	0.566
γ_2	2.586	2.539	2.823	3.251
		$\alpha = 10$		
γ_1	-0.637	-0.333	0	0.247
γ_2	3.190	2.818	2.746	2.901

As seen from Figure 1 and Table 1 that the beta distribution becomes

- Symmetric when $\alpha = \beta$
- Positively skewed when $\alpha < \beta$
- Negatively skewed when $\alpha > \beta$.

3 PARAMETER ESTIMATION

In this section, the estimators of the μ and σ parameters of the beta distribution are obtained with ML and MML estimation methods when the α and β parameters are known.

3.1 ML Estimation

Let $y_1, y_2, \ldots, y_n$ be random sample from the beta distribution with the location parameter μ, scale parameter σ and shape parameters α and β. Then the likelihood (L) function is given by

$$L = \left(\frac{\Gamma(\alpha + \beta)}{\Gamma(\alpha)\Gamma(\beta)}\right)^n \prod_{i=1}^{n} z_i^{\alpha-1}(1 - z_i)^{\beta-1} \qquad (2)$$

where $z_i = \frac{y_i - \mu}{\sigma}$ for $i = 1, 2, \ldots, n$.

Therefore, the log likelihood ($ln\ L$) function is obtained as

$$lnL = nln\Gamma(\alpha + \beta) - nln\Gamma(\alpha) - nln\Gamma(\beta) + (\alpha - 1)\sum_{i=1}^{n} ln\ (z_i) + (\beta - 1)\sum_{i=1}^{n} ln\ (1 - z_i) . \quad (3)$$

By calculating the partial derivatives of lnL in relation to the parameters μ and σ, the likelihood equations are acquired as

$$\frac{lnL}{\partial \mu} = -\frac{1}{\sigma}\left((\alpha - 1)\sum_{i=1}^{n} z_i^{-1} - (\beta - 1)\sum_{i=1}^{n}(1 - z_i)^{-1}\right) = 0 \qquad (4)$$

and

$$\frac{lnL}{\partial \sigma} = -\frac{1}{\sigma}\left(n(\alpha - 1) - (\beta - 1)\sum_{i=1}^{n} z_i(1 - z_i)^{-1}\right) = 0. \qquad (5)$$

However, there are no explicit solutions for the equations (4) and (5) due to the nonlinear functions of the unknown parameters. Therefore, we resort to the GA method for numerically solving the likelihood equations, see section 4 for details.

3.2 MML Estimation

Tiku and Akkaya (2004) obtained the explicit estimators of the location and scale parameters μ and σ of the beta distribution following the steps given below, see also Tiku (1967) in the context of MML methodology.

Step 1. The likelihood equations given in (4) and (5) are reformulated using standardized ordered observations $z_{(i)} = \frac{y_{(i)} - \mu}{\sigma}$ $(i = 1, 2, \ldots, n)$ as follows

$$\frac{\partial lnL}{\partial \mu} = -\frac{1}{\sigma}\left((\alpha - 1)\sum_{i=1}^{n} z_{(i)}^{-1} - (\beta - 1)\sum_{i=1}^{n}(1 - z_{(i)})^{-1}\right) = 0 \quad (6)$$

and

$$\frac{\partial lnL}{\partial \sigma} = -\frac{1}{\sigma}\left(n(\alpha - 1) - (\beta - 1)\sum_{i=1}^{n} z_{(i)}(1 - z_{(i)})^{-1}\right) = 0, \quad (7)$$

respectively, since complete sums are invariant to ordering.

Step 2. The nonlinear functions $z_{(i)}^{-1}$ and $(1 - z_{(i)})^{-1}$ in equations (6) and (7) are linearized by using the first two terms of the Taylor series expansion around $t_{(i)} = E(z_{(i)})$ as follows

$$z_{(i)}^{-1} \cong \alpha_{1i} - \beta_{1i}z_{(i)} \quad (8)$$

and

$$(1 - z_{(i)})^{-1} \cong \alpha_{2i} - \beta_{2i}z_{(i)}, \quad (9)$$

respectively. Here,

$$\alpha_{1i} = 2t_{(i)}^{-1}, \beta_{1i} = t_{(i)}^{-2}, \alpha_{2i} = (1 - t_{(i)})^{-1} - \beta_{2i}t_{(i)} \text{ and } \beta_{2i} = (1 - t_{(i)})^{-2}.$$

It should be noted that approximate $t_{(i)}$ values are obtained by solving the following equation

$$\int_0^{t_{(i)}} f(z)\, dz = \frac{i}{n+1} \quad (i = 1, 2, \ldots, n).$$

Step 3. The modified likelihood equations are obtained by incorporating the equations (8) and (9) into (6) and (7)

$$\frac{\partial lnL^*}{\partial \mu} = -\frac{1}{\sigma}\left((\alpha-1)\sum_{i=1}^{n}(\alpha_{1i}-\beta_{1i}z_{(i)}) - (\beta-1)\sum_{i=1}^{n}(\alpha_{2i}-\beta_{2i}z_{(i)})\right) = 0 \quad (10)$$

and

$$\frac{\partial lnL^*}{\partial \sigma} = -\frac{1}{\sigma}\left(n(\alpha-1) - (\beta-1)\sum_{i=1}^{n}z_{(i)}(\alpha_{2i}-\beta_{2i}z_{(i)})\right) = 0, \quad (11)$$

respectively.

Step 4. MML estimators of the parameters μ and σ are obtained by solving the equations (10) and (11) as given below

$$\hat{\mu} = K - D\hat{\sigma} \quad (12)$$

and

$$\hat{\sigma} = \frac{-B + \sqrt{B^2 + 4AC}}{2\sqrt{A(A-1)}} \quad (13)$$

where $K = \frac{\sum_{i=1}^{n} m_i y_{(i)}}{m}$, $D = \frac{\sum_{i=1}^{n} \delta_i}{m}$, $m = \sum_{i=1}^{n} m_i$, $B = \sum_{i=1}^{n} \delta_i (y_{(i)} - K)$, $C = \sum_{i=1}^{n} m_i (y_{(i)} - K)^2$,
$m_i = (\alpha-1)\beta_{1i} + (\beta-1)\beta_{2i}$, and $\delta_i = (\alpha-1)\alpha_{1i} - (\beta-1)\alpha_{2i}$.

MML and ML estimators are asymptotically equal. Hence, they are fully efficient under certain mild regularity conditions. Also, it is known that they are robust to reasonable deviations from the presumed model.

4 GENETIC ALGORITHM

GA, developed based on Darwinian evolutionary principles, is used to find the best or approximate best solution for the objective function in optimization problems, see Holland (1975). Clearly, it tries to reach the best solution by transferring the best chromosomes in the population to the next generation while eliminating the bad ones by imitating

mechanisms such as mutation and crossover in the evolutionary process. Since this method is a stochastic search method that does not require derivative information, it is frequently employed as a substitute for conventional gradient-based techniques such as Newton-Raphson. The working principles of GA are given in the following steps.

Step 1. Objective function, stopping criterion, search space and the initial parameters of the GA such as population size (N), number of elite chromosomes (E), selection rate (SR), mutation probability (MP), and crossover probability (CP) are determined. Here, the structure of a chromosome is given as follows

	Gene 1	Gene 2
Chromosome	μ	σ

and the objective function is chosen as lnL.

Step 2. The initial population consisting of N chromosomes is generated. This population is obtained by generating random numbers from a search space predetermined for each gene.

Step 3. Each chromosome in the population is evaluated according to its value in the objective function.

Step 4. By applying the elitism operator, predetermined number of elite chromosomes having the best fitness values are transferred to the next generation.

Step 5. The predetermined SR of the chromosomes having the worst fitness value is not transferred to the next generation. Then, new chromosomes are generated to replace them.

Step 6. According to the predetermined CP value, the genes of the selected chromosomes are mutually exchanged.

Step 7. Similar to Step 6, certain genes of the selected chromosomes are randomly changed with respect to the predetermined MP value.

Step 8. Steps 3-7 are reiterated prior to the predetermined stopping condition is met.

The determination of the initial parameters mentioned in the steps above affects the performance of GA. Specifically, the appropriate selection of the search space significantly increases the convergence speed of the GA. MML confidence intervals of the parameters expressing the genes of a chromosome are preferred as the search space instead of commonly used FSS, since these confidence intervals remarkably reduce the search space. Because of this feature, it is named as reduced search space (RSS), see Yalcinkaya et al. (2018). Different from FSS, RSS changes depending on the sample dynamically. Asymptotic confidence intervals for the beta distribution parameters μ and σ are defined as follows

$$\left(\hat{\mu}_{MML} - z_{\frac{\alpha}{2}} \sqrt{\widehat{Var}(\hat{\mu}_{MML})}, \hat{\mu}_{MML(B)} + z_{\frac{\alpha}{2}} \sqrt{\widehat{Var}(\hat{\mu}_{MML})} \right) \qquad (14)$$

and

$$\left(\hat{\sigma}_{MML} - z_{\frac{\alpha}{2}} \sqrt{\widehat{Var}(\hat{\sigma}_{MML})}, \hat{\sigma}_{MML(B)} + z_{\frac{\alpha}{2}} \sqrt{\widehat{Var}(\hat{\sigma}_{MML})} \right), \qquad (15)$$

respectively. See also Yalcinkaya et al. (2018, 2021, 2024) within the framework of parameter estimation using GA based on RSS.

5 SIMULATION STUDY

In this section, it is presented that we compare the performances of the GA based on FSS (GA-FSS) and GA based on RSS (GA-RSS) to obtain ML estimates of the location parameter μ and scale parameter σ of beta distribution. Moreover, MML estimators are also included in the simulation study to see their efficiencies since they were already calculated while obtaining the RSS. Mean, MSE, and DEF criteria are used in the Monte Carlo simulation study. If $\hat{\theta}_1, \hat{\theta}_2, \dots, \hat{\theta}_k$ be any estimators of the parameters $\theta_1, \theta_2, \dots, \theta_k$, then DEF defined as the joint efficiencies of the estimators is expressed as follows

$$DEF(\hat{\theta}_1, \hat{\theta}_2, \dots, \hat{\theta}_k) = MSE(\hat{\theta}_1) + MSE(\hat{\theta}_2) + \dots + MSE(\hat{\theta}_k). \quad (16)$$

All computations are done in R software. Without sacrificing generality, the values of μ and σ are taken to be 0 and 1, respectively. Sample sizes n and the shape parameters α and β (for both symmetric and skew cases) used in the simulation study are given as shown below.

	$n = 10, 25, 50, 100, 250, 500$
Symmetric cases	$(\alpha, \beta) = (2.5,2.5), (5,5), (10,10), (50,50)$
Skew cases	$(\alpha, \beta) = (3,5), (3,20), (5,3), (20,3)$

In the computation of GA, values of the initial parameters and the number of iterations are taken to be N=250, E=8, MP=0.1, CP=0.8 and 500, respectively. See also the following search spaces (FSS and RSS) used for μ and σ.

Search Space	μ	σ
FSS	(-0.5, 0.5)	(0.5,1.5)
RSS	CI in (14)	CI in (15)

For the estimators of μ and σ, the mean, MSE, and DEF values are given in Tables 2 and 3 for the symmetric and skew cases of the beta distribution, respectively.

Table 2: Mean, MSE, and DEF values for the estimators $\hat{\mu}$ and $\hat{\sigma}$: Symmetric cases

n	Method	$\hat{\mu}$ Mean	$\hat{\mu}$ MSE	$\hat{\sigma}$ Mean	$\hat{\sigma}$ MSE	DEF
		$(\alpha, \beta) = (2.5, 2.5)$				
	GA-RSS	0.0612	0.0134	0.8783	0.0388	0.0522
10	GA-FSS	0.0661	0.0137	0.8706	0.0388	0.0526
	MML	0.0695	0.0157	0.8635	0.0464	0.0621
	GA-RSS	0.0290	0.0041	0.9385	0.0125	0.0166
25	GA-FSS	0.0276	0.0041	0.9425	0.0129	0.0171
	MML	0.0360	0.0050	0.9268	0.0148	0.0199
	GA-RSS	0.0177	0.0017	0.9669	0.0049	0.0066
50	GA-FSS	0.0126	0.0017	0.9730	0.0049	0.0066
	MML	0.0220	0.0021	0.9557	0.0065	0.0086
	GA-RSS	0.0116	0.0008	0.9802	0.0022	0.0030
100	GA-FSS	0.0078	0.0009	0.9833	0.0023	0.0032
	MML	0.0143	0.0010	0.9712	0.0031	0.0042

	Method	Mean	MSE	Mean	MSE	DEF
	GA-RSS	0.0055	0.0002	0.9900	0.0006	0.0009
250	GA-FSS	-0.0016	0.0002	1.0011	0.0007	0.0010
	MML	0.0086	0.0003	0.9824	0.0009	0.0013
	GA-RSS	0.0029	0.0001	0.9944	0.0003	0.0004
500	GA-FSS	-0.0061	0.0002	1.0090	0.0005	0.0008
	MML	0.0063	0.0002	0.9890	0.0004	0.0006
$(\alpha, \beta) = (5, 5)$						
	GA-RSS	0.0486	0.0135	0.9028	0.0439	0.0575
10	GA-FSS	0.0452	0.0130	0.9053	0.0444	0.0574
	MML	0.0421	0.0135	0.9163	0.0454	0.0589
	GA-RSS	0.0175	0.0040	0.9583	0.0136	0.0177
25	GA-FSS	0.0218	0.0048	0.9595	0.0154	0.0203
	MML	0.0174	0.0046	0.9632	0.0155	0.0202
	GA-RSS	0.0105	0.0019	0.9750	0.0070	0.0090
50	GA-FSS	0.0091	0.0021	0.9813	0.0071	0.0093
	MML	0.0099	0.0024	0.9776	0.0077	0.0101
	GA-RSS	0.0032	0.0009	0.9935	0.0030	0.0040
100	GA-FSS	0.0063	0.0011	0.9890	0.0037	0.0048
	MML	0.0056	0.0011	0.9887	0.0037	0.0048
	GA-RSS	0.0029	0.0003	0.9952	0.0011	0.0015
250	GA-FSS	-0.0004	0.0004	1.0001	0.0012	0.0016
	MML	0.0028	0.0004	0.9925	0.0014	0.0018
	GA-RSS	0.0015	0.0001	0.9959	0.0005	0.0007
500	GA-FSS	0.0008	0.0002	0.9997	0.0007	0.0009
	MML	0.0034	0.0002	0.9934	0.0006	0.0008
	Method	Mean	MSE	Mean	MSE	DEF
$(\alpha, \beta) = (10, 10)$						
	GA-RSS	0.0524	0.0141	0.8990	0.0508	0.0649
10	GA-FSS	0.0392	0.0120	0.9199	0.0452	0.0573
	MML	0.0253	0.0131	0.9508	0.0479	0.0610
	GA-RSS	0.0174	0.0044	0.9696	0.0160	0.0205
25	GA-FSS	0.0122	0.0043	0.9764	0.0155	0.0199
	MML	0.0123	0.0051	0.9749	0.0184	0.0235
	GA-RSS	0.0106	0.0021	0.9810	0.0081	0.0103
50	GA-FSS	0.0071	0.0020	0.9863	0.0076	0.0097
	MML	0.0057	0.0023	0.9873	0.0091	0.0115
	GA-RSS	0.0039	0.0009	0.9928	0.0037	0.0047
100	GA-FSS	0.0043	0.0012	0.9911	0.0043	0.0056
	MML	0.0044	0.0011	0.9902	0.0041	0.0052
	GA-RSS	0.0021	0.0004	0.9951	0.0016	0.0020
250	GA-FSS	0.0017	0.0004	0.9967	0.0017	0.0021
	MML	0.0040	0.0005	0.9930	0.0019	0.0025
	GA-RSS	0.0011	0.0001	0.9976	0.0006	0.0008
500	GA-FSS	0.0003	0.0002	0.9987	0.0007	0.0009
	MML	0.0053	0.0002	0.9905	0.0010	0.0013
$(\alpha, \beta) = (50, 50)$						
	GA-RSS	0.0381	0.0119	0.9241	0.0475	0.0595
10	GA-FSS	0.0327	0.0121	0.9343	0.0474	0.0595
	MML	0.0186	0.0134	0.9628	0.0527	0.0662
	GA-RSS	0.0135	0.0039	0.9750	0.0156	0.0195
25	GA-FSS	0.0114	0.0048	0.9770	0.0193	0.0242
	MML	0.0083	0.0050	0.9836	0.0198	0.0249
	GA-RSS	0.0023	0.0020	0.9944	0.0081	0.0102
50	GA-FSS	0.0087	0.0025	0.9826	0.0096	0.0121
	MML	0.0015	0.0024	0.9968	0.0098	0.0123

100	GA-RSS	0.0033	0.0010	0.9927	0.0043	0.0054
	GA-FSS	0.0007	0.0012	0.9980	0.0049	0.0061
	MML	0.0008	0.0011	0.9969	0.0047	0.0059
250	GA-RSS	0.0007	0.0004	0.9981	0.0017	0.0021
	GA-FSS	0.0013	0.0004	0.9970	0.0017	0.0022
	MML	0.0008	0.0005	0.9982	0.0021	0.0026
500	GA-RSS	0.0018	0.0002	0.9965	0.0008	0.0010
	GA-FSS	0.0000	0.0002	0.9998	0.0009	0.0011
	MML	0.0028	0.0002	0.9943	0.0009	0.0012

Table 3. Mean, MSE, and DEF values for the estimators $\hat{\mu}$ and $\hat{\sigma}$: Skew cases

		$\hat{\mu}$		$\hat{\sigma}$		
n	Method	Mean	MSE	Mean	MSE	DEF
				$(\alpha, \beta) = (3, 5)$		
10	GA-RSS	0.0365	0.0065	0.8958	0.0439	0.0504
	GA-FSS	0.0327	0.0062	0.9096	0.0423	0.0485
	MML	0.0439	0.0073	0.9005	0.0466	0.0539
25	GA-RSS	0.0182	0.0020	0.9531	0.0143	0.0164
	GA-FSS	0.0190	0.0023	0.9541	0.0155	0.0179
	MML	0.0231	0.0025	0.9468	0.0168	0.0193
50	GA-RSS	0.0091	0.0009	0.9794	0.0061	0.0071
	GA-FSS	0.0070	0.0008	0.9803	0.0060	0.0069
	MML	0.0130	0.0010	0.9672	0.0075	0.0085
100	GA-RSS	0.0048	0.0004	0.9863	0.0028	0.0032
	GA-FSS	0.0049	0.0004	0.9865	0.0034	0.0038
	MML	0.0085	0.0004	0.9785	0.0036	0.0041
250	GA-RSS	0.0022	0.0001	0.9943	0.0011	0.0012
	GA-FSS	0.0008	0.0001	0.9974	0.0012	0.0014
	MML	0.0041	0.0001	0.9888	0.0014	0.0016
500	GA-RSS	0.0006	0.0000	0.9986	0.0005	0.0005
	GA-FSS	-0.0005	0.0000	1.0007	0.0006	0.0007
	MML	0.0032	0.0000	0.9925	0.0006	0.0007
				$(\alpha, \beta) = (3, 20)$		
10	GA-RSS	0.0131	0.0006	0.9030	0.0524	0.0531
	GA-FSS	0.0129	0.0007	0.9091	0.0455	0.0462
	MML	0.0154	0.0007	0.9358	0.0571	0.0579
25	GA-RSS	0.0058	0.0002	0.9591	0.0196	0.0199
	GA-FSS	0.0050	0.0002	0.9719	0.0194	0.0196
	MML	0.0071	0.0002	0.9660	0.0214	0.0217
50	GA-RSS	0.0033	0.0000	0.9775	0.0083	0.0084
	GA-FSS	0.0019	0.0000	0.9881	0.0098	0.0099
	MML	0.0045	0.0000	0.9775	0.0106	0.0107
100	GA-RSS	0.0013	0.0000	0.9915	0.0042	0.0042
	GA-FSS	0.0011	0.0000	0.9939	0.0041	0.0042
	MML	0.0019	0.0000	0.9965	0.0047	0.0047
250	GA-RSS	0.0000	0.0000	0.9966	0.0015	0.0015
	GA-FSS	0.0000	0.0000	1.0039	0.0019	0.0019

	MML	0.0000	0.0000	1.0001	0.0017	0.0017
500	GA-RSS	0.0003	0.0000	0.9965	0.0007	0.0008
	GA-FSS	-0.0006	0.0000	1.0064	0.0010	0.0010
	MML	0.0009	0.0000	0.9942	0.0009	0.0009

		$\hat{\mu}$		$\hat{\sigma}$		
n	Method	Mean	MSE	Mean	MSE	DEF
		$(\alpha, \beta) = (5, 3)$				
10	GA-RSS	0.0519	0.0214	0.9105	0.0417	0.0631
	GA-FSS	0.0592	0.0233	0.9072	0.0434	0.0668
	MML	0.0531	0.0234	0.9039	0.0459	0.0694
25	GA-RSS	0.0266	0.0072	0.9534	0.0134	0.0206
	GA-FSS	0.0257	0.0073	0.9579	0.0133	0.0206
	MML	0.0217	0.0085	0.9574	0.0159	0.0244
50	GA-RSS	0.0175	0.0037	0.9721	0.0064	0.0101
	GA-FSS	0.0129	0.0043	0.9780	0.0077	0.0120
	MML	0.0164	0.0041	0.9689	0.0075	0.0117
100	GA-RSS	0.0089	0.0018	0.9858	0.0030	0.0048
	GA-FSS	0.0057	0.0020	0.9902	0.0034	0.0055
	MML	0.0113	0.0020	0.9809	0.0035	0.0056
250	GA-RSS	0.0041	0.0006	0.9930	0.0011	0.0018
	GA-FSS	0.0009	0.0007	0.9974	0.0012	0.0020
	MML	0.0044	0.0007	0.9914	0.0013	0.0021
500	GA-RSS	0.0020	0.0003	0.9964	0.0005	0.0008
	GA-FSS	-0.0048	0.0003	1.0053	0.0006	0.0010
	MML	0.0006	0.0003	0.9988	0.0005	0.0009
		$(\alpha, \beta) = (20, 3)$				
10	GA-RSS	0.0626	0.0410	0.9266	0.0480	0.0890
	GA-FSS	0.0628	0.0397	0.9258	0.0462	0.0859
	MML	0.0509	0.0491	0.9347	0.0574	0.1065
25	GA-RSS	0.0305	0.0140	0.9642	0.0162	0.0303
	GA-FSS	0.0324	0.0133	0.9615	0.0155	0.0289
	MML	0.0240	0.0171	0.9692	0.0198	0.0369
50	GA-RSS	0.0191	0.0063	0.9780	0.0073	0.0136
	GA-FSS	0.0116	0.0070	0.9853	0.0079	0.0150
	MML	0.0208	0.0085	0.9746	0.0098	0.0183
100	GA-RSS	0.0059	0.0028	0.9926	0.0032	0.0060
	GA-FSS	0.0059	0.0037	0.9928	0.0042	0.0079
	MML	0.0121	0.0040	0.9848	0.0046	0.0087
250	GA-RSS	0.0039	0.0012	0.9955	0.0014	0.0027
	GA-FSS	0.0023	0.0014	0.9971	0.0016	0.0030
	MML	0.0040	0.0017	0.9949	0.0020	0.0038
500	GA-RSS	0.0017	0.0006	0.9979	0.0007	0.0013
	GA-FSS	-0.0014	0.0007	1.0012	0.0008	0.0016
	MML	0.0011	0.0010	0.9977	0.0011	0.0021

The following conclusions can be drawn from Tables 2 and 3 for each of the parameters μ and σ.

• The mean values of the GA-FSS and GA-RSS are more or less equal to each other in almost all cases.

• In symmetric cases, the performances of MML estimators, compared to others, improves as the values of the shape parameters increase according to the bias criterion when $n = 10$ and 25.

• According to MSE and DEF criteria, GA-FSS and GA-RSS performances are quite similar to one another when $n \leq 50$. Nevertheless, GA-RSS is the most efficient among the other estimators in the cases where $n > 50$.

• GA-RSS and GA-FSS are mostly superior than MML estimators compared to MSE and DEF criteria, but for $n \geq 100$, MML estimators show quite competitive performances.

• The joint efficiencies of $\hat{\mu}$ and $\hat{\sigma}$ based on GA-FSS get closer to those of GA-RSS as the beta distribution converges to normal distribution. For small values of shape parameters GA-RSS is significantly more effective.

• MSE values of all estimators decrease as the sample sizes increase as expected.

In this study, it should be noted that the FSS is chosen as narrow as possible to make fair comparisons, however this situation is not very realistic for practical point of view. Nevertheless, the performances of GA-RSS are found to be better or equal than those of GA-FSS according to Monte Carlo simulation results.

6 APPLICATION

In this section, the simulated data of size $n = 50$, generated from the $beta(\alpha = 5, \beta = 3)$ distribution with the location parameter $\mu = 0$ and scale parameter $\sigma = 1$, is used to demonstrate the estimation performance of GA-RSS showing superior performance among the others according to

the simulation results. The descriptive statistics of the data set are given in Table 4.

Table 4. The descriptive statistics for the simulated data

n	Min	Max	$\bar{x}$	Median	S^2	γ_1	γ_2
50	0.1303	0.8754	0.6080	0.6504	0.0261	-0.5922	2.9638

Beta QQ plot of the simulated data is shown in Figure 2.
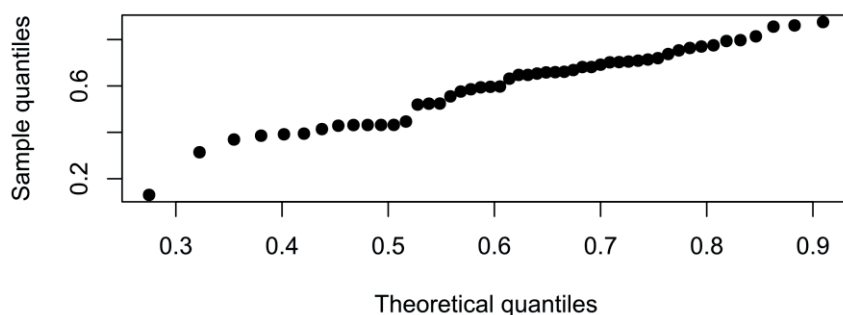
Figure 2. Beta QQ plot of the simulated data.

First, RSS is determined by using the MML confidence intervals based on the bootstrap MML estimates of the parameters and the corresponding standard errors. Then, ML based on GA-RSS estimates of the parameters μ and σ are obtained. Therefore, RSS is obtained for the parameters μ and σ as follows.

Parameters	μ	σ
RSS	$(-0.1307, 0.1589)$	$(0.7594, 1.1182)$

Then, the ML estimates based on GA-RSS for the parameters μ and σ are found to be $\hat{\mu} = -0.0143$ and $\hat{\sigma} = 0.9782$, respectively. Following null hypothesis

H_0: The simulated data is distributed as $beta(\alpha = 5, \beta = 3)$ with $\mu = -0.0143$ and $\sigma = 0.9782$

is tested to see the modelling performances of these estimate values by using Kolmogorov-Smirnov (K-S) test. As a result of the K-S test, the H_0 hypothesis is not rejected, since the p-value=0.5487 is greater than the presumed significance level $\alpha = 0.050$. Eventually, we infer that the $beta(\alpha = 5, \beta = 3)$ distribution with the location parameter $\mu = -0.0143$ and scale parameter $\sigma = 0.9782$ fits the simulated data according to the K-S test.

7 CONCULISON

In this study, we obtain ML and MML estimates of the unknown location parameter μ and scale parameter σ of the $beta(\alpha, \beta)$ distribution when the shape parameters are known. To obtain ML estimates of the unknown parameters, GA method based on two different search spaces (i.e., FSS and RSS) is used. A Monte Carlo simulation study is conducted to compare the efficiencies of these estimators. According to the of the simulation study results, it has been shown that the GA-RSS is more efficient with respect to the bias and MSE criteria in most of the symmetric and skew cases of the beta distribution. We also analyzed a simulated data set to show the implementation of the methodology. It is seen that simulation results are in agreement with the findings of the application of the simulated data. However, it should be noted that MML estimation method can be safely chosen in place of these iterative methods used for ML estimation because of its competitive performance and easy applicability.

REFERENCES

Ali, H., Akanihu, C. N., & Felix, J. (2023). Investigating the parameters of the beta distribution. World Journal of Advanced Research and Reviews, 19(1), 815-830.

Gnanadesikan, R., Pinkham, R. S., & Hughes, L. P. (1967). Maximum likelihood estimation of the parameters of the beta distribution from smallest order statistics. Technometrics, 9(4), 607-620.

Romesburg, H. C. (1976). Estimation of parameters in the beta distribution: comment. Decision Sciences, 7(3).

Fielitz, B. D., & Myers, B. L. (1975). Concepts, theory, and techniques: Estimation of parameters in the beta distribution. Decision Sciences, 6(1), 1-13.

Kottas, J. F., & Lau, H. S. (1978). On estimating parameters for beta distributions. Decision Sciences, 9(3), 526-531.

Bowman, K. O., & Shenton, L. R. (1992). Parameter estimation for the beta distribution. Journal of statistical computation and simulation, 43(3-4), 217-228.

Lau, H. S., & Hing-Ling Lau, A. (1991). Effective procedures for estimating beta distribution's parameters and their confidence intervals. Journal of Statistical Computation and Simulation, 38(1-4), 139-150.

Cordeiro, G. M., Da Rocha, E. C., Da Rocha, J. G. C., & Cribari-Neto, F. (1997). Bias-corrected maximum likelihood estimation for the beta distribution. Journal of Statistical Computation and Simulation, 58(1), 21-35.

Beckman, R. J., & Tietjen, G. L. (1978). Maximum likelihood estimation for the beta distribution. Journal of Statistical Computation and Simulation, 7(3–4), 253–258. https://doi.org/10.1080/00949657808810232

Cribari-Neto, F., & Vasconcellos, K. L. (2002). Nearly unbiased maximum likelihood estimation for the beta distribution. Journal of Statistical Computation and Simulation, 72(2), 107-118.

Owen, C. B. (2008). Parameter estimation for the beta distribution. Brigham Young University.

Ma, Z., & Leijon, A. (2010, March). Expectation propagation for estimating the parameters of the beta distribution. In 2010 IEEE international conference on acoustics, speech and signal processing (pp. 2082-2085). IEEE.

Yugandhar, C., & Haragopal, V. V. (2023). Local Information Based Parameter Estimation for Beta Distribution of First Kind. Aligarh Journal of Statistics, 43.

Othman, K. T. (2022). Using the nonparametric methods to estimate parameters of The Beta distribution.

Gelman, A., Carlin, J. B., Stern, H. S., & Rubin, D. B. (1995). Bayesian data analysis. Chapman and Hall/CRC.

Jambunathan, M. V. (1954). Some properties of beta and gamma distributions. The annals of mathematical statistics, 401-405.

Olea, R. A. (2011). On the use of the beta distribution in probabilistic resource assessments. Natural resources research, 20, 377-388.

Jun, C. H., & Yoo, C. S. (2012). Application of the beta distribution for the temporal quantification of storm events. Journal of Korea Water Resources Association, 45(6), 531-544.

Santana-e-Silva, J. J., Cribari-Neto, F., & Vasconcellos, K. L. (2022). Beta distribution misspecification tests with application to Covid-19 mortality rates in the United States. Plos one, 17(9), e0274781.

Yalçınkaya, A., Şenoğlu, B., & Yolcu, U. (2018). Maximum likelihood estimation for the parameters of skew normal distribution using genetic algorithm. Swarm and Evolutionary Computation, 38, 127-138.

Holland, J. H. (1975). An introductory analysis with applications to biology, control, and artificial intelligence. Adaptation in Natural and Artificial Systems. First Edition, The University of Michigan, USA.

Yalçınkaya, A., Yolcu, U., & Şenoğlu, B. (2021). Maximum likelihood and maximum product of spacings estimations for the parameters of skew-normal distribution under doubly type II censoring using genetic algorithm. Expert Systems with Applications, 168, 114407.

Yalçınkaya, A., Kılıç, A., & Şenoğlu, B. (2024). Estimating The Parameters of Generalized Logistic Distribution via Genetic Algorithm Based on Reduced Search Space. Journal of Mathematical Sciences, 1-17.

Tiku, M. L. (1967). Estimating the mean and standard deviation from a censored normal sample. Biometrika, 54(1-2), 155-165.

Tiku, M. L., & Akkaya, A. D. (2004). Robust estimation and hypothesis testing. New Age International.

Chapter 11

POINT ESTIMATION FOR KUMARASWAMY BURR TYPE XII DISTRIBUTION BASED ON TYPE II CENSORED DATA

Özge GÜRER[1]

Birdal ŞENOĞLU[2]

1 Dr., Ankara University, ORCID: 0000-0002-5565-5069, otanju@ankara.edu.tr

2 Prof. Dr., Ankara University, ORCID: 0000-0003-3707-2393, senoglu@science.ankara.edu.tr

1 INTRODUCTION

Censored samples are widely used in many disciplines such as medicine, economics, biology, engineering, etc. Therefore, there are many studies on the statistical analysis of censored data in the literature. The vast majority of these studies are from the fields of reliability and life testing, because it is often too expensive or impractical to continue the experiment until all the units fail. For the related literature, one may refer to Wu (2002), Wang (2011), Zhang et al. (2015), Nassr and Elharoun (2019), Xie et al. (2020), Kamal (2022), Kumar et al. (2024), etc.

Type II censoring, one of the most popular censoring schemes, is a condition where the experiment is started and/or terminated after a predetermined number of specific events have occurred. Many authors have used type II censoring scheme in parameter estimation problems. For example, Sarhan and Greenberg (1957) considered the estimation of the unknown parameters of one and two-parameter exponential distribution for type II censored samples. Harter and Moore (1966) developed iterative procedures for maximum likelihood (ML) estimation based on singly and doubly type II censored samples from normal populations. Tiku (1968) derived the modified maximum likelihood (MML) estimators for the parameters of log-normal distribution from a type II censored data. Balakrishnan and Chan (1992) derived the best linear unbiased estimator and approximate maximum likelihood estimator based on doubly type II censored samples for the scaled half logistic distribution. Singh et al. (2005) obtained the Bayes, ML and generalized ML estimators for the shape parameters of exponentiated-Weibull distribution under type II censored sample case. Makhdoom and Nasiri (2016) obtained the ML estimator for the exponential mean parameters under type II censoring by using EM algorithm. Pak et al. (2013) estimated the scale parameter of Rayleigh distribution under doubly type II censoring scheme by using ML methodology. Senoğlu and Tiku (2004) derived the MML estimators for the parameters of one-way analysis of variance (ANOVA) model under type II censoring when the error terms have generalized logistic distribution.

Ghosh and Nadarajah (2017) derived the Bayes estimates of the Kumaraswamy distribution based on singly and doubly type II censoring. Arslan et al. (2021) obtained explicit estimators for the location and scale parameters of Maxwell distribution under type II censoring scheme by using MML methodology.

Burr type XII ($BXII$) distribution is widely used in the context of statistical analysis of censored data, see for example Wingo (1993), Soliman (2005), Rastogi and Tripathi (2011), Panahi and Sayyareh (2014), Xin et al. (2018), Danish et al. (2018), Panahi (2019), Wang and Gui (2021), etc. $BXII$ distribution can accommodate many shapes due to its high flexibility, including some well-known distributions such as logistic, log-logistic, Lomax, Weibull, etc. Also, the cumulative distribution function (cdf) and the reliability function of $BXII$ distribution are defined explicitly, therefore its likelihood function for censored samples can easily be handled. Paranaiba et al. (2013) are motivated by the widespread and practical use of $BXII$ and the fact that more flexible distributions are still needed for more complex situations. They extended the $BXII$ distribution by inserting its cdf into the cdf of family of Kumaraswamy-Generalized (KwG) distributions defined by

$$F(x) = 1 - (1 - (G(x))^a)^b \qquad (1)$$

where a and b are the additional shape parameters and $G(x)$ denotes the cdf of baseline distribution, see Cordeiro and De Castro (2011) for the details of KwG distributions. Then, the resulting distribution is called as $KwBXII$. It should be noted that $KwBXII$ distribution has more flexible tails than $BXII$ distribution due to the additional shape parameters and can easily be used to model data from various fields of science.

In this study, the aim is to estimate the location and scale parameters of $KwBXII$ distribution by assuming the shape parameters are known under type II censored samples. ML is used as the estimation method. However, ML estimators cannot be obtained in closed form due to the intractable functions in the likelihood equations. Thus, we resort not only to the

iterative methods but also to the modified maximum likelihood (MML) methodology proposed by Tiku (1967). MML methodology linearize the nonlinear terms in the likelihood equations and provide explicit solutions for the unknown distribution parameters. The resulted MML estimators are asymptotically equivalent to ML estimators. An extensive Monte Carlo simulation study is conducted to compare the mentioned ML and MML estimators with respect to the *bias* and mean squares error (*MSE*) criteria. To the best of our knowledge, this is the first study addressing the ML and MML estimators of the location and scale parameters of *KwBXII* distribution in the context of type II censoring.

2 *KwBXII* DISTRIBUTION

The probability density function (pdf) and the corresponding cdf

of *KwBXII* distribution are given by

$$f(x) = \frac{abck}{\sigma} \left(\frac{x-\mu}{\sigma}\right)^{c-1} \left[1 + \left(\frac{x-\mu}{\sigma}\right)^c\right]^{-(k+1)} \left[1\right.$$
$$\left. - \left\{1 + \left(\frac{x-\mu}{\sigma}\right)^c\right\}^{-k}\right]^{a-1}$$
$$\times \left[1 - \left\{1 - \left[1 + \left(\frac{x-\mu}{\sigma}\right)^c\right]^{-k}\right\}^a\right]^{b-1} , \ x \geq$$

$$\mu, \ \mu \epsilon \mathbb{R}, \ a, b, c, k, \sigma \epsilon \mathbb{R}^+ \tag{2}$$

and

$$F(x) = 1 - \left[1 - \left\{1 - \left[1 + \left(\frac{x-\mu}{\sigma}\right)^c\right]^{-k}\right\}^a\right]^b, \tag{3}$$

respectively. Here, a, b, c and k are the shape parameters, μ is the location parameter and σ is the scale parameter. A random variable X having $KwBXII$ distribution with the aforementioned parameters is denoted by $X \sim KwBXII(a, b, c, k, \mu, \sigma)$. Figure 1 shows the pdf plots of $KwBXII$ distribution for some representative values of the shape parameters a, b, c and k.
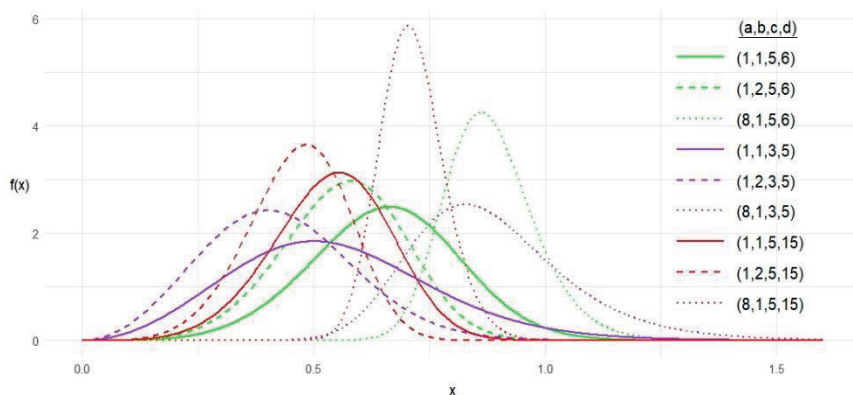
Figure 1. The pdf plots of $KwBXII$ distribution for some representative values of the shape parameters a, b, c and k.

See the simulated skewness and kurtosis values for the $KwBXII$ distribution given in Table 1.

Table 1. Skewness $\left(\sqrt{\beta_1}\right)$ and kurtosis (β_2) values of $KwBXII$ distribution for some representative values of the shape parameters a, b, c and k.

			(a,b)		
			(1,1)	(1,2)	(8,1)
(c,k)	(5,6)	$\sqrt{\beta_1}$	-0.0134	-0.1390	0.5143
		β_2	3.0088	2.9133	3.7003
	(3,5)	$\sqrt{\beta_1}$	0.5588	0.3467	0.8957
		β_2	3.6033	3.0424	4.8461
	(5,15)	$\sqrt{\beta_1}$	-0.1628	-0.2092	0.2771
		β_2	2.9032	2.8874	3.2292

It is clear that $KwBXII$ distribution reduces to $BXII$ distribution for $(a, b) = (1,1)$. It also contains many well-known distributions as sub-

models such as exponentiated $BXII$, KwLog-logistic, log-logistic, KwPareto type II, Pareto type II, KwWeibull, Weibull, etc.

3 ESTIMATION

This section is devoted to obtaining the ML and MML estimators of the location and scale parameters of $KwBXII$ distribution with known shape parameters for type II censored samples.

3.1 ML Estimation

Consider a sample of size n from $KwBXII(a, b, c, k, \mu, \sigma)$ distribution, in which the smallest r_1 and largest r_2 observations are censored. In other words, let

$$x_{(r_1+1)} \leq x_{(r_1+2)} \leq \cdots \leq x_{(n-r_2)}$$

be a type II censored sample of size $n - r_1 - r_2$ from $KwBXII(a, b, c, k, \mu, \sigma)$ distribution. Then, the corresponding likelihood (L) function is written as

$$L = \frac{n!}{r_1! r_2!} \left(\frac{1}{\sigma}\right)^{n-r_1-r_2} \left(\prod_{i=r_1+1}^{n-r_2} f(z_{(i)})\right) \left(F(z_{(r_1+1)})\right)^{r_1} \left(1 - F(z_{(n-r_2)})\right)^{r_2} \tag{4}$$

where $z_{(i)} = \frac{x_{(i)} - \mu}{\sigma}$, $z_{(r_1+1)} = \frac{x_{(r_1+1)} - \mu}{\sigma}$ and $z_{(n-r_2)} = \frac{x_{(n-r_2)} - \mu}{\sigma}$.

After taking the logarithm of L function, the log likelihood ($\ln L$) function is obtained as follows

$$\ln L = ln\left(\frac{n!}{r_1! r_2!}\right) - (n - r_1 - r_2) \ln \sigma + \sum_{i=r_1+1}^{n-r_2} \ln\left(f(z_{(i)})\right) + r_1 \ln\left(F(z_{(r_1+1)})\right) +$$

$$+ r_2 \ln\left(1 - F(z_{(n-r_2)})\right). \tag{5}$$

By taking the derivatives of $\ln L$ function with respect to the parameters μ and σ and setting them equal to zero, the following likelihood equations are obtained

$$\frac{\partial \ln L}{\partial \mu} = -\frac{1}{\sigma}\left(\sum_{i=r_1+1}^{n-r_2} g(z_{(i)}) + r_1 g_1(z_{(r_1+1)}) - r_2 g_2(z_{(n-r_2)})\right) = 0$$

$$\frac{\partial \ln L}{\partial \sigma} = -\frac{1}{\sigma}\left((n - r_1 - r_2) + \sum_{i=r_1+1}^{n-r_2} z_{(i)} g(z_{(i)}) + r_1 z_{(r_1+1)} g_1(z_{(r_1+1)})\right.$$

$$\left. -r_2 z_{(n-r_2)} g_2(z_{(n-r_2)})\right) = 0 \qquad (6)$$

where $g(z) = \frac{f'(z)}{f(z)}, g_1(z) = \frac{f(z)}{F(z)}$ and $g_2(z) = \frac{f(z)}{1-F(z)}$. It is obvious that the likelihood equations in (6) have no explicit solutions due to nonlinear functions of the unknown parameters. Thus, iterative methods are needed to solve these equations. In this study, we implemented the Nelder-Mead method by using the optim() function in R statistical software.

3.2 MML Estimation

Unlike ML methodology, in this subsection closed form solutions for the estimators of μ and σ are derived by using the MML methodology. In this way, some problems such as convergence to wrong root, convergence to multiple roots and non-convergence of iterations that can be caused by the iterative methods are avoided.

In order to obtain the MML estimators, firstly nonlinear functions g, g_1 and g_2 are linearized around the expected values of the standardized ordered statistics, i.e., $t_{(i)} = E(z_{(i)}), t_1 = E(z_{(r_1+1)})$ and $t_2 = E(z_{(n-r_2)})$, respectively, by using the first two terms of Taylor series expansion as follows

$$g(z_{(i)}) \cong \alpha_i - \beta_i z_{(i)}, \ g_1(z_{(r_1+1)}) \cong \alpha_1 - \beta_1 z_{(r_1+1)} \text{ and}$$
$$g_2(z_{(n-r_2)}) \cong \alpha_2 + \beta_2 z_{(n-r_2)} \qquad (7)$$

where

$$\alpha_i = \frac{f'(t_{(i)})}{f(t_{(i)})} + \beta_i t_{(i)}, \qquad \beta_i = -\left(\frac{f''(t_{(i)})f(t_{(i)}) - \left((f'(t_{(i)}))\right)^2}{\left(f(t_{(i)})\right)^2}\right), \qquad (i = r_1 + 1, \dots, n - r_2),$$

$$\alpha_1 = \frac{f(t_1)}{F(t_1)} + \beta_1 t_1, \beta_1 = -\left(\frac{f'(t_1)}{F(t_1)} - \frac{(f(t_1))^2}{(F(t_1))^2}\right), \alpha_2 = \frac{f(t_2)}{1-F(t_2)} - \beta_2 t_2$$

$$\text{and } \beta_2 = \frac{f'(t_2)}{1-F(t_2)} + \frac{(f(t_2))^2}{(1-F(t_2))^2}.$$

Here, $t_{(i)}$, $(i = r_1 + 1, \dots, n - r_2)$, t_1 and t_2 are calculated by solving the following equalities

$$F(t_{(i)}) = \frac{i}{n+1}, F(t_1) = \frac{r_1}{n+1} \text{ and } F(t_2) = 1 - \frac{r_2}{n+1}, \tag{8}$$

respectively. Secondly, linearized functions in (7) are incorporated into the likelihood equations in (6) and the following modified likelihood equations are obtained

$$\frac{\partial \ln L^*}{\partial \mu} = -\frac{1}{\sigma}\left(\sum_{i=r_1+1}^{n-r_2}(\alpha_i - \beta_i z_{(i)}) + r_1(\alpha_1 - \beta_1 z_{(r_1+1)}) - r_2(\alpha_2 + \beta_2 z_{(n-r_2)})\right) = 0$$

$$\frac{\partial \ln L^*}{\partial \sigma} = -\frac{1}{\sigma}\left((n - r_1 - r_2) + \sum_{i=r_1+1}^{n-r_2} z_{(i)}(\alpha_i - \beta_i z_{(i)}) + r_1 z_{(r_1+1)}(\alpha_1 - \beta_1 z_{(r_1+1)}) - r_2 z_{(n-r_2)}(\alpha_2 + \beta_2 z_{(n-r_2)})\right) = 0. \tag{9}$$

Finally, simultaneous solutions of the equations in (9) yield the MML estimators of μ and σ as

$$\hat{\mu} = K - D\hat{\sigma} \qquad \text{and} \qquad \hat{\sigma} = \frac{-B + \sqrt{B^2 + 4AC}}{2\sqrt{A(A-1)}} \tag{10}$$

where $K = \left\{\sum_{i=r_1+1}^{n-r_2} \beta_i x_{(i)} + r_1\beta_1 x_{(r_1+1)} + r_2\beta_2 x_{(n-r_2)}\right\}/m$, $D = \left\{\sum_{i=r_1+1}^{n-r_2} \alpha_i + r_1\alpha_1 - r_2\alpha_2\right\}/m$,

$m = \sum_{i=r_1+1}^{n-r_2} \beta_i + r_1\beta_1 + r_2\beta_2$, $A = n - r_1 - r_2$,

$B = \sum_{i=r_1+1}^{n-r_2} \alpha_i\left(x_{(i)} - K\right) + r_1\alpha_1\left(x_{(r_1+1)} - K\right) - r_2\alpha_2\left(x_{(n-r_2)} - K\right)$ and

$C = \sum_{i=r_1+1}^{n-r_2} \beta_i\left(x_{(i)} - K\right)^2 + r_1\beta_1\left(x_{(r_1+1)} - K\right)^2 + r_2\beta_2\left(x_{(n-r_2)} - K\right)^2.$

MML estimators offer several benefits, including asymptotic equivalence to ML estimators and high efficiency even with small sample sizes. Additionally, they are robust to outliers as they give small weights to the observations in the longer tails of the distribution. One may refer to Güven and Şenoğlu (2023) in the context of KwWeibull distribution under type II censoring, which is a sub-model of $KwBXII$ for $k \to \infty$. For complete samples, see Ergenç et al. (2022) in the context of KwWeibull distribution and also Akgül et al. (2019) in the context of $BXII$ distribution, which is a sub-model of $KwBXII$ for $(a, b) = (1,1)$.

4 MONTE CARLO SIMULATION

At this stage of the study, the ML ($\hat{\mu}_{ML}$ and $\hat{\sigma}_{ML}$) and MML ($\hat{\mu}_{MML}$ and $\hat{\sigma}_{MML}$) estimators obtained in the previous sections are compared through a Monte Carlo simulation study. While making comparisons, $bias$ and MSE criteria calculated using the following equalities are used

$$bias(\hat{\theta}) = E(\hat{\theta} - \theta) \text{ and } MSE(\hat{\theta}) = E(\hat{\theta} - \theta)^2. \qquad (11)$$

Deficiency (Def) criterion is also used to compare of the joint efficiencies of the ML and MML estimators for the location parameter μ and scale parameter σ. It is defined as given below

$$Def(\hat{\mu}, \hat{\sigma}) = MSE(\hat{\mu}) + MSE(\hat{\sigma}). \qquad (12)$$

During the simulation study, μ and σ are taken as 0 and 1, respectively, without loss of generality. Various combinations of sample sizes, numbers of censored observations and shape parameter values are considered, see Table 2. In the cases of interest, see also Table 1 for skewness and kurtosis values of the $KwBXII$ distribution.

Table 2. Sample sizes, numbers of censored observations and the shape parameter values used in the simulation study.

$n =$	10, 20, 50
$(r_1, r_2) =$	(0,0), (0,1), (1,0), (1,1), (0,2), (2,0), (1,2), (2,1), (2,2), (0,3), (3,0), (1,3), (3,1), (2,3), (3,2), (1,4), (4,1), (0,5), (5,0), (2,5)
$(c, k) =$	$(5, 6), (3, 5), (5, 15)$
$(a, b) =$	$(1, 1), (1, 2), (8, 1)$

Simulation results obtained using 10,000 Monte Carlo runs are presented in Tables 3 to 5. Conclusions drawn from these results are as follows.

From the *bias* perspective, MML estimator of the location parameter μ performs better than its competitor in almost every case. Only in some of the cases for $(a, b, c, k) = (1,1,3,5)$ and $(a, b, c, k) = (1,2,3,5)$ with a sample of size $n = 50$, the ML estimator of μ is less biased than $\hat{\mu}_{MML}$. For the scale parameter σ, the MML estimator has smaller bias than the corresponding ML estimator in all cases. It should also be noted that *bias* values for both ML and MML estimators of the parameters μ and σ decrease as the sample size n increases.

If to look at *MSE* values, the ML and MML estimators of the location parameter μ show similar performances in most of the cases. The cases where $\hat{\mu}_{ML}$ outperforms $\hat{\mu}_{MML}$ are observed when $(a, b) = (8,1)$, where skewness and kurtosis values are the highest regardless of the value of (c, k). For $(a, b) = (8,1)$ case, it is seen that the *MSE* values of $\hat{\mu}_{MML}$ gets closer to those of its counterpart as the sample size increases when $(c, k) = (5,6)$. The performances of $\hat{\mu}_{ML}$ and $\hat{\mu}_{MML}$ become similar as the sample size increases or the number of censored observations within small sample sizes increases when $(c, k) = (3,5)$. ML estimator of μ is superior only for $n = 10$ in complete sample case when $(c, k) = (5,15)$. For the scale parameter σ, it should firstly be noted that when the sample size is 50, performances of both estimators are very similar as expected in all cases. For other sample sizes, the results are needed to be explained in detail. When $(a, b, c, k) = (1,1,5,6)$, $\hat{\sigma}_{ML}$ is slightly more efficient than $\hat{\sigma}_{MML}$ for $n = 10$ and 20. When $(a, b, c, k) = (1,2,5,6)$, both estimators show

similar performances except for the complete sample case of $n = 10$, where $\hat{\sigma}_{MML}$ is observed to be more efficient. For $(a, b, c, k) = (1,1,3,5)$, $\hat{\sigma}_{ML}$ is superior for the complete sample case when $n = 10$ and 20, but as the number of censored observations increases, the performance of $\hat{\sigma}_{MML}$ surpasses its counterpart. For $(a, b, c, k) = (1,2,3,5)$, MML estimator of σ is more efficient than the corresponding ML estimator for $n = 10$. When $n = 20$, on the other hand, similar performances are observed, but $\hat{\sigma}_{MML}$ is more efficient for $(r_1, r_2) = (1,2)$. When $(a, b, c, k) = (1,1,5,15)$ and $(a, b, c, k) = (1,2,5,15)$, MML estimator of σ performs better than its rival for the sample sizes of 10 and 20 in almost all cases. For $(a, b) = (8,1)$, regardless of the value of (c, k), $\hat{\sigma}_{ML}$ estimator is more efficient than $\hat{\sigma}_{MML}$ estimators for $n = 10$ and 20.

In terms of Def criterion, results are very similar to those of MSE, therefore they are not reinterpreted here, for the sake of brevity.

As a result, researchers concerning about time and computational simplicity can comfortably prefer to use MML methodology, since it does not cause a considerable loss of efficiency even in the cases where ML is more efficient.

Table 3. Simulated *bias*, *MSE* and *Def* values for the MML and ML estimators of the location parameter μ and scale parameter σ; $(c, k) = (5, 6)$.

		$\hat{\mu}$				$\hat{\sigma}$					
		MML		ML		MML		ML			
n	(r_1, r_2)	bias	MSE	bias	MSE	bias	MSE	bias	MSE	Def_{MML}	Def_{ML}
						$(a, b) = (1, 1)$					
10	(0,0)	0.0206	0.0269	0.0537	0.0268	-0.0297	0.0567	-0.0802	0.0562	0.0836	0.0830
	(1,1)	0.0277	0.0366	0.0691	0.0365	-0.0414	0.0773	-0.1037	0.0768	0.1139	0.1133
20	(0,0)	0.0106	0.0125	0.0260	0.0124	-0.0142	0.0261	-0.0385	0.0259	0.0386	0.0383
	(1,1)	0.0087	0.0151	0.0269	0.0150	-0.0125	0.0313	-0.0403	0.0311	0.0464	0.0461
50	(0,0)	0.0057	0.0050	0.0107	0.0049	-0.0066	0.0103	-0.0151	0.0102	0.0153	0.0151
	(1,1)	0.0042	0.0052	0.0104	0.0052	-0.0053	0.0108	-0.0151	0.0107	0.0160	0.0159
	(2,2)	0.0056	0.0057	0.0125	0.0057	-0.0084	0.0116	-0.0191	0.0117	0.0173	0.0174
						$(a, b) = (1, 2)$					
10	(0,0)	0.0212	0.0197	0.0481	0.0199	-0.0384	0.0528	-0.0833	0.0534	0.0725	0.0733
	(1,0)	0.0205	0.0240	0.0531	0.0239	-0.0369	0.0634	-0.0907	0.0635	0.0874	0.0874
20	(0,0)	0.0128	0.0095	0.0247	0.0095	-0.0223	0.0254	-0.0427	0.0255	0.0349	0.0350
	(1,0)	0.0089	0.0106	0.0239	0.0106	-0.0157	0.0279	-0.0408	0.0279	0.0385	0.0385
	(2,1)	0.0107	0.0128	0.0278	0.0128	-0.0192	0.0338	-0.0478	0.0338	0.0466	0.0466
50	(0,0)	0.0062	0.0037	0.0099	0.0036	-0.0105	0.0098	-0.0171	0.0097	0.0135	0.0133
	(1,0)	0.0050	0.0039	0.0102	0.0039	-0.0081	0.0101	-0.0170	0.0102	0.0140	0.0141
	(2,1)	0.0044	0.0041	0.0102	0.0041	-0.0081	0.0108	-0.0178	0.0108	0.0149	0.0149
	(3,2)	0.0050	0.0044	0.0112	0.0044	-0.0091	0.0119	-0.0196	0.0119	0.0163	0.0163
						$(a, b) = (8, 1)$					
10	(0,0)	0.0149	0.0452	0.0647	0.0438	-0.0124	0.0622	-0.0732	0.0569	0.1074	0.1007
	(0,1)	0.0260	0.0486	0.0740	0.0480	-0.0266	0.0671	-0.0850	0.0659	0.1157	0.1139
20	(0,0)	0.0074	0.0215	0.0334	0.0211	-0.0062	0.0296	-0.0379	0.0290	0.0511	0.0501
	(0,1)	0.0092	0.0227	0.0331	0.0225	-0.0085	0.0312	-0.0377	0.0308	0.0539	0.0533
	(0,2)	0.0117	0.0237	0.0356	0.0236	-0.0114	0.0328	-0.0406	0.0324	0.0565	0.0560
50	(0,0)	0.0013	0.0083	0.0119	0.0082	-0.0005	0.0114	-0.0136	0.0112	0.0197	0.0194
	(0,1)	0.0030	0.0085	0.0128	0.0084	-0.0025	0.0117	-0.0145	0.0117	0.0202	0.0201
	(0,2)	0.0045	0.0086	0.0141	0.0086	-0.0043	0.0119	-0.0160	0.0119	0.0205	0.0205
	(0,3)	0.0039	0.0088	0.0133	0.0088	-0.0036	0.0122	-0.0151	0.0121	0.0210	0.0209
	(1,3)	0.0033	0.0090	0.0130	0.0090	-0.0027	0.0124	-0.0146	0.0123	0.0214	0.0213
	(2,3)	0.0046	0.0097	0.0147	0.0096	-0.0045	0.0133	-0.0167	0.0132	0.0230	0.0228
	(1,4)	0.0053	0.0094	0.0151	0.0094	-0.0053	0.0130	-0.0171	0.0129	0.0224	0.0223

Table 4. Simulated $bias$, MSE and Def values for the MML and ML estimators of the location parameter μ and scale parameter σ; $(c,k) = (3,5)$.

		$\hat{\mu}$				$\hat{\sigma}$					
		MML		ML		MML		ML			
n	(r_1,r_2)	bias	MSE	bias	MSE	bias	MSE	bias	MSE	Def_{MML}	Def_{ML}
					$(a,b)=(1,1)$						
10	(0,0)	0.0368	0.0162	0.0519	0.0163	-0.0453	0.0584	-0.0907	0.0579	0.0746	0.0742
	(0,1)	0.0411	0.0164	0.0542	0.0166	-0.0541	0.0613	-0.0966	0.0617	0.0777	0.0783
20	(0,0)	0.0207	0.0073	0.0255	0.0071	-0.0211	0.0269	-0.0430	0.0261	0.0342	0.0332
	(0,1)	0.0262	0.0073	0.0294	0.0072	-0.0352	0.0274	-0.0526	0.0275	0.0347	0.0347
	(0,2)	0.0272	0.0077	0.0301	0.0076	-0.0377	0.0288	-0.0541	0.0289	0.0365	0.0365
	(1,2)	0.0188	0.0089	0.0285	0.0091	-0.0258	0.0324	-0.0527	0.0328	0.0413	0.0419
50	(0,0)	0.0120	0.0026	0.0115	0.0025	-0.0123	0.0099	-0.0182	0.0097	0.0125	0.0122
	(0,1)	0.0132	0.0027	0.0121	0.0026	-0.0168	0.0101	-0.0208	0.0100	0.0128	0.0126
	(0,2)	0.0139	0.0028	0.0128	0.0027	-0.0190	0.0105	-0.0226	0.0103	0.0133	0.0130
	(1,2)	0.0097	0.0030	0.0115	0.0030	-0.0112	0.0110	-0.0195	0.0111	0.0140	0.0141
	(0,3)	0.0148	0.0028	0.0135	0.0027	-0.0202	0.0103	-0.0233	0.0102	0.0131	0.0129
	(1,3)	0.0086	0.0030	0.0103	0.0030	-0.0109	0.0111	-0.0190	0.0111	0.0141	0.0141
	(2,3)	0.0085	0.0033	0.0118	0.0033	-0.0108	0.0117	-0.0210	0.0118	0.0150	0.0151
	(0,5)	0.0142	0.0028	0.0127	0.0027	-0.0201	0.0109	-0.0227	0.0107	0.0137	0.0134
	(2,5)	0.0084	0.0034	0.0117	0.0034	-0.0113	0.0127	-0.0215	0.0127	0.0161	0.0161
					$(a,b)=(1,2)$						
10	(0,0)	0.0292	0.0094	0.0398	0.0095	-0.0528	0.0512	-0.0914	0.0520	0.0606	0.0615
	(0,1)	0.0353	0.0104	0.0460	0.0106	-0.0697	0.0591	-0.1084	0.0609	0.0695	0.0715
20	(0,0)	0.0185	0.0045	0.0214	0.0045	-0.0307	0.0242	-0.0468	0.0242	0.0287	0.0287
	(0,1)	0.0211	0.0047	0.0233	0.0046	-0.0377	0.0257	-0.0519	0.0258	0.0304	0.0304
	(0,2)	0.0213	0.0048	0.0239	0.0047	-0.0407	0.0273	-0.0552	0.0274	0.0321	0.0321
	(1,2)	0.0151	0.0055	0.0228	0.0056	-0.0272	0.0306	-0.0522	0.0311	0.0361	0.0367
50	(0,0)	0.0107	0.0017	0.0101	0.0016	-0.0185	0.0090	-0.0222	0.0089	0.0107	0.0105
	(0,1)	0.0107	0.0017	0.0097	0.0017	-0.0179	0.0093	-0.0205	0.0092	0.0110	0.0109
	(0,2)	0.0110	0.0017	0.0100	0.0017	-0.0197	0.0097	-0.0220	0.0095	0.0114	0.0112
	(0,3)	0.0110	0.0017	0.0099	0.0017	-0.0196	0.0099	-0.0216	0.0091	0.0116	0.0108
	(1,3)	0.0080	0.0018	0.0094	0.0018	-0.0137	0.0103	-0.0208	0.0104	0.0121	0.0122
	(2,3)	0.0067	0.0020	0.0093	0.0020	-0.0124	0.0112	-0.0215	0.0113	0.0132	0.0133
	(1,4)	0.0081	0.0018	0.0096	0.0019	-0.0160	0.0105	-0.0232	0.0106	0.0123	0.0125
					$(a,b)=(8,1)$						
10	(0,0)	0.0216	0.0436	0.0685	0.0421	-0.0136	0.0672	-0.0785	0.0633	0.1108	0.1054
	(0,1)	0.0306	0.0459	0.0733	0.0455	-0.0250	0.0707	-0.0841	0.0686	0.1166	0.1141
	(0,2)	0.0382	0.0496	0.0825	0.0496	-0.0367	0.0779	-0.0974	0.0766	0.1275	0.1262
20	(0,0)	0.0091	0.0206	0.0327	0.0203	-0.0044	0.0319	-0.0376	0.0309	0.0525	0.0512
	(0,1)	0.0115	0.0212	0.0324	0.0210	-0.0071	0.0328	-0.0366	0.0321	0.0540	0.0531
	(0,2)	0.0168	0.0222	0.0371	0.0222	-0.0134	0.0346	-0.0420	0.0342	0.0568	0.0564
50	(0,0)	0.0034	0.0080	0.0127	0.0079	-0.0014	0.0124	-0.0146	0.0122	0.0204	0.0201
	(0,1)	0.0041	0.0079	0.0124	0.0078	-0.0026	0.0122	-0.0145	0.0121	0.0201	0.0199
	(0,2)	0.0056	0.0082	0.0136	0.0081	-0.0040	0.0126	-0.0154	0.0125	0.0208	0.0206
	(0,3)	0.0049	0.0082	0.0127	0.0082	-0.0036	0.0128	-0.0148	0.0127	0.0210	0.0209

(r_1,r_2)	bias	MSE	bias	MSE	bias	MSE	bias	MSE	Def_{MML}	Def_{ML}
(1,3)	0.0042	0.0088	0.0129	0.0087	-0.0023	0.0135	-0.0145	0.0134	0.0223	0.0221
(1,4)	0.0060	0.0090	0.0146	0.0090	-0.0049	0.0138	-0.0169	0.0137	0.0228	0.0227
(0,5)	0.0063	0.0084	0.0141	0.0084	-0.0049	0.0130	-0.0159	0.0129	0.0214	0.0213
(2,5)	0.0047	0.0096	0.0139	0.0095	-0.0033	0.0146	-0.0160	0.0145	0.0242	0.0240

Table 5. Simulated $bias$, MSE and Def values for the MML and ML estimators of the location parameter μ and scale parameter σ; $(c,k) = (5,15)$.

		$\hat{\mu}$				$\hat{\sigma}$					
		MML		ML		MML		ML			
n	(r_1,r_2)	bias	MSE	bias	MSE	bias	MSE	bias	MSE	Def_{MML}	Def_{ML}
						$(a,b) = (1,1)$					
10	(0,0)	0.0226	0.0179	0.0479	0.0181	-0.0423	0.0528	-0.0861	0.0537	0.0707	0.0718
	(1,0)	0.0211	0.0217	0.0519	0.0218	-0.0401	0.0618	-0.0927	0.0624	0.0835	0.0842
20	(0,0)	0.0125	0.0085	0.0237	0.0086	-0.0227	0.0247	-0.0424	0.0249	0.0332	0.0335
	(1,0)	0.0111	0.0098	0.0251	0.0098	-0.0210	0.0278	-0.0453	0.0280	0.0376	0.0378
	(2,1)	0.0119	0.0109	0.0282	0.0110	-0.0229	0.0318	-0.0511	0.0321	0.0427	0.0431
50	(0,0)	0.0068	0.0033	0.0101	0.0033	-0.0119	0.0095	-0.0181	0.0095	0.0128	0.0128
	(1,0)	0.0028	0.0035	0.0075	0.0035	-0.0058	0.0100	-0.0142	0.0100	0.0135	0.0135
	(2,1)	0.0033	0.0038	0.0088	0.0038	-0.0066	0.0109	-0.0162	0.0109	0.0147	0.0147
	(3,2)	0.0039	0.0039	0.0099	0.0039	-0.0072	0.0114	-0.0176	0.0114	0.0153	0.0153
						$(a,b) = (1,2)$					
10	(0,0)	0.0173	0.0136	0.0388	0.0137	-0.0393	0.0520	-0.0812	0.0526	0.0656	0.0663
	(1,0)	0.0179	0.0166	0.0441	0.0166	-0.0414	0.0621	-0.0920	0.0626	0.0787	0.0792
	(2,0)	0.0179	0.0202	0.0482	0.0199	-0.0412	0.0740	-0.0991	0.0736	0.0942	0.0935
20	(0,0)	0.0109	0.0065	0.0201	0.0065	-0.0237	0.0245	-0.0418	0.0247	0.0310	0.0312
	(1,0)	0.0089	0.0071	0.0206	0.0071	-0.0212	0.0265	-0.0439	0.0268	0.0336	0.0339
	(2,0)	0.0101	0.0079	0.0231	0.0080	-0.0229	0.0296	-0.0479	0.0299	0.0375	0.0379
	(2,1)	0.0090	0.0086	0.0231	0.0086	-0.0209	0.0329	-0.0486	0.0330	0.0415	0.0416
50	(0,0)	0.0062	0.0025	0.0089	0.0025	-0.0131	0.0095	-0.0184	0.0095	0.0120	0.0120
	(1,0)	0.0034	0.0027	0.0073	0.0027	-0.0077	0.0100	-0.0153	0.0100	0.0127	0.0127
	(2,0)	0.0042	0.0028	0.0087	0.0028	-0.0093	0.0105	-0.0179	0.0105	0.0133	0.0133
	(2,1)	0.0038	0.0028	0.0085	0.0028	-0.0091	0.0106	-0.0182	0.0106	0.0134	0.0134
	(3,0)	0.0029	0.0029	0.0077	0.0029	-0.0071	0.0106	-0.0163	0.0107	0.0135	0.0136
	(3,1)	0.0046	0.0029	0.0096	0.0029	-0.0103	0.0109	-0.0200	0.0109	0.0138	0.0138
	(3,2)	0.0030	0.0031	0.0081	0.0031	-0.0072	0.0117	-0.0173	0.0117	0.0148	0.0148
	(4,1)	0.0035	0.0032	0.0087	0.0032	-0.0083	0.0118	-0.0184	0.0118	0.0150	0.0150
	(5,0)	0.0038	0.0031	0.0090	0.0031	-0.0088	0.0114	-0.0187	0.0114	0.0145	0.0145
						$(a,b) = (8,1)$					
10	(0,0)	0.0137	0.0283	0.0515	0.0278	-0.0172	0.0579	-0.0725	0.0564	0.0862	0.0842
	(0,1)	0.0247	0.0324	0.0634	0.0323	-0.0329	0.0660	-0.0895	0.0656	0.0984	0.0979
20	(0,0)	0.0063	0.0133	0.0255	0.0132	-0.0078	0.0271	-0.0359	0.0268	0.0404	0.0400
	(0,1)	0.0103	0.0147	0.0292	0.0146	-0.0136	0.0300	-0.0412	0.0298	0.0447	0.0444
	(0,2)	0.0102	0.0157	0.0296	0.0156	-0.0135	0.0321	-0.0419	0.0319	0.0478	0.0475
	(1,2)	0.0118	0.0172	0.0325	0.0171	-0.0158	0.0348	-0.0459	0.0346	0.0520	0.0517
50	(0,0)	0.0022	0.0052	0.0100	0.0052	-0.0027	0.0107	-0.0141	0.0106	0.0159	0.0158

(0,1)	0.0030	0.0054	0.0105	0.0053	-0.0038	0.0109	-0.0148	0.0108	0.0163	0.0161
(1,2)	0.0032	0.0059	0.0109	0.0059	-0.0040	0.0120	-0.0152	0.0120	0.0179	0.0179
(0,3)	0.0027	0.0056	0.0103	0.0056	-0.0033	0.0113	-0.0144	0.0113	0.0169	0.0169
(1,3)	0.0047	0.0059	0.0124	0.0059	-0.0063	0.0120	-0.0176	0.0120	0.0179	0.0179
(1,4)	0.0041	0.0061	0.0119	0.0061	-0.0055	0.0124	-0.0169	0.0124	0.0185	0.0185

5 APPLICATION

This section shows the implementation of the proposed methodology on a simulated data set, which consist of 18 observations from $KwBXII(a = 8, b = 1, c = 3, k = 5, \mu = 0, \sigma = 1)$ distribution and 2 observations from $KwBXII(a = 8, b = 1, c = 3, k = 5, \mu = 0, \sigma = 4)$ distribution. The purpose of generating the simulated data in this way is to create outliers which are defined as the observations that are distant from the majority of the data. After obtaining a random sample of size $n = 20$, they are sorted in an ascending order as shown below:

0.6659	0.6892	0.6918	0.6947	0.7618	0.7694	0.7993	0.8074	0.8570	0.8617
0.8826	0.9007	0.9150	0.9583	0.9907	1.0416	1.1414	1.1462	3.5081	3.8689

In order to identify the distribution of the simulated data set, Q-Q plot technique is used. As it can be seen from $KwBXII$ Q-Q plot in Figure 2 that the largest two observations (3.5081 and 3.8689) are located far from the entire data set, whereas the remaining observations do not deviate much from a straight line. Therefore, after censoring the largest two observations,
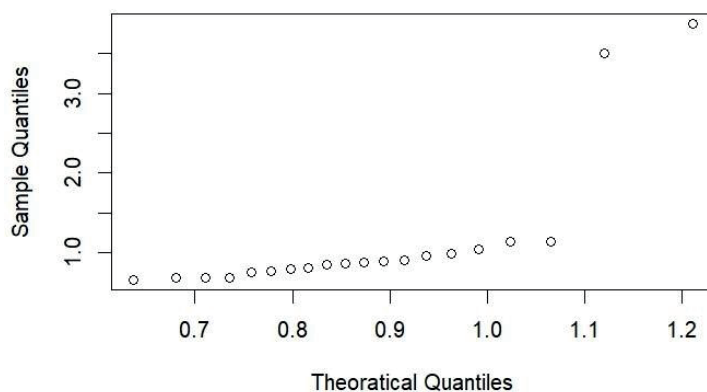
it can be concluded that *KwBXII* distribution provides a good fit for the remaining 18 observations as expected.

Figure 2. *KwBXII* Q-Q Plot for the simulated data (n=20).

Then, ML and MML estimates for the location and scale parameters of *KwBXII* distribution are obtained for the simulated data set. Here, it should be realized that r_1 and r_2 are taken as 0 and 2, respectively. Table 6 shows the estimate values for the parameters μ and σ and the corresponding bootstrap standard errors.

	ML	MML
μ	-0.0040 (0.0102)*	-0.0289 (0.0100)*
σ	1.0238 (0.0163)*	1.0577 (0.0177)*

Table 6. ML and MML estimates for the location parameter μ and scale parameter σ of *KwBXII* distribution.

*: Bootstrap standard errors

It is clear from Table 6 that both ML and MML estimates have negligible biases. If we compare ML and MML estimates with respect to bootstrap standard errors, it is seen that they are close to each other for the location parameter μ. On the other hand, the standard error of ML estimate of the scale parameter σ is slightly lower than the corresponding MML estimate.

It should be noticed that when outliers are found in the data set, using the method given in this study, robust and efficient statistical inferences can be made about the rest of the data with the help of estimators obtained by censoring outlying observations. See Tiku (1982) in the context of outliers and censoring.

6 CONCLUSION

This study is concerned with the estimation of the location and scale parameters of *KwBXII* distribution with known shape parameters under type II censoring. In the estimation phase, ML methodology is utilized. However, due to the lack of closed form solutions for the likelihood

equations, iterative methods are required. To avoid potential problems created by these methods, the use of MML methodology is considered and the MML estimators for the unknown parameters of *KwBXII* distribution are derived. Proposed MML estimators are then compared with the iteratively obtained ML estimators in terms of their biases and efficiencies using Monte Carlo simulation. Simulation results show that as the sample size n increases, the performances of the MML and ML estimators become similar as expected. In this study, the point to be emphasized is that the performances of the MML estimators are quite close to those of ML estimators even for small sample sizes. Therefore, it can be concluded that the proposed methodology provides an alternative for researchers who prioritize time and computational simplicity by ensuring minimal loss in efficiency.
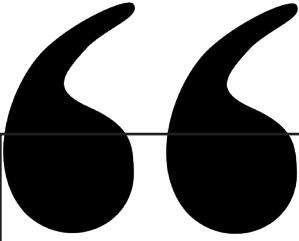
REFERENCES

Akgül, F. G., Acıtaş, Ş., & Şenoğlu, B. (2019). Estimation of the location and the scale parameters of Burr Type XII distribution. *Communications Faculty of Sciences University of Ankara Series A1 Mathematics and Statistics*, *68*(1), 1030-1044.

Arslan, T., Acitas, S., & Senoglu, B. (2021). Parameter estimation for the two-parameter Maxwell distribution under complete and censored samples. *REVSTAT-Statistical Journal*, *19*(2), 237-253.

Balakrishnan, N., & Chan, P. S. (1992). Estimation for the scaled half logistic distribution under type II censoring. *Computational statistics & data analysis*, *13*(2), 123-141.

Cordeiro, G. M., & De Castro, M. (2011). A new family of generalized distributions. *Journal of statistical computation and simulation*, *81*(7), 883-898.

Danish, M. Y., Arshad, I. A., & Aslam, M. (2018). Bayesian inference for the randomly censored Burr-type XII distribution. *Journal of Applied Statistics*, *45*(2), 270-283.

Ergenç C., Güven G., & Şenoğlu B. (2022). "Estimating Parameters of Kumaraswamy Weibull Distribution" 6th International Conference on Mathematics "*An Istanbul Meeting for World Mathematicians*" 21-24 June, 2022, Istanbul, Turkey.

Ghosh, I., & Nadarajah, S. (2017). On the Bayesian inference of Kumaraswamy distributions based on censored samples. *Communications in Statistics-Theory and Methods*, *46*(17), 8760-8777.

Güven, G., & Şenoğlu, B. (2023). Statistical Inference for the Kumaraswamy Weibull Distribution under Doubly Type II Censoring. *International Studies In Science And Mathematics*, 219.

Harter, H. L., & Moore, A. H. (1966). Iterative maximum-likelihood estimation of the parameters of normal population from singly and doubly censored samples. *Biometrika*, *53*(1-2), 205-213.

Kamal, M. (2022). Parameter Estimation Based on Censored Data under Partially Accelerated Life Testing forHybrid Systems due to Unknown Failure Causes. *CMES-Computer Modeling in Engineering & Sciences*, *130*(3).

Kumar, K., Kumar, S., Garg, R., & Kumar, I. (2024). Reliability estimation for inverse Pareto lifetime model based on unified hybrid censored data. *International Journal of System Assurance Engineering and Management*, 1-10.

Makhdoom, I., & Nasiri, P. (2016). Maximum likelihood estimation of exponential distribution under type-II censoring from imprecise data. *Journal of Fundamental and Applied Sciences*, *8*(2), 697-714.

Nassr, S. G., & Elharoun, N. M. (2019). Inference for exponentiated Weibull distribution under constant stress partially accelerated life tests with multiple censored. *Communications for Statistical Applications and Methods*, *26*(2), 131-148.

Pak, A., Parham, G. A., & Saraj, M. (2013). On estimation of Rayleigh scale parameter under doubly type-II censoring from imprecise data. *Journal of Data Science, 11*(2), 305-322.

Panahi, H., & Sayyareh, A. (2014). Parameter estimation and prediction of order statistics for the Burr Type XII distribution with Type II censoring. *Journal of Applied statistics*, *41*(1), 215-232.

Panahi, H. (2019). Estimation for the parameters of the Burr type XII distribution under doubly censored sample with application to microfluidics data. *International Journal of System Assurance Engineering and Management*, *10*(4), 510-518.

Paranaíba, P. F., Ortega, E. M., Cordeiro, G. M., & Pascoa, M. A. D. (2013). The Kumaraswamy Burr XII distribution: theory and practice. *Journal of Statistical Computation and Simulation*, *83*(11), 2117-2143.

Rastogi, M. K., & Mani Tripathi, Y. (2011). Estimating a parameter of Burr type XII distribution using hybrid censored observations. *International Journal of Quality & Reliability Management, 28*(8), 885-893.

Sarhan, A. E., & Greenberg, B. G. (1957). *Estimation of the parameters of the one- and two-parameter single exponential distribution from singly and doubly censored samples.* North Carolina State University. Dept. of Statistics.

Senoglu, B., & Tiku, M. L. (2004). Censored and truncated samples in experimental design under non-normality. *Statistical Methods, 6*(2), 173-199.

Singh, U., Gupta, P. K., & Upadhyay, S. K. (2005). Estimation of parameters for exponentiated-Weibull family under type-II censoring scheme. *Computational statistics & data analysis, 48*(3), 509-523.

Soliman, A. A. (2005). Estimation of parameters of life from progressively censored data using Burr-XII model. *IEEE Transactions on Reliability, 54*(1), 34-42.

Tiku, M. L. (1967). Estimating the mean and standard deviation from a censored normal sample. *Biometrika, 54*(1-2), 155-165.

Tiku, M. L. (1968). Estimating the parameters of log-normal distribution from censored samples. *Journal of the American Statistical Association, 63*(321), 134-140.

Tiku, M. L. (1982). Robust statistics for testing equality of means or variances. *Communications in Statistics-Theory and Methods, 11*(22), 2543-2558.

Wang, J. (2011). Estimation of lifetime distribution with missing censoring. *Journal of Data Science, 9*(3), 331-343.

Wang, X., & Gui, W. (2021). Bayesian estimation of entropy for burr type xii distribution under progressive type-ii censored data. *Mathematics, 9*(4), 313.

Wingo, D. R. (1993). Maximum likelihood methods for fitting the Burr type XII distribution to multiply (progressively) censored life test data. *Metrika*, *40*(1), 203-210.

Wu, S. J. (2002). Parameter estimation of the two-parameter exponential distribution under step-stress accelerated test with censoring. *Journal of Information and Optimization Sciences*, *23*(2), 355-365.

Xie, L., Ren, J., Song, J., & Wu, N. (2020, August). A knowledge synthesis method for Weibull distribution estimation with four right-censored life data. In *2020 Asia-Pacific International Symposium on Advanced Reliability and Maintenance Modeling (APARM)* (pp. 1-4) *IEEE.*

Xin, H., Zhu, J., Sun, J., Zheng, C., & Tsai, T. R. (2018). Reliability inference based on the three-parameter Burr type XII distribution with type II censoring. *International Journal of Reliability, Quality and Safety Engineering*, *25*(02), 1850010.

Zhang, J., Ng, H. K. T., & Balakrishnan, N. (2015). Statistical inference of component lifetimes with location-scale distributions from censored system failure data with known signature. *IEEE Transactions on Reliability*, *64*(2), 613-626.

Chapter 12

DATA ENVELOPMENT ANALYSIS

Hülya EMİNÇE SAYGI[1]

1 Prof. Dr. Hülya EMİNÇE SAYGI
Ege University Faculty of Fisheries, Department of Aquaculture
https://orcid.org/0000-0002-3408-6709

1. **Definitions and Concepts Related to Data Envelopment Analysis (DEA)**

Recently intensely Competitive landscape, in the face against globalization and technological developments, businesses must increase their productivity by determining the efficiency level of their activities to survive and stably continue their activities. The criteria based on which the company's performance criteria are determined or measured are depicted in Figure 1.
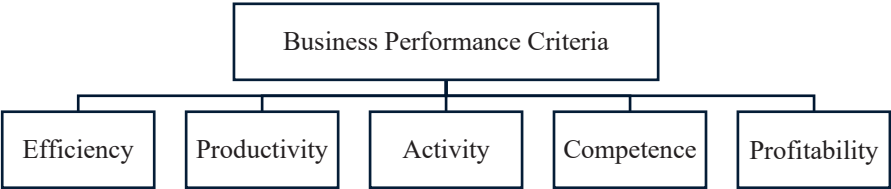

Figure 1. Performance Criteria of the Business

Therefore, performance measures must be calculated to understand whether the business can meet its performance. (Sayıştay 2002). To use resources optimally, companies must assess their relative performance in the sector in which they compete and simultaneously identify their efficiency limits by identifying companies to use as benchmarks. It aims to use the enterprises' resources most effectively in the current competitive environment. Company executives need measurements and valuations to identify deviations from the company's targeted plans and to see the company's position in the market against its competitors. Productivity analysis is one of the methods used for this.

An examination of the concepts of efficiency and effectiveness in the literature shows that the efficiency of a production unit can usually be expressed as a comparison of the actual and optimum values of its inputs and outputs. It is found by dividing the actual output by the maximum output obtained from the input. It is also expressed as the ratio of the minimum level of input required to produce the desired quantity of output to the actual level of input (Lovell, 1993; Gedik, 2011; Zho, 2015).

It is used to measure the performance of a homogeneous DMU, which produces a single type of output or outputs using inputs measured at different levels. (Zhu, 2015).

DEA is an improved version of the linear programming method. Therefore, these DMUs, called "Decision Making Units (DMU)" in the literature, can have very broad definitions such as businesses, companies, organizations and countries that are responsible for transforming some inputs into some outputs. As a result, the best DMUs that Within the observation set, units that produce the maximum output combination with the minimum input combination are determined and these DMUs form the efficient frontier. The model attempts to measure the efficiency of other DMUs in accordance with this limit. The terms used in DEA are as follows (Figure 2).

Input
- The variables evaluated by the DMU to obtain an output are called inputs.

Output
- The results of the processing and consumption of inputs are called products.

Variable
- These are the input-output factors used in the process.

Homogeneity
- It is the similarity between units.

Efficiency
- It is calculating the maximum output given a fixed input or a fixed output given a minimum input.

Activity
- It is defined as producing maximum output using the available input.

DMU
- Businesses, institutions, etc. that obtain similar outputs thanks to similar inputs are the units whose relative effectiveness is examined.

Effective DMU
- The target efficiency ratio is 1. This is an indication that the unit is more successful than other decision units.

Figure 2 Terms used in DAE

DEA is a linear programming method used to compare the relative productivity levels of DMUs and to estimate the production frontier or best practice frontier as an alternative to multifactor, in particular ratio analysis and parameterized methods (Buyukkeklik et. al., 2016). In other words, DEA measures DMU efficiency across multiple input-output variables, while also revealing levels of inefficiency. With this feature, DEA can help managers determine the input reduction and/or output increase required in inefficient units.

2. History of the DEA

DEA is based on the concept of the "efficient frontier" in Farrell's paper "The Measurement of Production Effectiveness" (Farrel, 1957). This application was developed in a study by Charnes, et al. in 1978. In the study conducted by Charnes, the technical efficiency of schools was estimated with multiple inputs and outputs, assuming prices as unimportant. It was thanks to this technique that they introduced the DEA to the literature, which allows the analysis of cases in which there are a large number of inputs and outputs (Okursoy and Tezsürücü, 2014; Jalili and Özbek, 2019). They came up with the DEA formula, known as the CCR method, and a study of this formula was published in the "European Journal of Operations Research". This study was the first to start DEA studies. Their research, published in the European Journal of Operations Research, led to the development of the DEAs. This study was the first to start DEA studies.

DEA was first used in Edwardo Rhodes' doctoral thesis at Carnigie Mellon University, where educational programs were evaluated (Charnes et al., 1994). In addition, Analysis has become a powerful tool. In particular, it can measure the relative technical efficiency of many DMUs in almost all sectors (Charnes et al., 1978; Seiford, 1997; Timor and Lorcu, 2010; Zho, 2015) (Figure 3). The CCR method was first used to measure economies of scale by Banker, Charnes and Cooper (BCC) in 1984 with some later modifications (Zho, 2015). This new scale, foresaw a change in the formulation of CCR for return and technical efficiency estimation, became a much more efficient scale, and provided an answer to how the CCR linear programming formula should be used for estimating returns to scale. (Basen, 1994).

The importance of DEA in recent years, together with practical and

theoretical advances, is now widely recognized as an effective tool for data analysis (Akdoğan, 2012). There are studies in the following areas in the literature (Figure 3).
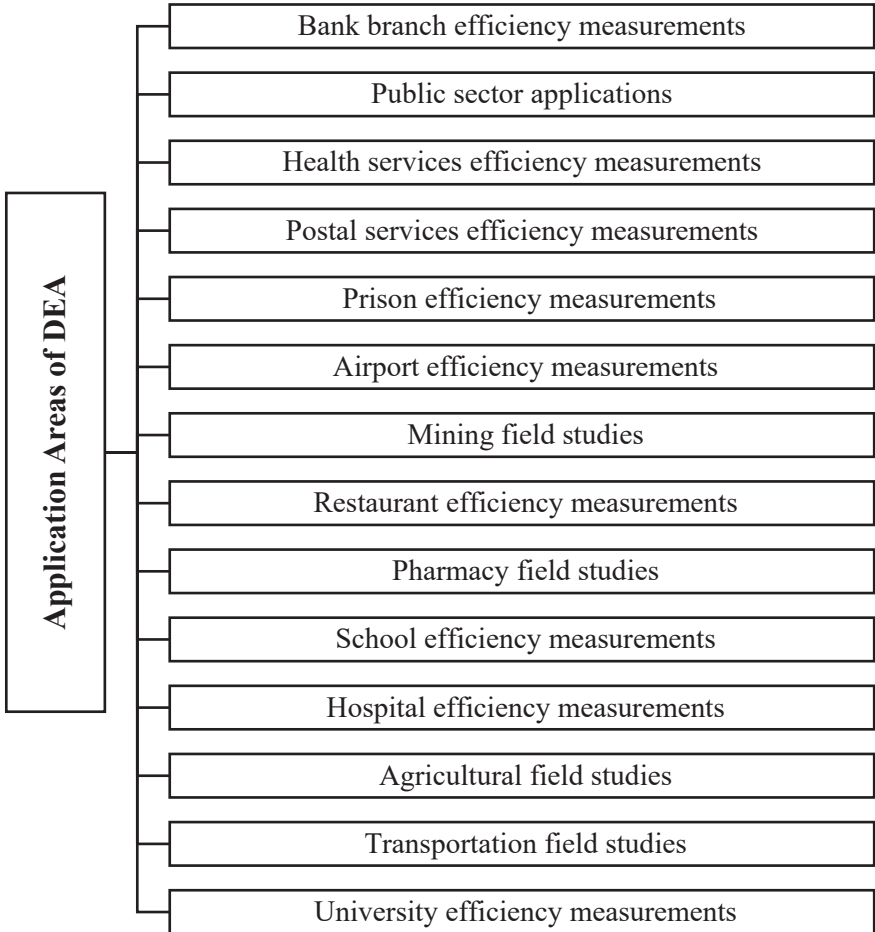

Figure 3 Application Areas of DEA

3. DEA Models

DEA can be used in two ways: input-oriented and output-oriented. Input-orientated modelling looks at the most efficient combination of inputs to generate a given output, while output-orientated modelling looks at the maximum combination of outputs that a given combination of inputs

can generate. This is an attempt to find a maximum combination of outcomes for a given combination of inputs (Piran et al., 2020). It is at this point that the DEA finds the best observations in the set of observations and determines the efficiency bound. The objective is to maximise the outputs (Charnes et al., 1994; Zho, 2015).

What all DEA models have in common is that they identify which DMUs constitute the efficiency frontier and which DMUs are effective or ineffective at that frontier.

DEA is an improved form of the variable programming method. This form is valid for linear programming where the objective function is maximized or minimized under restrictive constraints, and the use of a limited number of permissions is not desired, and the DEA models are also valid for those that are dormant (Tarım, 2001; Öztürk, 2014) (Figure 4).
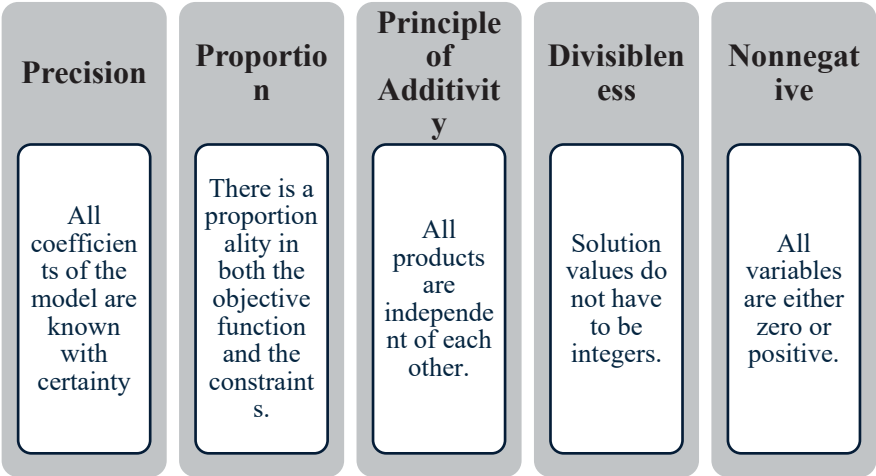
Precision	Proportion	Principle of Additivity	Divisibleness	Nonnegative
All coefficients of the model are known with certainty	There is a proportionality in both the objective function and the constraints.	All products are independent of each other.	Solution values do not have to be integers.	All variables are either zero or positive.

Figure 4. Assumptions of DEA

As in linear programing models, DEA also requires efficient use of limited resources. The objective function can take the form of minimization or maximization. DMUs in this analysis are homogeneous units whose performance is under review and comparison. These economic units are responsible for transforming inputs into outputs. This analysis divides DMUs into "effective" and "ineffective". Effective ones create an efficiency limit, and the others try to reduce this limit. A reference set is created for ineffective values and target values are determined. Thus, strategies can be developed for each DMU to enhance its effectiveness.

The efficiency of the whole DMU is expected to be between 0 and 1 under the constraints specified in the DEA. The efficient DMU is expressed as 1. An efficiency value of 1 indicates that the DMU is 100% efficient. These units constitute the efficiency limit. The DMU with efficiency values less than 1 is called "inefficient DMU" and the source and amount of its inefficiency are defined. Therefore, the DMU or its manager can take the necessary precautions to eliminate the problem of this inefficiency, the source and amount of which are known, and separate target values can be determined for each. To convert these inequalities into a linear programming problem, the denominator of the objective function in the maximizing form is set=1 (Ulucan, 2000).

The DEA models can be divided into two groups: those with constant returns to scale and those with variable returns to scale. Many DEA models have been developed. Analysis can be done by considering fixed and variable situations according to the scale and in cases where the model used is input and output-oriented or unbiased. Models are classified by orientation: "Input-orientated", "Output-orientated" and "non-orientated" modelling (Kecek, 2010).

These are models proposed by Charnes, Cooper and Rhodes (CCR) in 1978 based on the distance of inefficient units from the production frontier. These are also models that have been calculated under the assumption of constant returns to scale. the overall technical efficiency.

The other model, which calculates the value of pure technical efficiency in variable movements to scale, was proposed by Banker, Charnes and Cooper (BCC) in 1984. There are two ways to increase the effectiveness of a DMU.

The model can be input oriented or output oriented. Input-oriented modelling looks at how much input must be reduced without changing the amount of production. The input level is kept constant in output driven models. With the current level of input, they look at how much output needs to be increased to ensure the effectiveness of the decision unit.

Input-oriented models are used to minimize the amount of input. They predict the extent to which ineffective decision-making units' input should be reduced. This means trying to find the optimal mix of inputs to produce the most efficient mix of outputs (Vurur, & Özdemir, 2024).

The purpose of output orientation models is the maximisation of output. It can be stated that it is appropriate to increase the outputs of ineffective DMUs to increase their efficiency. In other words, it is investigated how many output combinations can be obtained with the input combination considered (Cooper et al, 2011; Vurur, & Özdemir, 2024).
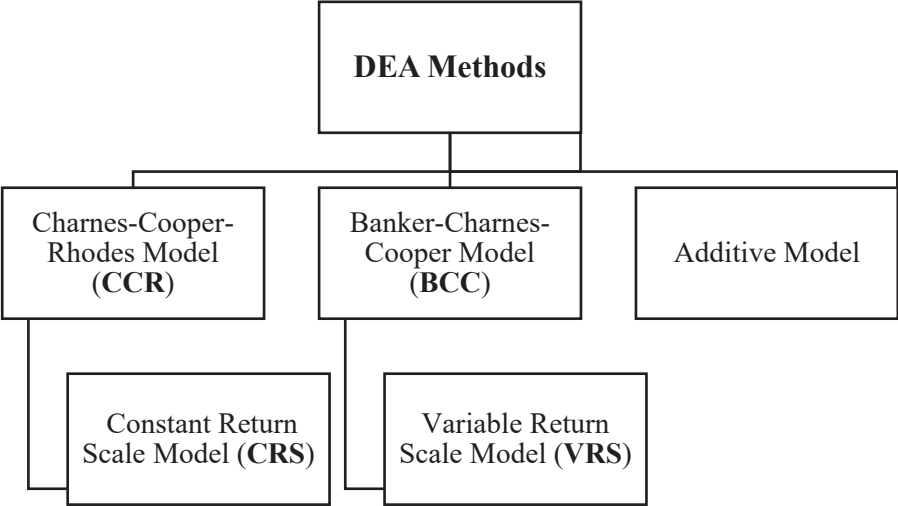

Figure 5. DEA Methods

In short, there are three methods used in the DEA. These are the CCR (Charnes, Cooper, Rhodes) procedure, the BCC (Banker, Charnes, Cooper) procedure and the addition procedure. (Figure 5).

These models may fall into two categories: constant returns to scale and variable returns to scale. Additive model used in productivity measurement that cannot be said to be input or output-oriented, i.e., have no focus (Zho, 2015).

3.1. CCR Method

Charnes, Cooper and Rhodes contributed the CCR model, the first DEA model, to the literature, improving Farrell's 1957 efficiency measure from single output/multiple input to multiple output/multiple input. According to Charnes, Cooper and Rhodes' definition of CCR, it is as follows.

1. 1. Unless one or more inputs are increased or some other outputs are decreased, no output can be increased.
2. No input can be reduced except by reducing some of the outputs or other inputs.

In this model, also known as a ratio model, you can either use an 'inputs-based' model, which minimizes those inputs which produce an output, or an 'outputs-based' model, which optimizes an output from observed inputs. In general, an efficiency analysis is generally performed. At the same time, an analysis is made about which resources are sufficient and which resources are idle in this model (Ergülen et al., 2019). There are two groups of CCR models to consider. The first is input-orientated and the other is output-orientated (Bolayır and Ergülen, 2022).

3.1.1. CCR model with input orientation

The input-centred CCR model is used to achieve the same level of output no matter how much the amount of input needs to be reduced (Cumhur, 2017). In DEA models, it is assumed that "n" decision units will be copied, and "s" number of decision units are output using "m" number of decision units. Table 1 shows the primal and dual applied representations of the input CCR models. Under the condition of free use of inputs and constant returns (CRS) under standard technology conditions, the input-oriented CCR model, where inputs are minimized and outputs are assumed to be at a constant level, is shown as follows: (Cooper et al., 2004, Hsu and Lin, 2007; Özden, 2008; Bhanot, & Singh, 2018; Bolayır and Keyifli, 2022).

Table 1. CCR model with input orientation

Primal	Dual
Objective Function	**Objective Function**
$$maxh_k = \sum_{i=1}^{p} u_{ij}y_{ij}$$	$$minq_j$$
Restrictors	**Restrictors**
$$\sum_{i=1}^{p} y_{ij} - \sum_{i=1}^{k} v_{ij}x_{ij} \leq 0,$$ $$j = 1,2,\dots,n$$ $$\sum_{i=1}^{k} v_{ij}x_{ij} = 1$$ $$u_{ij} \geq 0, i = 1,2,\dots,p$$ $$v_{ij} \geq, i = 1,2,\dots,k$$	$$\sum_{j=1}^{n} \lambda_{ij}y_{ij} \geq y_{ij}, i = 1,2,\dots,p$$ $$q_j x_{ij} - \sum_{j=1}^{n} \lambda_{ij}x_{ij} \geq 0, i = 1,2,\dots,k$$ $$\lambda_{ij} \geq 0, j = 1,2,\dots,n$$ $$-\infty \leq q_j \leq +\infty$$

The variables of the model presented in Table 1 are defined in the following way: u_{ij} and v_{ij}: weight of the i-th output input of the j-th DMU; y_{ij} and x_{ik}: i-th Output/ input used by the j-th DMU; k: No. of input, p: No. of outputs, n: No. of of DMUs

Table 1 shows that the dual models have variables q, in contrast to the original models.Since the solution path of both models will be the same, it is equivalent to the effectiveness of k (Bolayır and Keyifli, 2022).

This model aims at maximizing the weighted mean of the outputs of the DMUs whose efficiency we want to calculate, and in the boundary conditions it ensures that the weighted mean of the inputs of the DMUs whose efficiency we want to calculate are equal to one. In the other constraint, the weighted averages of the outputs for all DMU are ensured to be smaller than the inputs. As a result, the output/input ratio can be a maximum of 1 for each DMU, while the optimum output average for each DMU can be a maximum of 1 (Banker, 1984).

3.1.2. CCR model with output orientation

Obtaining the maximum output component for a given input component is the objective of the CCR output model. The difference between these models from the models with features entered is that the capacity entered with weighting can be changed to minimize the expansion to the amount measured with weighting (Doğan, 2010).

In other words, when the constant return (CRS) assumption is used, the Output Oriented CCR model is built to maximize the output value without requiring further inputs.

In

Table **2**, it is seen that the dual model has variables and, which are different from the primal model (Bolayır and Ergülen, 2022).

Table 2. Output-oriented CCR model

Primal	Dual
Objective Function	**Objective Function**
$\min f_j = \sum_{i=1}^{p} v_{ij} x_{ij}$	$\max Z_j$
Restrictors	**Restrictors**

$$\sum_{i=1}^{k} v_{ij}x_{ij} - \sum_{i=1}^{p} u_{ij}y_{ij} \geq 0, \qquad j = 1,2,\dots,n$$

$$\sum_{i=1}^{k} u_{ij}y_{ij} = 1$$

$$u_{ij} \geq 0, i = 1,2,\dots,p$$

$$v_{ij} \geq, i = 1,2,\dots,k$$

$$\sum_{j=1}^{n} \eta_{ij}x_{ij} \leq x_{ij}, i = 1,2,\dots,k$$

$$Z_j y_{ij} - \sum_{j=1}^{n} \eta_{kj}y_{ij} \leq 0, i = 1,2,\dots,p$$

$$\eta_{ij} \geq 0, j = 1,2,\dots,n$$

$$-\infty \leq Z_j \leq +\infty$$

Using this model, the aim is to calculate efficiency by minimising the weighted average of the decision unit's inputs. Also in the constraints, the weighted average of the outputs of the decision unit is 1 for the calculation of efficiency. In the other constraint, the weighted average of the outputs for all DMU is provided to be smaller than that of the inputs. As a result, the output/input ratio is at least 1 for each decision-making unit, and the optimum output average for each decision-making unit can be at least 1 (Banker, 1984).

3.2. BCC Model

DEAs have been used successfully for many years. It was developed by Banker, Charnes and Cooper and is also known as the BCC model, named after the authors' initials. Banker, Charnes and Cooper were inspired by the studies of CCR in this study and developed increasing, constant and decreasing assumptions to measure the efficiency of DMUs in the BCC model. Although there is a constant return assumption in the CCR model, the variable return assumption of the BCC model is thought to be more suitable for real life (Ergülen et al., 2020). The BCC model estimates the technical efficiency of transactions at a certain scale and determines whether they are increasing, decreasing or constant based on the scale required for detailed use. It also makes a distinction between them. The BCC model is divided into two inputs with variable returns to scale and output-oriented (Sarı, 2010; Zho, 2015).

The BCC model was created by modifying the assumptions of the existing CCR model developed by Banker, Charnes and Cooper in 1984. In the CCR model, which accepts the constant return assumption, the production boundary represents a straight line passing through the origin in the case of input and output. Again, in the BCC model, a constant term should be added to the sum of the input and output indicators to move the production boundary away from the origin and make it more flexible (Zho,

2015). Using the model, variable returns to scale can be for all DMUs. The boundary of the BCC model is always below the CCR boundary. Therefore, the efficiency score of the CCR model may be equal to and smaller than the efficiency score of the BCC model. The addition of the so-called convexity constraint to the model makes the difference between the BCC and CCR models. Suppose this constraint is $\sum_{j=1}^{n} \lambda_j = 1$, it indicates that the variable returns to scale assumption is accepted, if it is =1 the assumption of decreasing returns to scale is accepted, and if it is =1 it indicates that the assumption of increasing returns to scale is accepted (Zho, 2015). Thus, only technical efficiency of each DMU is measured in this model. In this model, a DMU must have both scale efficiency and technical efficiency to qualify as effective, while a DMU need only have technical efficiency to qualify as effective (Kabakuş, 2014).

3.2.1. Input-Oriented BCC Model

Input-oriented BCC models determine the optimal combination of inputs, similar to CCR models (Kazançıoğlu, 2008). This model predicts that approaching the efficiency limit is possible by reducing inputs proportionally. Table 3 shows the primal and dual models of the entered BCC model (Cooper et al., 2004; Uzgören and Şahin, 2013; Bolayır and Keyifli, 2022).

Table 3. Input-Oriented BCC model

Primal	Dual
Objective Function	Objective Function
$$maxh_i = \sum_{i=1}^{p} u_{ij}y_{ij} - u_0$$	$$minq_j$$
Restrictors	Restrictors
$$\sum_{i=1}^{p} u_{ri}y_{ri} - \sum_{i=1}^{k} v_{ij}x_{ij} \leq 0, \qquad j = 1,2,\ldots,n$$ $$\sum_{i=1}^{k} v_{ij}x_{ij} = 1$$ $$u_{ij} \geq 0, i = 1,2,\ldots,p$$ $$v_{ij} \geq, i = 1,2,\ldots,k$$	$$\sum_{j=1}^{n} \lambda_{ij}y_{ij} \geq y_{ij}, i = 1,2,\ldots,p$$ $$q_j x_{ij} - \sum_{j=1}^{n} \lambda_{ij}x_{ij} \geq 0, i = 1,2,\ldots,k$$ $$\sum_{j=1}^{n} \lambda_{ij} = 1$$ $$\lambda_{ij} \geq 0, j = 1,2,\ldots,n$$ $$-\infty \leq q_j \leq +\infty$$

The Variables of the model in Table 1 are defined as: u_{ij} and v_{ij}: weight of i-th output/input of j-th DMU; y_{ij} and x_{ij}: i-th output/input

produced by the j-th DMU; k: No. of input; p: No. of outputs; n: No. of
of DMUs

When the input-oriented CCR model is compared with the input-oriented BCC model, it is seen that in the BCC model, in addition to the CCR model, there is another variable u_0 (Zho, 2015). In the BCC model, to measure the effectiveness of the DMU, the u_0 variable included in this model is checked whether it is positive (decreasing returns), zero (constant returns) or negative (increasing returns). According to the state of variable u_0, if $u_0<0$, it is scaled increasing, if $u_0=0$, it is scaled constant and if $u_0>0$, it is scaled decreasing (Doğan, 2010).

3.2.2.   Output-Oriented BCC Model

The principle of output maximisation at constant input, which is generally observed in output-oriented models, remains valid for the BCC model. The assumption of variable returns in the input-output model is retained in the BCC model (Zho, 2015).

The output-oriented BCC model emerges because of adding the $\sum_{j=1}^{n} \eta_j = 1$ convexity constraint to the CCR model (Zho, 2015; Cumhur, 2017).

This output-oriented model means minimising inputs and maximising outputs without changing the given resources. Table 4 shows the primary and dual models of the BCC model.

Table 4. Output-Oriented BCC model

Primal	Dual
Objective Function	Objective Function
$$minf_i = \sum_{i=1}^{s} v_{ij}x_{ij} + v_0$$	$$maxZ_j$$
Restrictors	Restrictors
$$\sum_{i=1}^{k} v_{ij}x_{ij} - \sum_{i=1}^{p} u_{ij}y_{ij} \geq 0, \qquad j=1,2,\dots,n$$ $$\sum_{i=1}^{k} u_{ij}y_{ij} = 1$$ $$v_{ij} \geq 0, i=1,2,\dots,k$$ $$u_{ij} \geq, i=1,2,\dots,p$$ $$v_0 \ serbest$$	$$\sum_{j=1}^{n} \eta_{ij}x_{ij} \leq x_{ij}, i=1,2,\dots,k$$ $$Z_jy_{ij} - \sum_{j=1}^{n} \eta_{kj}y_{ij} \leq 0, i=1,2,\dots,p$$ $$\sum_{j=1}^{n} \eta_{ij} = 1$$ $$\eta_{ij} \geq 0, j=1,2,\dots,n$$ $$-\infty \leq Z_k \leq +\infty$$

This output-oriented model translates into minimizing inputs and maximizing outputs without any change in the given resources.

If we compare the output-oriented CCR model with the BCC model, the BCC model contains a variable v_0 in addition to the CCR model (Colak, 2023). These are positive, zero or negative, depending upon whether they are increasing, constant or decreasing. Depending on the status of the variable V_0, $V_0 < 0$ indicates declining economies of scale, $V_0 = 0$ indicates constant economies of scale and $V_0 > 0$ indicates increasing economies of scale (Zho, 2015; Bolayır and Ergülen, 2022).

3.3. Additive Model

This model acts as a bridge between the inefficiency analyses previously defined by Charnes and Cooper and this process. This model also provides a quantitative commentary on why the specified DMUs are inefficient. It is possible to perform an efficiency analysis on the assumption of economies of scale, although it is called non-directional (Sarı, 2010). It is known that the additive model corresponds to the envelopment model in the BCC model, one of the DEA models. Again, by removing the Σ condition from the specified additive model, we obtain the equivalent variation of the same model to the CCR model (Doğan, 2006). This model is a model that can evaluate input-oriented and output-oriented versions simultaneously. The main purpose of using this model is to evaluate the excess of inputs and the deficiency of outputs simultaneously and to reach inefficient DMUs by performing an analysis on the efficiency frontier (Baz, 2021).

It is a model developed by Charnes, Cooper, Golany, Seiford and Stutz in 1985. The additive model evaluates together two types of orientations made separately by the CCR and BCC models for input and output. Although there are many versions, the most basic is the one supported by linear programming. (Cook and Seiford, 2009).

Objective Function:

$$max = \sum_{i=1}^{p} s_r^+ + \sum_{i=1}^{k} s_i^-$$

Restrictions:

$$\sum_{j=1}^{n} y_{ij}\lambda_j - s_j^+ = y_{jo}$$

$$\sum_{j=1}^{n} x_{ij}\lambda_j - s_j^- = x_{io}$$

$$\sum_{j=1}^{n} \lambda_j = 1$$

$$\lambda_j, s_j^+, s_j^- \geq 0$$

s_j^-: The idle value of the ith input of the jth DMU

s_j^+: The idle value of the ith output of the jth DMU

In particular, it is used to calculate which point on an inefficient DMU's efficiency frontier is furthest away from an efficient DMU's efficiency frontier. As a result of this model, the efficiency value cannot be obtained, but it can be said whether the DMUs are efficient or not by looking at the slacker variable values. If both slacker variables s_r^+=0 and output deficiency s_r^-=0 are determined, it can be said that the DMU is efficient according to the additive model. If any or both values are not zero, it is said that the values of those that are different from zero define the sources and the amounts of inefficiency in the appropriate inputs and outputs. The additive model combines DEA with Charnes-Cooper inefficiency analysis and is based on variable returns to scale (Kıran, 2008; Zho, 2015).

In addition to these models, additive models developed in Charnes, et al., 2001, have been developed for the case where neither input nor output is oriented. In this model, input excess and output excess are considered together.

The "s" values shown as the slacker variable in the model are used to decide whether the relevant decision-making unit is effective or not. If these values are equal to 0, it is said to be relatively effective, if at least one of them is different from 0, that decision-making unit is said to be ineffective.

4. Application of DEA

In DEA applications, it is considered important that the DMU subject to analysis have certain common features and perform similar

functions towards the same goal. It also requires that market conditions are similar and that productivity characteristics are the same for all units in the group, except for density and size differences (Kayalıdere and Kargın, 2004).

Before conducting DEA, some basic questions such as what the purpose of performance measurement is, what the DMUs should be, whether the intended inputs and outputs will meet the desired performance, whether there is enough DMUs and which model should be appropriate need to be answered (Imanirad et al., 2013). Answering these questions will allow the application to proceed more healthily and correctly. In addition, completing some steps completely and correctly to perform the analysis will be effective in reaching the correct results. These steps are listed as follows by Ramanathan (2003) (Deniz, 2009) (**Hata! Başvuru kaynağı bulunamadı.**).
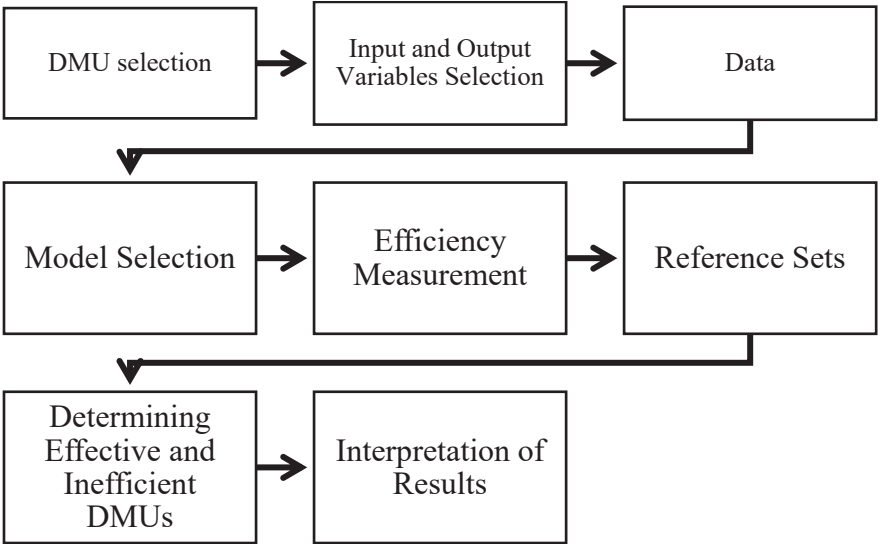
4.1. DMU Selection

It is advantageous to have a large data set to complete a DEA study. Boussofiane et al. (1991) stated that the number of DMUs must be at least the product of the number of inputs and outputs. Therefore, determining the efficiency of each DMU is based on flexibility in choosing the weights to be assigned to the input and output values. There are two factors that affect the selection of DMUs for a study. These are the homogeneity of the DMUs and the number of DMUs. The most

important thing to remember when selecting DMUs is that they should be homogeneous. This means that DMUs should be similar and work towards similar goals. Apart from this, even if their sizes and units are different, they should obtain similar outputs using similar inputs to make a healthy measurement. If they are not homogeneous, the efficiency scores may reflect fundamental differences in the environment rather than any inefficiency. To overcome this, what needs to be done is to divide the DMUs into homogeneous groups. However, this requires many DMUs (Haas and Murphy, 2003). Cluster analysis, multi-stage DEA and scale return analysis are performed to determine the homogeneity in the data set.

There is a direct proportion between the increase in the number of DMUs and the achievement of better results. The increase in this number increases the chance of capturing units with higher performance, which will enable the determination of the efficiency limit. However, increasing this number brings with it a problem such as negatively affecting homogeneity. To prevent these situations, some approaches have been developed in determining the number (Table 5). On the other hand, Cook et al., (2014) state that these opinions are not a rule or obligation and do not have a statistical basis. All these views are stated for the purpose of greater convenience.

Table 5. References related to DMU issue

Input	Output	Minimum	Reference
3	4	12	Golany and Roll, 1989
k	p	k+p+1	Boussofiane et al.,1991
2	4	8	Bowlin, 1998
k	p	$(k + p) < \dfrac{n}{3}$	Friedman and Sinuany-Stern, 1998
k	p	(k+p) *2	Dyson et al., 2001
k	p	(k+p+1)	Deliktaş, 2002
k	p	(k+p) *2	Sezen and Doğan, 2005

In contrast to the approaches given above, if the number of DMUs is less than the number of inputs and outputs, the number of inputs and outputs can be reduced accordingly. Some authors have proposed Regardless of the size of the dataset, DEA-based efficiency models can help

differentiate between DMUs more effectively (Andersen and Petersen, 1993; Rousseau and Semple, 1995; Doyle and Green, 1994; Zho, 2015).

4.2. Input-output selection

The most fundamental point of DEA is to determine the inputs and outputs that will best reveal the efficiency of DMUs and ensure that they can be compared with each other in a healthy way. There are no fixed rules set to determine inputs and outputs. However, when determining inputs and outputs, it is necessary to have knowledge about the functioning and structures of the DMUs whose efficiency measurements are targeted (Zho, 2015). This information helps to identify impacts and define relationships between inputs and outputs (Banker, 1992). Therefore, the selection of inputs and outputs is important in DEA. However, one of the most important difficulties encountered in DEA arises in determining the inputs and outputs. DEA plays an important role in defining the relationships and simplifying complex problems and determining the inputs and outputs. In practice, inputs and outputs that are dependent on the production process should be selected. Overlooking any of the input-output variables may cause the DMU efficiency to yield different results (Öncü and Aktaş, 2007). Inputs that go through a certain process are needed for a production or service to be realized. However, this process may not always appear as a simple process of single input and single output or multiple inputs and single output, but as a more complex process. While in a simple process, the best things to do to reach the desired outcome, what is input and what is output, can be clearly observed, as the process becomes more complex, the effects start to mix, inputs and outputs become more difficult to determine, and cause and effect relationships begin to increase.

After selecting DMUs, determining input and output variables and obtaining reliable data, the question of which model should be used for analysis needs to be answered. Based on the classification in DEA models, it is first necessary to determine which assumption will be used and then whether it will be input-oriented or output-oriented.

Çağlar (2003) states that if it is observed that the increase in output increases by the same amount with a direct proportion to the increase in inputs, it is fixed returns to scale, and if an increase or decrease in

output increase is less or more than the increased amount, it is a variable return to scale. In addition, the CCR model measures the assumption of constant returns to scale and total efficiency, while the BCC model measures the assumption of variable returns to scale and technical efficiency. Efficiency scores may be lower in the CCR model, so both scale and technical efficiency must be ensured (Behdioğlu and Özcan, 2009; Zho, 2015).

4.3. Availability and reliability of data

In DEA, once the process of defining the inputs and outputs has been completed, the phase of accessing this data begins. If these data cannot be accessed for any decision-making unit or if there is a suspicion that the data is not reliable, that decision-making unit is either removed from the analysis or other input-output variables are tried to be determined. However, due to the structure of DEA, removing a DMU from the analysis will affect the relative efficiency of the other DMUs. Therefore, determining safe and high-quality inputs and outputs is very important for the reliability of DEA analysis.

Although DEA allows the use of multiple inputs and outputs to measure efficiency, this cannot include all variables considered relevant. This means that variables need to be identified and included in the model by considering how DMUs are structured and operate. Another important point is that, as in all other studies, the data should be reliable and available. A study in which some of the variables that seem important are obtained and some are not, leads to incomplete and incorrect results.

4.4. Determination of the activity values

The efficiency value of each DMU is in the range [0,1]. DMUs with an efficiency value of 1 are considered fully efficient, and at the same time, they constitute the efficiency boundary. DMUs with an efficiency value between 0 and 1 are determined as inefficient DMU (Bakırcı, 2006).

After determining the most suitable model, the most effective DMUs are determined because of the analysis and their efficiency scores are given a value of 1. The efficiency scores of ineffective DMUs will be less than 1. For each DMU, it identifies the detailed use of inputs and outputs, the shortfalls and surpluses, and the actions needed to improve

efficiency.

Increasing the number of variables tends to reduce the discriminating power of DEA. By including these unimportant inputs or outputs in the model, ineffective DMUs can appear effective. (Yıldırım, 2010). For this reason, input and output selections should be made correctly.

The input variables used should best reveal the efficiency status to be measured. In the early applications of DEA, it has become more apparent over time whether the variables used should be inputs or outputs. In some cases, variables can be used as both inputs and outputs, depending on how clear the purpose of the study is (Imanirad et al., 2013).

All DMUs become more effective as the number of inputs and outputs used in the application increases. Therefore, the DMU cannot reflect its real effectiveness. If the number of inputs and outputs is increased in the application, the number of DMUs to be used should also be increased. (Öncü and Aktaş, 2007; Zho, 2015).

4.5. Determination of reference sets

In DEA, ineffective DMU are tried to be likened to effective decision-making units. The set formed by these effective DMU to which they try to be likened is called the reference set (Depren, 2008).

In order to realize the activation, reference sets are used. Reference sets show how the ineffective DMU should improve the effective DMUs in percentage slices. When these features are provided, reference sets can be created for the ineffective DMU, and comparisons can be made in addition to efficiency measurement. However, if the homogeneity condition is not provided, this comparison will not be healthy. (Ramanathan, 2003).

4.6. Interpretation of the results

After examining the DMUs, common findings are investigated for effective and ineffective DMU belonging to the observation set where inputs and outputs are considered.

5. Advantages and Disadvantages of DEA

In the literature, DEA is a method that measures the relative efficiencies

of DMU in the presence of inputs and outputs consisting of multiple and different measurement units and is also called "Efficiency Analysis". This method is based on linear programming and is not parametric. Nonparametric methods measure the distance of the efficiency value to the efficiency limit. The advantages of these methods are that they do not make assumptions about the structure of production units and that more than one explained and explanatory variable can be used. They do not, however, include a term for the random errors. For this reason, the errors made are transferred to the model. Thus, the efficiency limit is determined incorrectly. This situation can be seen as a disadvantage of nonparametric methods. Nonparametric methods are more flexible than parametric methods. An upper efficiency limit is created for all units included in the analysis. The conclusion that "they are not effective" is reached for all units deviating from the limit. For this reason, nonparametric methods are used more frequently instead of parametric methods (Cooper et al., 2007).

This method is a very effective tool when used correctly. The advantages of using DEA can be listed as follows;

1.Unlike parametric methods, there is no need for any functional relationship between input and output.

2.DEA can process many inputs and outputs.

3.Input-output factors may have different units.

4.Compared units have a homogeneous structure among themselves (İnan, 2000).

5.It is possible to compare DMU with other DMU or different combinations of these units.

6.DMU with many inputs and outputs can be used in efficiency measurements.

7.Input and output values may be in different units. DEA does not require a functionality that correlates inputs and outputs. DMU whose efficiencies are measured with DEA are compared with DMU that have full efficiency in a coherent manner.

8.Provides important guidance on making ineffective DMU more effective.

9.It allows DMU to better understand production processes. Because it does not require a functional form between inputs and outputs, it can perform analyses with many input and output variables (Kecek, 2010).

In addition to the advantages of DEA, there are also some disadvantages. These disadvantages are;

1.DEA is very sensitive to measurement errors because it is evaluated as an endpoint technique (Govindarajan, 2003).

2.2. There is no point in interpreting these scores in terms of absolute efficiency, but they are sufficient to measure the performance of DMU.

3.Since it is a static analysis, it performs a cross-sectional analysis between the DMU data in a single period. Since a completely different linear programming model needs to be solved for each DMU, it takes too much time to calculate in large-scale problems. However, this problem has been eliminated by today's computer programs.

4.For DEA, which measures relative efficiency based on a certain sample, some observations of the sample that may have very small or large input and output values may create problems in the formation of the efficiency limit (Karasoy, 2000).

5.DEA is not considered suitable for statistical hypothesis testing because it is not a parametric method (İnan, 2000).

6.It is not sensitive to categorical and abstract components (for example, measurement of service quality) (Erken and Emiral, 2002).

7.Solving large-scale problems with DEA can be computationally time-consuming since it will be necessary to solve a separate linear model for each decision point (Ma &Li, 2024).

In DEA, the high sensitivity to input and output variables and the high sensitivity of the variables to be selected and used to the input and output values and their being too large or too small make the efficiency limit difficult.

Referanslar

Ada, S., Öncü, S., & Aktaş, R. (2007). Yeniden yapılandırma döneminde Türk bankacılık sektöründe verimlilik değişimi. Yönetim ve Ekonomi Dergisi, 14(1), 247-266.

Akdogan, H. (2012). The efficiency of police stations in the city of Ankara: an application of data envelopment analysis. Policing: an international journal of police strategies & management, 35(1), 25-38.Andersen and Petersen (1993),

Andersen, P., & Petersen, N. C. (1993). A procedure for ranking efficient units in data envelopment analysis. Management science, 39(10), 1261-1264.

Bakırcı, F. (2006). A measurement of efficiency on sectoral basis: An analysis with DEA. Atatürk University: Journal of Economics and Administrative Sciences, 20(2), 199-217.Banker, 1984).

Banker, R. D. (1992). Selection of efficiency evaluation models. Contemporary Accounting Research, 9(1), 343-355.).

Banker, R. D., Charnes, A., & Cooper, W. W. (1984). Models for estimating technical and returns-to-scale efficiencies in DEA. Management Science, 30(5), 1078-1092.Basen, 1994

Bayram, G. (2023). Paradigm Change in Industrial and Systems Engineering (Doctoral dissertation, Marmara Universitesi (Turkey)).

Baz, H. A. (2021). Veri zarflama analizi ile bankacılık sektöründe etkinliğin ölçülmesi: borsa İstanbul üzerinde bir uygulama. YayımlanmamıG yüksek lisans tezi, Korkut Ata Üniversitesi, Osmaniye.

Behdioğlu, S., Özcan,G. (2009), Veri Zarflama Analizi Ve Bankacılık Sektöründe Bir Uygulaması, Süleyman Demirel Üniversitesi İktisadi Ve İdari Bilimler Fakültesi Dergisi, C.14, S.3, Ss. 301-326

Bhanot, N., & Singh, H. (2018). Benchmarking Performance Indicators of Indian Rail Freight by DEA Approach. In Encyclopedia of Information Science and Technology, Fourth Edition (pp. 587-600). IGI Global.

Bolayır, B. ve Keyifli, N. (2022). E-devlet uygulamalarının yolsuzluk üzerindeki etkisinin veri zarflama analizi yöntemiyle incelenmesi: OECD ülkeleri örneği. Nevşehir Hacı Bektaş Veli Üniversitesi SBE Dergisi, 12(1), 1-18.

Boussofiane, A., Dyson, R. G. ve Thanassoulis, E. (1991). Applied data envelopment analysis. European Journal of Operational Research, 52(1), 1-15.

Bowlin, W.F., 1998, Measuring performance: An introduction to data

envelopment analysis (DEA), Journal of cost analysis, 7, 3-27.

Buyukkeklik, A., Dumlu, H., & Evci, S. (2016). Measuring the efficiency of turkish SMEs: A data envelopment analysis approach. International Journal of Economics and Finance, 8(6), 190-200.

Çağlar A., (2003), "Veri Zarflama Analizi İle Belediyelerin Etkinlik Ölçümü", (Yayımlanmamış Doktora Tezi, Hacettepe Üniversitesi Fen Bilimleri Enstitüsü), Ankara. Charnes, A., Cooper, W. W., & Rhodes, E. (1978). Measuring the efficiency of decision making units. European journal of operational research, 2(6), 429-444.

Charnes, A., Cooper, W. W., Golany, B., Seiford, L., & Stutz, J. (1985). Foundations of data envelopment analysis for Pareto-Koopmans efficient empirical production functions. Journal of econometrics, 30(1-2), 91-107..

Charnes, A., Cooper, W., Lewin, A. Y., & Seiford, L. M. (1997). Data envelopment analysis theory, methodology and applications. Journal of the Operational Research society, 48(3), 332-333.

Charnes, C., Rötteler, M., & Beth, T. (2001). On homogeneous bent functions. In Applied Algebra, Algebraic Algorithms and Error-Correcting Codes: 14th International Symposium, AAECC-14 Melbourne, Australia, November 26–30, 2001 Proceedings 14 (pp. 249-259). Springer Berlin Heidelberg.,

Colak, Z., (2023). Efficiency measurement of real estate investment trusts traded in BIST with data envelopment analysis and Malmquist total factor productivity index. Journal of Economics, Finance and Accounting (JEFA), 10(1), 1-20.

Cook, W. D., & Seiford, L. M. (2009). Data envelopment analysis (DEA)–Thirty years on. European journal of operational research, 192(1), 1-17.

Cooper, W. W., Seiford, L. M. ve Zhu, J. (2004). Data envelopment analysis: History, models and interpretations. W. W. Cooper, L. M. Seiford and J. Zhu (Ed.), In Handbook on data envelopment analysis (pp. 1-39), Chapter 1. Boston: Kluwer Academic Publisher.

Cooper, W. W., Seiford, L. M., & Zhu, J. (2011). Data envelopment analysis: History, models, and interpretations. Handbook on data envelopment analysis, 1-39.

Cooper, W. W., Seiford, L. M., Tone, K., & Zhu, J. (2007). Some models and measures for evaluating performances with DEA: past accomplishments and future prospects. Journal of Productivity Analysis, 28, 151-163.

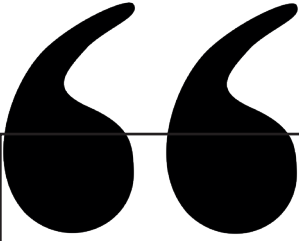Cooper, W.W., Seiford L.M., Tone, K., "Data Envelopment Analysis: A

Comphrehensive Text with Models, Application, References and DEA-Solver Software", Kluwer Academic Publishers, Boston, (2000).

Cumhur, Y. (2017). Türkiye'deki il belediyelerinin etkinliklerinin 2009 yerel seçimleri özelinde veri zarflama analizi yöntemi ile değerlendirilmesi. Çağdaş Yerel Yönetimler, 26(4), 1-41.

Delikdaş, E., (2002), Türkiye Özel Sektör İmalat Sanayinde Etkinlik Ve Toplam Faktör Verimliliği Analizi, Odtü Geliğtirme Dergisi, Cilt: 29, Sayı: 3-4, Ss.251

Deniz, N.,(2009), Türkiye'deki İllerin Kaynak Kullanımına Göre Göreli Etkinliklerinin Klasik Ve Bulanık Veri Zarflama Analizi Yöntemleriyle Belirlenmesi, Anadolu Üniversitesi Fen Bilimleri Enstitüsü, Yüksek Lisans Tezi, Eskişehir.

Depren, Ö., "Veri Zarflama Analizi Ve Bir Uygulama", Yüksek Lisans Tezi, Yıldız Teknik Üniversitesi Fen Bilimleri Enstitüsü, İstanbul, 3, 5-12, 17-18, 26, 28-29, 31-44, (2008).

Doğan, N. Ö. (2006). Veri zarflama analizi ile belediyelerde performans ölçümü: Kapadokya bölgesi örneği. Yayımlanmamıĝ yüksek lisans tezi, Erciyes Üniversitesi, Kayseri.

Doğan, Z. (2010). 1992 yılında kurulan devlet üniversitelerinin etkinliğinin veri zarflama analizi ile araştırılması. Yayımlanmamıĝ yüksek lisans tezi, Abant Ġzzet Baysal Üniversitesi, Bolu.

Doyle, J., & Green, R. (1994). Efficiency and cross-efficiency in DEA: Derivations, meanings and uses. Journal of the operational research society, 45(5), 567-578.

Dyson, R.G., Allen, R., Camanho, A.S., Podinovski, V.V., Sarrico, C.S. & Shale, E.A., 2001, Pitfalls and protocols in DEA, European journal of operational research, 132, 245-259.

Ergülen A., Öcal, F. M., Harmankaya, İ., (2020). 1992'de Kurulan Devlet Üniversiteleri Üzerine Bölgesel Veri Zarflama Analizi Uygulaması, International Journal Entrepreneurship And Management Inquiries, Güz Dönemi Cilt, 3, Sayı 5, 175-190.

Ergülen, A., Kazan, H. ve Ünal Z. (2019). Yoğun rekabet ortamında performans değerlendirme: Ġç Anadolu bölgesindeki devlet üniversitelerinin, veri zarflama analizi yöntemiyle performans ölçümü. European Journal of Managerial Research (EUJMR), 3(4), 59-64.

Erken, N., & Emiral, F. (2002). Türk Bankacılık Sisteminde Etkinlik Analizi (Veri Zarflama Analizi Uygulanması). Active Mayıs Haziran, 1-32.

Farrell, M.J., (1957). "The Measurement of Productive Efficiency", Journal of the Royal Statistical Society, 120(3);253-290.

Friedman, L., & Sinuany-Stern, Z. (1998). Combining ranking scales and selecting variables in the DEA context: The case of industrial branches. Computers & Operations Research, 25(9), 781-791.

Gedik, M. (2011). Vergi rekabeti etkinlik değerlendirmesi: OECD üyesi ülkeler için veri zarflama analizi uygulaması. Maliye Dergisi, 160, 329-350.Farrel, 1957.

Golany, B. & Roll, Y., 1989, An application procedure for DEA, Omega, 17(3), 237-250.

Govindarajan, R., Rastogi, S., Vijayakumar, M., Shirwaikar, A., Rawat, A. K. S., Mehrotra, S., & Pushpangadan, P. (2003). Studies on the antioxidant activities of Desmodium gangeticum. Biological and pharmaceutical Bulletin, 26(10), 1424-1427.

Haas, D. A., & Murphy, F. H. (2003). Compensating for non-homogeneity in DMU in data envelopment analysis. European Journal of Operational Research, 144(3), 530-544.

Hsu, C. S., & Lin, J. R. (2007). Mutual fund performance and persistence in Taiwan: a non-parametric approach. The Service Industries Journal, 27(5), 509-523.

Imanirad, R., Cook, W. D., & Zhu, J. (2013). Partial input to output impacts in DEA: Production considerations and resource sharing among business subunits. Naval Research Logistics (NRL), 60(3), 190-207.

İnan, A., (2000), "Banka Etkinliğinin Ölçülmesi Ve Düşük Enflasyon Sürecinde Bankacılıkta Etkinlik", Bankacılar Dergisi (34).

Jalili, M., & Ozbek, M. E. (2019). Efficiency Benchmarking Framework for Highway Patrol Agencies and Implementation for the Wyoming Highway Patrol. Infrastructures, 4(3), 40.

Karasoy, H., (2000), "Veri Zarflama Analizi", Yüksek Lisans Tezi, Yıldız Teknik Üniversitesi, Fbe, İstanbul, (Yayımlanmamış)

Kayalıdere, K. ve Kargın.(2004), Çimento ve Tekstil Sektörlerinde Etkinlik Çalışması ve Veri Zarflama Analizi, Dokuz Eylül Üniversitesi", Sosyal Bilimler Enstitüsü Dergisi, Cilt 6, Say_:1, 2004, s. 196-219.

Kazançoğlu, Y. (2008). Lojistik yönetimi sürecinde tedarikçi seçimi ve performans değerlendirilmesinin yöneylem araştırması teknikleri ile gerçekleştirilmesi: AHP (analitik hiyerarşik süreç) ve DEA (veri zarflama analizi). Ege Üniversitesi, Sosyal Bilimler Enstitüsü, İşletme Anabilim

Dalı, Doktora Tezi, İzmir.

Kecek, G. (2010). Veri Zarflama Analizi Teori ve Uygulama Örneği. Siyasal Basım Yayım.180s.

Kıran, B. (2008) Kalkınmada Öncelikli İllerin Ekonomik Etkinliklerinin Veri Zarflama Analizi Yöntemi İle Değerlendirilmesi, Yüksek Lisans Tezi, Çukurova Üniversitesi Sosyal Bilimler Enstitüsü İşletme Anabilim Dalı: Adana

Lovell, C. K. (1993). Production frontiers and productive efficiency. The measurement of productive efficiency: techniques and applications, 3, 67.

Ma, Z., & Li, H. (2024). A new parallel framework algorithm for solving large-scale DEA models. Expert Systems with Applications, 241, 122687.

Okursoy, A., & Tezsürücü, D. (2014). Veri Zarflama Analizi ile Göreli Etkinliklerin Karşılaştırılması: Türkiye'deki İllerin Kültürel Göstergelerine İlişkin Bir Uygulama. Journal of Management & Economics/Yönetim ve Ekonomi, 21(2).

Özbek, A. (2019). Türkiye'deki İllerin Edas ve WASPAS Yöntemleri ile Yaşanabilirlik Kriterlerine Göre Siralanmasi. Kırıkkale Üniversitesi Sosyal Bilimler Dergisi, 9(1), 177-200.

Özden, Ü. H. (2008). Veri zarflama analizi (VZA) ile Türkiye'deki vakıf üniversitelerinin etkinliğinin ölçülmesi. İstanbul Üniversitesi İşletme Fakültesi Dergisi, 37(2), 167-185.

Öztürk, Y. E. (2014). Veri zarflama analizi ve hastane etkinliğinin ölçülmesinde kullanımı. *Selçuk Üniversitesi Sosyal Bilimler Meslek Yüksekokulu Dergisi*, 12(1-2), 97-118.

Piran, F. S., Lacerda, D. P., & Camargo, L. F. R. (2020). Analysis and management of productivity and efficiency in production systems for goods and services. CRC Press.

Ramanathan R. (2003), An Introduction To Data Envelopment Analysis A Tool For Performance Measurement, Sage Publications, New Delhi.

Rousseau, J. J., & Semple, J. H. (1995). Two-person ratio efficiency games. Management Science, 41(3), 435-441.

Sarı, N. B. (2010). Belediye toplu taşıma hizmetlerinin etkinliğinin veri zarflama analizi ile ölçümü ve iyileştirilmesi. YayımlanmamıꞬ yüksek lisans tezi, Çukurova Üniversitesi, Adana.

Sayıştay, S. I. P. Ö. İ. (2002). Önaraştırma Raporu. Sayıştay Yayını, Ankara, 9.

Seiford, L. M. (1997). A bibliography for data envelopment analysis (1978-1996). Annals of Operations Research, 73(0), 393-438.

Sezen, B., Doğan, E., (2005), Askeri Bir Tersaneye Bağlı Atölyelerin Karğılağtırmalı Verimlilik Değerlendirmesi: Bir Veri Zarflama Yöntemi Uygulaması, Havacılık Ve Uzay Teknolojileri Dergisi, Cilt: 2, Sayı: 2, Ss. 82

Tarım, A., (2001). Veri Zarflama Analizi: Matematiksel Programlama Tabanlı Göreli Etkinlik Ölçümü Yaklaşımı T.C. Sayıştay Başkanlığı Yayınları, No:15, Ankara. S. 8.

Timor, M., & LORCU, F. (2010). Türkiye ve Avrupa Birliğine Üye Ülkelerin Sağlık Sistem Performanslarının Kümeleme ve Veri Zarflama Analizi ile Karşılaştırılması. Yönetim-İstanbul Üniversitesi İşletme Fakültesi İşletme İktisadı Enstitüsü Dergisi 21(65).

Ulucan, A. (2011). Measuring the efficiency of Turkish universities using measure-specific data envelopment analysis. Sosyoekonomi, 14(14), 182-196.

Uzgören, E. ve ġahin, G. (2013). Measurement of the performances of Dumlupınar University vocational high schools using data envelopment analysis method. Journal of Management Economics and Business, 9(18), 91-110. https://doi.org/10.11122/ijmeb.2013.9.18.148

Vurur, S., & Özdemir, L. (2024). Comparison of Efficiency Levels of Turkish Insurance Companies with VZA Malmquist Total Factor Efficiency Analysis. In Cross-Disciplinary Impacts on Insurance Law: ESG Concerns, Financial and Technological Innovation (pp. 127-145). Cham: Springer Nature Switzerland.

Yıldırım, İ. E., (2010), Veri Zarflama Analizinde Girdi Ve Çıktıların Belirlenmesindeki Kararsızlık Problemi İçin Temel Bileşenler Analizine Dayalı Bir Çözüm önerisi, İstanbul Üniversitesi İşletme Fakültesi Dergisi, C: 39, S: 1, Ss. 141-153.

Zhu, J. Data Envelopment Analysis: A Handbook of Models and Methods; Springer: Boston, MA, USA, 2015; Volume 221, 472p.

Zhu, J., & Cook, W. D. (Eds.). (2007). Modeling data irregularities and structural complexities in data envelopment analysis. Springer Science & Business Media, 333p.

Chapter 13

k-TYPE SLANT HELIX FOR NON NULL CURVES IN THE PSEUDO-GALILEAN SPACE $\mathbb{G}_1^4$ *

Esra ERBEK[1]

Mehmet BEKTAŞ[2]

1.Intrudoction

Many geometric concepts have been expressed and proven with the help of Frenet equations of a unit speed curve in Euclidean space [1-3]. Examining the equivalents of these theories established in Euclidean space for timelike, spacelike and null curves in Lorentz-Minkowski space has been the subject of research for geometers [4-6]. From this perspective, new theories for timelike, spacelike and null curves have been put forward and proven. In recent years, Euclidean space and Lorentz-Minkowski space have been the correspondences and differences of the studies carried out for the theory of curves have been examined in Galilean spaces, and new perspectives have been established [7-9]. In parallel with all these, examining the theories for curves in Euclidean space, Lorentz Minkowski space and Galilean space in Pseudo-Galilean space, as another field of study, has revealed a different perspective [10-12].

The aim of this study is to express and prove new theories by defining the concept of k-type helix for curves in Euclidean space, Lorentz Minkowski space and Galilean space in Pseudo-Galilean spaces.

2.Preliminaries

The Minkowski space-time E_1^4 is the Euclidean 4- space E^4 equipped with indefined flat metric given by

$$\langle x, y \rangle_M = -x_1 y_1 + x_2 y_2 + x_3 y_3 + x_4 y_4, \tag{1}$$

for any two vectors $x = (x_1, x_2, x_3, x_4)$ and $y = (y_1, y_2, y_3, y_4)$ in rectangular coordinate system of E_1^4. Since $\langle ., . \rangle_M$ is an indefinite metric, an arbitrary vector $x \neq 0 \in E_1^4$ can be spacelike, timelike and null (lightlike), if $\langle x, x \rangle_M$ is positive, negative or zero, respectively. In particular the vector $x = 0$ is a spacelike vector, [6]. The norm (length) of a vector $x \in E_1^4$ is given by $\|x\|_M = \sqrt{|\langle x, x \rangle_M|}$. An arbitrary curve $\alpha(s)$ in E_1^4 can locally be spacelike, timelike and null (lightlike), if all its

velocity vectors $\alpha'(s)$ are respectively spacelike, timelike and null (lightlike). A null curve $\alpha(s)$ is parameterized by pseudo-arc s if $< \alpha''(s), \alpha''(s) >_M = 1$. On the other hand, a non-null curve α is parametrized by the arclength parameter s if $< \alpha'(s), \alpha'(s) >_M = \pm 1$.

3.Pseudo-Galilean Geometry $\mathbb{G}_1^4$

We will use the terminology and notations in [13] unless told otherwise.

Let $\boldsymbol{a} = (x, y, z, w)$ and $\boldsymbol{b} = (x_1, y_1, z_1, w_1)$ be vectors in the pseudo-Galilean space $\mathbb{G}_1^4$. The scalar product in the pseudo-Galilean space $\mathbb{G}_1^4$ is defined by

$$\langle \boldsymbol{a}, \boldsymbol{b} \rangle_{\mathbb{G}} = xx_1.$$

A vector $\boldsymbol{a} = (x, y, z, w)$ is said to be isotropic or special vector if $x = 0$. Otherwise, $\boldsymbol{a} = (x, y, z, w)$ is called a non-isotropic. All unit non-isotropic vectors and isotropic vectors are of the form $\boldsymbol{a} = (x, y, z, w)$, $x \neq 0$ and $\boldsymbol{p} = (0, y, z, w)$, respectively. Let $\boldsymbol{p} = (0, y, z, w)$ and $\boldsymbol{q} = (0, y_1, z_1, w_1)$ be two isotropic vectors. Then, the special scalar product of isotropic vectors $\boldsymbol{p}$ and $\boldsymbol{q}$ is defined by

$$\langle \boldsymbol{a}, \boldsymbol{b} \rangle_\delta = yy_1 + zz_1 - ww_1.$$

The orthogonality of vectors in pseudo-Galilean space $\mathbb{G}_1^4$, $\boldsymbol{a} \perp_{\mathbb{G}} \boldsymbol{b}$, means that $\langle \boldsymbol{a}, \boldsymbol{b} \rangle_{\mathbb{G}} = 0$ for $\langle \boldsymbol{a}, \boldsymbol{a} \rangle_{\mathbb{G}} \neq 0$. So, all isotropic vectors are orthogonal to the non-isotropic vectors. Also, the $\delta -$orthogonality of isotropic vectors $\boldsymbol{p}$ and $\boldsymbol{q}$ means that $\langle \boldsymbol{p}, \boldsymbol{q} \rangle_\delta = 0$.

The norm of a vector **a** is defined by

$$\|\boldsymbol{a}\|_{\mathbb{G}} = |x|,$$

and **a** is called a unit vector if $\|\boldsymbol{a}\|_{\mathbb{G}} = 1$. The norm of an isotropic vector $\boldsymbol{p}$ is defined by

$$\|\boldsymbol{p}\|_\delta = \sqrt{|y^2 + z^2 - w^2|}$$

and p is called a unit isotropic vector if $\|p\|_\delta = 1$. Briefly, the vectors in $\mathbb{G}_1^4$ are divided into two classes: the non-isotropic vector or the isotropic vectors which are spacelike, timelike or null.

Let $a = (x, y, z, w)$, $b = (x_1, y_1, z_1, w_1)$ and $c = (x_2, y_2, z_2, w_2)$ be at least one non-isotropic vector in the pseudo-Galilean space $\mathbb{G}_1^4$, we introduce the vector product of a, b and c as the following:

$$a \times b \times c = - \begin{vmatrix} 0 & e_2 & e_3 & -e_4 \\ x & y & z & w \\ x_1 & y_1 & z_1 & w_1 \\ x_2 & y_2 & z_2 & w_2 \end{vmatrix}.$$

Especially, the vector product of isotropic vectors $p = (0, y, z, w)$, $q = (0, y_1, z_1, w_1)$ and $r = (0, y_2, z_2, w_2)$ is introduced

$$p \times q \times r = - \begin{vmatrix} e_1 & e_2 & e_3 & -e_4 \\ 0 & y & z & w \\ 0 & y_1 & z_1 & w_1 \\ 0 & y_2 & z_2 & w_2 \end{vmatrix}.$$

Here, e_1, e_2, e_3 and e_4 are coordinate direction vectors which satisfy at follows:

$$e_1 \times e_2 \times e_3 = e_4,$$

$$e_2 \times e_3 \times e_4 = e_1,$$

$$e_3 \times e_4 \times e_1 = e_2,$$

$$e_4 \times e_1 \times e_2 = -e_3.$$

Let $\{D, E, F, G\}$ be vectors in $\mathbb{G}_1^4$.

    i.   If D is a unit non-isotropic vector and $\{E, F\}$ are unit isotropic spacelike vectors and G is a unit isotropic timelike vector, then $\{D, E, F, G\}$ is called an orthonormal basis of $\mathbb{G}_1^4$.

    ii.   If D is a unit non-isotropic vector and E is a unit isotropic spacelike vector, $\{F, G\}$ are unit isotropic lightlike vectors such

that $\langle F, G \rangle_\delta = -1$, $\{D, E, F, G\}$ is called a null basis (or null frame) of $\mathbb{G}_1^4$.

4. Construction of Frenet-Serret Frame in $\mathbb{G}_1^4$

Let α be a curve in $\mathbb{G}_1^4$ given first by

$$\alpha(t) = (x(t), y(t), z(t), w(t)),$$

where $x(t), y(t), z(t), w(t) \in C^4$ (the set of four-times continuously differentiable functions) and t run through a real interval. If $\frac{dx(t)}{dt} \neq 0$, then the curve α is called an admissible curve. Otherwise, the curve α is called a non-admissible curve. From now on, we denote differentiation with respect to t by a dash.

An admissible curve given first by

$$\alpha(t) = (x(t), y(t), z(t), w(t)),$$

where $x'(t) \neq 0$, the parameter of arc length is defined by

$$ds = |x'(t)dt| = |dx|.$$

For briefly, we assume $ds = dx$ and $s = x$ as the arc length of the curve α. Let an admissible curve α of the class $C^r (r \geq 3)$ parameterized by arclength x, given in coordinate form $\alpha(x) = (x, y(x), z(x), w(x))$. The first vector of the Frenet-Serret frame, namely the tangent vector of α is defined by

$$T(x) = \alpha'(x) = (1, y'(x), z'(x), w'(x)).$$

Since T is a unit vector, so, we may express $\langle T, T \rangle_\mathbb{G} = 1$. Differentiating the last equation with respect to x, we have $\langle T', T \rangle_\mathbb{G} = 0$. Note that $T'(x)$ can be a timelike, spacelike or null vector:

So, we have computed Frenet-Serret formulas with respect to three conditions of $T'(x)$.

Only if $T'(x)$ is timelike, the Frenet-Serret formulas are obtained as follows.

$$\begin{bmatrix} T' \\ N' \\ B_1' \\ B_2' \end{bmatrix} = \begin{bmatrix} 0 & k_1 & 0 & 0 \\ 0 & 0 & k_2 & 0 \\ 0 & k_2 & 0 & k_3 \\ 0 & 0 & -k_3 & 0 \end{bmatrix} \begin{bmatrix} T \\ N \\ B_1 \\ B_2 \end{bmatrix}. \tag{2}$$

In cace the Frenet-Serret formulas in cases where $T'(x)$ is spacelike and null can also be looked at [13].

Let α be a admissible curve with the Frenet frame $\{T, N, B_1, B_2\}$ in G_1^4 and u is a constant vector field in G_1^4. If there is $c_1 \in IR$ such that $\langle T, u \rangle = c_1$, then α curve is called 1- type slant helix (or general helix), If there is $c_2 \in IR$ such that $\langle N, u \rangle = c_2$, then α curve is called 2- type slant helix (or slant helix), If there is $c_3 \in IR$ such that $\langle B_1, u \rangle = c_3$, then α curve is called 3- type slant helix and If there is $c_4 \in IR$ such that $\langle B_2, u \rangle = c_4$, then α curve is called 4- type slant helix [14].

5. k −type slant helix

Along with the study, the special scalar product will be denoted by $\langle . , . \rangle$.

Theorem 5.1. Let $\alpha: I \to \mathbb{G}_1^4$, $\alpha = \alpha(x)$ be a regular curve with curvatures $k_1(x), k_2(x)$ and $k_3(x)$. If the curve α is a 1 −type slant helix in $\mathbb{G}_1^4$ and $k_i (1 \le i \le 3)$ is not zero, then $\langle N, u \rangle = \langle B_1, u \rangle = \langle B_2, u \rangle = 0$.

Proof. Let $\alpha = \alpha(x)$ be a 1 −type slant helix in $\mathbb{G}_1^4$.

Then there is a $c_1 \in \mathbb{R}$, such that

$$\langle T, u \rangle = c_1. \tag{3}$$

If we take derivative of both sides of (3), use (2)

$$\langle N, u \rangle = 0 \tag{4}$$

if we take derivative of both sides of (4), use (2)

$$\langle B_1, u \rangle = 0 \tag{5}$$

Finally, if we take derivative of both sides of (5) use (2) and (4), we obtain

$$\langle B_2, u \rangle = 0. \tag{6}$$

Theorem 5.2. Let $\alpha: I \to \mathbb{G}_1^4$, $\alpha = \alpha(x)$ be a regular curve with $k_1(x)$, $k_2(x)$ and $k_3(x)$ such that $k_2(x)$ and $k_3(x) \neq 0$. If α is a $2-$type slant helix and $k_2(x) = k_3(x)$, then α is a $4-$type slant helix.

Proof. Let $\alpha = \alpha(x)$ be a $2-$type slant helix in $\mathbb{G}_1^4$.

Then there is a $c_2 \in \mathbb{R}$ such that

$$\langle N, u \rangle = c_2 \tag{7}$$

if we take derivative of both sides of (7), use (2)

$$\langle B_1, u \rangle = 0. \tag{8}$$

If we take derivative of both sides of (8), use (2) and (7), we obtain

$$\langle B_2, u \rangle = -c_2. \tag{9}$$

In this case, α is a $4-$type slant helix.

Theorem 5.3. Let $\alpha: I \to \mathbb{G}_1^4$, $\alpha = \alpha(x)$ be a regular curve with curvatures $k_1(x), k_2(x)$ and $k_3(x)$. If α is a $3-$type slant helix and $k_2(x) = k_3(x)$, then

$$\langle N, u \rangle = -\langle B_2, u \rangle \tag{10}$$

Proof. Let $\alpha = \alpha(x)$ be a $3-$type slant helix in $\mathbb{G}_1^4$.

Then there is a $c_3 \in \mathbb{R}$, such that

$$\langle B_1, u \rangle = c_3 \tag{11}$$

If we take derivative of both sides of (11), use (2) we obtain (10).

Theorem 5.4. Let $\alpha: I \to \mathbb{G}_1^4, \alpha = \alpha(x)$ be a regular curve with $k_1(x)$, $k_2(x)$ and $k_3(x)$ such that $k_2(x)$ and $k_3(x) \neq 0$. If α is a $4-$type slant helix and $k_2(x) = k_3(x)$, then α is a $2-$type slant helix.

Proof. Let $\alpha = \alpha(x)$ be a $4-$type slant helix in $\mathbb{G}_1^4$.

Then there is a $c_4 \in \mathbb{R}$, such that

$$\langle B_2, u \rangle = c_4 \tag{12}$$

if we take derivative of both sides of (12), use (2)

$$\langle B_1, u \rangle = 0 \tag{13}$$
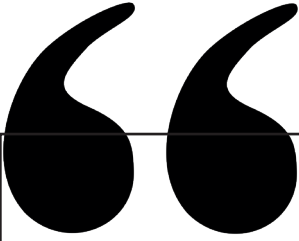
and we take derivative of both sides of (13), use (2)

$$\langle N, u \rangle = -c_4$$

this completes of proof.

References

[1] Yeneroğlu, M., & Duyan, A. (2024). Assocıated Curves Accordıng To Bıshop Frame In 4-Dımensıonal Euclıdean Space. *Journal of Science and Arts*, *24*(1), 105-110.

[2] Mazlum, S. G., Şenyurt, S., & Bektaş, M. (2022). Salkowski Curves and Their Modified Orthogonal Frames in E³ . *Journal of New Theory*, (40), 12-26.

[3] Çiçek Çetin, E., & Bektaş, M. (2019). The Characterization of Affine Symplectic Curves in $\mathbb{R}$4. *Mathematics*, *7*(1), 110.

[4] Saad, M. K., Abdel-Baky, R. A., Alharbi, F., & Aloufi, A. (2020). Characterizations of some special curves in Lorentz-Minkowski space. *Mathematics and Statistics*, *8*(3), 299-305.

[5] Sager, I., Abazari, N., Ekmekci, N., & Yayli, Y. (2011). The classical elastic curves in Lorentz-Minkowski space. *Int. J. Contemp. Math. Sciences*, *6*(7), 309-320.

[6] Hanif, M., Hou, Z. H., & Nisar, K. S. (2018). On special kinds of involute and evolute curves in 4-dimensional Minkowski space. *Symmetry*, *10*(8), 317.

[7] Elsharkawy, A., Tashkandy, Y., Emam, W., Cesarano, C., & Elsharkawy, N. (2023). On Some Quasi-Curves in Galilean Three-Space. *Axioms*, *12*(9), 823.

[8] Elzawy, M., & Mosa, S. (2023). Equiform rectifying curves in Galilean space G4. *Scientific African*, *22*, e01931.

[9] Bektas, M., Ergut, M., and Ögrenmiş, A.O. (2013). Special curves of 4D Galilean space Int. J. Math. Eng. Sci., 2 (3).

[10] Arfah, A. (2022). On Involutes of Admissible Non-Lightlike Curves in Pseudo-Galilean 3-Space. *Cumhuriyet Science Journal*, *43*(1), 82-87.

[11] Yoon, D. W. (2013). Surfaces of revolution in the three dimensional pseudo-Galilean space. *Glasnik matematički*, *48*(2), 415-428.

[12] Milin Šipuš, Ž., & Divjak, B. (2012). Surfaces of Constant Curvature in the Pseudo-Galilean Space. *International Journal of Mathematics and Mathematical Sciences*, *2012*(1), 375264.

[13] Akbıyık, M., & Yüce., S. (2021). 4-dimensional pseudo-Galilean geometry. *Cumhuriyet Science Journal*, *42*(4), 890-905.

[14] Ali, A., L´opez R., and Turgut,M., (2012). k-type partially null and pseudo null slant helices in Minkowski 4-space, Math. Commun. 17, 93-103.

Chapter 14

THE HOSOYA-TYPE PELL LENGTHS AND THE BASIC HOSOYA-TYPE PELL LENGTHS OF THE FOX GROUPS $G_{1,T}$

Ömür DEVECİ[1]

1 Prof. Dr., Kafkas University, Faculty of Science and Letters, Department of Mathematics, odeveci36@hotmail.com, ORCID: 0000-0001-5870-5298.

1. INTRODUCTION

It is well known that the Pell sequence $\{P_n\}$ is defined by the following homogeneous linear recurrence relation:

$$P_{n+2} = 2P_{n+1} + P_n$$

for $n \geq 0$, with initial conditions $P_0 = 0$ and $P_1 = 1$.

The study of the linear recurrence sequences in groups began with the earlier work of Wall (Wall, 1960) where the ordinary Fibonacci sequences in cyclic groups were investigated. Other work on the Fibonacci sequences in cyclic groups is discussed in, for example, (Chang, 1986; Lü & Wang, 2007; Renault, 2013; Shah, 1968; Vinson, 1963). In the mid-eighties, Wilcox studied the Fibonacci sequences in abelian groups in (Wilcox, 1986). In (Campbell, Doostie, & Robertson, 1990), the theory was expanded to non-abelian groups by Campbell et al. There, they defined the Fibonacci orbit and the basic Fibonacci orbit of a 2-generator group. We also have the following definition of Fibonacci orbit for a finitely generated group $G = \langle A \rangle$, where $A = \{a_1, a_2, \ldots a_n\}$:

Definition 1.1 The Fibonacci orbit of with respect to the generating set A, written $F_A(G)$, is the sequence $x_i = a_{i+1}$, $0 \leq i \leq n-1$, $x_{i+n} = \prod_{j=1}^{n} x_{i+j-1}$ for $i \geq 0$.

If the sequence $F_A(G)$ is periodic, then the length of the period is called the Fibonacci lenght of G with respect to the generetaing set A, written $LEN_A(G)$ (Campbell P. , 2003; Campbell & Campbell , (2009)

Let G be a 2-generator group and let

$$X = \{(x_1, x_2) \in G \times G \mid \langle \{x_1, x_2\} \rangle = G\}.$$

The notation (x_1, x_2) is said to be a generating pair for G. If G is a 2-generator group and (x_1, x_2) is a generating pair of G, then every element of G can be written as a word

$$(x_1)^{\alpha_1} (x_2)^{\alpha_2} (x_1)^{\alpha_3} \cdots (x_1)^{\alpha_{n-1}} (x_2)^{\alpha_n}$$

where $\alpha_i \in \mathbb{Z}$, $1 \le i \le n$.

The concept of Fibonacci length for two or more generators has also been considered; see, for example, (Aydin & Dikici, 1998; Campbell & Campbell, 2004; Campbell C. , Campbell, Doostie, & Robertson, 2004; Deveci, Karaduman, & Campbell, 2011; Doostie & Golamie, 2000; Karaduman & Aydın, 2003; Knox, 1992; Ozkan, 2003). In next process, some special linear recurrence sequences defined by the aid of group elements have been studied by many authors; for example, (Akuzum & Deveci, 2020; Cetinalp, Yılmaz, & Deveci, 2024; Deveci, Akdeniz, & Akuzum, 2017; Deveci, Akuzum, & Colin, 2018; Deveci, Akuzum, & Uğurlu, 2018; Deveci, Artun, & Akuzum, 2017) (Deveci, Erdag, & Güngoz, 2022; Deveci & Karaduman, 2015; Deveci & Shannon, 2021; Deveci & Shannon, 2018; Erdag & Deveci, 2022) (Erdag & Deveci, 2018; Erdag, Deveci̇, & Karaduman, 2022; Hashemi & Mehraban, 2022; Hulk, Erdag, & Deveci, 2023; Kuloglu, Ozkan, & Shannon, 2022; Mehraban, Gulliver, Boulaaras, Hosseini, & Hincal, 2024; Mehraban & Hashemi, 2023) (Ozkan, 2014). In (Peters, Deveci, & Arıkanoglu, Is Submitted), Peters et al. contributed to theory via the Hosoya-type Pell r-orbits of the 2-generator groups. In their paper they defined this sequence by considering Hosoya triangle and Pell sequence:

Definition 1.2 (Peters, Deveci, & Arıkanoglu, Is Submitted) Let r be a positive integer and let P_r be the rth Pell number. For generating pair $(x_1, x_2) \in X$, we define the Hosoya-type Pell r-orbits of the 2-generator group G as follows:

$$a_0^r = x_1, a_1^r = x_2, a_{n+2}^r = \left(a_n^r\right)^{-P_r} \left(a_{n+1}^r\right)^{P_{r+1}}, (n \ge 0).$$

For the generating pair (x_1, x_2), we denote the rth Hosoya-type Pell orbit of G by $P_{(x_1, x_2)}^{h,r}(G)$.

Theorem 1.1 (Peters, Deveci, & Arıkanoglu, Is Submitted) Let G be a 2-generator group and let (x_1, x_2) be a generating pair of . If G is finite, then the rth Hosoya-type Pell orbit of G with respect to the generating pair (x_1, x_2), $P_{(x_1, x_2)}^{h,r}(G)$ is periodic for every positive integer r.

The length of the period of the sequence $P_{(x_1, x_2)}^{h,r}(G)$ is denoted by $l_{(x_1, x_2)}^{h,r}(G)$.

Definition 1.3 (Peters, Deveci, & Arıkanoglu, Is Submitted) Let the rth Hosoya-type Pell orbit of G, $P_{(x_1, x_2)}^{h,r}(G)$ be simply periodic for a constant positive integer r. For generating pair $(x_1, x_2) \in X$, the basic r^{th} Hosoya-type Pell orbit $\overline{P_{(x_1, x_2)}^{h,r}}(G)$ of basic length m is a sequence of group elements $b_0^r, b_1^r, b_2^r, \ldots, b_n^r, \ldots$, each term is defined

$$b_0^r = x_1, b_1^r = x_2 \text{ and } b_{n+2}^r = \left(b_n^r\right)^{-P_r}\left(b_{n+1}^r\right)^{P_{r+1}}, (n \geq 0)$$

where $m \geq 1$ is the least integer, with

$$b_0^r = b_m^r \theta, b_1^r = b_{m+1}^r \theta, \, b_2^r = b_{m+2}^r \theta, \ldots, b_m^r = b_{2m}^r \theta,$$
$$b_{m+1}^r = b_{2m+1}^r \theta, \ldots, b_{(i-1)\cdot m}^r = b_{i\cdot m}^r \theta, b_{(i-1)\cdot m+1}^r = b_{i\cdot m+1}^r \theta, \ldots$$

for some $\theta \in AutG$.

Since b_m^r and b_{m+1}^r generate and the terms succeding $b_{m+2}^r, b_{m+3}^r, \ldots$, depend on b_m^r, b_{m+1}^r for their values, it follows that the automorphism θ is uniquely determined. The length of the period of the sequence $\overline{P_{(x_1, x_2)}^{h,r}}(G)$ is denoted by $\overline{l_{(x_1, x_2)}^{h,r}}(G)$.

The Fox groups $G_{1,t}$, are finite metacyclic groups of order $|t-1|^3$, having generators of order $(t-1)^2$, see (Benson & Mendelsohn, 1966; Campbell C. , Campbell, Doostie, & Robertson, 2004; Campbell & Robertson, 1976). They are presented by

$$\langle x, y : xy = y^t x, \; yx = x^t y \rangle.$$

The relations of $G_{1,t}$ imply the relation $x^{t-1} = y^{1-t}$.

In this work, we obtain lengths of the periods of the sequences $P_{(x,y)}^{h,1}\left(G_{1,t}\right)$ and $\overline{P_{(x,y)}^{h,1}}\left(G_{1,t}\right)$ for $t \geq 3$.

2. MAIN RESULTS

A sequence is periodic if, after a certain point, it consists only of repetitions of a fixed subsequence. The number of terms in the shortest repeating subsequence is called the period of the sequence. In addition, if the first k terms in the sequence form a repeating subsequence then the sequence is simply periodic with period k. For example, the sequence $\{a,b,c,d,b,c,d,b,c,d,\ldots\}$ is periodic after the initial term a and has period 3 and also the sequence $\{a,b,c,d,a,b,c,d,a,b,c,d,\ldots\}$ is simply periodic with period 4.

We shall now address the 1st Hosoya-type Pell lengths and the basic 1st Hosoya-type Pell lengths of the Fox groups $G_{1,t}$ for $t \geq 3$.

Theorem 2.1 Let t be an integer such that $t \geq 3$.

i) For $t = 3$, the sequence $P_{(x,y)}^{h,1}\left(G_{1,3}\right)$ is simply periodic and $l_{(x,y)}^{h,1}\left(G_{1,3}\right) = \overline{l_{(x,y)}^{h,1}}\left(G_{1,3}\right) = 2$.

ii) For $t \geq 4$, the sequence $P^{h,1}_{(x,y)}\left(G_{1,t}\right)$ is simply periodic and the lengths $l^{h,1}_{(x,y)}\left(G_{1,t}\right)$ and $\overline{l^{h,1}_{(x,y)}}\left(G_{1,t}\right)$ are as folows:

(1) If t is a positive even integer, then $l^{h,1}_{(x,y)}\left(G_{1,t}\right) = (t-1)^2$ and $\overline{l^{h,1}_{(x,y)}}\left(G_{1,t}\right) = t-1$.

(2) If is a positive odd integer, then $l^{h,1}_{(x,y)}\left(G_{1,t}\right) = \dfrac{(t-1)^2}{2}$ and $\overline{l^{h,1}_{(x,y)}}\left(G_{1,t}\right) = t-1$.

Proof. We prove this by direct calculation. We first note that the 1$^{\text{st}}$ Hosoya-type Pell orbit of the Fox groups $G_{1,t}$ with respect to the generating pair (x,y) is as follows:

$$a^1_0 = x, a^1_1 = y, a^1_{n+2} = \left(a^1_n\right)^{-1}\left(a^1_{n+1}\right)^2, (n \geq 0).$$

i) The sequence $P^{h,1}_{(x,y)}\left(G_{1,3}\right)$ is

$$\{x, y, x, y, x, y, \ldots\}$$

which has period 2 and the basic period 2 since $x\theta = x$ and $y\theta = y$ where is the identity transform.

ii) For $t \geq 4$, the rth Hosoya-type Pell orbit $P^{h,1}_{(x,y)}\left(G_{1,t}\right)$ has the following pattern:

$$a^1_0 = x, a^1_1 = y, \ldots,$$
$$a^1_{t-1} = x^{(t-2)^2}, a^1_{1+t-1} = y^{2t-1}, \ldots,$$
$$a^1_{2t-2} = x^{(t-2)^4}, a^1_{1+2t-2} = y^{(2t-1)^2}, \ldots,$$
$$a^1_{3t-3} = x^{(t-2)^6}, a^1_{1+3t-3} = y^{(2t-1)^3}, \ldots,$$
$$a^1_{i\cdot(t-1)} = x^{(t-2)^{2i}}, a^1_{1+i\cdot(t-1)} = y^{(2t-1)^i}, \ldots,$$

which implies that the sequence is simply periodic with period $i \cdot (t-1)$. Since , we need the smallest positive integer i such that

$$(t-2)^{2i} \equiv 1 mod (t-1)^2$$

and

$$(2t-1)^{2i} \equiv 1 mod (t-1)^2.$$

Let $(t-1)$ be denoted by a. Then, by the binomial expansion, we get

$$(a-1)^{2i} = \sum_{k=0}^{2i} a^{2i-k} (-1)^k \binom{2i}{k}$$

and

$$(2a+1)^i = \sum_{k=0}^{i} (2a)^{i-k} \binom{i}{k} = (2a)^i + (2a)^{i-1} \cdot \binom{i}{1} + (2a)^{i-2} \cdot \binom{i}{2}$$

$$+ \cdots + 4a^2 \cdot \binom{i}{i-2} + 2i \cdot a + 1.$$

To determine the period of the sequence we concentrate on finding the smallest positive integer i such that

$$2i \cdot a \equiv 1 \left(\mod a^2 \right).$$

(1) If a is odd, then $i = a = t-1$. Thus we obtain $l_{(x,y)}^{h,1} \left(G_{1,t} \right) = (t-1)^2$ and $\overline{l_{(x,y)}^{h,1}} \left(G_{1,t} \right) = t-1$ since $x\theta = x^{(t-2)^{2t-4}}$ and $y\theta = y^{(2t-1)^{t-2}}$ where θ is an outer automorphism of order $t-1$.

(2) If a is even, then $i = \dfrac{a}{2} = \dfrac{t-1}{2}$. Thus we obtain

$l_{(x,y)}^{h,1}\left(G_{1,t}\right) = \dfrac{(t-1)^2}{2}$ and $\overline{l_{(x,y)}^{h,1}}\left(G_{1,t}\right) = t-1$ since $x\theta = x^{(t-2)^{t-3}}$ and

$y\theta = y^{(2t-1)^{\frac{t-3}{2}}}$ where θ is an outer automorphism of order $\dfrac{t-1}{2}$.

We now give examples of calculating the 1st Hosoya-type Pell lengths and the basic 1st Hosoya-type Pell lengths of the Fox groups $G_{1,t}$.

Example 2.1 The sequences $P_{(x,y)}^{h,1}\left(G_{1,4}\right)$ and $P_{(x,y)}^{h,1}\left(G_{1,5}\right)$ are as follows, respectively:

$$\left\{x, y, x^{-1}y, x^4, y^7, y^2x^{-1}, x^7, y^4, y^{-1}x^{-1}, x, y,...\right\},$$

and

$$\left\{x, y, x^{-1}y^2, y^{-1}x^2, x^9, y^9, x^7y^2, y^3x^{-2}, x, y,...\right\}.$$

Firstly, we consider the sequence $P_{(x,y)}^{h,1}\left(G_{1,4}\right)$. Considering $|x| = |y| = 9$, we obtain $l_{(x,y)}^{h,1}\left(G_{1,4}\right) = 9$ and $\overline{l_{(x,y)}^{h,1}}\left(G_{1,4}\right) = 3$ since $x\theta = x^{16} = x^7$ and $y\theta = y^{49} = y^4$ where θ is an outer automorphism of order 3.

Now we concentrate on finding the lengths and the basic lengths of the sequence $P_{(x,y)}^{h,1}\left(G_{1,5}\right)$. Using an analogous argument as the above we see that $l_{(x,y)}^{h,1}\left(G_{1,5}\right) = 8$ and since $x\theta = x^9$ and $y\theta = y^9$ where θ is an outer automorphism of order 2.

REFERENCES

Akuzum, Y., & Deveci, O. (2020). The Hadamard-type k-step Fibonacci sequences in groups. *Comm. Algebra, 48*(7), 2844-2856.

Aydin, H., & Dikici, R. (1998). General Fibonacci Sequences in Finite Groups. *Fibonacci Quarterly, 36*(3), 216-221.

Benson, C., & Mendelsohn, N. (1966). A calculus for a certain class of word problems in groups. *J. Comb. Theory, 1*, 202-208.

Campbell , P. (2003). Fibonacci length and efficieny in group presentations. *Ph.D. Thesis, University of St Andrews.*

Campbell, C. M., Doostie, H., & Robertson, E. F. (1990). *Fibonacci Length of Generating Pairs in Groups in Applications of Fibonacci Numbers.* (V. 3. al., Dü.) Kluwer Academic Publishers.

Campbell, C., & Campbell , P. ((2009). The Fibonacci lengths of binary polyhedral groups and related groups. *Cong. Numerantium, 194*, 95-102.

Campbell, C., & Campbell, P. (2004). *On the Fibonacci length of powers of dihedral groups. In Applications of Fibonacci numbers,* (Cilt 9). Dordrecht, The Netherlands.: F. T. Howard, Ed., Kluwer Academic Publisher.

Campbell, C., & Robertson, E. (1976). On a group presentation due to Fox. *Canad. Math. Bull.,,* 247-248.

Campbell, C., Campbell, P., Doostie, H., & Robertson, E. (2004). Fibonacci lengths for certain metacyclic groups. *Algebra Colloq., 11*(2), 215-229.

Cetinalp, E., Yılmaz, N., & Deveci, O. (2024). The cyclic-Fibonacci hybrid sequence in groups. *J. Mahani math. Res., 13*(2), 411-422.

Chang, D. (1986). Higher-order Fibonacci sequences modulo m. *Fibonacci Quart., 24*(2), 138-139.

Deveci, O., & Karaduman, E. (2015). The Pell Sequences in Finite Groups. *Utilitas Mathematica, 96*, 263-276.

Deveci, O., & Shannon, A. (2018). The quaternion-Pell sequence. *Commun. Algebra, 46*(12), 5403-5409.

Deveci, O., & Shannon, A. (2021). The complex-type k-Fibonacci sequences and their applications. *Comm. Algebra, 3*, 1352-1367.

Deveci, O., Akdeniz, M., & Akuzum, Y. (2017). The Periods of The Pell p-Orbits of Polyhedral and Centro-Polyhedral Groups. *Jordan J. Math. Stat., 10*(1), 1-9.

Deveci, O., Akuzum, Y., & Colin, M. (2018). The recurrence sequences via polyhedral groups. *Commun. Fac. Sci. Univ. Ank. Ser. A1 Math. Stat., 67*(2), 99-115.

Deveci, O., Akuzum, Y., & Uğurlu, G. (2018). The k-step Fibonacci sequences via Hurwitz matrices. *An. Stiint . Univ. Al. I. Cuza Ia si. Mat. (N.S.), 64*((f.1)), 121-134.

Deveci, O., Artun, G., & Akuzum, Y. (2017). The Fibonacci p-Sequences and the Padovan p-Sequences in the Extended Triangle Groups. *Romai J.*(13), 19-25.

Deveci, O., Erdag, O., & Güngoz, U. (2022). The complex-type cyclic-Fibonacci sequence and its applications. *J. Mahani Math. Res., 12*(2), 235-246.

Deveci, O., Karaduman, E., & Campbell, C. (2011). On the k-nacci sequences in finite binary polyhedral groups. *Algebra Colloq., 18*(1), 945-954.

Doostie, H., & Golamie, R. (2000). Computing on the Fibonacci lengths of finite groups. *Int. J. Appl. Math., 4*, 149-156.

Erdag, O., & Deveci, O. (2018). The arrowhead-Pell-random-type sequences in finite groups. *AIP Conference Proceedings. 1991.* AIP Publishing LLC.

Erdag, O., & Deveci, O. (2022). The Complex-type Cyclic-Jacobsthal Sequence and its applications. E. O. (Ed.) içinde, *Teoriden Uygulamaya Fizik Ve Matematik Alanında Akademik Çalışmalar II* (s. 197-212). Ankara, Iksad Publications House.

Erdag, O., Deveci̇, O., & Karaduman, E. (2022). The complex-type cyclic-Pell sequence and its applications. *Turkish J. Sci., 7*(3), 202-210.

Hashemi, M., & Mehraban, E. (2022). The generalized order k-Pell sequences in some special groups of nilpotency class 2. *Commun. Algebra, 54*(2), 1768-1784.

Hulk, S., Erdag, O., & Deveci, O. (2023). Complex-type Narayana sequence and its application. *Maejo Int. J. Sci. Technol., 17*(2), 163-176.

Karaduman, E., & Aydın, H. (2003). General 2-step Fibonacci sequences in nilpotent groups of exponent p and nilpotency class 4. *Appl. Math. Comp., 141*(2-3), 491-497.

Knox, S. (1992). Fibonacci Sequences in Finite Groups. *Fibonacci Quarterly, 30*, 116-120.

Kuloglu, B., Ozkan, E., & Shannon, A. (2022). The Narayana sequence in finite groups. *Fibonacci Quart., 60*(5), 212-221.

Lü, K., & Wang, J. (2007). k-step Fibonacci Sequence Modulo m. *Utilitas Mathematica, 71*, 169-178.

Mehraban, E., & Hashemi, M. (2023). Fibonacci length and the generalized order k-Pell sequences of the 2-generator p-groups of nilpotency class 2. *Journal Algebra Appl., 22*(3), 2350061.

Mehraban, E., Gulliver, T., Boulaaras, S., Hosseini, K., & Hincal, E. (2024). New sequences from the generalized Pell p- numbers and mersenne numbers and their application in cryptography. *AIMS Mathematics, 9*(5), 13537-13552.

Ozkan, E. (2003). 3-step Fibonacci sequences in nilpotent groups. *Appl Math. Comput., 144*(2-3), 517-527.

Ozkan, E. (2014). Truncated Lucas sequences and its period. *Appl Math. Comput., 232*, 285-291.

Peters, J., Deveci, O., & Arıkanoglu, B. (Is Submitted). Hosoya-Pell cyclic proximity groups. *Application of HP sinusoidal polinomials in modulating oscillatory waveforms emamating from vibrating systems.*

Renault, M. (2013). The period, rank, and order of the (a, b)-Fibonacci sequence Mod m. *Math. Magazine, 86*(5), 372-380.

Shah, A. (1968). Fibonacci sequence modulo m. *Fibonacci Quart., 6*(2), 139-141.

Vinson, J. (1963). The relations of the period modulo m to the rank of application of m in the Fibonacci sequence. *Fibonacci Quart., 1*(2), 37-45.

Wall, D. D. (1960). Fibonacci series modulo m. *The American Mathematical Monthly, 67*, 525-532.

Wilcox, H. (1986). Fibonacci Sequences of Period n in Groups. *Fibonacci Quart, 24*(4), 356-361.